Development of biofluid biomarkers for Huntington's disease

A thesis submitted for
the degree of Doctor
of philosophy

Lauren Mary Byrne
Student no. 14094153

University College London, 2019

For Peter...

being a Byrne,

and all that that entails

Declaration of authorship and originality

I, Lauren Mary Byrne, confirm that the work presented in this thesis is my own. Where information has been derived from other sources, I confirm that this has been indicated in the thesis.

Lauren Mary Byrne

Abstract

Though no treatments can currently prevent onset or slow progression of Huntington's disease (HD), many huntingtin-lowering drug candidates targeting the root cause of HD are in the development pipeline. This brings much hope that disease-modifying treatments for HD will be a reality. However, success of potential candidates may be hindered by a lack of sensitive tools to measure biological efficacy over short intervals.

Decades of attempts to develop robust biofluid biomarkers of HD progression has yielded little success or replication of results. Cerebrospinal fluid (CSF), fluid that bathes the brain and is enriched for brain-specific proteins, is a plausible target for uncovering neuropathologically relevant markers of HD. However, a lack of standardisation of collection protocols, biological rationale and technological sensitivity has hampered the progress of CSF biomarkers within the field of HD. At the core of this thesis lies the HD-CSF study – a single-site CSF collection study, with a standardised protocol designed to generate high-quality CSF and blood with matched clinical and phenotypic data. It is the first CSF collection prospectively designed for longitudinal sampling and having matching MRI data.

Mutant huntingtin protein (mHTT) can be quantified in CSF and has been identified as having high potential as a biomarker of HD progression. Further, the interpretation of drug-induced lowering of mHTT in the CNS relies upon elucidation of the natural history of CSF mHTT in HD gene carriers. Neurofilament light (NfL) has emerged as a promising marker of neuronal damage that can be measured in CSF and blood. This thesis includes the first reports of blood NfL in HD, head to head comparison of NfL and mHTT, and assessment of longitudinal alterations in mHTT and NfL, in addition to proposed biomarkers of specific pathogenic pathways. The work in this thesis will have significant implications for the use of NfL and mHTT as pharmacodynamic markers of HD.

Impact Statement

Huntington's Disease (HD) is a devastating, slowly-progressive, neurodegenerative disease which is dominantly-inherited. Around 8000 people in the UK are thought to be affected by HD, with many more at risk of inheriting it. Despite the knowledge of the exact cause – a defect in the HTT gene that results in toxic Huntingtin protein (mHTT) – since 1993, there are no disease-modifying therapies that could stop or even slow this fatal disease. Over 100 therapeutics have been trialled in HD with only two being licensed for HD symptoms. One issue that may contribute to this low success rate is the lack of measures sensitive enough to detect efficacy. Extensive research efforts have produced robust imaging biomarkers. However, there has been little progress with biochemical markers.

In this thesis, I have identified a blood-based biomarker of neuronal injury that is highly relevant to the biological underpinnings of HD pathology – neurofilament light (NfL) – and demonstrated that it has robust prognostic ability for HD. This is the first blood test to possess these attributes. This work received the 2017 HD Insight of the year award from the Huntington Study Group.

In September 2015, the HD field entered a new era when the first targeted huntingtin-lowering therapeutic candidate entered a phase 1b/2a trial and later showed dose-dependent mHTT reduction in CSF. This thesis has generated essential natural history data of the longitudinal dynamics of mHTT in CSF. These data have been shared with several collaborators, including industry and non-profit partnerships, to bring forward the application of both mHTT and NfL as clinical trial endpoints. This is already facilitating the interpretation of huntingtin-lowering trials.

I have established a longitudinal collection of high-quality Cerebrospinal fluid (CSF) and matched blood, clinical and MRI data – the HD-CSF study. HD-CSF is now a resource available for the HD community and will continue to facilitate biofluid biomarker development for years to come. The hierarchical statistical approach presented here offers a framework for evaluating biofluid biomarkers for HD and the strength of NfL and mHTT sets a benchmark for prospective biomarkers. This methodology may also be applicable to other neurodegenerative diseases.

Each results chapter of this thesis has resulted in a publishable piece of work. Three have already been disseminated in journals including Lancet Neurology and Science Translational Medicine, with one soon to be submitted for publication at the time of completing this thesis. The work has also been presented at several global conferences via platform talks and poster presentations.

I anticipate that NfL and mHTT will act as key surrogate endpoints essential to the design of future prevention trials for HD. Further down the line when disease-modifying therapies are a reality for HD, I believe testing NfL in blood will be integrated into the gold standard of HD clinical management and be used to make decisions on when to initiate treatments in premanifest HD mutation carriers.

Acknowledgements

First and foremost, I thank all the HD patients and family members who selflessly gave their time, their strength and copious amounts of their biofluids. A lumbar puncture is no mean feat and agreeing to multiple, all for the global fight against HD, is extraordinary.

The work in this thesis would not have been possible without the funding from the Medical Research Council which covered the costs of the HD-CSF study and my salary for four years; CHDI who supplied the sample collection kits and electronic data capture portal for HD-CSF as well as the TRACK-HD samples and data used in Chapter 3; Roche for funding the quantification of mHTT used in Chapters 4 and 5; the Huntington's Disease Society of America who are funding the continuation of this work with my postdoctoral fellowship which has supported my salary since July 2019.

To my secondary supervisor, Sarah Tabrizi, thank you for everything that you are, everything that you do and everything you have done for the HD field. You are the reason I came to UCL for my masters, and subsequently this PhD. I am grateful to be a member of the Huntington's disease centre that you have created. I thank Henrik Zetterberg, my other secondary supervisor, whose insights into the field of biofluid biomarker development have been invaluable and whose positivity made every research meeting pure joy.

Much of the work presented in this thesis has arisen from collaboration. I thank all the TRACK-HD investigators for generating such a high quality resource. Thanks to Doug Langbehn for the statistical analysis of this dataset in Chapter 3. I thank Dr Zetterberg's lab in Gothenburg for analysing NfL in these samples and neurogranin in the pilot CSF study. Amanda Heslegrave supplied the protocol for the TREM2 assay and supported me in their lab space at the UK DRI Fluid Biomarker lab. Evotec performed the quantification of mHTT in HD-CSF with the funding from Roche, all of which I am very grateful.

The global HD community is phenomenal. Open, collaborative, passionate and determined. The disease and the families impacted are always at the forefront of every decision. Coming from an HD family myself, I am so overwhelmingly proud to now be a member. I have received so much support over the last 4 years and forged several personal and professional relationships within this wonderful community. Of particular note Emily Machiela – my front-seat rebel conference/drinking buddy; Tamara Maiuri, Rachel Harding and Sarah Hernandez – other aspiring women in the HD field; George Yhorling and the HDSA; Cat Martin and the HD Youth Organisation; and personal heroes to me, Dr Jeff Carroll and Charles Sabine.

To the entire UCL Huntington's disease centre, I thank you for for creating such a supportive and engaging environment: Rachel Scahill, Sarah Gregory, Nicola Robertson, Stef Brown, Gail Owens, Carlos Estevez, Peter McColgan, Davina Hensman, Paul Zeun, Hannah Furby, Kat Schubert, Gill Bates, Joe Hamilton, Emma Bunting, Michael Flower, Christian Landles, and Ed Smith. A special thanks to Eli Johnson and Helen Crawford – for being my research big sisters when first starting my PhD; Marina Papoutsi – for being an excellent Masters supervisor, teaching me good scientific rigour and continuing to be a source of pragmatic advice; James Behagg – for always having the answer to any administrative problem and beyond; Jessica Lowe and Daniela Rae – for their special care at times when I really needed it; Akshay Nair – for being my personal psychiatrist and confidante and helping me get help when I needed it.

Peer support has been essential for managing my emotional and mental well-being throughout these four years. To Heather Ging and Lea R'Bibo who have been there from the beginning. Our wine-fuelled venting was greatly appreciated. To Grace O'Regan and Caroline Casey, I am so glad we grew so close in our last year and could support each other through the lowest points. I am so proud of you all as we each make it over the finish line.

I have had the most amazing support over the years from my friends outside of the UCL PhD bubble. These acknowledgements would not be complete if I did not mention ICGAC. I have shared some of the best moments of my life with the members of that club, not to mention a bottle or two of Bucky! To the old boys who taught us to honour the old ways: Lavery, Finzo, Dunners and a special mention of Dr Frank O'Neill, who has not only helped me have the craic but has helped me academically, from reading over my undergraduate Biology essays to helping me prepare for my PhD viva. To KC, PC, JMF, John McGuckin and all my craic heures. To Ruth Reynolds and Sinead Ward, the triad will live on. In particular, I want to thank from the bottom of my heart, Sinead and my close friend Marlene Osei-Asante, who supported me through one of the biggest challenges in my life and a big step towards being able to begin this PhD – getting tested for Huntington's disease.

Having a stable home environment and caring housemates has been extremely important to me throughout my thesis. Xenia, Uther, Sophie, Andy and Alex – Although we have now moved on to the next phase of our lives the Highgate sticker club will always be fond memories. And to Ruth, my current housemate who and has had to put up with me during these last 6 months of writing up. Thank you for your support and making this time easier.

There are two people I must give tremendous thanks to, for this thesis would not be what it is without them. To my primary supervisor Ed Wild, thank you for your generosity and kindness, all the opportunities you have provided me and for giving me a space where I can speak my mind and (sometimes) disagree with you. To my colleague Filipe Rodrigues, thank you for your constant steadiness, making me a better scientist and your ability to deal with my ever changing mood. I trust you completely and I am so glad to call you both close friends. I hope to always work with you both in some capacity throughout my career.

Last, but in no way least, I want to thank my family who suffer the impact of this disease every day. To the whole extended Byrne family, may we all continue to support each other as this disease enters the next generation. My siblings, Kyle and Jodie, I love you so much and wish I could make it so HD was something you and your growing families never had to worry about in your future. Jodie, you have always pushed me and told me I could do anything I set my mind to. To my mother, Roisin, you have to deal with so much and continue to worry about everyone else over yourself. Thank you for always supporting and loving me through everything I do. I dedicate this thesis in particular to my father, Peter, whose deterioration over these last four years has served as a poignant reminder of where I have come and where I still need to go; what I have gained, and sadly, what I have lost. I will forever and always be a Byrne.

Table of Contents

List of Tables

Lists of Figures

Abbreviations

AD	Alzheimer's disease
ANOVA	Analysis of variance
ASO	Anti-sense Oligonucleotide
AUC	Area under the curve
BEST	Biomarker, EndpointS and other Tools
CAG	Cytosine-adenine-guanine
CAP	CAG Age product
CI	Confidence interval
CNS	Central nervous system
CSF	Cerebrospinal fluid
cUHDRS	Composite Unified HD rating scale
CV	Coefficient of Variance
DBS	Disease burden score
DCS	Diagnostic Confidence Score
EBM	Event-based modelling
ECL	Electrochemiluminescence
ELISA	Enzyme-linked immunosorbent assay
FDA	Food and Drug Administration
HD	Huntington's disease
HPLC	High Performance Liquid Chromatography
HR	hazard ratio
HTT	Huntingtin gene
HTT	Huntingtin protein
ICC	Intraclass correlation coefficient
KA	Kynurenic acid
KP	Kynurenine pathway
LLoQ	Lower limit of quantification
LoD	Limit of detection
mHTT	Mutant huntingtin protein
MRI	Magnetic resonance imaging
MSD	Mesoscale discovery
NfL	Neurofilament light chain
NHNN	National Hospital for Neurology and Neurosurgery
NIH	National Institute of Health
N4PB	Neurology 4-plex B assay

PBAs	Problem Behaviour Assessment – short
PCR	Polymerase Chain reaction
PreHD	Premanifest HD
QA	Quinolinic acid
ROC	Receiver operating characteristic
SD	Standard deviation
SE	Standard Error
Simoa	Single molecule array
SCN	Stroop Colour Naming
SD	Standard deviation
SDMT	Symbol digit modalities test
SMC	Single Molecule Counting
SWR	Stroop Word Reading
TFC	Total Functional Capacity
TIV	Total intracranial volume
TMS	Total Motor Score
TR-FRET	Time-resolved Förster resonance energy transfer
UCL	University College London
UCLH	University College London Hospitals
UHDRS	The Unified Huntington's disease rating scale '99
VFC	Verbal Fluency - Categorical

Chapter 1 Introduction

The introduction provides the background needed to set the context of my work. I reflect on the HD field at the time of beginning my PhD, in particular the state of biofluid biomarkers for HD. Within each data chapter, I provide an introduction that reflects the time when the work was published. Finally, in my discussion chapter, I summarise my findings with respect to developments in the field since the beginning of my PhD, providing my future perspective of biofluid biomarkers for Huntington's Disease.

1.1 Huntington's disease

Huntington's disease (HD) is an adult-onset, dominantly inherited neurodegenerative disease, that currently lacks any therapies capable of slowing or modifying its disease course. The disease progression is slow and relentless, more so than more common neurodegenerative diseases such as Alzheimer's disease (Rodrigues et al., 2017). Life expectancy after the onset of motor symptoms typically spans 15-25 years. There are approximately 12 in 100,000 people suffering from HD in the United Kingdom with many more at risk (Evans et al., 2013). Although a relatively rare disease, it is the one of the most common genetic cause of dementia and offers an excellent model disease to study the earliest signs of neurodegeneration. It is primarily a neurological disease and has historically been treated within the neurology speciality, although is frequently handled within genetics and psychiatric services. However, it is being increasingly recognised that a multidisciplinary approach is required to effectively meet the needs of these patients suffering from a complex combination of symptoms.

1.1.1 Clinical manifestations

Motor

HD was formerly known as Huntington's chorea and these uncontrollable 'dance-like' involuntary movements remain the hallmark of HD. Other common motor signs include irregular eye movements, unsteady balance, dystonia and abnormal gait (Ross et al., 2014). At earlier stages of disease, the hyperkinetic movements are more prominent but at later stages patients begin to suffer from more slowness of movement (bradykinesia) as well as stiffness and rigidity (Dorsey et al., 2013). By the end of the disease, HD patients cannot walk, speak or even swallow and need 24-hour care. The most common causes of death at this stage are pneumonia and heart failure. Juvenile onset HD (when neurological symptoms develop before the age of 21) usually manifests with a hypokinetic phenotypic composed of parkinsonism, dystonia and tremors (Nance and Myers, 2001).

Cognitive

The cognitive disturbances in HD can vary between patients with disturbed cognitive performance often present up to 10 years before the manifestation of motor symptoms (Papoutsi et al., 2014; Ross et al., 2014). Early on patients develop deficits with executive function and working memory, making it very difficult for them to multi-task and manage their job performance. Decision making, disinhibition and ability to rationalise are also disrupted (Craufurd et al., 2001). As the disease progresses they can become increasingly mentally inflexible, with varying severity of perseveration highly common

and a challenging behaviour to deal with for caregivers (Craufurd et al., 2001). Emotion recognition and social cognition are also impacted in HD and this can significantly impact their relationships with family and friends. In the later stages of the disease the cognitive deficits become more generalised leading to widespread affliction of high-level cognitive function (Bates et al., 2014). These symptoms are often underlined by a lack of insight into their own disease or abilities (McCusker and Loy, 2014).

Neuropsychiatric

Most HD patients will suffer from some psychiatric and behavioural disturbances throughout the course of their disease (Craufurd et al., 2001). The most common psychiatric symptoms are low mood, depression, anxiety and apathy (Van Duijn et al., 2014). However, some patients can suffer from symptoms such as psychosis, obsessive compulsive disorder and mania. Psychiatric symptoms are often the most debilitating and cause difficulties for family and caregivers. Treatment for neuropsychiatric features of HD are based mainly on expert opinion and usually managed with anti-depressants or anti-psychotics (Teixeira et al., 2016). Unlike motor and cognitive deficits, neuropsychiatric symptoms lack a clear association with disease progression as they can relapse and remit through the course of disease. The exception to this is apathy which has an association with disease duration (Craufurd et al., 2001).

Diagnosis

The motor symptoms (more specifically chorea) – being the most characteristic and present in most cases of HD – have historically been the main qualification for diagnosis. Clinical diagnosis has classically been defined by the manifestation of unequivocal motor abnormalities that cannot be otherwise explained (Huntington Study Group, 1996; Reilmann et al., 2014). This unsurprisingly complicates the estimation of age of onset as many HD mutation carriers present differently often with the cognitive or behavioural changes manifesting before the motor symptoms. In this thesis, HD mutation carriers who have had a clinical diagnosis are classified as (motor) manifest HD and those who do not have sufficient signs and symptoms to have a clinical diagnosis are premanifest HD (PreHD).

1.1.2 Genetics

HD is a monogenic disorder with a dominant pattern of inheritance. The single mutation causing the disease was discovered in 1993 (The Huntington's Disease Collaborative Research Group, 1993). An expansion of the CAG repeat within exon 1 of the *HTT* gene encodes a mutant form of the huntingtin protein (mHTT) which has a toxic gain of function

with a propensity to misfold and aggregate, ultimately leading to neuronal death (Bates et al., 2014).

The number of CAG repeats has an inverse relationship with the age of onset, with longer repeats tending to cause an earlier onset of disease (Andrew et al., 1993; Langbehn et al., 2010; Snell et al., 1993). Over 40 CAG repeats leads to a fully penetrant disease risk within an average lifespan. With larger CAG repeats (usually greater than 60), HD mutation carriers can manifest symptoms before the age of 21, which is known as Juvenile onset HD (Rubinsztein et al., 1996). Between 36 and 39 inclusive is known as the reduced penetrance range, where individuals may or may not manifest HD symptoms within an average lifespan. Those between 27 and 35 are not at risk of inheriting the disease themselves but do hold a risk of passing a disease causing mutation to their offspring (Nance et al., 1998). This is due to a phenomenon in which the CAG length tends to increase from one generation to the next – known as anticipation – and caused by meiotic instability of this trinucleotide repeat (Duyao et al., 1993). In addition to the meiotic instability that drives generational increases of the inherited CAG repeat length, somatic instability is present with extremely large CAGs found in affected brain regions from HD patients compared to their blood-derived genetic test (Kennedy et al., 2003; Telenius et al., 1994). This may be a driving mechanism of disease progression but currently cannot be assessed *in vivo*.

Despite a strong relationship with CAG repeat length, there is large variability in age of onset of neurologic symptoms for a given length. In the most common pathogenic allele range (40-45 CAGs), there can be 20-40 years difference in the age of onset of individuals with the same CAG length (The U.S.-Venezuela Collaborative et al., 2004). CAG accounts for approximately 67% of the variation in age of onset, suggesting that other factors must influence and modify the HD phenotype (Gusella and MacDonald, 2009). Although these factors could be environmental or even stochastic, genetic modifiers offer the potential of new drug targets that could be uncovered directly in humans using modern genetics. The first well-powered genome-wide association study in HD revealed several hits from genes within DNA repair and handling pathways (Lee et al., 2015).

1.1.3 Pathobiology

Despite many years of research since its discovery, the exact role of huntingtin is still unclear. An intracellular protein, huntingtin is involved in many cellular pathways and has many interactors (Bates et al., 2015). Huntingtin is ubiquitously expressed throughout all cell types which means the effects of mHTT are likely wide and could impact many

systems (Saudou and Humbert, 2016). Knock-out of *HTT* are embryonically lethal, indicating that it is essential for healthy development (Zeitlin et al., 1995). The *HTT* knock-out mice have lethality at embryonic day 7.5 to 8.5, around the very beginning of the development of the nervous system (Liu and Zeitlin, 2017). Further, the expression of *HTT* transcripts is higher within the CNS than peripheral tissues (Saudou and Humbert, 2016). Taken together, this suggests that Huntingtin plays an important role more specifically in neurodevelopment.

Neuropathology

The classification system for staging HD neuropathology was reported back in 1985 which classifies the severity of HD pathology into five grades – 0-4 (Vonsattel et al., 1985). Localised atrophy within the striatum and selective vulnerability of medium spiny neurons (MSNs) are hallmarks of the earliest signs of HD neuropathology (Ferrante et al., 1987; Reiner et al., 1988). HD post-mortem brains show widespread atrophy in both grey and white matter with a 30% mean loss in brain weight (De La Monte et al., 1988). mHTT forms aggregates that are deposited in inclusions within the cytoplasm, nucleus and dystrophic neurites (Davies et al., 1997; DiFiglia et al., 1997).

In addition to degeneration of neurons, there is evidence for neuroinflammation and reactive gliosis, with increases in numbers and activation of astrocytes, microglia and oligodendrocytes (Bates et al., 2014). This is thought to start initially within and around the striatum (Hedreen and Folstein, 1995; Myers et al., 1991) but later present throughout the brain (Sapp et al., 2001; Tai et al., 2007). HLA-DR-positive (reactive) microglia are found within the neostriatum in close proximity to vulnerable MSNs and this pattern appears to be distinct from that in other neurodegenerative diseases (McGeer et al., 1988). Increased binding of a peripheral type benzodiazepine binding sites (PTBBS) ligand – a biochemical change occurring during astrocytosis and microglial activation – in HD brain tissue suggests inflammatory gliosis within in the putamen and frontal cortex (Meßmer and Reynolds, 1998). Furthermore, there is evidence for components within the complement pathway being increased within HD striatal neurons, myelin and astrocytes compared to that from controls, which are thought to be produced locally from reactive microglia (Singhrao et al., 1999).

Prior to the degeneration of MSNs, there is evidence for early synaptic dysfunction including altered transmission/activity and excitability in brains of HD patients and animal models (Smith-Dijak et al., 2019). It has been shown that mHTT impairs processes for synaptic maintenance impacting those physiological events that modulate learning and cognitive flexibility, including the long-term plasticity of the neuron and transmission (Shirasaki et al., 2012; Turrigiano, 2017; Wang et al., 2017; Watt and Desai, 2010). The

earliest occurrence of synaptic alterations is thought to begin at the corticostriatal synapse (Plotkin and Surmeier, 2015; Veldman and Yang, 2018). Using repetitive Transcranial magnetic stimulation of the motor cortex as a proxy for long term depression in corticospinal projections, it was shown in preHD human subjects that there is altered cortical synaptic plasticity and excitability long before onset of overt symptoms (Orth et al., 2010; Schippling et al., 2009). In HD mouse models, similar impaired synaptic plasticity has been demonstrated within the cortex (Cummings et al., 2007, 2006; Dallérac et al., 2011), the striatum (Plotkin et al., 2014; Sepers et al., 2018) and the hippocampus (Kolodziejczyk et al., 2014; Milnerwood et al., 2006). Further alterations in neuronal activity have been reported including the balance between excitation and inhibition of cortical pyramidal neurons (Cummings et al., 2009). Finally, mHTT appears to cause alterations in many neurotransmitters and signalling pathways involved in synaptic transmission including dopamine, glutamate, GABA, adenosine and BDNF (Smith-Dijak et al., 2019).

MRI modalities has permitted the exploration of HD neuropathology *in vivo.* Structural MRI studies have reflected the patterns seen in histopathological studies with earliest changes in striatal volume detected over 10 years from predicted onset (Paulsen et al., 2008; Tabrizi et al., 2009). Longitudinal imaging studies have also highlighted the global atrophy throughout the disease, in particular significant and widespread white-matter loss (Tabrizi et al., 2013, 2012, 2011). A small PET-MRI study in HD patients showed widespread microglial activation with greater activation in the striatal region that correlates with disease severity (Pavese et al., 2006).

1.1.4 Treatment and clinical monitoring

At present, there is no way to reverse or slow the progressively debilitating symptoms of HD. Current treatment methods focus on treating the symptoms. For example, treating the psychiatric disturbances with anti-depressants and anti-psychotics; chorea with Tetrabenazine; sleep with melatonin (McColgan and Tabrizi, 2018). Given the complex clinical features of HD, specialist multidisciplinary care can be beneficial for HD clinical management, incorporating specialist therapies including neuro-physiotherapists (to help support physical well-being as long as possible), speech and language (for difficulties speaking and swallowing), and occupational health (Novak and Tabrizi, 2010). Specialist HD multidisciplinary clinics can be led by healthcare professionals from several disciplines, including neurology, psychiatry and genetics. Clinical rating scales have been developed to classify and monitor patients which are outlined in Chapter 2 (Huntington Study Group, 1996). These are used to characterise the overt motor,

functional, cognitive and neuropsychiatric symptoms and are usually administered by an experienced physician (Ross et al., 2014).

1.1.5 Current therapeutic candidates

As of June 2019, there are 30 clinical trials ongoing for HD – based on those registered on clinicaltrials.gov (Rodrigues et al., 2019a). This includes clinical trials of 16 pharmacological, 8 invasive non-pharmacological, and 6 non-invasive non-pharmacological therapeutic candidates. Of particular excitement are the therapies aimed at targeting huntingtin and lowering its expression. The first huntingtin-lowering therapeutic – an antisense oligonucleotide (ASO) – entered human trials in September 2015 (Rodrigues and Wild, 2017). There are now several huntingtin-lowering candidates at various stages of the therapeutic pipeline (Wild and Tabrizi, 2017).

Over 100 clinical trials have been conducted in Huntington's disease (HD), with a very low success rate (Travessa et al., 2017), and there is only low quality evidence that selected symptomatic interventions have a beneficial effect on HD (Mestre et al., 2009a), while evidence of disease modification has not been reported yet. Two possible explanations exist for this: either the drugs did not work, or they worked and we were unable to detect the benefit in the time period of the clinical trial.

Clinical rating scales have consistently been used as primary end points in interventional studies of HD (Mestre et al., 2009b, 2009c). However, they lack the sensitivity to repeatedly measure changes over 1-2 years due to low signal-to-noise ratio (Mestre et al., 2018b, 2018a; Schobel et al., 2017) and may be partly responsible for the lack of disease-modifying therapies for HD. The low signal-to-noise ratio of rating scales may be driven by the human administration and error making them subject to inter- and intra-rater variability (Winder et al., 2018). They also have floor/ceiling effects due to their inherent purpose, characterising individuals with overt clinical symptoms (Mestre et al., 2018b, 2018a). For these reasons, they might not be the most effective way to measure efficacy of therapeutics for premanifest HD mutation carriers, the group of affected individuals most likely to have the greatest long-term benefit of treatment with a disease modifying therapy.

1.2 The quest for biomarkers

1.2.1 Applications of biomarkers

By definition, a biomarker is an entity that can be objectively quantified to give an indication of natural physiological variation, disease-related processes or in the context of interventional studies, pharmacological response and efficacy (FDA-NIH Biomarker Working Group, 2016). More specifically, they can aid clinical decision making by more accurately defining diagnosis and prognosis, stratifying patients for clinical trials, and if a successful disease modifying therapy is developed, detecting the earliest signs of disease and thus the window of opportunity to begin treatment. They are distinct from clinical outcome assessments which are direct measures of an individual's well-being, function or survival (Califf, 2018). Both may be used as predefined endpoints for clinical trials; however, biomarkers will require extensive validation before they can be used as the primary basis of regulatory approval required to bring a drug to market.

The biomarker subtypes, as outlined by the FDA/NIH developed Biomarker, EndpointS and other Tools (BEST) resource are summarised in Table 1. Each subtype has their own criteria, but a single biomarker could meet the requirements to be used in multiple applications.

If possible, a biomarker should be readily accessible in that it is relatively easy to obtain a measurement and therefore will have the least impact on the patient's well-being to obtain. Most importantly, quantification should be reliable, objective and there must be a strong biological reasoning that it is truly representing a physiological process. The ultimate goal of developing robust biomarkers is to have a fully validated and evaluated tool that could be used as a surrogate endpoint for clinical trials or to inform clinical decision making. To obtain this level of regulatory approval a potential biomarker will need to go through an extensive and formal validation process. Both analytic validation of the technique used to assess the biomarker and the clinical validation of the biomarker itself must be considered. There are guidelines provided by regulatory authorities (EMA, 2008; FDA-NIH Biomarker Working Group, 2016) to streamline this process but no candidate has yet achieved this for HD.

Another important consideration of a candidate biomarker is whether it can be used across disease models and therefore be used as a translational biomarker that could speed up or streamline preclinical therapeutic development.

Table 1 The applications for candidate biomarkers.

Adapted from the FDA-NIH Biomarker Working Group (2016). Examples of what the candidates were for the respective applications for HD in 2016

Application	Definition	Examples in HD
Diagnostic	Able to detect the presence of disease or pathology; it could also sub-characterise an individual within a particular disease	Genetic diagnosis + UHDRS Diagnostic confidence level (The Huntington's Disease Collaborative Research Group, 1993; Huntington Study Group, 1996)
Monitoring	Able to give an indication of disease status over time or to aid clinical decision-making or to provide evidence of drug effect	UHDRS (Huntington Study Group, 1996)
Pharmacodynamic or response	Specifically able to show a biological response to a drug or environmental agent	Could CSF mHTT show response to huntingtin-lowering? (Wild et al, 2015)
Predictive	Able to identify or predict individuals that are more likely to have a favourable or unfavourable effect from exposure to a drug or environmental agent	CAG age Product (CAP) score (Ross et al., 2014)
Prognostic	Able to identify the likelihood of a clinical event, disease recurrence or disease progression	Could genetic modifiers define prognosis in the future? (Lee et al., 2015)
Safety	Able to indicate the likelihood, presence, or extent of toxicity after exposure to a drug or environmental agent	Depends on intervention
Susceptibility/risk	Able to indicate the potential to develop a disease but who does not currently have clinical symptoms	Predictive genetic testing – CAG repeat length in *HTT* gene (The Huntington's Disease Collaborative Research Group, 1993)
Surrogate	An endpoint supported by a strong mechanistic rationale to expect that an effect on the surrogate endpoint would be correlated to clinical benefit endpoint	Could CSF mHTT meet this in the future? (Wild et al, 2015)

1.2.2 Biomarkers for Huntington's disease

There has been extensive work to generate and develop biomarkers of HD disease progression from various domains including clinical, quantitative motor, cognitive, neuroimaging and biofluids (Biglan et al., 2013; Dorsey et al., 2013; Ross et al., 2014; Tabrizi et al., 2013). Rigorous head-to-head comparison of potential candidates in studies such as TRACK-HD has generated much success, particularly in structural imaging modalities such as whole brain and caudate volume, which were some of the earliest measures to become detectably and significantly altered between preHD and healthy controls over a 12-month interval (Tabrizi et al., 2011). Outcome measures with the strongest effect sizes over the 36-months of TRACK-HD have subsequently been incorporated in the assessment battery of current clinical trials in early HD (NCT03761849, 2019; Tabrizi et al., 2019, 2013).

Biofluids

Biofluids are any biological fluids which can be secreted, excreted for collection or obtained through medical procedures such as venepuncture or lumbar puncture. This includes commonly collected fluids for medical monitoring, such as blood or urine, but also other fluids such as Cerebrospinal fluid (CSF), saliva or sweat. The concentrations of molecules that we can measure from these fluids are referred to as biochemical markers and studying them in disease can help inform us about the specific physiology or biological mechanisms of an ongoing pathological process. Many biological molecules can be quantified in biofluids including proteins, RNA and DNA. Which fluid we choose to look at is often governed by two core aspects 1) how accessible the fluid is i.e. how invasive and expensive of a procedure is needed to obtain it, and 2) how likely we are to find disease-relevant alterations in such a fluid.

There are several potential benefits of using biofluids for biomarker development compared to other media. Harnessing well-established molecular biological methodology, highly specific and robust assays can be developed which produce repeatable and objective measurements. For example, antibodies can be raised against a specific antigen of interest with high binding affinity and selectivity over other molecules. With the ability to generate multiplex assays, there is the potential to measure multiple analytes from one sample at the same time. As assay platforms become more high-throughput, bulk processing is becoming increasingly possible with the capability of analysing hundreds of samples in one run. Biofluids can also be collected and stored for years in biobanks, which creates the potential for continued biomarker discovery as technologies advance and methods become more sensitive. Further, biobanking allows baseline and follow-up samples to be analysed together, reducing some artefacts that can otherwise creep in where measurements have to be done in real time, such as rater drift or MRI scanner upgrades. Another highly desirable attribute of a biomarker is its translatability. Many animal models produce the same biofluids as humans which could offer easier translation of biofluid biomarkers across multiple disease models to enhance preclinical therapeutic development.

Biofluid biomarkers for Huntington's disease

This thesis focuses on CSF and blood for biofluid biomarker discovery. CSF is the clear colourless fluid surrounding the spinal cord and brain, and is contained within the central nervous system (CNS). It is relatively more difficult and expensive to obtain than some other biofluids due to the invasive nature of the lumbar puncture procedure. Nevertheless, CSF remains a highly desirable fluid to study disease-related alterations in the CNS, with 20% of its proteins thought to be brain-derived (Reiber, 2003) and a 1.8 fold CSF/blood enrichment for brain-specific proteins (Fang et al., 2009).

CSF biomarker development for HD has been trailing behind that in other neurodegenerative diseases (Andersen et al., 2017; Burchell and Panegyres, 2017; Pawlowski et al., 2017). A need for better diagnostic tools in other diseases, which HD has had since 1993 with the definitive genetic test, may have been a driver. This is evident with a lot of biomarker studies in other neurodegenerative diseases focusing on differential diagnostic markers, in attempts to distinguish between the overlapping phenotypes (Bjerke and Engelborghs, 2018; Ewers et al., 2015; Gmitterová et al., 2018; Magdalinou et al., 2014; Vranová et al., 2014).

Moreover, investigation of CSF in HD has had several shortcomings. Many studies had low sample numbers and therefore lack the power to show results. There has been a lack of consistency in reporting and standardisation of sample collection and processing, including time of day, fasting and the plasticware used (Byrne and Wild, 2016). Different materials used in sample handling can affect protein concentration. Polystyrene and polyethylene tubes have been shown to artefactually diminish CSF levels of amyloid beta compared with polypropylene tubes, through adsorption of the protein to the plastic surface (Lewczuk et al., 2005). Similar effects may well be seen with any other protein; most have not been investigated for such technical effects. Other granular technical considerations such as aliquot size can have a significant effect on the measured levels of proteins (Toombs et al., 2013). Careful planning and due diligence around all aspects of biofluid studies are paramount. In addition to the handling of samples, the controls used in several studies were other patients with other neurological disorders and not matched for age or gender (Enna et al., 1977; Heyes et al., 1992, 1991; Jeitner et al., 2001; Manyam et al., 1990). Finally, there were often loose connections to biological underpinnings of disease, most likely driven by the fact that many CSF studies took place before the discovery of the HD gene itself as depicted in Figure 1 (Byrne and Wild, 2016). In blood and more accessible fluids, even less systematic work has been done.

Despite considerable effort in studying biofluids from HD patients, there has been little success in identifying biochemical markers with a direct connection to relevant features of pathology or clinical severity (Byrne and Wild, 2016; Scahill et al., 2012). In 2018, we extensively reviewed past biofluid biomarker efforts (Rodrigues et al., 2018). Here I will briefly summarise proposed biofluid biomarkers for HD and their state of validation (as of 2016), with a particular focus on CNS-relevant biomarkers likely to be used in current and planned clinical trials.

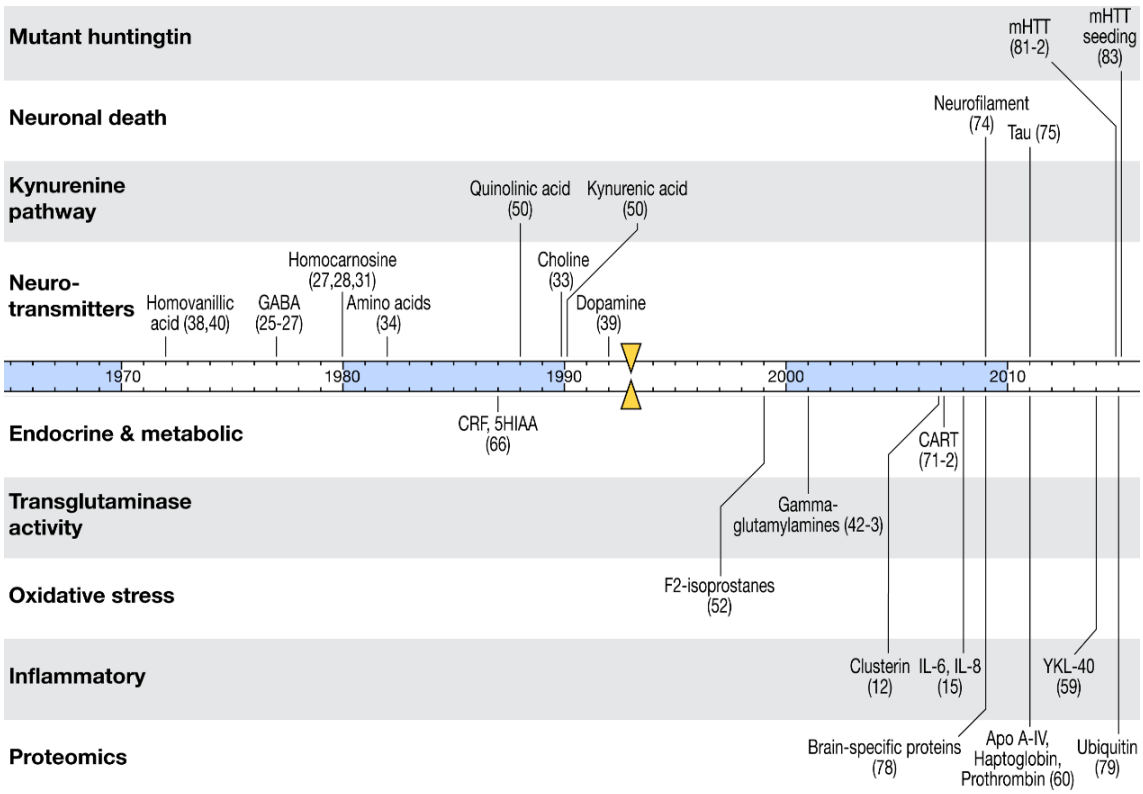

Figure 1 A timeline of CSF biomarker studies in HD from 2016.

This figure was adapted from a review we wrote at the beginning of my PhD (Byrne and Wild, 2016). Substances previously reported to change significantly in HD compared to controls are marked by the year of first published finding. The yellow triangular markers indicate the identification of the HTT gene as the cause of HD in 1993. The numbers in brackets indicate the citations as numbered from the references in the original review.

Huntingtin protein

Understanding the function of the huntingtin protein and its mutant counterpart has been a major focus of HD research since the gene was discovered in 1993. With many approaches aimed at reducing the expression of mHTT, its quantification in CSF has been highly desirable. However, this has proven extremely challenging. With the huntingtin protein (and therefore mHTT) being expressed ubiquitously (Saudou and Humbert, 2016), it is hard to distinguish CNS-derived mHTT from that generated peripherally. mHTT is a large, aggregation-prone intracellular protein, and since HD generally progresses slowly, mHTT would be expected to be released very gradually into the CSF from dying neurons. Consequently, its CSF concentration is certainly extremely low and several generations of improvement in antibodies and mHTT-quantifying assays failed to yield a method sensitive enough to quantify it.

The first detection of mHTT in biofluids was achieved in 2009 by Weiss and colleagues, who quantified soluble mHTT in human whole blood, isolated erythrocytes and buffy coats – the portion of an anticoagulated blood sample that contains the majority leucocytes and platelets following centrifugation – using a highly sensitive time-resolved Förster resonance energy transfer (TR-FRET) assay (Paganetti et al., 2009; Weiss et

al., 2009). The assay relies on a specific antibody pair: 2B7, which binds N-terminal huntingtin; and MW1, which binds to expanded polyglutamine tracts. mHTT in erythrocytes and buffy coats was significantly higher in HD patients (n=5) compared to controls (n=4). The same method was also used to quantify mHTT in isolated monocytes, B cells and T cells in eight preHD mutation carriers, 18 manifest HD and 12 healthy controls, revealing significant differences not only between individuals with and without the HD mutation, but also across the three disease stages (Weiss et al., 2012).

Successful quantification of mHTT in CSF was only achieved in early 2015 (Wild et al., 2015). A single molecule counting (SMC) immunoassay was used with the same 2B7-MW1 antibody combination to quantify mHTT at femtomolar sensitivity. mHTT was significantly higher in manifest HD and preHD compared to controls with a roughly three-fold difference seen between preHD and manifest. mHTT also correlated with clinical phenotype as measured by motor and cognitive scores. These findings were shown in two independent cohorts of 12 participants in London and 40 in Vancouver.

Shortly afterwards, Southwell and colleagues reported mHTT quantification in CSF with immunoprecipitation and flow cytometry (IP-FCM) using a combination of MW1 and HDB4 antibodies, the latter recognizing a C-terminal binding site (Southwell et al., 2015). They confirmed the presence of mHTT in mutation carriers but not controls and a tendency to rise with onset and clinical manifestations. They went on to show that the assay was capable of detecting mHTT in CSF from Hu97/18 mice expressing human mHTT, and that the signal in CSF was correlated significantly with brain mHTT level after intracerebroventricular administration of a huntingtin-lowering antisense oligonucleotide. These findings suggest a likely neuronal origin for mHTT detected in CSF and affirm its promise as a highly pathogenically relevant biomarker for huntingtin-lowering trials.

All forms of mutant huntingtin are not alike, and a means of quantifying the most pathogenic forms in CSF would be valuable. Tan and colleagues developed a cell-based aggregation assay to quantify the proportion of cells with aggregates, and the amount of aggregates in lysate. They demonstrated that seeding of aggregation could be triggered by synthetic polyglutamine oligomers and by CSF from transgenic rats and human HD patients (Tan et al., 2015). The study provides the first evidence that CSF could be used to study not only the quantity of mHTT but its pathogenic properties.

Markers of neuronal damage

Neurodegeneration is readily detectable as an early feature of HD both pathologically (Dunlap, 1927) and non-invasively through neuroimaging (Terrence et al., 1977). However, proteins released by dying neurons that can be quantified in CSF have been studied much more comprehensively in other neurological diseases than in HD. Tau

protein (a component of microtubules) and the light subunit of neurofilament triple protein (NfL, a component of the neuronal cytoskeleton) are reasonably well-established as markers of neuronal death that appear to be widely applicable across neurodegenerative diseases (Blennow et al., 2010). Tau in particular is already in clinical use in the diagnostic process of Alzheimer's disease alongside with levels of beta-amyloid species. NfL has generated excitement in recent years with its strong potential as a diagnostic biomarker for mild traumatic brain injury in high contact sports such as boxing (Neselius et al., 2012) and as an efficacy biomarker for effective treatment of Multiple Sclerosis (Kuhle et al., 2015).

Tau and NfL have both been examined in several HD cohorts. NfL levels were higher in the CSF of 35 HD patients compared to 35 matched controls, and correlated with UHDRS Total Functional Capacity (Constantinescu et al., 2009), a clinical measure of disease progression. The same group measured CSF levels of tau and found a significant elevation in HD, though, due to overlap, tau could not provide categorical distinction between groups and showed no correlations with clinical measures (Constantinescu et al., 2011). Vinther-Jenson and colleagues found no group differences in CSF tau (Vinther-Jensen et al., 2016). However, our own group found higher CSF tau in HD mutation carriers and significant associations with several UHDRS components (Rodrigues et al., 2016a). CSF NfL was reported again to have increased concentrations in HD mutation carriers compared to controls and also to be associated with an estimate for the burden of CAG expansion, CAP score (Vinther-Jensen et al., 2016). As with many initial biomarker findings in HD, these results had yet to be replicated in larger, longitudinal cohorts (as of 2016).

Inflammatory markers

There has been a long line of evidence suggestion the presence of neuroinflammation in HD (See Neuropathology). Over activation of myeloid cells, including microglia, and subtle abnormalities of the innate immune system, are among the earliest biochemical changes that had so far been detected in HD patients (Björkqvist et al., 2008; Dalrymple et al., 2007). Most of this work has been carried out in peripheral blood or ex vivo cells (Träger et al., 2014) but in 2007 Dalrymple and colleagues found that plasma elevations of clusterin were mirrored in CSF from 20 patients and 10 controls (Dalrymple et al., 2007). Their finding of elevated IL-6 and IL-8 in blood plasma was reproduced in patient CSF in 2008 by Björkqvist, *et al* (Björkqvist et al., 2008).

More recently, YKL-40, a member of the glycosyl hydrolase family 18 and thought to be a marker of microglial activation (Aronson et al., 1997) was investigated as a CSF marker in 54 HD mutation carriers (27 manifest and 27 preHD) after reported elevation in other diseases associated with neuroinflammation (Vinther-Jensen et al., 2014). YKL-40 was

noted to increase with age in healthy controls but, after age-correction only a trend of elevated YKL-40 was seen in manifest HD that did not reach statistical significance. However, we found in our own cohort that age-adjusted YKL-40 was elevated in HD mutation carriers and associated with both motor and functional decline (Rodrigues et al., 2016b). In 2016, a compound aimed at modulating microglial activity was being trialled as a novel therapeutic candidate (Legato-HD trial of laquinimod - NCT02215616, 2016). Despite this trial failing to meet its primary endpoint, YKL-40 and other microglial and inflammatory markers remain of interest as potential HD biomarkers. It may be that an emphasis on standardisation of CSF collection and processing methods, to eliminate variation from time of day, medication or diet, can reveal these substances to be useful markers reflecting relevant and tractable disease-related changes in HD.

Similar to other neurodegenerative diseases, there is evidence for increased clusterin levels as well as cytokines IL-6 and IL-8 (Dalrymple et al., 2007). A small sample proteomic study detected significantly higher levels of prothrombin and haptoglobin which are both additional proteins associated with inflammatory response (Huang et al., 2011).

Kynurenine pathway

The NMDA receptor agonist Quinolinic acid (QA), and the concept of excitotoxicity as a contributor to neuropathology, became of interest in HD CSF after it was discovered that direct intra-striatal administration is selectively toxic to medium spiny neurons and produces deficits that mimic some aspects of HD. Before the identification of the causative gene, QA-lesioned rodents were the main experimental model for HD.

QA is a downstream product of the kynurenine pathway, by which the neurotransmitter amino acid tryptophan is degraded in mammals (Vécsei et al., 2013). As well as its possible role in HD neuropathology, affirmed by subsequent work in animal models and human post-mortem samples (Bohár et al., 2015; Sathyasaikumar et al., 2010), the pathway and in particular the enzyme kynurenine mono-oxygenase, is a high-priority target for therapeutic development (Wild and Tabrizi, 2014). Its study in CSF also serves to illustrate the historical shortcomings in the field and the urgent need for greater rigour.

From the observations in animal and human brains, it was initially hypothesised that an increase would be seen in QA in HD patient CSF. However, in one study using a radioenzymatic assay, no significant difference was observed (Schwarcz et al., 1988). This study included just 10 patients and 7 controls and was most likely underpowered to detect an effect, especially given that its controls were patients with schizophrenia and there was no standardisation of dietary conditions (known to affect KP metabolite levels)

or the time of day when samples were collected, and no information recorded about medications or the processing of CSF samples.

In a second study three years later, a similar result was found but this was a faithful replication inasmuch as it suffered the same shortcomings as the original work: small subject numbers (9 patients and 9 'hospital patient' controls), no standardisation of sampling or processing conditions and insufficient information about possible confounds such as medication (Heyes et al., 1991).

In a broad-ranging study in 1992, Heyes and colleagues set out to quantify several KP metabolites in CSF from HD patients and a broad range of other neurological and physical diseases. The total number of subjects was large but the HD sample relatively small and inconsistently reported (the number of patients was reported as both 30 and 13). Using High Performance Liquid Chromatography (HPLC) they found CSF levels of the neuroprotective metabolite kynurenic acid (KA) were lower in HD than in controls, and a similar pattern in Alzheimer's disease; CSF QA was elevated in inflammatory disease but not altered in neurodegenerative diseases. The decreased KA finding echoed an earlier report from 23 HD patients and 50 controls "undergoing myelography or being evaluated for fever or headache" by Beal and colleagues (Heyes et al., 1992).

This cluster of publications on CSF kynurenine pathway metabolites is edifying. There were strong reasons to suspect that relevant, disease-related alterations in metabolites ought to be detectable in CSF; but the only studies available to us were conducted using inconsistent methods over two decades ago – before we could even be certain that the patient volunteers had HD rather than a phenocopy syndrome – and yielded mixed or negative results we cannot interpret because they likely lacked the power to test their hypotheses definitively.

A need for standardisation

The investigators in these early studies established the field using the methods and standards of the day, and it would be unfair to judge them by standards that have changed dramatically in the intervening decades. More recent efforts were still disappointingly limited by basic inconsistencies of methodology and power. The importance and need of prospective study design and rigorous standardisation of data and sample collection was evident. Advanced methodologies for sensitively, accurately and reproducibly quantifying metabolites in biofluids that could be harnessed for biomarker development in HD had just emerged in 2016 (See 2.4.1 Immunoassays).

1.3 The scope of this thesis

1.3.1 The imminent need

The relentless and slow progression of HD is particularly problematic for therapeutic development as it makes quantifying significant clinical decline in the time frame of a clinical trial extremely difficult. As I have already discussed, a further obstacle to clinical trial success is the clinical rating scales which are consistently used as primary end points in interventional studies of HD. Their rater-induced variability and lack of sensitivity means that they would not be suitable for measuring efficacy of therapeutics in premanifest HD mutation carriers for preventative trial designs – the group of affected individuals most likely to have the greatest long term benefit of treatment with a disease modifying therapy.

The need for sensitive, objective and clinically relevant biomarkers is imminent. The first targeted 'huntingtin-lowering' therapy, Ionis-HTTRx (now RG6042 or Tominersen) – an anti-sense oligonucleotide specifically designed to target the root cause of HD, huntingtin itself, and lower its expression – is now (December 2019) in a phase 3 pivotal efficacy trial (NCT03761849, 2019). The results of the phase 1b/2a (NCT02519036) showed remarkable safety and tolerability as well as dose dependent lowering of mHTT in the CNS (Tabrizi et al., 2019). There are several other candidates targeting *HTT* expression via different mechanisms and delivery routes all within various stages of therapeutic development: allele selective ASOs; viral-administrated gene therapies; orally available small molecules etc. (Wild and Tabrizi, 2017). There are more pressing reasons than ever to wish to know what HD-related changes can be found, or what drug-induced changes can be detected. It is therefore crucial that we have a robust toolkit for assessing the therapeutic candidates' ability to slow disease progression. In my thesis work, I set out to advance this tool kit with highly sensitive biofluid biomarkers that have strong biological evidence in connection to the underlying mechanisms of HD pathology. In order to correctly interpret alterations in CSF mHTT in the clinical trial setting and other exploratory biochemical markers in response to a therapeutic, it was essential that the longitudinal dynamics in the natural history of HD must first be determined.

The core challenge was to replicate findings of proposed biofluid biomarkers in larger and well characterised cohorts with standardised longitudinal sampling to ensure high quality measures. HD-CSF was designed with this in mind and has allowed direct comparison of prospective biomarkers with established clinical and structural imaging biomarkers of HD progression. Beyond this thesis, HD-CSF will be a resource for the HD community to facilitate future biofluid biomarker development for HD.

1.3.2 Thesis Aims

1) To establish an 80-participant longitudinal cohort of HD individuals and healthy controls, who have undergone a standardised CSF and blood sampling protocol with matching high quality clinical and MRI data.
2) To investigate mHTT in CSF as a potential target engagement biomarker for future clinical trials.
3) To further explore markers of neurodegeneration, in particular, Neurofilament light chain by using the cohorts available to me, mainly HD-CSF and TRACK-HD.
4) To investigate mHTT and NfL in parallel to compare their properties as HD biomarkers.
5) To characterise the longitudinal dynamics of mHTT and NfL.
6) To investigate other prospective biomarker candidates.

Chapter 2 General Methods

As each results chapter relates to published work, the methods specific to them are set out in that chapter. Here, the general methods used for this thesis are briefly discussed, where a consideration of their general principle may be informative.

2.1 Clinical procedures

All assessments were performed by an experienced rater or clinician.

2.1.1 Genetic testing

Genetic diagnosis was completed for any participant at-risk or with a family history of HD studied in this thesis, including those from an HD family; manifest and premanifest individuals and gene negative family controls (subjects who were at risk of HD but have been confirmed not to have the expanded CAG tract) had a confirmed CAG repeat length. Those participants coming from the National Hospital for Neurology and Neurosurgery had their test performed by the Neurogenetics Laboratory. The method used there is as follows:

- DNA was extracted using an NA3000 automated DNA extractor (AutoGen, MA).
- PCR amplification was performed of the *HTT* CAG repeat region followed by size fractionation and fragment analysis using an Applied Biosystems 3730XL genetic analyser and GeneMapper software (Applied Biosystems, CA).

For participants recruited from outside the National Hospital of Neurology and Neurosurgery, the CAG repeat length was extracted from the information collected with their Enroll-HD data. Healthy controls who had no family history of HD did not undergo genetic testing. More information regarding the HD mutation can be found in 1.1.2 Genetics. Throughout this thesis, CAG repeat length is referred to as CAG.

2.1.2 Clinical rating scales

The Unified Huntington's disease rating scale '99 (UHDRS)

The UHDRS is a collection of rating scales designed and selected to characterise all clinical manifestations of HD (Huntington Study Group, 1996). It encompasses four categories of clinical assessment: motor, cognitive, behavioural and functional. The UHDRS scores used in the current thesis include:

Total Motor Score (TMS)

The TMS is a combined score for all aspects of HD-related motor abnormalities (maximum of 124 points). This incorporates assessment for hyperkinetic disorders (chorea and dystonia), the hypokinetic disorder (bradykinesia) and impairment of voluntary movements.

Diagnostic Confidence Score (DCS)

The DCS is based on a clinical assessment in which a clinician rates how confident they are in classifying the HD mutation carrier as motor manifest HD. This decision is based on the unequivocal presence of motor abnormalities that cannot otherwise be explained (Biglan et al., 2013). The rating is as follows: 0 = normal and 4 = motor abnormalities that are unequivocal signs of HD (≥99% confidence).

Total Functional Capacity (TFC)

The TFC is a combined score assessing the individual's ability to work, complete household finances, perform activities of daily living and whether they can be cared for at home (13 = fully functional and independent; 0 = complete dependence for all care). Clinical staging is based on this score as described in Shoulson and Fahn (1979).

Cognitive assessments

This thesis uses the following tests from the UHDRS to measure each participant's cognitive performance:

Symbol digit modalities test (SDMT)

The SDMT is a 90 second task that involves the participant using a key to replace symbols with corresponding numbers (Smith, 1973). It assesses executive function, working memory and processing speeds of the subject.

Stroop Word Reading (SWR)

The SWR is a simple 1 minute reading task usually performed prior to the Stroop colour naming and Stroop Interference tasks (Scarpina and Tagini, 2017). It assesses reading speed, processing speed and working memory of the subject. The Stroop Interference component is not part of the core assessments completed in Enroll-HD and so was not included in this thesis.

Stroop Colour Naming (SCN)

The SCN is a 45 second task where the participant names the colour in coloured blocks at speed. It assesses processing speed and working memory of a subject using a less automated task (Scarpina and Tagini, 2017).

Verbal Fluency - Categorical (VFC)

For the VFC test, participants are asked to name as many animals as they can in 1 minute. It assesses the subjects' verbal ability and executive control (Shao et al., 2014).

Problem Behaviour Assessment – short (PBAs)

The PBAs was designed by the European Huntington's disease working group specifically to assess and quantify behaviour symptoms in HD. It has 16 components which are scored by frequency within the last month (from 0 - 4, with 0 = never and 4 =

almost always) and severity of the symptoms (from 0 - 4, with 0 = no problem and 4 = having a major impact on the patient, family or carers (Callaghan et al., 2015)). The PBAs was not used as an outcome in this thesis due to its lack of association with disease duration.

Comorbidities

All participants had their medical history taken and were asked about comorbidities. For all subjects in the HD-CSF study, these metrics were recorded within the Enroll-HD electronic data capture as part of their Enroll-HD visit. For the HD-CSF study, participants were also asked and assessed specifically for any comorbidities that might make the lumbar puncture procedure unsafe e.g. a blood clotting disorder. These were exclusion criteria for this study (see the full study protocol in the appendix).

Medications

All medications and non-pharmacological therapies were recorded for all participants.

2.1.3 Estimates for the burden of CAG pathology

Disease burden score (DBS)

The DBS is a measure of the CAG length related burden of pathology, and was first described in (Penney et al., 1997). It is calculated by completing the following equation: [CAG-35.5] x age of participant.

CAG x age product (CAP) score

The CAP score is similar to the DBS score, as CAP score is also a product of age and CAG. It was introduced to be a more neutral term (Ross et al., 2014) – in that it does not oversell the score as a surrogate of disease burden – with the most commonly used version known as the standardised CAP score and calculated by completing the equation: $100 \times$ age of participant $\times [(CAG - L) \div S]$, where S is a normalizing constant estimated by (Langbehn et al., 2004), and L is a scaling constant that anchors CAG length approximately at the lower end of the distribution relevant to HD pathology. This equation was designed so that the CAP score is approximately 100 at the patient's expected onset. L = 30 and S = 627 here are based on the re-estimation from (Langbehn et al., 2004).

2.2 Participant classification

In this thesis, various terminology has been used in the clinical classification of research participants. Presented here is a summary and definition of the terms common to most of the cohorts used:

HD mutation carrier – all individuals who have tested positive for an expanded *HTT* CAG repeat mutation (> 35 CAG) whether or not they have manifested clinical symptoms for HD.

Disease stage – classification of motor manifest individuals (DCS = 4) based on TFC score (Bates et al., 2014; Huntington Study Group, 1996). TFC 11-13 = stage 1; TFC 7-10 = stage 2; TFC 4-6= stage 3; TFC 1-3 = stage 4; TFC 0 = stage 5 (Shoulson and Fahn, 1979).

Premanifest HD (PreHD) – HD mutation carriers (only CAG > 40 were included in the cohorts used in this thesis due to the reduced penetrance for CAGs 36 – 39) without manifest motor abnormalities (DCS < 4).

Manifest HD – HD mutation carriers (CAG > 36) with manifest motor abnormalities (DCS = 4)

Early HD – stage 1 and 2 (i.e. TFC 7-13)

Moderate HD – stage 3

Advanced HD – stage 4

Healthy controls – were either HD family members confirmed to be gene negative (CAG <= 36) or individuals without a family history of HD, usually spouses, who were clinically well with no neurological symptoms and a similar age to HD mutation carriers.

2.3 Patient cohorts

The data and samples used in this thesis have been collected from several patient cohorts outlined below. Figure 2 outlines where samples and data from each cohort have been used in within this thesis. I coordinated HD-CSF which has involved recruiting all 80 participants, managing all study activities, assisting with sample collection and performing the cognitive and behavioural assessments. All cohort studies were performed in accordance with the declaration of Helsinki with all participants providing written informed consent before enrolment.

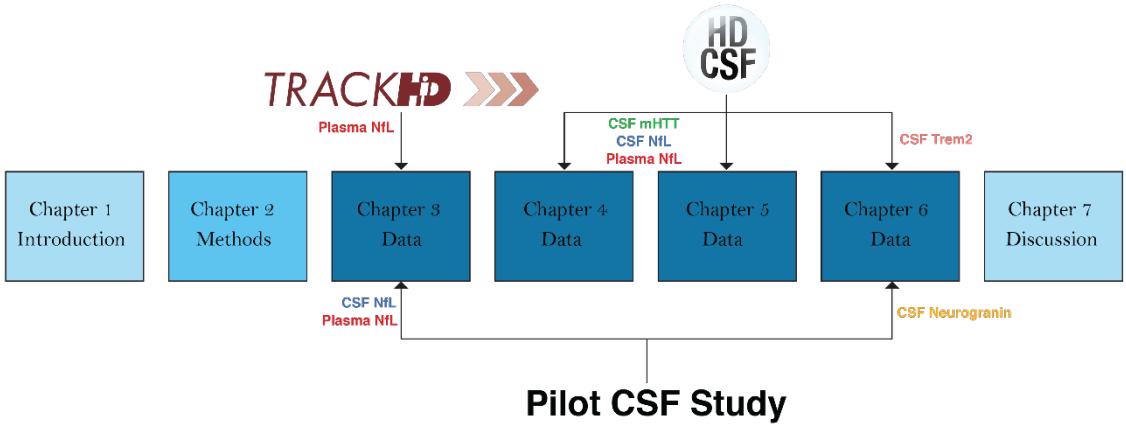

Figure 2 A schematic of how the samples and data from cohorts have been used in this thesis.

Chapters 3 through 6 are the data chapters of this thesis. Arrows designate which cohorts were used for each data chapter. Which biofluid and analyte investigated is also indicated.

HD-CSF

HD-CSF is, to our knowledge, the first longitudinal CSF collection in HD patients who are well characterised phenotypically with matching MRI data. The study was designed with the intention of collecting high quality biofluids and matched clinical and phenotypic data for the development of biomarkers for HD. The primary aim of the study was to quantify mHTT concentration in CSF in order to obtain essential natural history data that could eventually inform huntingtin-lowering clinical trials.

Ethics approval was obtained from the London - Camberwell St Giles Research Ethics Committee. 80 participants (20 healthy controls, 20 preHD and 40 early-moderate HD) were recruited from the NHNN/UCL/UCLH HD Multidisciplinary Clinic and the Enroll-HD study. All participants went through the core Enroll-HD assessments, including the UHDRS TFC, TMS and cognitive battery.

The study design included a screening visit up to 30 days before the sampling visit. This was to ensure that safety assessments could be performed before the lumbar puncture. The safety assessments included a full neurological exam, medical history assessment

for comorbidities and a blood test to check for any clotting abnormalities. Participants with any indication of inflammation or infection were also excluded. If the participant had an Enroll-HD visit within 60 days of the screening visit, then the UHDRS assessments were used from that Enroll-HD visit. Otherwise the UHDRS assessments were completed at the screening visit. Sample collections were completed in a standardized manner. In summary, lumbar punctures were carried out between 9 - 10.30 am post 12 hr fasting, samples were collected on ice and processed within 30 mins of collection using standard kits of polypropylene plasticware. Standardised time of day and fasting was to minimise diurnal and metabolic variation in the proteins measured. The use of polypropylene was to minimise effects of adsorption that could confound concentration of proteins (Perret-Liaudet et al., 2012). The aliquot volume size was also standardised (300uL) to minimise the confounding impact of aliquot storage volume on protein concentration (Toombs et al., 2013). Blood collection was performed within 30 mins of CSF collection using lithium heparin tubes for plasma. Microscopy was used as a quality check (for CSF), cells were removed by centrifugation and the remaining plasma was frozen and stored at −80 °C. As an optional study component, some participants had a repeat sampling visit between four and eight weeks after the main sampling visit. Both the screening visit and the sampling visit were repeated in a 24-month follow-up. Full details of the study procedures as well as the inclusion/exclusion criteria can be found in the study protocol (Appendix).

Pilot CSF study

As a precursor to HD-CSF, a pilot CSF collection was carried out at UCL to obtain preliminary data. Ethics approval was obtained from the Central London Research Ethics Committee. 37 participants (14 healthy controls, 3 preHD and 20 early-moderate HD) were recruited from the NHNN/UCL/UCLH HD Multidisciplinary Clinic between 2013 and 2015. All patients were assessed using the UHDRS. Individuals with infectious, inflammatory, or other concomitant CNS disorders or significant comorbidities were excluded. Sample collection and storage procedures were as described for HD-CSF (with the exception of blood being collected in sodium heparin cell-preparation BD Vacutainer tubes to isolate plasma) and previously published (Wild et al., 2015).

TRACK-HD

TRACK-HD was a four year longitudinal, multi-site, observational study of HD, designed with quality control and assurance similar to that of a clinical trial, to rigorously test head-to-head potential biomarkers of disease progression (Tabrizi et al., 2013, 2012, 2011, 2009). In 2008, 366 participants were enrolled at four study sites (London, Leiden, Paris, and Vancouver). At each of the annual study visits, participants were subject to an extensive battery of assessments, including 3-Tesla T1 volumetric MRI, clinical,

cognitive, quantitative motor, and neuropsychiatric assessments. The full details and protocol were previously published (Tabrizi et al., 2013, 2012, 2011, 2009).

Disease stages 1 and 2 were defined HD1 and HD2 respectively. PreHD had a TMS < 5 and a DBS > 250 to ensure that they were not motor manifest and that they were not so far from onset that disease related changes would be undetectable in the time frame of the study. PreHD participants were split into two sub-groups at the group median of predicted years to onset (10.8) (furthest from, and closest to onset, preHD A and preHD B respectively).

Enroll-HD

Enroll-HD is an ongoing global observational longitudinal study that assesses participants annually. It was set up to not only study the natural history of HD and better understand its progression, but also to be a platform for other HD research and to facilitate recruitment for clinical trials. HD family members including manifest, premanifest, genetically tested or at-risk can take part. Healthy controls (usually spouses or gene-negative siblings) also take part, but can be community controls. All participants are subject to blood donation at their baseline visit in order to confirm their genotype status in the study. Each subsequent visit involves an update of medical history, comorbidities, medication, the core UHDRS assessments and clinical assessment of HD characteristics. As of 17th December 2019, 21,948 people from the HD community are actively participating at 181 sites in 19 countries worldwide. HDClarity is a platform study of Enroll-HD which is a global CSF collection initiative. HD-CSF is a sister study to HDClarity, and uses the same sampling protocol, sampling kits and electronic data capture based in the Enroll-HD electronic portal.

2.4 Biofluid analyte quantification methods

2.4.1 Immunoassays

Immunoassays are techniques used to detect and quantify specific proteins and other macromolecules and can be completed using a variety of formats. They are so named because they use antibodies which are immunologically raised against the protein or molecule of interest. An immunocomplex is formed between the antibody and the protein of interest, which causes it to become isolated. This is usually coupled with fluorescent labelling that can be detected and quantified by various reader technologies.

Enzyme-linked immunosorbent assays (ELISA)

ELISA is the most commonly used immunoassay format and was first described in 1960 (Engvall and Perlmann, 1972, 1971; Yalow and Berson, 1960). ELISA's employ enzymes which generate an observable colour change upon binding the enzyme substrate. This colour change can be detected and quantified by plate readers when a threshold on light detection is set at specific wavelengths. The step-by-step process of an ELISA is summarised in Figure 3A.

Direct ELISAs

Direct ELISAs are the simplest form of an ELISA. This assay involves coating the plate surface with the protein or molecule of interest via adsorption. The enzyme is conjugated to an antibody which is specific to the molecule of interest. Conjugation of the enzyme to the antibody is usually through a chemical linker such as streptavidin-biotin binding. This directly binds the enzyme to the molecule of interest (Figure 3B). The higher the concentration of the molecule of interest, the more binding of enzyme and therefore the greater the colour change and subsequent signal generated.

Indirect ELISAs

Similarly, to direct ELISAs, in indirect ELISAs the molecule of interest can be adsorbed directly onto the plate. However, the enzyme is attached to the immunocomplex *indirectly* via a secondary antibody that recognises the primary antibody bound to the molecule of interest (Figure 3C).

Sandwich ELISAs

The sandwich ELISA format (also known as a 'capture assay') is the gold standard in ELISA formats. It maximises specificity and sensitivity by using two antibodies that bind to the molecule of interest, normally at different epitopes. The plate is coated with a capture antibody which binds to the molecule of interest. The immunocomplex 'sandwich' is complete when a detection antibody (which is conjugated to the enzyme either directly [Figure 3B] or indirectly [Figure 3C]) is bound to the captured molecule of interest.

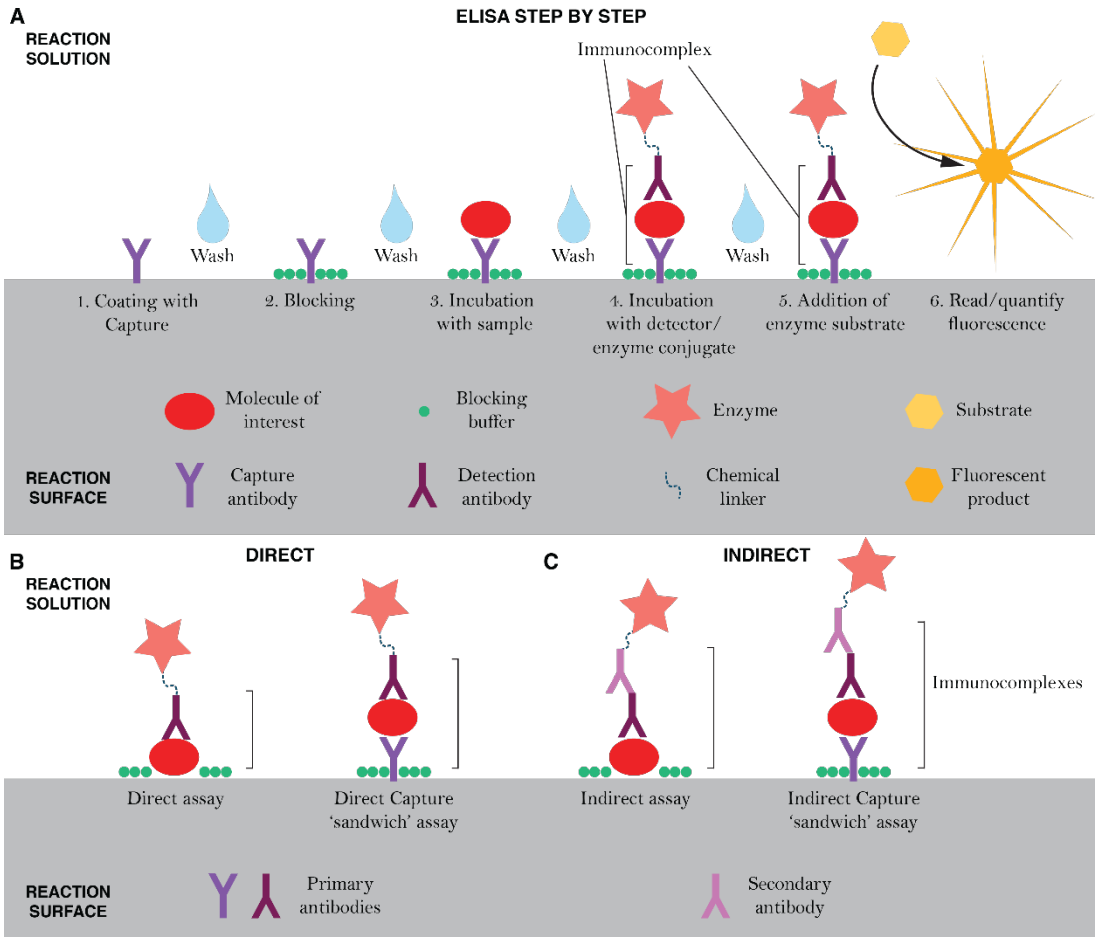

Figure 3 Summary of ELISA methodological steps and types.

A. The classical analytical steps involved in a ELISA include: 1. Coating a surface with the capture antibody (or the molecule of interest if in the direct assay format in B). 2. The blocking step blocks any unbound surface with the blocking buffer to minimise non-specific binding to the surface. 3-4. There are a series of incubations in the order of sample>detector/enzyme conjugate. However, in some formats the sample and detector may be incubated together in the same step and/or the enzyme is added as a separate step. 5. The enzyme substrate is added and the colour change reaction occurs. 6. The amount of colour change or fluorescence is quantified using a plate reader. Each step is separated by a wash step to remove any unbound substances. B. Direct assays have the molecule of interest directly bound with the enzyme (or fluorescent label) via the primary detection antibody. This can also be implemented in the capture 'sandwich' format. C. Indirect assays have the molecule of interest bound indirectly to the enzyme (or fluorescent label) via a secondary antibody which is bound to the primary detection antibody. This can also be implemented in the capture 'sandwich' format.

Electrochemiluminescence (ECL)

ECL utilises electron transfer and the ability of some molecules to emit light when in an excited state. The mesoscale discovery (MSD) immunoassay platform employs this method in their technology. They use specially designed kits with electrodes running along the bottom of each well. The protocol is similar to a sandwich ELISA but replaces the enzyme with a conjugated Sulfo-Tag. The Sulfo-Tag emits light when an electrical current passes through the electrode. This platform was used to quantify TREM2 in Chapter 6.

Ultrasensitive immunoassays

In the last five to ten years, new technologies have emerged with sensitivity ranges that significantly surpass that of the standard ELISA. These advancements have facilitated

the first immunoassay that is sensitive enough to quantify mHTT in CSF (Wild et al., 2015) which was essential to showing target engagement in the first ever HTT-lowering trial. Where the standard ELISA format uses a well plate as the reaction surface, the two leading immunoassay technologies both employ a bead-based approach to reach ultrasensitive detection of proteins (Figure 4):

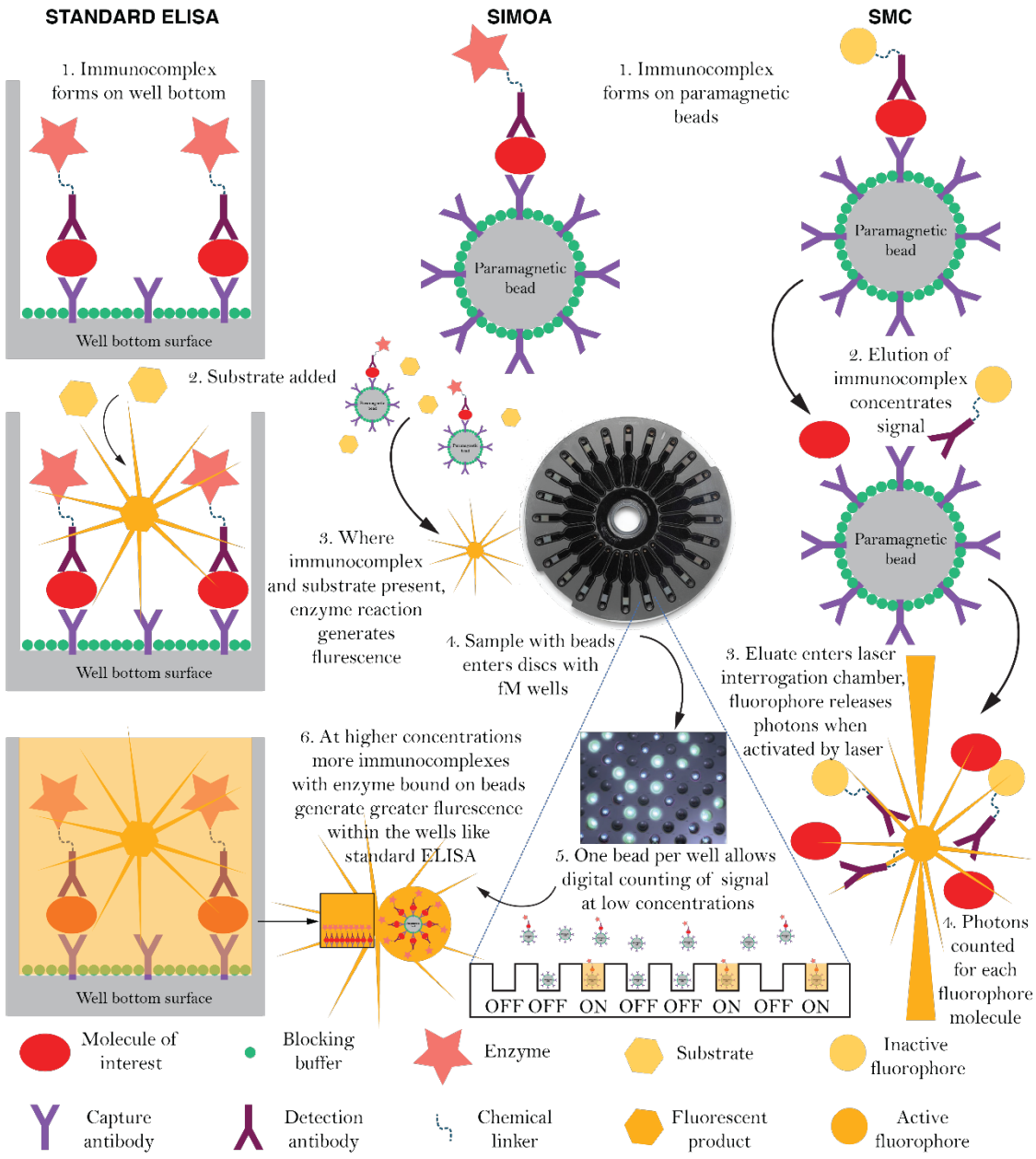

Figure 4 Comparison of ultrasensitive technologies with standard ELISAs

1. The two ultrasensitive technologies, Simoa and SMC, use paramagnetic beads to isolate the immunocomplex instead of the bottom of a well plate like a standard ELISA. However, they differ after this step. Simoa uses an ELISA based set-up: 2. like in the standard ELISA, the enzyme substrate is added to the solution with the immunocomplexes. 3. When the immunocomplex and enzyme are present, the enzyme reaction generates a fluorescent signal. 4. At this point the Simoa process differs from a standard ELISA; the solution containing the bead-bound immunocomplexes is added to special discs which contain femtomolar sized wells. 5. Only one bead can fit per femtomolar well. This allows counting in 'ON/OFF' binary fashion when only some beads have bound immunocomplex at lower concentrations. 6. At higher concentrations, most beads will have multiple bound immunocomplexes i.e. all wells will be 'ON'. The total florescence in the well signal is then read in an analogue fashion to work out a concentration, similar to how the signal is read in a standard ELISA. For SMC: 1. Instead of an enzyme a fluorophore is bound to the immunocomplex. 2. After immunocomplexes are formed on beads, they are eluted from the beads into a smaller volume, concentrating the signal. 3. The eluate is drawn into SMC™ Erenna

via a capillary tube into a very small laser interrogation chamber. 4. Photons of light are generated by single fluorescently labelled molecules and counted as digital events.

Simoa® HD-1 Analyser platform - Quanterix

Single molecule array (Simoa®) technology employs paramagnetic beads which act as the binding surface for the capture antibodies in an ELISA-based format. Simoa® then uses discs containing femtomolar wells that can fit only one bead per well. At low concentrations there will only be one immunocomplex per bead, if any, which allows for extremely sensitive detection. The process is described in Figure 4: the HD-1 Analyser can detect a signal from one immunocomplex which allows for 'digital' detection as the reader can count in an 'ON-OFF' binary fashion. At higher concentrations there will be many immunocomplexes bound to be the beads and therefore captured in the femtomolar wells. This generates greater fluorescent signal per well and triggers the analogue counting phase, facilitating a larger dynamic range to be achieved by this platform.

Single molecule counting (SMC™) Erenna® platform - Singulex

SMC™ Erenna® platform also uses paramagnetic particles to capture the molecule of interest. The process is then similar to that of a sandwich ELISA, except the detector antibody is labelled with a fluorophore rather than an enzyme (Figure 4). SMC™ achieves its sensitivity by eluting the immunocomplex from the beads and concentrating the signal. The eluate containing the fluorophore then enters a laser interrogation chamber where each single fluorophore molecule generates a bursts of light (photon) when it passes through the laser. These bursts are then quantified to calculate a concentration.

2.4.2 Assays used for biofluid analytes investigated in this thesis

All samples were analysed in blinded conditions to disease status. Each analyte was quantified using the same batch of reagents (for measurements in a given cohort). Quantification methods for each analyte are described below:

NfL

In Chapters 3 and 4, the levels of CSF-derived NfL were quantified using the NF-light ELISA according to the manufacturer's instructions (UmanDiagnostics, Umeå, Sweden). In the HD-CSF 24 month follow up Chapter 5, CSF-derived NfL was quantified using the Neurology 4-plex B (N4PB) Simoa® assay which was commercially available from Quanterix. The concentration of NfL derived from plasma was measured with Simoa® technology by either: a Simoa® homebrew method for TRACK-HD and pilot HD-CSF cohorts in Chapter 3 (Rohrer et al., 2016); or the commercially available NF-Light Simoa® kits for the HD-CSF cohort at baseline in Chapter 4, as per the manufacturer's

instructions (Quanterix, Lexington, MA, USA); or the N4PB Simoa® assay which was commercially available from Quanterix for the HD-CSF 24-month follow-up in Chapter 5.

mHTT

CSF levels of mHTT included in Chapter 4 and 5 were quantified using the SMC™ Erenna® platform (Singulex) at a clinical research facility (Evotec, A.G), using a protocol as previously described (Wild et al., 2015)). The assay has been extensively validated by Fodale and colleagues (Fodale et al., 2017) who found that the signal generated by the assay was dependent on HTT fragment size and polyglutamine length of the protein, as well as concentration. It is currently used in all huntingtin-lowering programs to assess the pharmacodynamics of the molecule (NCT02519036, 2015; NCT03225833, 2017; NCT03761849, 2019; NCT04120493, 2019).

Neurogranin

Neurogranin was quantified for Chapter 6 using an in-house ELISA at the Zetterberg lab in Gothenburg, as previously published (Wellington et al., 2016).

TREM2

Concentrations of TREM2 were quantified on the Meso Scale Discovery SECTOR Imager 2400, using an adapted protocol from Kleinberger et al., (2014). Further details can be found in Chapter 6.

Haemoglobin

To determine CSF contamination by blood and haemolysis, haemoglobin concentration was assessed using multi-wavelength spectrophotometric readings.

2.5 Statistical approach

Here the general statistical framework used in this thesis is outlined. Any study specific approaches are discussed in detail in the relevant chapters. Any statistical analysis not performed by myself is so stated in the contributions section of the relevant chapters. Results throughout this thesis are defined as statistically significant with a threshold level of $p < 0.05$. Analyses performed by the author were with Stata version 14 software (StataCorp, College Station, Texas, USA).

2.5.1 Data collection and management

The data collection and management of the HD-CSF study involved collecting information directly from patients and generating source data (stored in hospital notes and research study folders), as well as logging data into an electronic data capture form (set up for the HDClarity study within the Enroll-HD study platform). This data was then extracted to Excel and/or Stata spreadsheets. MRI analysis and biofluid analyte data was generated separately to clinical data and then collated after quality control.

The other cohorts used for Chapters 3 and 6, TRACK-HD and the pilot CSF study, were retrospective analyses where datasets had already been collected by the team or shared with us through collaboration. The NfL data for these studies was generated retrospectively and collated with the previously collected phenotypic data after quality control.

2.5.2 Study power

HD-CSF was designed by Dr Wild as part of his MRC Clinical Scientist Fellowship. The sample number per disease group was chosen based on a power calculation for detecting group differences in mHTT. This power calculation was performed using CSF mHTT values (quantified using the same SMC™ method) from the 12-subject pilot CSF study data used in the first publication of the mHTT assay (Wild et al., 2015). Detecting cross-sectional differences between control and HD (90% power at 5% significance) requires very small numbers. For sample size estimations for longitudinal change, annualised change in mHTT was estimated using imputed data from the cross-sectional data, extrapolating from the number of years typically from stage 1 to stage 2 HD. The 20 subjects per group gives >90% power to detect predicted longitudinal change in CSF mHTT over two years.

NfL had been previously shown to be increased in HD patient CSF in two cohorts (Constantinescu et al., 2009; Vinther-Jensen et al., 2016), both of which had smaller participant numbers than HD-CSF. TRACK-HD was one of the largest collections of high quality blood plasma and imaging data and was therefore adequately powered to distinguish whether or not NfL concentrations were also increased in blood plasma of HD patients. There was no previously reported data on CSF concentration of TREM2 or neurogranin in HD patients, therefore we performed power calculations to ensure we had the power to show negative results after completing the study.

2.5.3 Team Wild statistical pipeline for assessing biomarkers

In Team Wild, we aim to standardise and pre-specify methods across different analytes; we seek to minimise the effect of confounding variables; we use methods appropriate to the distribution of the data; and we seek to identify biology-related patterns using a hierarchical approach to minimise multiple comparisons. To achieve this, we have developed a general stepwise order of analysis when assessing a new potential biomarker for HD.

Before running analyses

Assessing for normality

It is generally best practise to use parametric tests where possible for several reasons: they have more statistical power; they allow for covariate adjustment; and the equivalent non-parametric tests are not comparable. Distributions of all analytes of interest were tested for normality (visually and statistical assessment of kurtosis and skew) and transformed where appropriate. For the pilot CSF study, which had a small sample number (and therefore would be difficult to reliably make assumptions on the normality of data), either non-parametric tests or 1000 rep bootstrapping with parametric tests were employed instead of transformation.

Assessing for potential confounding variables

The influence of potential confounders was considered at two levels:

1. The recruitment of participants for HD-CSF and TRACK-HD were so performed to ensure balanced groups for demographics such as age and gender. Controls were balanced for age against the combined HD mutation carrier group.
2. Demographic variables were investigated for a confounding effect on the analytes in healthy controls.

3. Other variables based on the literature would also be assessed for a confounding effect e.g. blood contamination of CSF that would impact the signal for mHTT.

Any variables found to have significant association with the analyte, or had any other justifiable reasoning, were included as covariates in subsequent analyses to control for this effect.

A priori analysis plan

To reduce multiplicity and avoid false positive results, we always pre-specified the main analysis in a hypothesis driven manner based on the current literature. With new analytes we followed a stepwise approach in which the next analysis phase would only be performed following significant findings. Anything outside the *a priori* plan was considered exploratory or a secondary analysis.

Stepwise analysis

Cross-sectional

1. Control vs HD mutation carriers - unpaired two-tailed t-test or Wilcoxon log-rank test was used to test two-group comparisons.
2. Groupwise differences - Intergroup differences were assessed using one-way ANOVA or kruskal-wallis tests or multiple regressions (to adjust for covariates) with post-hoc pairwise wald tests.
3. Associations with other scores for clinical severity (most robust measures based on the literature) - motor, functional, cognitive and brain volume, Pearson's and partial correlations were used.

Secondary analyses:

1. Relationship with age and CAG – analyses were repeated to include age and CAG or some function of their terms as covariates. This was used to assess a biomarkers' association with clinical outcomes independent to the best known predictors of HD progression.
2. Stability over a short time period – if a biomarker is to be using in the clinical setting we must first characterise the natural fluctuations within an individual over a short time period.
3. Discriminatory ability – using receiver operator characteristic curves, we can assess, an analytes ability to distinguish between two disease groups and compare against other disease groups.
4. Power calculations – if unsure about whether a study is sufficiently powered to show a result, we perform power calculations retrospectively on the data.

5. Sample size calculations – to inform clinical trial design, we can estimate the number of subjects required per arm needed to show altering of biomarkers at various effect sizes.

Longitudinal

Using longitudinal data from multiple time points allows us to further explore the dynamics of these biomarker throughout HD progression. We can perform a number of investigations to characterise this:

1. Assessment of analyte trajectories over time, including group-wise differences in trajectories and rates of change –
    a. Generalised mixed effects models were generated separately for defined disease groups to incorporate repeated measures; the biofluid analyte as the dependent variable; fixed effects applied for age (and CAG in HD mutation carriers); random intercept per participant and random slope for age were also applied.
    b. Rates of change in the analytes for each disease group can then by estimated from these mixed effects models
2. Repeated measures can be used to increase power for assessing cross-sectional associations –
    a. Mixed effects models incorporating matched analyte and outcome data from multiple visits including random intercept for participant effect.
3. Comparison of the prognostic ability of a single baseline measurement versus the rate of change in analyte –
    a. Annualised rate of change in clinical and imaging outcomes were computed by follow-up value minus baseline value divided by the time interval in years
    b. Baseline analyte values or annualised rate of change in analytes were then compared with annualised rate of change in outcomes using partial correlations and/or mixed effects models.

Outliers

In the presence of outliers or a participant who could influence the analysis, we ran a sensitivity analysis and repeated the tests excluding those data points.

Multiple comparisons

For multiple group comparisons, bonferroni correction was included throughout the thesis. If a different approach was used, it is stated and justified within the relevant results chapter.

Chapter 3 Neurofilament light protein in blood as a potential biomarker of neurodegeneration in Huntington's disease: a retrospective cohort analysis

This chapter is based on data previously published in the Lancet Neurology, of which I was first author (Byrne et al., 2017). For the first time, we reported neurofilament light protein in blood and its potential prognostic biomarker for HD.

3.1 Introduction

A key pathological feature of HD is the slow yet relentless increase in neuronal dysfunction and subsequent death, beginning predominately with medium spiny neurons in the striatum, then progressing to a more widespread global atrophy (1.1.3 Neuropathology). Given its position as a core disease process in HD, proteins related to neuronal damage serve as a compelling target for robust biomarkers of HD progression. As mentioned in 1.1.3 Neuropathology, the success achieved in neuroimaging measures of brain atrophy provides further reasoning for developing biochemical markers of neuronal damage, with the evidence suggesting that these neuronal alterations precede manifestation of clinical symptoms (Paulsen et al., 2008; Tabrizi et al., 2009). Moreover, in 1.2.2 Biofluids, I outlined the rationale for biofluid biomarkers over neuroimaging biomarkers. Biochemical measures of neuronal integrity would likely fluctuate with the current state of neuronal health and may not be constrained by the historical damage that has already occurred like structural neuronal loss quantified in MRI. For this reason, biochemical markers could provide a more efficient measure of drug-induced neuronal protection and a cheaper alternative to neuroimaging measures.

The best candidates we currently have for biochemical biomarkers of neuronal damage in HD were in fact appropriated from the extensive biofluid biomarker research in other neurodegenerative diseases (Pawlowski et al., 2017). As discussed in 1.2.2 Markers of neuronal damage, probably most notable and a major focus of this current thesis is neurofilament light protein (NfL). Neurofilaments are major components of the cytoskeleton in neurons and are essential for maintaining the axonal caliber. NfL is the smallest of three subunits and is released from what are believed to be damaged or dying neurons. Cerebrospinal fluid (CSF) levels of NfL are higher in several neurodegenerative diseases, such as Alzheimer's disease, amyotrophic lateral sclerosis (Rosengren et al., 1996), and frontotemporal dementia (Rosengren et al., 1996; Waldö et al., 2013). NfL has also been shown to be higher in the CSF of HD patients in several different cohorts (Constantinescu et al., 2009; Niemelä et al., 2017; Vinther-Jensen et al., 2016; Wild et al., 2015).

In theory, CSF – being enriched for brain-derived proteins (Reiber, 2003) – offers vast potential of uncovering biofluid biomarkers of neuronal damage (1.2.2 Biofluids). However, measuring a molecule that is indicative of relevant HD-related CNS pathology in a more accessible fluid, such as blood, is a highly desirable alternative. A cross-sectional study has shown levels of mHTT in blood leucocytes to be associated with clinical severity (Weiss et al., 2012), but a peripheral measurement of mHTT – which is ubiquitously expressed – is unlikely to be directly related to CNS pathology (1.2.2

Huntingtin protein). Markers of peripheral pathology therefore would not be suitable for assessing therapeutics delivered directly into the CNS, like the current HTT-lowering candidates (Wild and Tabrizi, 2017).

With the advancement in ultrasensitive immunoassay technology (2.4.1 Ultrasensitive immunoassays), it is now possible to detect NfL in blood, equally in both serum and plasma (Keshavan et al., 2018; Kuhle et al., 2016). Increased blood levels of NfL have been shown cross-sectionally in Alzheimer's disease, amyotrophic lateral sclerosis (Gaiottino et al., 2013) frontotemporal dementia (Rohrer et al., 2016), and atypical parkinsonism (Hansson et al., 2017), and longitudinally in amyotrophic lateral sclerosis (Lu et al., 2015), progressive supranuclear palsy (Rojas et al., 2016) and frontotemporal dementia (Meeter et al., 2016; Steinacker et al., 2017).

The cohorts studied previously (before the publication on which this chapter is based) have been genetically and pathologically heterogeneous and one study involving presymptomatic individuals used small numbers of individuals with different genotypes (Meeter et al., 2016). TRACK-HD followed HD mutation carriers over three years at different stages of disease, including preHD, and matched healthy controls (2.3 TRACK-HD). It was a multi-site observational study designed with rigorous quality control, comparable to that in clinical trials. They tested head-to-head an extensive battery of potential HD biomarkers from a range of domains including clinical scales, 3T MRI modalities, quantitative motor and cognitive tools, and blood sampling. This genetically uniform disease cohort facilitates the study of neurodegeneration in the premanifest phase of individuals with the same core pathology and identifying patterns in disease progression.

Before the work from this chapter was published, there had been no previous study in HD patients reporting NfL levels in blood. We investigated plasma NfL as a potential prognostic marker of neurodegeneration and disease progression for HD.

3.2 Aim

The primary questions we aimed to answer were 1) Are plasma NfL concentrations raised in Huntington's disease and do they increase with disease stage? 2) Is there a relationship between plasma NfL levels in preHD individuals and subsequent disease onset? 3) Do NfL levels in plasma correlate with established measures of subsequent disease progression, in particular, brain atrophy? 4) Are CSF and plasma levels of NfL associated with each other, thus supporting a predominantly CNS origin of plasma NfL?

3.3 Methods

3.3.1 TRACK-HD cohort

Using samples and data from the TRACK-HD study we performed a retrospective analysis of 298 participants who had available plasma samples at baseline and at a follow-up visit (see 2.3 TRACK-HD). Participant classification was based on TFC in manifest HD patients and DBS in preHD. Disease stages 1 (TFC 11-13) and 2 (TFC 7-10) were defined HD1 and HD2 respectively. PreHD had a TMS < 5 and a DBS > 250 to ensure no motor abnormalities were present and that they were not so far from onset that disease related changes would be undetectable within the time frame of the study. PreHD participants were split into two sub groups at the group median of predicted years to onset (10.8) (furthest from and closest to onset preHD A and preHD B respectively).

BD Vacutainer tubes with EDTA (Franklin Lakes, NJ, USA.) were used to collect blood at each visit. Sample processing to isolate plasma was as described previously (Borowsky et al., 2013) and samples were frozen then stored at −80°C. Full study details were previously described (Tabrizi et al., 2013, 2012, 2011, 2009).

To minimise the number of statistical comparisons, the most robust predictors of HD progression [based on their effect sizes from TRACK-HD (Tabrizi et al., 2013, 2012, 2011, 2009)] were chosen *a priori* as outcomes of interest and included: volumetric imaging measures – whole-brain, grey and white matter, ventricular, caudate and putamen volume; cognitive measures – SDMT and SWR; and clinical measures – UHDRS TMS and TFC.

3.3.2 MRI Processing

T1 volumetric MRI scans went through extensive quality control and a blinded analysis by specialist image analysts using standardised and rigorously optimised techniques. Briefly, cross-sectional putamen volumes were calculated by automated segmentation; whole-brain, caudate, lateral ventricles, and total intracranial volumes by semi-automated segmentation; and grey-matter and white-matter volumes by voxel-based morphometry. The boundary shift integral technique was used to calculate longitudinal changes in whole-brain, ventricles, and caudate, and voxel compression mapping within voxel-based morphometry segmentations to assess changes in grey-matter and white-matter volume. All cross-sectional imaging measures were calculated as a percentage of total intracranial volume.

3.3.3 Pilot CSF study

The Pilot CSF samples and data was used to assess the origin of NfL and confirm that plasma NfL was reflective of neuronal pathology. The details of this collection are outlined in 2.3 Pilot CSF study.

3.3.4 NfL quantification

The quantification of NfL was performed externally in Henrik Zetterberg's lab in University of Gothenburg. CSF levels of NfL were quantified using the NF-light ELISA according to the manufacturer's instructions (UmanDiagnostics, Umeå, Sweden). Plasma NfL concentration was measured with ultrasensitive single-molecule array (Simoa) technology by an in-house homebrew method (Rohrer et al., 2016) (Quanterix, Lexington, MA, USA). All NfL values were within the linear ranges of the assays.

3.3.5 Statistical analysis

For TRACK-HD data analysis, an a priori statistical analysis plan was designed jointly by myself, Ed Wild and Doug Langbehn, and executed by Doug Langbehn who was the statistician involved in the core TRACK-HD publications, using SAS (v9.4, SAS Institute Inc, Cary, NC, USA) using SAS/STAT 14.1. The analysis was finalised and interpreted jointly.

A natural log-transformation of NfL concentrations in plasma was used to normalise the distribution of values for all analyses. NfL had no association with sex and study site, thus, they were not used as covariates. Based on other HD phenomena and their significant association with the higher order terms, a polynomial model of age and CAG (most commonly reported predictors of HD progression) was used to adjust their interacting effects (Table 2).

Cross-sectional analysis: Group comparisons at baseline were measured using ANOVA. Scatter plots were outcomes of interest matched to plasma concentrations of NfL for the corresponding study visit. Linear models including random slope for participant effect were used to assess cross-sectional associations incorporating individuals' baseline and follow-up measurements. For simplicity, cross-sectional associations with NfL are described with Pearson's correlations between NfL concentrations and matched outcomes. However, all p values were derived from analogous random effects repeated measurement models, which allow proper inference but lack unambiguously defined corresponding correlation statistics.

Longitudinal analysis: for scatter plots, differences in outcome variables between baseline and follow-up were converted to annualised rates and plotted against baseline plasma NfL. Longitudinal changes in NfL concentrations were assessed with correlated

random intercept and slope models. Similar to cross-sectional analyses, longitudinal associations were described with Pearson's correlations between baseline NfL concentrations and the annualised rates of change in other outcomes. All p values were derived from the analogous random effects repeated measurement models. Longitudinal analyses of TFC changes only included manifest HD subjects due to negligible change in preHD individuals (i.e. ceiling effect).

To calculate hazard ratios (HRs), Cox proportional hazard survival modelling was used with 95% CIs for the correlation between baseline NfL concentration and subsequent onset of HD within 3 years in preHD individuals. The number of confirmed new diagnoses was too small (n=18) to include multiple covariates simultaneously, but their pattern was consistent with the proportional odds assumption. Thus, other known risk factors previously identified in the TRACK-HD data were controlled separately to assess non-redundancy of NfL concentrations as a risk factor.

The data from the pilot CSF study were analysed by the author. Due to the small size of the cohort, the data was analysed without transforming the data. Instead 1000 rep bootstrapping was used to run parametric tests. PreHD and manifest HD subjects were pooled into one HD group for this analysis. Wilcoxon rank sum tests were used for group comparisons. Bootstrapped Pearson's correlation was used to assess association between CSF and plasma NfL.

Table 2 Relationships between plasma NfL, age and CAG repeat.

A. Relationship between plasma NfL (log), age and HTT CAG repeat count in HD mutation carriers, examined using a polynomial function allowing for interactions with these predictors, their squares and all potential interactions. Age was centred at 50 years; CAG count at 42. DF, 198 degrees of freedom. B. Relationship between plasma NfL (log) and age in controls, 96 residual degrees of freedom. The relationship is essentially linear. (The non-significant Age^2 term is retained for consistency with the above model for participants with HTT CAG expansion.)

A)

Effect	Estimate	Standard Error	t Value	P value
Intercept	3·8007	0·03814	99·65	<.0001
Age	0·03408	0·003735	9·12	<.0001
CAG	0·1866	0·02227	8·38	<.0001
Age × CAG	-0·00456	0·002469	-1·85	0·0661
Age^2	-0·00106	0·00036	-2·95	0·0036
CAG^2	-0·02331	0·006174	-3·78	0·0002
Age^2 × CAG	-0·00026	0·000105	-2·47	0·0143
Age × CAG^2	-0·00091	0·000279	-3·24	0·0014

B)

Effect	Estimate	Standard Error	t Value	P value
Intercept	2·7463	0·05044	54·45	<.0001
Age	0·02061	0·004162	4·95	<.0001
Age^2	0·000066	0·000333	0·2	0·8435

3.4 Results

3.4.1 NfL levels increase with HD disease severity

Baseline and follow-up plasma samples were available from 298 out of 366 TRACK-HD participants who completed the 3-year TRACK-HD study. 293 had paired plasma samples from the 3-year follow-up visit, four from the 2-year visit, and one from the 1-year visit. Table 3 outlines the demographic and clinical characteristics of TRACK-HD participants at baseline.

Plasma NfL concentrations and selected biomarker measures at the study baseline are presented by disease group in Table 4. Raw plasma NfL concentrations at baseline were 2.6 times higher in HD mutation carriers than in controls (mean 3.63 [SD 0.54] log pg/mL vs 2.68 [0.52] log pg/mL, p<0.00001). At baseline, plasma NfL levels were significantly elevated in all HD subgroups than those in controls and raised with advancing disease stage, with the exception of stage 2 (HD 2) versus stage 1 (HD 1) (Figure 5 and Table 5). However, the HD 2 subgroup had significantly higher NfL than PreHD A (early) (mean difference 0.785 [SE 0.113], p<0.0001) and PreHD B (late) (0.348 [0.102], p=0.0017).

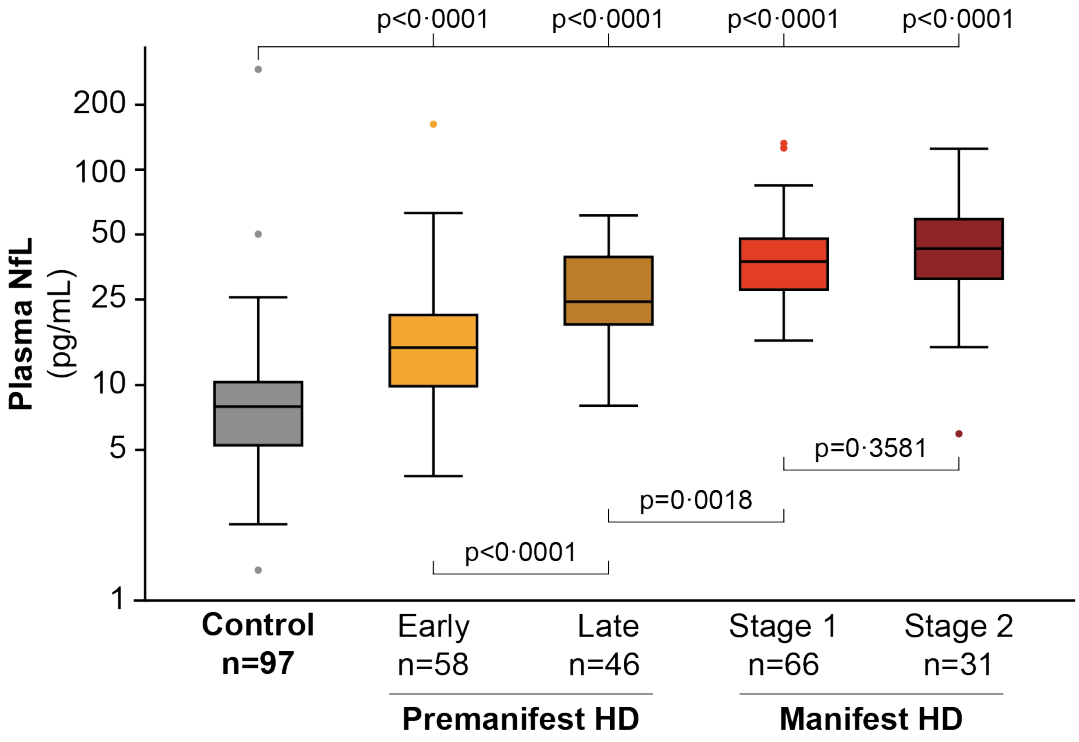

Figure 5 Associations between plasma NfL and disease stage.

In 201 HD mutation carriers and 97 controls we present baseline plasma NfL levels by disease stage. Boxes show first and third quartiles, the central band shows the median, and the whiskers show data within 1·5 IQR of the median. The dots represent outliers. Data were log transformed for comparisons.

Table 3 Baseline characteristics of each cohort.

A. TRACK-HD cohort. **B.** Pilot CSF cohort. Values are mean ± SD. CAP, standardised CAG-age product score; 5yr onset prob, conditional probability of onset within 5 years (Langbehn et al, Am J Hum Genet 2009: 135B, 397-408). Disease duration is based on a rater's estimation of disease onset. Disease duration was available for 90 of the TRACK-HD manifest HD subjects. *pooled HD group includes 3 preHD for CSF and 2 preHD for plasma.

	A. TRACK-HD cohort					B. Pilot CSF cohort			
Group	**Control**	**preHD A**	**preHD B**	**HD 1**	**HD 2**	**Control**		**HD***	
n	97	58	46	66	31	14	(13 plasma)	23	(17 plasma)
		104		97					
Age	46·08 ± 9·91	41·22 ± 8·52	40·68 ± 8·94	47·70 ± 10·32	51·29 ± 8·23	43·52 ± 13·17		50·11 ± 11·28	
Sex (M:F)	41:56	26:32	22:24	27:39	17:14	04:10		10:13	
CAG	N/A	42·14 ± 1·84	44·17 ± 2·39	43·62 ± 3·37	43·55 ± 2·46	N/A		43·6 ± 2·43	
TMS	1·51 ± 1·63	2·19 ± 1·42	2·96 ± 1·89	19·33 ± 9·28	30·29 ± 9·82	N/A		28·65 ± 22·11	
TFC	12·99 ± 0·10	12·90 ± 0·41	12·76 ± 0·78	12·27 ± 0·85	8·74 ± 1·06	13 ± 0		10·04 ± 3·04	
CAP	N/A	77·62 ± 7·88	88·93 ± 6·75	99·26 ± 12·67	108·54 ± 12·41	N/A		106·15 ± 19·20	
5yr onset prob	N/A	0·14 ± 0·061	0·32 ± 0·085	0·44 ± 0·16	0·53 ± 0·15	N/A		N/A	
Disease duration	N/A	N/A	N/A	5·53 ± 6·68	8·74 ± 4·68	N/A		N/A	

Table 4 Baseline measures in the TRACK-HD cohort.

NfL, clinical and imaging measure values by subgroup. Values are mean ± SD.

	Control	**preHD A**	**preHD B**	**HD 1**	**HD 2**
n	97	58	46	66	31
Plasma NfL	18·11 ± 25·61	28·36 ± 22·24	39·39 ± 14·19	52·18 ± 20·52	57·48 ± 23·82
log plasma NfL	2·68 ± 0·52	3·17 ± 0·56	3·61 ± 0·37	3·89 ± 0·35	3·96 ± 0·48
SDMT	53·54 ± 8·99	52·83 ± 9·69	49·8 ± 11·36	37·35 ± 9·14	31·00 ± 9·42
SWR	107·07 ± 16·29	102·19 ± 15·43	96·70 ± 17·55	84·56 ± 15·01	70·19 ± 19·87
Whole-brain	81·30 ± 3·61	80·57 ± 3·63	78·54 ± 4·41	76·19 ± 4·57	71·69 ± 3·94
Caudate	0·55 ± 0·058	0·48 ± 0·066	0·45 ± 0·073	0·38 ± 0·076	0·33 ± 0·06
Putamen	0·70 ± 0·075	0·62 ± 0·10	7·42 ± 1·15	0·46 ± 0·93	0·43 ± 0·055
Grey matter	46·36 ± 3·61	46·1 ± 2·92	669·29 ± 77·01	42·98 ± 3·39	40·69 ± 3·74
White matter	32·94 ± 1·88	32·47 ± 1·53	31·08 ± 1·83	30·14 ± 2·14	28·78 ± 2·22
Ventricles	1·12 ± 0·65	1·11 ± 0·53	1·26 ± 0·59	1·77 ± 0·84	2·36 ± 1·25

Table 5 Plasma NfL group comparisons with confidence intervals and effect sizes.

Effect size is least square mean difference scaled by residual standard deviation in the underlying ANOVA model. CAP score, normalised CAG-age product score.

Group 1	**Group 2**	**Difference Between Means**	**95% Confidence Limits**		**Effect Size**	**P-value**
Control	**preHD A**	-0·49	-0·644	-0·336	2·21	<0·0001
Control	**preHD B**	-0·928	-1·094	-0·762	4·18	<0·0001
Control	**HD 1**	-1·213	-1·36	-1·065	5·46	<0·0001
Control	**HD 2**	-1·276	-1·467	-1·084	5·75	<0·0001
preHD A	**preHD B**	-0·438	-0·621	-0·255	1·97	<0·0001
preHD A	**HD 1**	-0·722	-0·889	-0·556	3·25	<0·0001
preHD A	**HD 2**	-0·785	-0·992	-0·579	3·54	<0·0001
preHD B	**HD 1**	-0·285	-0·463	-0·106	1·28	<0·0001
preHD B	**HD 2**	-0·348	-0·563	-0·132	1·57	0·0007
HD 1	**HD 2**	-0·063	-0·265	0·139	0·28	0·5115

3.4.2 A CAG-dependent genetic dose-response relationship

Plasma NfL concentrations were positively associated with age in controls and all HD subgroups. In HD mutation carriers, NfL levels had a significant positive association with CAG-age product and disease burden score, estimates for the degree of exposure to the expanded CAG and its toxicity (Table 6 and Figure 6A), but a CAG-dependent quadratic function of age model best characterised the non-linear relationship of NfL with age and CAG (Table 2). There is a distinct a CAG-dependent genetic dose response relationship evident when we consider each CAG separately (Figure 6B, Figure 7). Overall plasma NfL increased with CAG for a given age. The higher the CAG, the earlier the age for increasing plasma NfL levels and the steeper the initial slope which eventually levelled out at older ages. Thus, maximum predicted NfL concentrations became similar. In contrast, the association between plasma NfL and age in controls – who lack the expanded CAG – was approximately linear (slope 0.02 log pg/mL per year [SE 0.0042], p<0.0001; Figure 6B; Figure 7).

Table 6 Plasma NfL associations with CAP score and 5-year conditional onset probability.

	n	Pearson r	p-value
CAP score	201	0·589	<0·0001
5yr onset prob	201	0·589	<0·0001

3.4.3 NfL is cross-sectionally associated with outcomes of interest

In HD mutation carriers, cross-sectional plasma NfL concentrations showed negative associations with cognitive measures and with the MRI volumetrics for putamen, caudate, and grey and white matter remaining significant after controlling for the combined effects of age and CAG (Figure 8, Table 7). The negative association of whole-brain volume, did not remain significant after adjustment. TMS and lateral ventricle volume had significant positive associations with plasma NfL persisting after adjustment for age and CAG (Figure 8, Table 7).

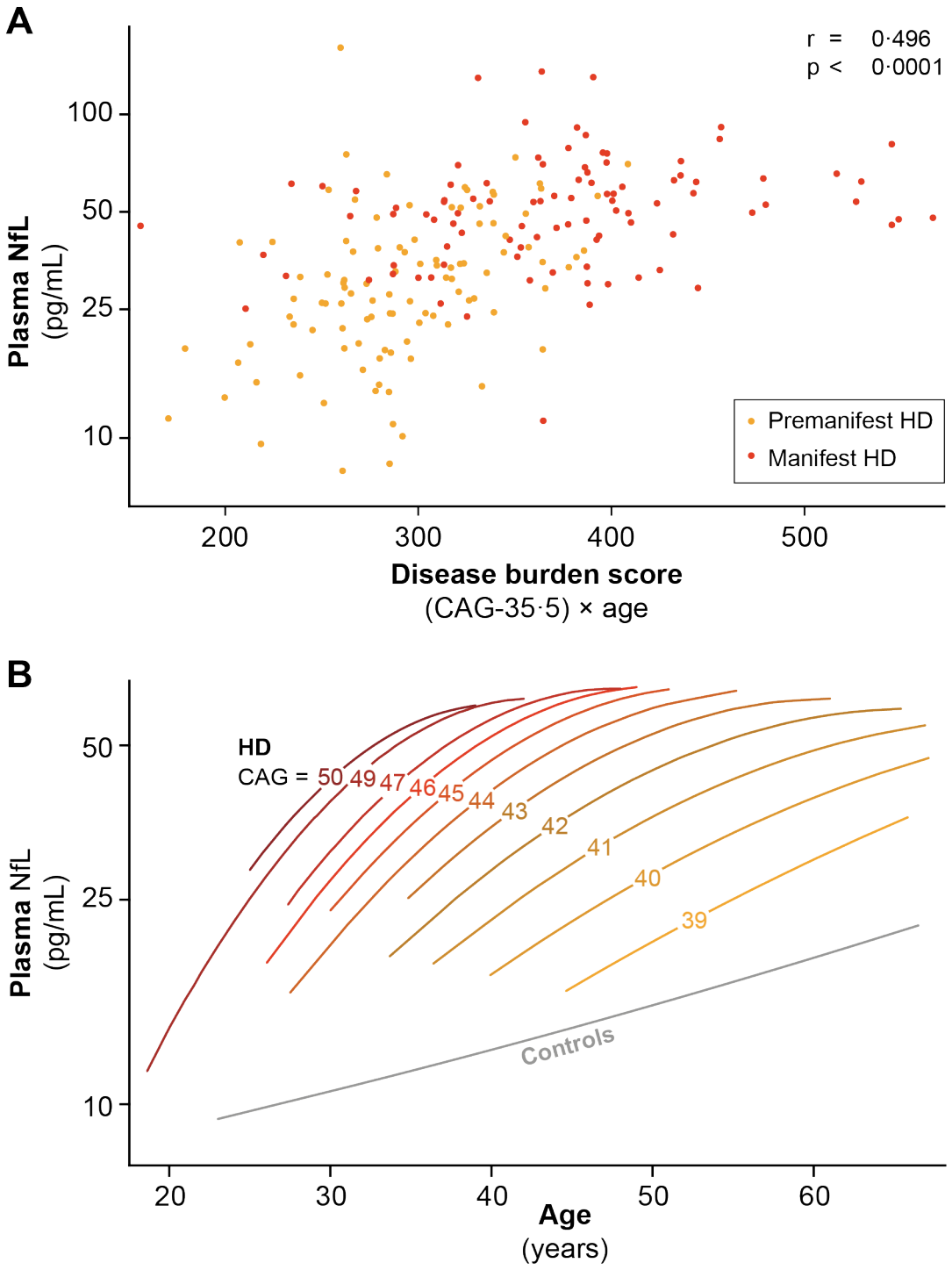

Figure 6 Relationship between plasma NfL, age and CAG.

A. NfL and 'disease burden score' in 201 HD mutation carriers. The 'disease burden score' of Penney et al. (Ann Neurol 1997; 41(5):689-92) is an estimate of an individual's lifetime exposure to mutant huntingtin based on age and CAG repeat length. Given by DBS = (CAG − 35.5) × age, it is closely related to the normalised CAG-age product score which standardises such that a score of 100 represents the predicted age of onset from the conditional probability model of Langbehn et al. (Clin Genet 2004; 65(4):267-77). B. its association with age and CAG, modelled with a polynomial function of age, CAG, their squares, and their interactions. The lines show quadratic fit for all participants with a given CAG repeat count or all controls. Each increase in CAG was associated with higher and more steeply rising plasma NfL levels. Predicted values are truncated at the vertical inflection point of the parabola. Data points for each individual CAG repeat count and for controls are provided in Figure 7. HD=HD mutation carriers. Log transformed plasma NfL data presented.

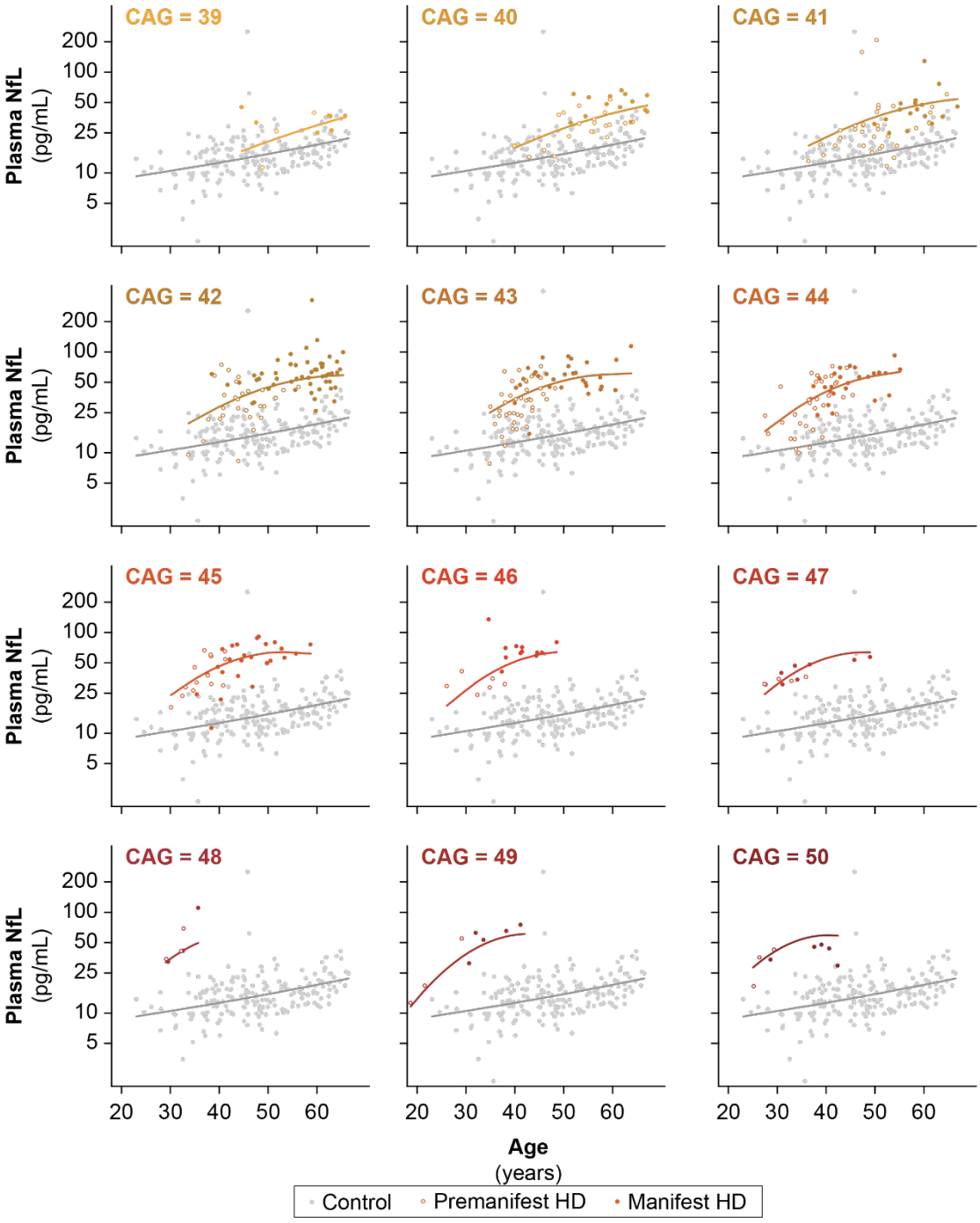

Figure 7 Relationship between plasma NfL and age for each individual.

CAG repeat count and controls, modelled as per Figure 6B.

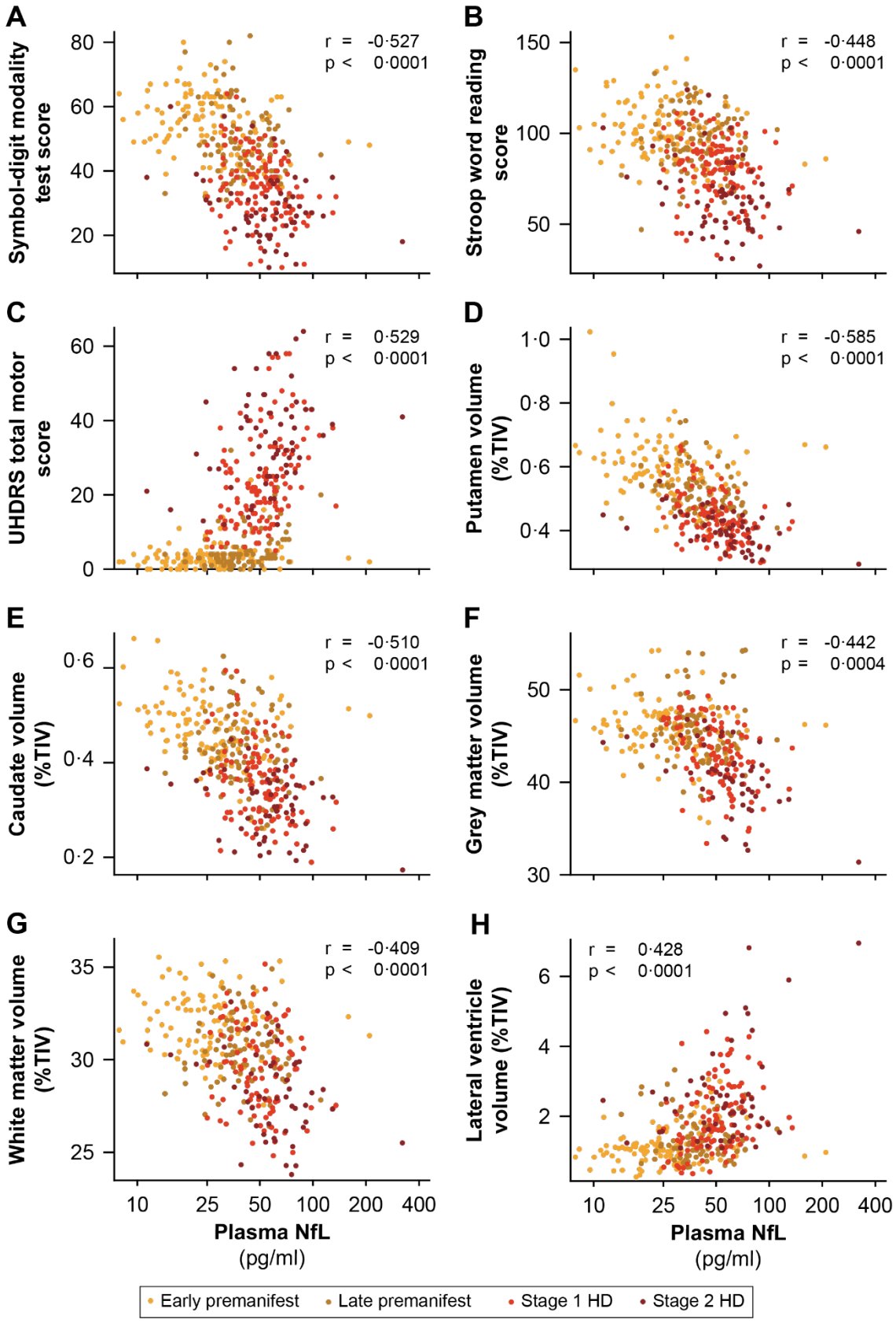

Figure 8 Baseline plasma NfL cross-sectional associations with outcome measures of interest.

A, B. Association with cognitive scores. C. Association with motor function. D–H. Associations with global and regional brain volumes, expressed as percentages of total intracranial volume. Log transformed plasma NfL data presented. Unadjusted Pearson's r presented with p-values derived from random effects repeated measures models as shown in Table 7. Includes both measures from each participant.

Table 7 Plasma NfL cross-sectional associations with outcome measures.

Adjusted values are adjusted for age and CAG and their interactions. The associations are described with Pearson's correlations, however, p values were derived from analogous random effects repeated measurement models to incorporate both measurements from baseline and follow-up for each participant. TMS, total motor score; TFC, total functional capacity; SDMT, Symbol digit modalities test; SWR, stroop word reading. Brain volumes were percentage of total intracranial volume.

Cross-sectional	Unadjusted		Adjusted	
	Pearson's r	P-value	Pearson's r	P-value
TMS	0.529	<0.0001	0.246	<0.0001
TFC	-0.360	<0.0001	-0.213	0.0219
SDMT	-0.527	<0.0001	-0.293	<0.0001
SWR	-0.448	<0.0001	-0.239	0.0042
Whole-brain	-0.447	<0.0001	-0·120	0·1500
Caudate	-0.510	<0.0001	-0.187	0.0170
Putamen	-0.585	<0.0001	-0.286	<0.0001
Grey matter	-0.442	0.0004	-0·198	0.0004
White matter	-0.409	<0.0001	-0·121	0.0480
Ventricles	0.428	<0.0001	0·260	<0.0001

3.4.4 NfL concentrations increase over time in HD mutation carriers

There was a significant increase from baseline in plasma NfL concentrations by 0.060 log pg/mL per year (SE 0.012, p<0.0001) in PreHD, and by 0.026 log pg/mL per year (0.0129, p=0.0442) in manifest HD. The change in controls was not significant (0.018 log pg/mL per year [0.0128], p=0.171). PreHD had a higher rate of increase than controls (0.043 log pg/mL per year [0.018], p=0.0161) but did not differ significantly than manifest HD (0.034 log pg/mL per year [0.018], p=0.0547). The rate of increase in manifest HD and controls did not differ (0.009 log pg/mL per year [0.018], p=0.630). A greater increase in preHD conforms to the non-linear relationship observed between levels of NfL with age, and CAG.

3.4.5 Baseline plasma NfL is associated with disease onset

Out of 104 individuals who were preHD at baseline, 18 progressed or 'pheno-converted' to manifest HD during the course of the study. Baseline plasma NfL concentration was significantly associated with subsequent disease onset (HR 3.29 per 1.0 log pg/mL, 95% CI 1.48-7.34, p=0.0036; Figure 9A), even after adjustment for age and CAG (3.03 per 1.0 log pg/mL, 1.07-8.60, p=0.0371) and separate adjustment for each baseline brain volume measure (Table 8), all previously reported predictors of onset (Long et al., 2017a). The highest mean sensitivity and specificity for risk of diagnosis within 3 years were when NfL concentration was 3.61 log pg/mL at baseline, as shown in the receiver operating characteristic curve (Figure 10), which is similar to the baseline median value for preHD participants of 3.69 log pg/mL. When splitting the preHD group by their median

baseline NfL levels, those with lower baseline NfL were more likely to remain premanifest (Figure 9B, Table 8B).

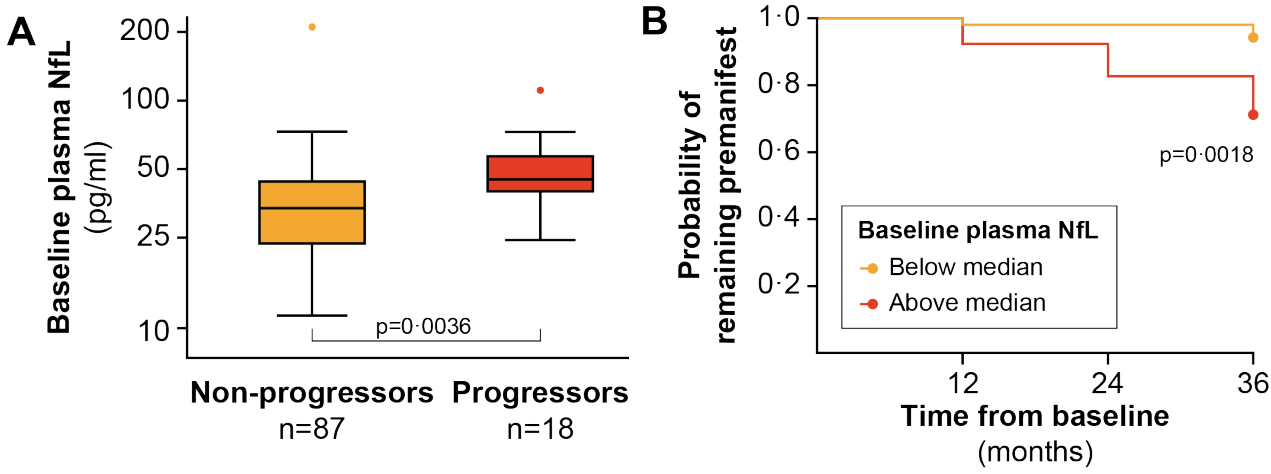

Figure 9 Baseline plasma NfL associations with progression to manifest Huntington's disease.

A. Baseline plasma NfL concentration in individuals who were preHD at baseline by diagnosis status at 3 years. P-value generated from Cox proportional hazard survival modelling B. Kaplan-Meier plot showing longitudinal survival in the premanifest phase among HD mutation carriers with baseline plasma NfL levels above or below the median. The Cox proportional hazards model is the more sensitive of the two models presented here. See Table 8.

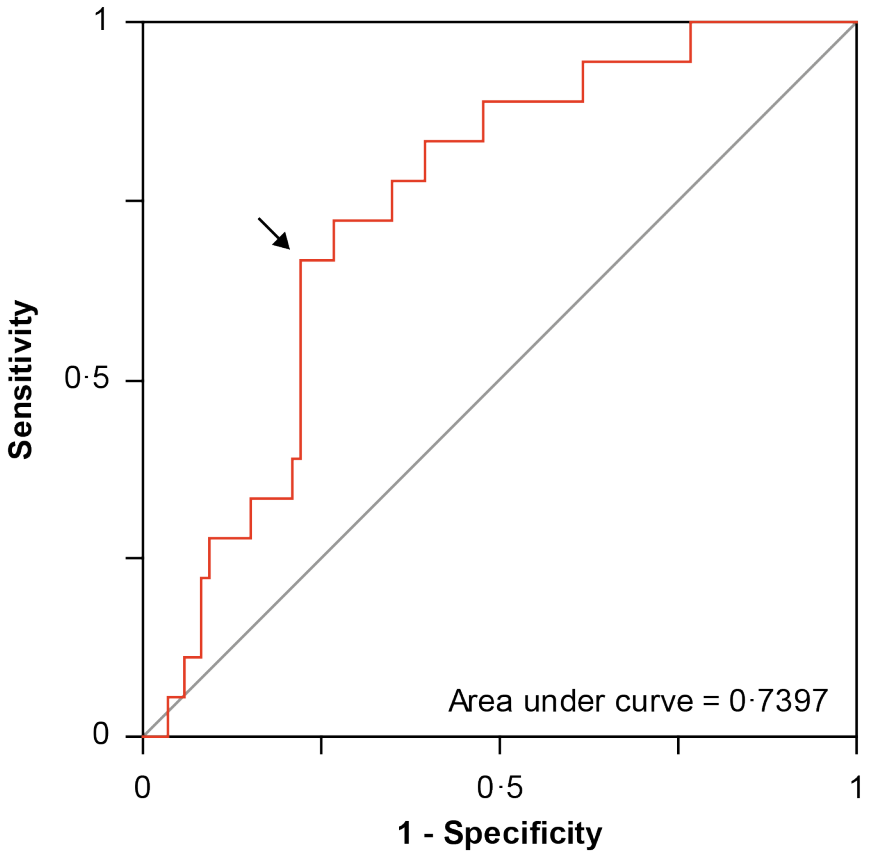

Figure 10 Receiver operating characteristic (ROC) curve showing diagnosis risk within 36 months in the premanifest cohort.

The point of highest mean sensitivity (0·667) and specificity (0·779), indicated by arrow, was at plasma NfL=3·61 log[pg/ml], close to the premanifest HD median value of 3·69.

Table 8 A. Further detail of survival analysis in premanifest cohort.

B. Tests of equality in the survival analysis using log-rank and Wilcoxon tests. P values given are asymptotic approximations. An exact permutation method for real-valued log-rank scores (exactRankTests v0.8-29 package for R v3.3.3), gave a 2-sided p value of 0.00247. C. Log hazard ratio for the prediction of new diagnosis as a function of log plasma NfL concentrations after controlling for other known predictors. Analysis was done in the group that was premanifest at baseline. Due to the limited number of new diagnoses (18 over 36 months), covariate adjustments were controlled one at a time, except for age, CAG length, and their interaction. The log NfL hazard ratio is little changed by additional of any of these covariates, suggesting that NfL is a risk predictor that is not redundant with other known predictors. (a)For context, the standard deviation of log NfL concentration in at-risk preHD subjects was 0·39 log(pg/ml).

A	Time (yrs)	Survival	Failure	Survival SE	Failed	Remaining	95% CI	
	NfL above median							
	0	1.000	0.000	0	0	52	_	_
	1	0.923	0.077	0.037	4	48	0.851	0.996
	2	0.827	0.173	0.0525	9	43	0.724	0.930
	3	0.712	0.289	0.0628	15	37	0.588	0.835
	NfL below median							
	Time (yrs)	**Survival**	**Failure**	**Survival SE**	**Failed**	**Remaining**	**95% CI**	
	0	1.000	0.000	0	0	52	_	_
	1	0.981	0.019	0.019	1	51	0.944	0.999
	3	0.942	0.058	0.0323	3	49	0.879	0.999

B	Test	Chi-Square	P value
	Log-Rank	9.720	0.0018
	Wilcoxon	9.721	0.0018

C	Covariate controlled	NfL log Hazard Ratio per log(pg/ml)[a]	Standard error	p-value
	None	1·192	0·409	0·0036
	Age, CAG, Age × CAG	1·109	0·532	0·0371
	Caudate volume	1·084	0·451	0·0162
	Putamen volume	1·213	0·548	0·0269
	Whole-brain volume	1·060	0·436	0·0151
	Ventricular volume	1·119	0·435	0·0101
	White-matter volume	1·052	0·453	0·0201
	Grey-matter volume	1·092	0·455	0·0163
	UHDRS Total Motor Score	0·866	0·451	0·0549
	Speeded tapping mean inter-tap time (nondominant hand)	1·318	0·406	0·0011
	Symbol-digit modality test	0·923	0·449	0·0398
	Indirect circle tracing time	1·512	0·471	0·0013
	Paced tapping at 3 Hz (inverse standard deviation)	0·990	0·472	0·0358
	Spot-the-Change	1·152	0·445	0·0096

3.4.6 Baseline NfL has independent prognostic value

Plasma NfL concentrations at baseline were associated with cognitive and functional decline over three years (Figure 11, Table 9) but only SDMT remained significant after adjustment for age and CAG. There were strong positive associations, after age and CAG adjustment, with atrophy of the caudate, whole-brain, grey and white matter and with ventricular expansion (Figure 11, Table 9). Change in motor score was not significantly associated with levels of NfL at baseline. Associations withstanding adjustment for age and CAG suggests that NfL in plasma has independent prognostic

value for HD progression. To further explore the independent prognostic value of plasma NfL we additionally controlled for diagnostic status with age and CAG while assessing baseline plasma NfL and its association with atrophy. The associations with more global atrophy measures of whole-brain, grey matter and white matter and ventricular expansion remained significant, independently from diagnostic status. When preHD and manifest HD were considered separately, independent associations for change in whole-brain, grey matter and ventricular volume were significantly stronger in manifest HD than preHD (Table 10).

Table 9 Baseline plasma NfL longitudinal associations with outcome measures.

Adjusted values are adjusted for age and CAG and their interactions. The associations are described with Pearson's correlations between baseline plasma NfL values and the annualised rate of change in the outcome measures, however, p values were derived from analogous random effects repeated measurement models. TMS, total motor score; TFC, total functional capacity; SDMT, Symbol digit modalities test; SWR, stroop word reading. Brain volumes were percentage of total intracranial volume.

Longitudinal	**Unadjusted**		**Adjusted**	
	Pearson's r	**P-value**	**Pearson's r**	**P-value**
TMS	0.112	0.0592	0.076	0.3704
TFC	-0.289	0.0264	-0.151	0.1107
SDMT	-0.374	<0.0001	-0·173	0.0010
SWR	-0.248	0.0033	-0·040	0.4057
Whole-brain	0.602	<0.0001	0.320	<0.0001
Caudate	0.178	0.0087	0.199	0.0043
Putamen	-0.029	0.7602	-0.064	0.8854
Grey matter	0.518	<0.0001	0.242	0.0190
White matter	0.588	<0.0001	0.327	<0.0001
Ventricles	-0.589	<0.0001	-0.323	0.0002

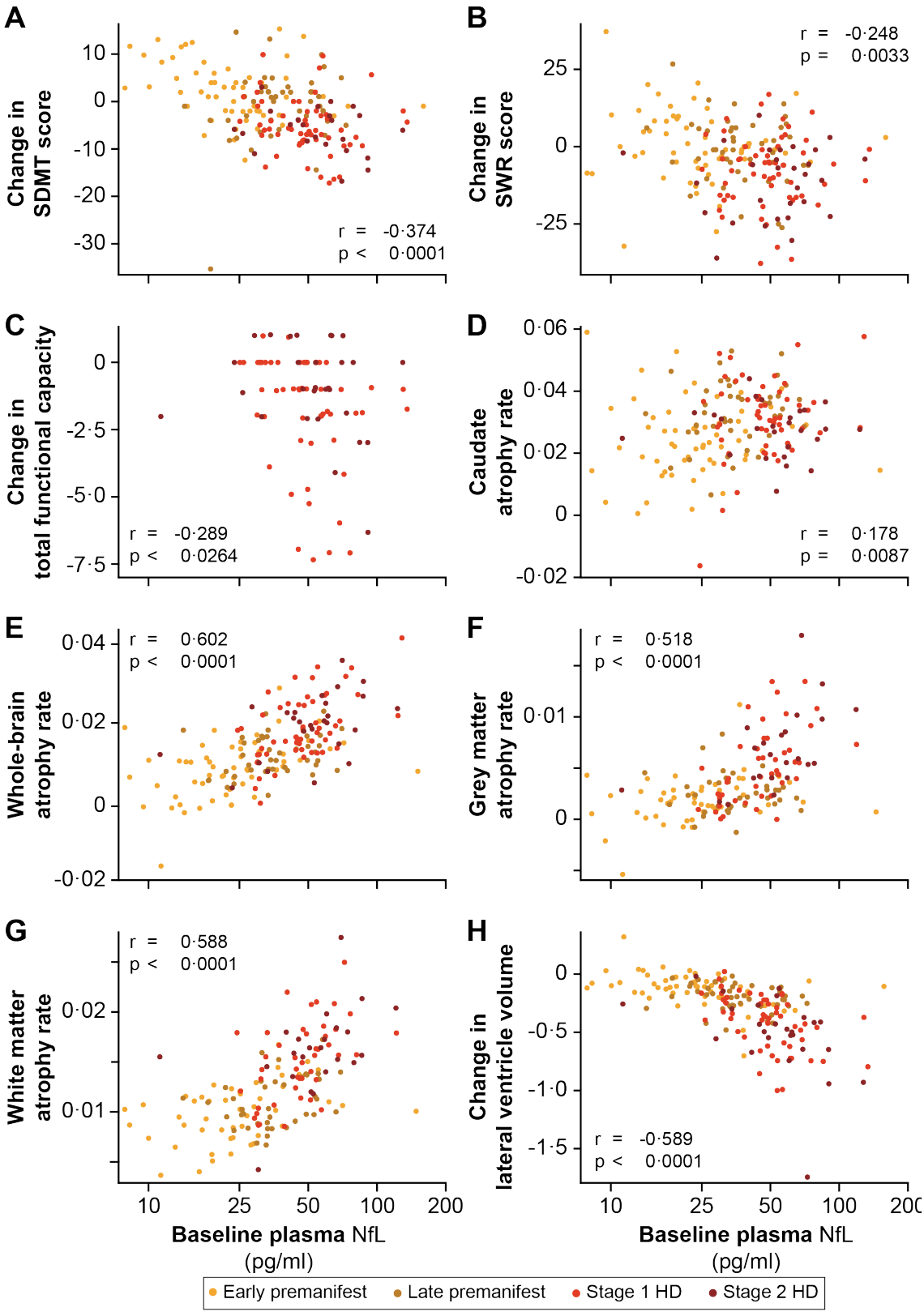

Figure 11 Associations of baseline plasma NfL and longitudinal change in outcome measures.

A, B. Associations with cognitive scores. C. Association with functional capacity. D–H. Associations with global and regional brain volumes, expressed as percentages of total intracranial volume. By convention, negative values for change in lateral ventricle volumes indicate ventricular expansion (ie, brain atrophy). Unadjusted Pearson's r presented with p-values derived from random effects repeated measures models as shown in Table 9.

Table 10 The prognostic value of baseline NfL for longitudinal brain volume change in preHD and manifest HD.

After examining longitudinal predictive power of baseline plasma NfL for longitudinal brain volume change measures across all mutation carriers, it was re-examined controlling for group (premanifest or manifest HD) to examine whether plasma NfL offers additional prognostic power beyond that of group status. Where these analyses were significant, we then examined for the interaction between premanifest and manifest HD to determine whether there was a significantly different relationship with NfL between the two groups. Such relationships were identified for whole-brain and grey matter atrophy and lateral ventricle expansion, all of which were more strongly predicted by NfL in the manifest HD group. Regression estimate represents the least square mean slope for preHD and early HD. Unit for 'estimate' is percent TIV change per log(pg/ml) plasma NfL. * represents the group with the significantly stronger NfL association. For context, the standard deviation of log NfL concentration in preHD subjects was 0·39 log(pg/ml) and in early HD was 0·52log(pg/ml).

Longitudinal measure	**Adjusting for age, CAG and group**		**PreHD vs Early HD Interaction**					
	Regression estimate	**p-value**	**PreHD slope estimate**	**p-value**	**Early HD slope estimate**	**p-value**	**Estimate difference**	**p-value**
Putamen	0·00039	0·8161	0·00016	0·928	0·00061	0·816	0·00045	0·884
Caudate	0·00134	0·0279	0·00177	0·008	0·00091	0·343	0·00086	0·436
Whole brain	0·205	<0·0001	0·129	0·0007	0·282*	<0·0001	0·153	0·043
White matter	0·08	<0·0001	0·048	0·004	0·112	0·002	0·064	0·082
Grey Matter	0·077	<0·0001	0·011	0·496	0·144*	<0·0001	0·143	< 0·0001
Lateral Ventricle	-0·0606	<0·0001	-0·024	0·004	-0·097*	<0·0001	0·073	0·002

3.4.7 Plasma levels of NfL are representative of CNS levels

We explored the relationship of plasma NfL levels with NfL in CSF from an independent cohort of 37 participants (the Pilot CSF study, London). HD individuals had higher median CSF NfL levels than controls (HD: 1871 pg/mL, IQR 1312-2461 vs Controls: 300 pg/mL, 234-368, p<0.0001, Figure 12A). 30 participants had matched plasma samples, which again had significantly different median NfL concentrations between HD and controls (HD: 31.7 pg/mL, IQR 24.9–50.6 vs Controls: 9.9 pg/mL, 8.4–13.7, Figure 12B). NfL concentrations in plasma and CSF were highly correlated (Figure 12C), with median CSF levels 46.4 times greater than plasma. The HD group had higher CSF:plasma ratio then controls (62.11 vs 30.1, p<0.0001).

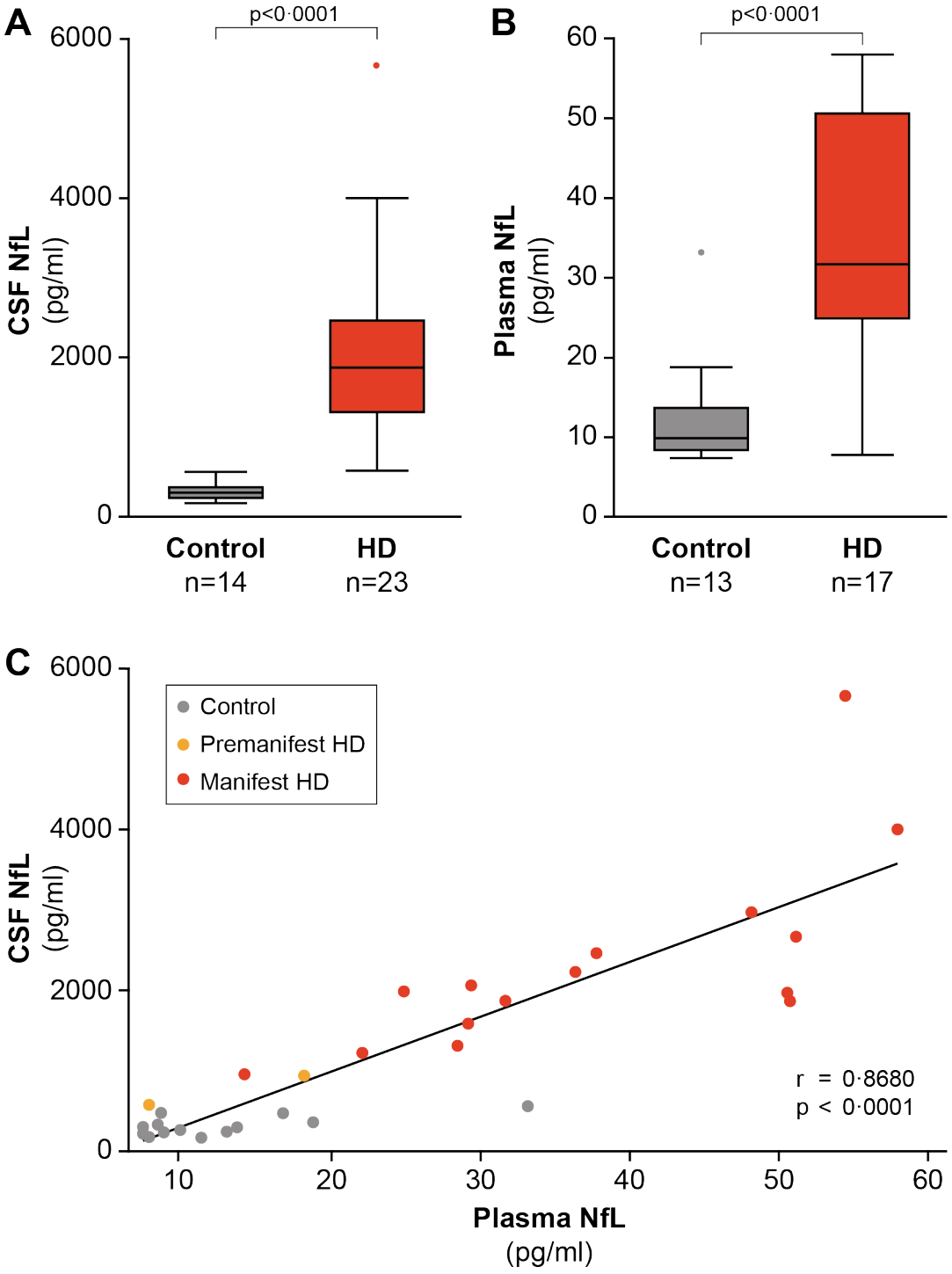

Figure 12 NfL concentrations in paired CSF and plasma samples.

Raw NfL concentrations in A. CSF and B. plasma in HD mutation carriers and controls. C. Bootstrapped Pearson's correlation between NfL concentration in CSF and plasma. HD = HD mutation carriers

3.5 Discussion

3.5.1 Summary

This is the first study reporting NfL concentrations in plasma from HD patients. Not only did we find higher levels in HD compared to controls, but levels rose with progressing disease stage. Notably, plasma NfL was significantly higher in preHD individuals over 10 years from their predicted onset, which no other biofluid biomarker has achieved to date. A major strength of this study is the quality of the TRACK-HD cohort – *A priori* designed to have rigorous quality control and assurance and so powered to develop a battery of robust biomarkers for use in multi-site clinical trials. Using the measures from TRACK-HD previously reported to have the strongest effect sizes (Tabrizi et al., 2013), we showed that plasma NfL concentration at a particular timepoint reflected clinical severity, as depicted by measures for motor and cognitive performance, and global and regional brain volume. NfL concentration increased most steeply in individuals who were preHD at baseline and participants with longer CAG. This striking relationship with plasma NfL and CAG with age is consistent with a CAG-dependent genetic dose-response. Additionally, adjusting associations for the combined effects of age and CAG and their interactions indicates plasma NfL's ability to independently predict clinical features of HD over and above the foremost predictors of disease progression. We showed that baseline levels of plasma NfL were a prognostic indicator of onset over the three-year period beyond that of other known indicators. Baseline plasma NfL was also independently associated with the rate of decline in cognitive function and rate of brain atrophy. To our knowledge, this level of longitudinal prognostic power over many modalities has not been substantiated by any substance in any biofluid for HD.

3.5.2 A dynamic blood biomarker of ongoing neuronal damage

In addition to validating the main plasma findings and previously reported findings in CSF (Constantinescu et al., 2009; Niemelä et al., 2017; Vinther-Jensen et al., 2016; Wild et al., 2015) in a second and independent cohort, the added value of having matched plasma and CSF allowed us to investigate the CNS origin of plasma NfL. The close correlation with CSF levels together with the strong associations with brain atrophy measures provide evidence to support this.

Despite the strong association cross-sectionally between plasma NfL concentrations and the striatal measures of caudate and putamen volume, we found that baseline NfL was more greatly associated with longitudinal reduction in whole-brain than striatal volume. This indicates that a single measurement of NfL in plasma is more representative of the ongoing rate of global neuronal damage. NfL, being a key component of neuronal

cytoskeleton, is present in all neurons (centrally and peripherally), and therefore not expected to be region specific. Furthermore, although disproportional atrophy of the striatum is characteristic of the earliest stages of the disease, whole-brain atrophy has been depicted throughout the span of the disease (Tabrizi et al., 2013). By this means, it would be expected that successful treatment of CNS pathology should lower NfL levels in both CSF and blood. Indeed, lowering of NfL in response to treatment has been reported in clinical trials for Multiple sclerosis (Amor et al., 2014; Kuhle et al., 2015). All in all, the current results with the added perspective from the literature suggest an efficient and more accessible route to quantify neuronal damage may be achieved via plasma NfL.

3.5.3 Limitations

There were several limitations to this study. Firstly, and most crucially, the variability in plasma NfL levels within each HD subgroup was such that it impossible to make prognostic assumptions on an individual patient level at this time. Therefore, much more study in many cohorts is needed before the full clinical relevance of NfL in both plasma and CSF can be understood. This will involve gathering NfL data from many observational cohorts to fully characterise its dynamics throughout the natural history of HD. Secondly, despite the statistical significance achieved, some of the associations of plasma NfL with outcome measures were relatively modest, particularly with longitudinal change. This is likely influenced by inherent variability of NfL levels but it is also important to reiterate the shortcomings of clinical and cognitive measures in objectively quantifying longitudinal change, heavily impeded by intra- and inter- rater variability. In a similar sense, reliable measurement of longitudinal striatal atrophy is extremely difficult with the relatively small sizes of the caudate and putamen. Therefore, we cannot make conclusive physiological inference regarding the association of NfL and global brain atrophy relative to its association with a disproportionate striatal atrophy. Thirdly, TRACK-HD only recruited preHD individuals up to 15 years from predicted onset and manifest HD individuals with early HD (stage 1 and 2). Having no data for NfL in later stages of disease as well as those who are much further from onset restricts any presupposition we can make on the role of NfL in the full span of the disease course. Fourthly, the pilot HD-CSF study was not powered for direct comparison of CSF and plasma NfL therefore, based on the data presented in this study, we cannot determine whether plasma is as good as a predictor of disease outcome or whether CSF will have added prognostic value. The main restriction to finding an answer to these questions is that there has been no such cohort with CSF collection in HD that is large enough in size, with rich phenotypic data and collected longitudinally. HDClarity (NCT02855476) is an ongoing global multi-site CSF collection initiative aimed at creating a resource of high

quality CSF and matched plasma with well characterised clinical data from over 600 participants from early preHD to advanced stage HD, which will facilitate the required head-to-head comparison of plasma vs CSF NfL as well as NfL versus other biofluid biomarkers. Additionally, I have recruited the 80 participant HD-CSF cohort (2.3 HD-CSF) which I have used to address some of these questions about NfL as part of this thesis (see Chapter 4 and 5).

3.5.4 Future perspectives

It is my opinion that the results of this study present plasma NfL as a very promising prognostic marker for ongoing neuronal damage and HD progression. A distinct advantage of NfL over imaging biomarkers is the indication of the current rate of neuropathology that can be achieved with a single measurement, saving time, money and side stepping the difficulties with interpreting longitudinal measurements. Once validated to regulatory standards, this could greatly facilitate the conduct of clinical trials of interventions expected to ameliorate neuronal damage.

We suggest incorporating quantification of plasma NfL in future observational studies and therapeutic trials for HD as well as retrospectively in blood samples collected in previous trials and cohorts to further understand plasma NfL's ability to represent neuronal damage and prognostic outcome.

3.6 Contributions and collaborations

This work has involved a collaborative effort between several organisations and individuals. Dr Wild and I conceived the project, designed the experiment, and obtained the samples. An initial outline of the project plan was discussed with my secondary supervisor Prof Henrik Zetterberg, who had developed both the NF-Light ELISA and Simoa home-brew set up and agreed to quantify NfL in all samples collaboratively at Gothenburg. First, I shipped the Pilot CSF study CSF and plasma samples to Gothenburg, which had previously been collected by Dr Wild and were stored at the Institute of Neurology. NfL data was generated by Henrik's team in Gothenburg and sent back to me. I designed and performed the statistical analysis of this first batch of samples. With the positive pilot data, I drafted a request for access to the TRACK-HD plasma samples from CHDI which Dr Wild reviewed and we submitted together. Once approved TRACK-HD plasma samples were sent directly to Gothenburg for NfL analysis. At this point we invited Prof Doug Langbehn – who was the statistician for all the previous TRACK-HD study publications – to perform the statistical analyses. Before the TRACK-HD NfL data was received, I was involved in all discussions with Doug and together we conceived an *a priori* analysis plan. I was directly involved in working with Doug at every stage, which included reviewing reports, interpreting the results, checking for inconsistencies and finalising the analyses that were to be included in the final manuscript. I developed the core message from the results, supervised by Dr Wild, and wrote the manuscript, including preparing all the figures, collating all edits from co-authors and responding to reviewers.

Chapter 4 Parallel evaluation of mutant huntingtin and neurofilament light as biofluid biomarkers of Huntington's disease: Cross-sectional analysis from HD-CSF study baseline data

This chapter is based on data previously published in Science Translational Medicine, of which I was joint first author (Byrne et al., 2018b). For the first time, we compared mutant huntingtin and neurofilament light protein head-to-head and their relative properties as biomarkers for HD. This was the baseline analysis of the HD-CSF study.

4.1 Introduction

As I have discussed already (1.1.2 Genetics), the single mutation underlying Huntington's disease (HD), a CAG repeat expansion in the *HTT* gene, has been known since the mapping of gene in 1993 (The Huntington's Disease Collaborative Research Group, 1993). This encodes the causative agent, mutant huntingtin protein (mHTT), which is the upstream trigger to the cascade of events (1.1.3 Pathobiology) ultimately leading to the death of neurons and manifestation of HD (Ross et al., 2014). In 2015, the global HD community started a new era, with the first therapy designed to target the source of HD itself and reducing its expression (see 1.1.5 Current therapeutic candidates), entering human clinical trials (clinicaltrials.gov, NCT02519036, 2015).

In 1.3 The scope of this thesis, I emphasised the need for sensitive biomarkers – that can predict progression and report on target engagement to inform trial design and therapeutic development – now with multiple targeted 'huntingtin-lowering' therapies in various phases of clinical development (Rodrigues and Wild, 2018; Wild and Tabrizi, 2017). In a potential future where these prospective therapies are disease modifying, there will be an immediate need (1.3.1 The imminent need) for tools to aid stratification of premanifest HD mutation carriers (preHD) entering preventative trials. In subsequent years, tools will then be necessary for guiding decisions on when to begin treatment in seemingly healthy HD mutation carriers (1.2.1 Applications of biomarkers). Current clinical assessments and rating scales will be limited for this purpose by their nature of being designed to classify overt clinical symptoms (Mestre et al., 2018b, 2018a, 2018d, 2018c, 2016). Through longitudinal observational studies, robust clinical, cognitive and structural neuroimaging biomarkers of HD progression have emerged (Tabrizi et al., 2013, 2012, 2011, 2009). As already discussed in this thesis (1.2.2 Biofluid biomarkers for Huntington's disease), establishing biochemical markers that reflect early CNS pathobiology and predict progression and therapeutic response has proven more challenging (Byrne and Wild, 2016).

In 1.2.2 Huntingtin protein, I outlined the events leading to the first reported quantification of levels of mHTT in the CNS using a single-molecule counting immunoassay (Wild et al., 2015). mHTT concentration in CSF was associated with clinical severity, independently of known predictors – age and *HTT* CAG repeat length. This assay was used to demonstrate successful huntingtin lowering in the first phase 1/2 clinical trial of a huntingtin-lowering therapy, the intrathecally administered antisense oligonucleotide HTT_{Rx} (NCT02519036; Ionis Pharmaceuticals, 2017; Rodrigues and Wild, 2018; Tabrizi et al., 2019). Without this essential tool, the trial would have been unable to show proof of concept and target engagement. A technical validation of the assay has been

published (Fodale et al., 2017), bringing it closer to regulatory standards. However, the performance of CSF mHTT in terms of clinical sensitivity, specificity and intra-individual stability over time – important characteristics for designing adequately powered biomarker-supported clinical trials – has not been assessed in a clinical cohort.

Neurofilament light protein (NfL; as introduced in 1.2.2 Markers of neuronal damage) is the smallest of three subunits of neurofilaments and a key component to the neuronal cytoskeleton. With neuronal injury it is released into CSF (Shahim et al., 2016b); several studies have reported increased NfL in CSF from HD patients and correlates with clinical severity (Constantinescu et al., 2009; Rodrigues et al., 2016b; Vinther-Jensen et al., 2016; Wild et al., 2015). I have already discussed within this thesis the striking potential of NfL (Chapter 3), measured in blood using an ultrasensitive Single molecule array (Simoa)-based assay, as a prognostic HD biomarker (Byrne et al., 2017). Baseline plasma NfL predicted numerous aspects of subsequent disease course, including rates of brain atrophy and cognitive decline, and disease onset in premanifest HD mutation carriers. We also showed a strong correlation between plasma and CSF levels of NfL, indicating a CNS origin of NfL detected in plasma. Further to this, we have shown that NfL in plasma predicts regional atrophy in disease-associated brain areas (Johnson et al., 2018). Soylu-Kucharz and colleagues also showed that NfL in CSF and blood is a potential translational biomarker in the R6/2 mouse model of HD (Soylu-Kucharz et al., 2017). However, our understanding of the potential value of NfL as a biomarker is limited by the lack of a large, well-phenotyped cohort in which to study the relative performance of NfL in both plasma and CSF.

These two proteins – mHTT as the pathogenic agent and a pharmacodynamic marker of huntingtin-lowering, and NfL as a marker of neuronal damage – have the potential to form a powerful biofluid biomarker combination that could facilitate disease-modifying trials in HD. However, they have never been measured in parallel in CSF and blood from a cohort of HD mutation carriers and controls. Assessment of multiple biomarkers in the same individuals enables the head-to-head evaluation of clinical performance characteristics necessary to inform clinical trial design. The event-based model (EBM) (Fonteijn et al., 2012) is a data-driven and probabilistic method that computationally models disease-related biomarker changes as a sequence of events in which individual factors become detectably abnormal. It uses the biomarker distributions in healthy and disease populations to infer normal and abnormal thresholds. MRI derived biomarker orderings which have provided insight into the pathological sequence of events in Alzheimer's disease (Oxtoby et al., 2018; Young et al., 2014), multiple sclerosis (Eshaghi et al., 2017), and HD (Wijeratne et al., 2018), have been determined using this method. However, studies in HD investigating the temporal order in which biofluid markers alter

during the disease course relative to more established clinical and MRI measures were lacking before the results from this chapter were published.

The HD-CSF study (see 2.3 HD-CSF) was designed to generate a resource of high-quality CSF matched with blood plasma, along with phenotypic and neuroimaging data, to facilitate the development of biofluid biomarkers for HD. Study procedures were designed to maximise consistency of data and sample acquisition and processing.

4.2 Aim

Using the baseline samples and data from HD-CSF, we aimed to assess mHTT in CSF and NfL in CSF and plasma head-to-head for the first time, comparing their relative performance as HD biomarkers in the context of matching clinical, cognitive and MRI data. We compared their diagnostic ability using Receiver operating characteristic (ROC) analysis and their within-subject stability using samples from an optional repeat sampling visit 4-8 weeks after the baseline sampling. We calculated sample size requirements for clinical trials using lowering in mHTT or NfL as outcome measures. Finally, the temporal sequence in which the measured biomarker outcomes become abnormal was assessed using event-based modelling, to determine when these biofluid biomarkers are detectably altered in HD.

4.3 Methods

4.3.1 Participants

Eighty participants (20 healthy controls, 20 premanifest HD and 40 manifest HD) were recruited from the NHNN/UCL/UCLH HD Multidisciplinary Clinic as part of the HD-CSF study (2.3 HD-CSF). The HD-CSF study was conducted according to Declaration of Helsinki principles and was approved by the London - Camberwell St Giles Research Ethics Committee. All participants gave written informed consent prior to inclusion in the study.

All participants underwent the core Enroll-HD assessments which includes the UHDRS assessments: Total functional capacity, Total motor score, Symbol digit modalities test, Verbal fluency categorical, Stroop color naming and Stroop word reading (https://www.enroll-hd.org/). MRI scans and the repeat sampling visits between four and eight weeks after the baseline sampling visit were optional. HD mutation carriers had a CAG repeat length ≥ 40. Manifest HD mutation carriers were defined by having a diagnostic confidence score (DCS) = 4 and PreHD as having a DCS of < 4. Stages of HD are defined by TFC score (Stage 1, TFC 11-13; Stage 2, TFC 10-7; Stage 3, TFC 7-10). Early HD includes stages 1 and 2. Moderate HD is stage 3. Healthy controls were recruited contemporaneously and age-matched to HD mutation carriers and were clinically well with low risk of incidental neurological disease. The full HD-CSF study protocol is included in the Appendix.

Data from the multisite TRACK-HD study were used in the event-based model analysis. This involved 290 participants out of the 366 enrolled at baseline (95 healthy controls, 103 PreHD and 92 Early HD), all of which had baseline data for plasma NfL and quality controlled imaging data. Details of the participants and the study protocol – including MRI acquisition and plasma NfL quantification – have been previously published (Byrne et al., 2017; Johnson et al., 2018; Wijeratne et al., 2018). The same data were used in (Chapter 3).

4.3.2 Sample collection and processing

Sample collections were standardized as previously described (Byrne et al., 2018a; Wild et al., 2015). In summary, lumbar punctures were carried out between 9 and 10.30am, post 12-hour fasting, samples were collected on wet ice and processed within 30 minutes of collection by centrifugation and freezing using standard kits containing polypropylene plasticware supplied by the HDClarity study (http://hdclarity.net). Blood collection was performed within 30 minutes of CSF collection. CSF and blood plasma were isolated by centrifugation and frozen at -80°C.

4.3.3 Analyte Quantification

All samples were analysed blinded to disease status and clinical data. Each analyte was quantified using the same batch of reagents for all samples. mHTT levels in CSF were measured in triplicate using a single-molecule counting immunoassay (Singulex) as previously described (Fodale et al., 2017; Wild et al., 2015). CSF levels of NfL were quantified in duplicate using the NF-light ELISA according to the manufacturer's instructions (UmanDiagnostics, Umeå, Sweden). Plasma NfL concentration was measured in duplicate with ultrasensitive Simoa technology – the commercially available NF-Light® kits, as per the manufacturer's instructions (Quanterix, Lexington, MA, USA). CSF mHTT levels were undetectable in healthy controls and above the limit of detection (LoD) of the assay (8 fM) in all HD mutation carriers. NfL in both CSF and blood plasma was above the LoDs of each assay (100 pg/mL and 0.105 pg/mL respectively) in all participants. All NfL values were within the linear ranges of the assays. Haemoglobin concentration was measured using a commercial ELISA (E88-134, Bethyl Laboratories Inc.) to determine CSF contamination by blood. mHTT in plasma was not quantified as it was previously shown that it does not correlate with levels in the CNS and therefore was not considered to be neuropathologically relevant (Wild et al., 2015).

4.3.4 MRI Acquisition

T1-weighted MRI data were acquired on a 3T Siemens Prisma scanner using a protocol optimised for this study. Images were acquired using a 3D MPRAGE sequence with a TR = 2000ms and TE = 2.05ms. The protocol had an inversion time of 850ms, flip angle of 8 degrees, matrix size 256 x 240mm. 256 coronal partitions were collected to cover the entire brain with a slice thickness of 1.0 mm. Parallel imaging acceleration (GRAPPA, R = 2) was used and 3D distortion correction was applied to all images.

4.3.5 Structural MRI Processing

All T1-weighted scans passed visual quality control check for the presence of significant motion or other artefacts prior to processing. Bias correction was performed using the N3 procedure (Sled et al., 1998). A semi-automated segmentation procedure via MIDAS was used to generate volumetric regions of the whole-brain and total intracranial volume (TIV) as previously described (Freeborough et al., 1997; Scahill et al., 2003; Whitwell et al., 2001). In addition, SPM12 'Segment' (MATLAB version 2012b) was used to measure the volume of the grey and white matter (Ashburner and Friston, 2000). Finally, MALP-EM was used to quantify caudate volume (Ledig et al., 2015). MALP-EM is an automated tool used to segment MRI scans into regional volumes, and has previously been validated for use in HD cohorts (Johnson et al., 2017). Default settings were used, for both SPM12 segmentations and MALP-EM caudate regions, no scans failed processing after visual quality control of segmentations by experienced raters to ensure accurate

delineation of the regions. Demographic MRI volumes were presented adjusted for TIV. All MRI analyses used brain volumes as percentage of TIV.

4.3.6 Event-based model

The previously published event-based model (EBM) by Wijeratne and colleagues (Wijeratne et al., 2018), was adapted to include the biomarkers that were a priori selected for the HD-CSF study. The HD-CSF EBM was constructed using a subset of the HD-CSF cohort, with a requirement that subjects must have measurements for every biomarker (Controls = 15; preHD = 16; HD = 32). Biomarkers were adjusted for age and TIV using frequentist residual control. Since mHTT was below the lower level of quantification (LLoQ) in controls and therefore had a standard deviation equal to zero, the control mHTT distribution's standard deviation was set to reflect the LLoQ for mHTT of 6.5fM (as reported in Fodale et al (2017)). As with Wijeratne et al. (2018), constrained mixture models (a probabilistic method were distributions of likelihoods are generated for normal and abnormal for each biomarker) were fit to the control and manifest HD distributions for each biomarker (Figure 13). Sequence estimation was initialised using greedy ascent (an iterative process that adjusts the model and builds on each previous estimation) and optimised using Markov Chain Monte Carlo sampling (a step that allows the optimisation of a desired probabilistic distribution where variables are autocorrelated with one another). Subjects were staged according to their most likely position in the event sequence for each biomarker.

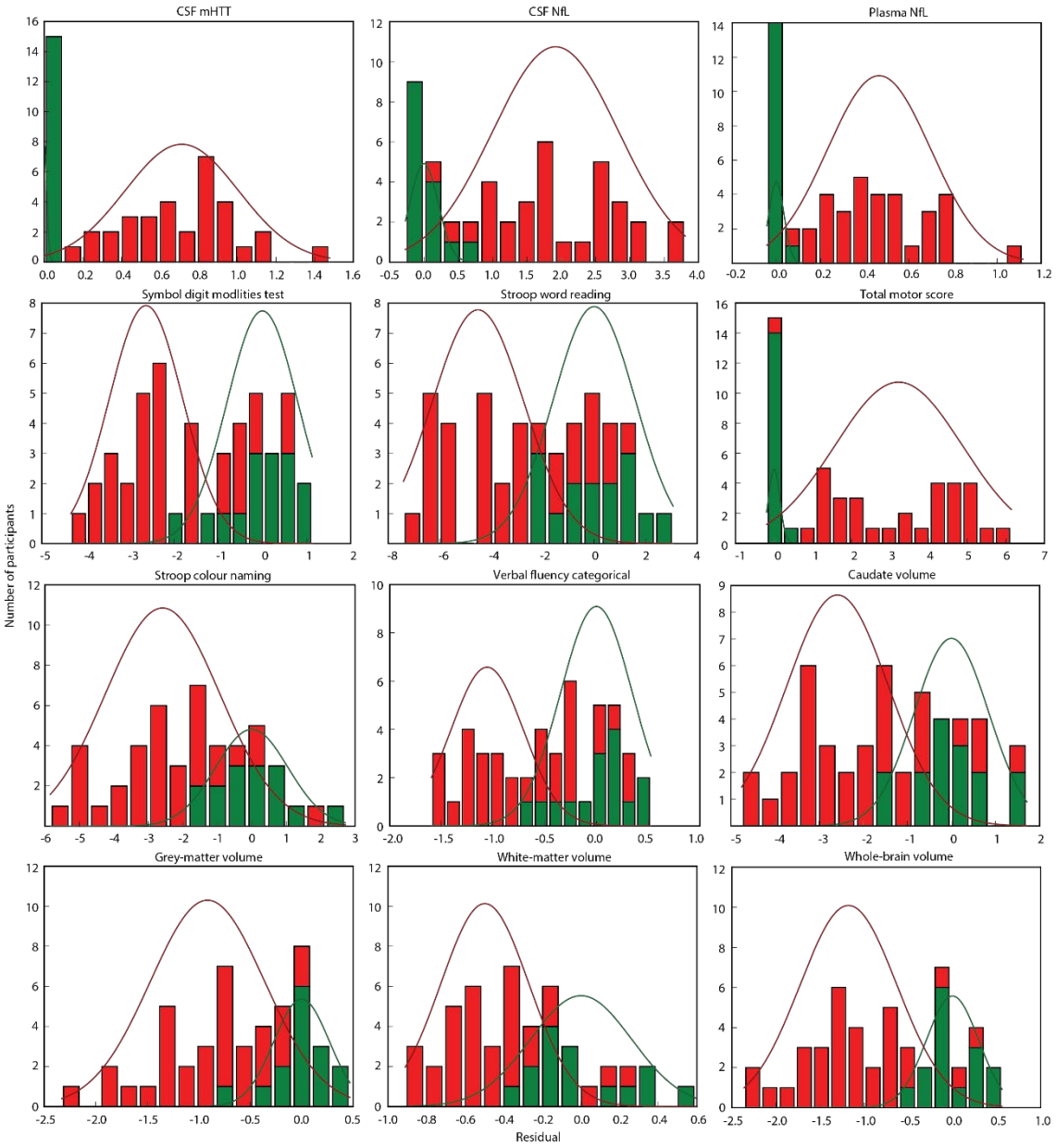

Figure 13 The residual distributions for each measure used in the HD-CSF EBM.

The residual distributions and corresponding constrained mixture model fits for controls (green; N=15) and manifest HD (red; N=32) which were used in the HD-CSF EBM to define normal and abnormal for each measure. Measured variables are age and TIV adjusted.

4.3.7 Statistics

Analyses were performed with the statistical package Stata 14.2 (StataCorp, Texas, USA). Significance level was defined as $p<0.05$.

Analyte distributions were tested for normality and, if necessary, arithmetical transformations were evaluated to produce normality. CSF mHTT had a normal distribution. CSF and plasma NfL were non-normally distributed; a natural logarithm transformation produced an acceptable normal distribution for both CSF and plasma NfL,

as previously shown (Byrne et al., 2017), therefore transformed values were used for all analyses.

Potentially confounding demographic variables (age, gender, blood contamination) were examined in preliminary analyses and those found to be significant were included as covariates for subsequent analyses. All analyses were repeated with adjustment for both age and CAG repeat length – a planned second-level analysis – to assess each analyte's associations with measures beyond the known combined effect of age and *HTT* CAG repeat length.

The clinical and imaging outcome measures were pre-specified based on previously published evidence that these measures were most robustly associated with disease progression (Byrne et al., 2017; Tabrizi et al., 2013, 2012). We used unpaired two-sample t-test/ANOVA or the Pearson's chi-squared test to assess intergroup differences of baseline characteristics. Intergroup comparisons of analytes were tested using multiple linear regressions using either age or both age and CAG repeat length as covariates. Correlations were tested using Pearson's correlation and partial correlations for covariate adjustment.

To understand the diagnostic power of the studied analytes ability to differentiate healthy controls and HD mutation carriers, and premanifest from manifest HD, we produced receiver operating characteristics (ROC) curves for each analyte and compared the areas under the curves (AUC) formally using the method suggested by DeLong and colleagues (DeLong et al., 1988).

We performed sample size calculations to inform the design of therapeutic trials aiming to lower these analytes by a range of desired therapeutic effect sizes. Log-transformed values were used for each analyte. The assumption for inter-subject variability was based on the variability in the change from baseline to 6 weeks in HD mutation carriers. No change over time was assumed for the hypothetical control arm of the trial. On the basis of these assumptions, we derived the sample size per arm required to detect a given control-adjusted percent reduction in the treatment arm with 80% power and two-sided 5% type I error.

4.4 Results

4.4.1 HD-CSF demographics are well matched between groups except for age

At the HD-CSF baseline, 80 participants (20 healthy controls, 20 preHD, and 40 manifest HD mutation carriers (manifest HD) ranging from early to moderate stage HD) were recruited and completed the core assessments. Demographics and clinical characteristics of the cohort are presented in Table 11.

Table 11. Baseline characteristics of the HD-CSF cohort.

Intergroup differences were assessed using ANOVA or unpaired two-sample t-tests (with the exception of gender which was assessed using a 2 by 3 Pearson's chi-squared test). Brain volumes are adjusted for total intracranial volume. Values are mean ± SD, except where stated otherwise. Values presented for CSF and plasma NfL concentration are natural log transformed and p-values are adjusted for age and Bonferroni corrected. P-values for CSF mHTT concentration are adjusted for age and Bonferroni corrected. Other p-values are not adjusted for multiple comparisons. PreHD, premanifest HD mutation carriers; Manifest HD, manifest HD mutation carriers; CAG, CAG triplet repeat count; CSF, cerebrospinal fluid; mHTT, mutant huntingtin protein; NfL, neurofilament light protein.

	Control	PreHD	Manifest HD	ANOVA p-value	Control vs PreHD p-value	PreHD vs Manifest HD p-value
n	20	20	40			
Age (years)	50.7 ± 11.0	42.4 ± 11.1	56.0 ± 9.4	<0.0001	0.012	<0.0001
Males (%)	10 (50)	10 (50)	22 (55)	0.905	1.000	0.714
CAG	N/A	42.0 ± 1.6	42.8 ± 2.2	N/A	N/A	0.179
Disease burden score	N/A	267.1 ± 61.9	395.5 ± 94.6	N/A	N/A	<0.0001
Total functional capacity	13 ± 0	13 ± 0	9.4 ± 2.7	<0.0001	1.000	<0.0001
Total motor score	2.35 ± 2.4	2.80 ± 2.8	37.3 ± 19.3	<0.0001	0.919	<0.0001
Symbol digit modalities test	50.9 ± 10.4	55.6 ± 9.3	27.2 ± 12.6	<0.0001	0.198	<0.0001
Stroop color naming	75.8 ± 13.1	81.3 ± 10.1	45.7 ± 16.9	<0.0001	0.236	<0.0001
Stroop word reading	100.2 ± 17.4	105.1 ± 11.8	59.6 ± 23.6	<0.0001	0.436	<0.0001
Verbal fluency, categorical	24.3 ± 4.1	23.3 ± 3.4	14.3 ± 5.8	<0.0001	0.523	<0.0001
Whole brain volume (mL)	1195 ± 55.8	1187 ± 49.7	1052 ± 70.1	<0.0001	0.709	<0.0001
White matter volume (mL)	439.6 ± 32.64	430.4 ± 28.1	382 ± 34	<0.0001	0.433	<0.0001
Grey matter volume (mL)	705.9 ± 51.6	709 ± 46.4	593.5 ± 61.4	<0.0001	0.879	<0.0001
Caudate volume (mL)	7.1 ± 0.8	6.1 ± 1.1	4.0 ± 1.2	<0.0001	0.009	<0.0001
CSF mHTT (fM)	0 ± 0	46.4 ± 21.8	73.7 ± 28.7	<0.0001	<0.0001	0.0010
CSF NfL (log pg/mL)	6.7 ± 0.5	7.5 ± 0.7	8.5 ± 0.4	<0.0001	<0.0001	<0.0001
Plasma NfL (log pg/mL)	2.9 ± 0.4	3.3 ± 0.6	4.2 ± 0.4	<0.0001	<0.0001	<0.0001

The preHD group was significantly younger than the control and manifest HD groups, a consequence of their selection as individuals too young to have developed HD symptoms; the control group was recruited to match the mean age of all HD mutation carriers (p=0.061). Therefore, age adjustment was included in all analyses. There were no inter-group differences in gender. As expected there were no intergroup differences between controls and the preHD groups for functional, motor and cognitive scores, but there were differences between the preHD and the manifest HD groups.

In all 80 participants, mHTT was quantified in CSF, and NfL in both CSF and plasma. CSF mHTT was quantifiable in all HD mutation carriers, but was below the detection threshold in all healthy controls, as expected. Thus, controls were excluded from the

analysis of confounding variables for mHTT. CSF mHTT, CSF NfL and plasma NfL concentrations were significantly associated with age (Figure 14A-C; CSF mHTT in HD mutation carriers r=0.260, p=0.0449; CSF NfL in controls r=0.681 p=0.0009, and in HD mutation carriers r=0.643 p<0.00001; plasma NfL in controls r=0.844 p<0.00001, and in HD mutation carriers r=0.639 p<0.00001). There was no apparent gender effect on any of the analytes (Figure 14D-E; CSF mHTT in HD mutation carriers p=0.1919; CSF NfL in controls p=0.0924, and in HD mutation carriers p=0.3735; plasma NfL in controls p=0.2247, and in HD mutation carriers p=0.3950). Assessing the effect of blood contamination in CSF, haemoglobin was not significantly associated with the concentration of either CSF mHTT (Figure 14J-L; r=-0.132, p=0.2445) or CSF NfL r=-0.1306, p=0.2484).

Only CSF mHTT concentrations were associated directly with CAG repeat length (Figure 14G-I; CSF mHTT r=0.376, p=0.0031; CSF NfL r=0.253, p=0.0511; plasma NfL r=0.230, p=0.0776). CAG repeat length is the primary driver of HD and its product with age is strongly associated with disease progression. As a secondary analysis, we repeated all subsequent analyses to include both age and CAG repeat length as covariates. This step assesses whether the analyte has independent power to predict cross-sectional disease characteristics, beyond the known best-known predictors of HD disease progression.

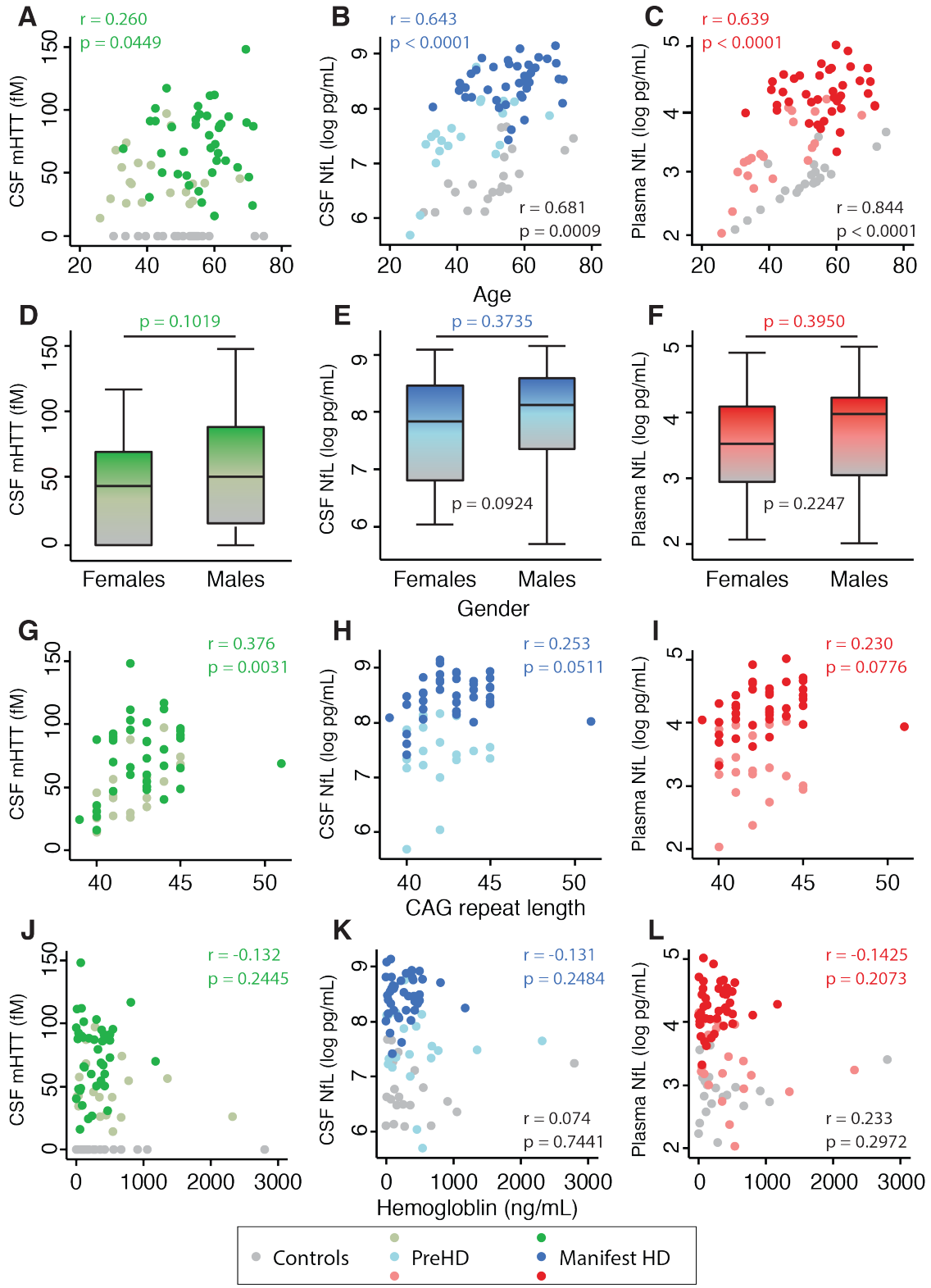

Figure 14 Assessments for potential confounding variables.

(A-C) Correlations between age and (A) CSF mHTT, (B) CSF NfL and (C) plasma NfL. (D-F) The mean difference of analyte by gender for (D) CSF mHTT, (E) CSF NfL and (F) plasma NfL. (G-I) Correlations with CAG repeat length and (G) CSF mHTT, (H) CSF NfL and (I) plasma NfL. (J-L) Correlations between haemoglobin and (J) CSF mHTT, (K) CSF NfL and (L) plasma NfL. NfL values are natural log transformed. Correlations are represented by r and p values generated from Pearson's correlations. P values for mean differences were generated using a two-sided two-sample t-test. r and p values were generated using either controls only (grey; N=20) or HD mutation carriers only (coloured; N=60). Only HD mutation carriers were included in the analyses involving mHTT or CAG repeat length as controls do not have detectable mHTT or CAG repeat length in the disease range. CSF, cerebrospinal fluid; mHTT, mutant huntingtin; NfL, neurofilament light.

4.4.2 mHTT and NfL increase with disease progression

The concentrations of CSF mHTT, CSF NfL and plasma NfL were all significantly higher in HD mutation carriers compared to controls (p=<0.0001 for all three analytes; Figure 15). Concentrations of each analyte were also significantly higher in manifest than premanifest HD, and in premanifest HD than controls even after Bonferroni correction for multiple comparisons (Figure 15 and Table 11). The manifest HD group had significantly higher CSF NfL and plasma NfL than preHD even after adjustment for age and CAG repeat length, also surviving multiplicity correction (CSF mHTT p=0.1520; CSF NfL p=0.0148; plasma NfL p=0.0008).

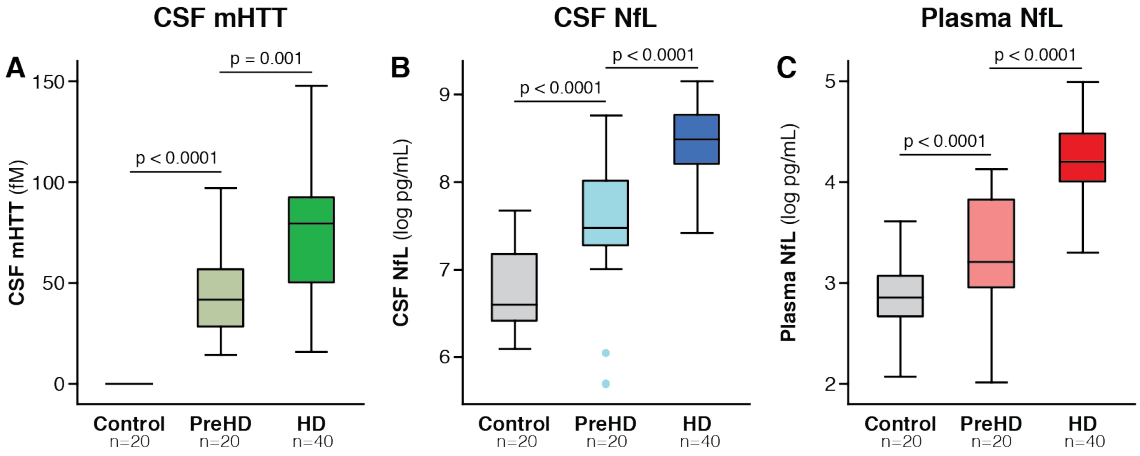

Figure 15 Comparison of analyte concentrations across disease stage.

A) CSF mHTT; B) CSF NfL; C) plasma NfL. Boxes are the interquartile range with horizontal lines representing the median value. Whiskers are upper and lower adjacent values with dots outside representing values 1.5 x interquartile range above or below the 25th or 75th percentile. P values were generated from multiple linear regression to adjust for confounders and are Bonferroni corrected. PreHD, premanifest Huntington's disease; HD, Huntington's disease; CSF, cerebrospinal fluid; mHTT, mutant huntingtin; NfL, neurofilament light.

4.4.3 Plasma NfL is most strongly associated with clinical severity

Among HD mutation carriers there were significant associations between CSF mHTT, CSF NfL, and plasma NfL concentration and all pre-specified UHDRS clinical measures: Total functional capacity, Total Motor Score, Symbol digit modalities Test, Stroop color naming, Stroop word reading, and Verbal fluency categorical (Figure 16, Table 12). When CAG repeat length was adjusted for in addition to age, the associations between plasma NfL and the clinical measures remained statistically significant.

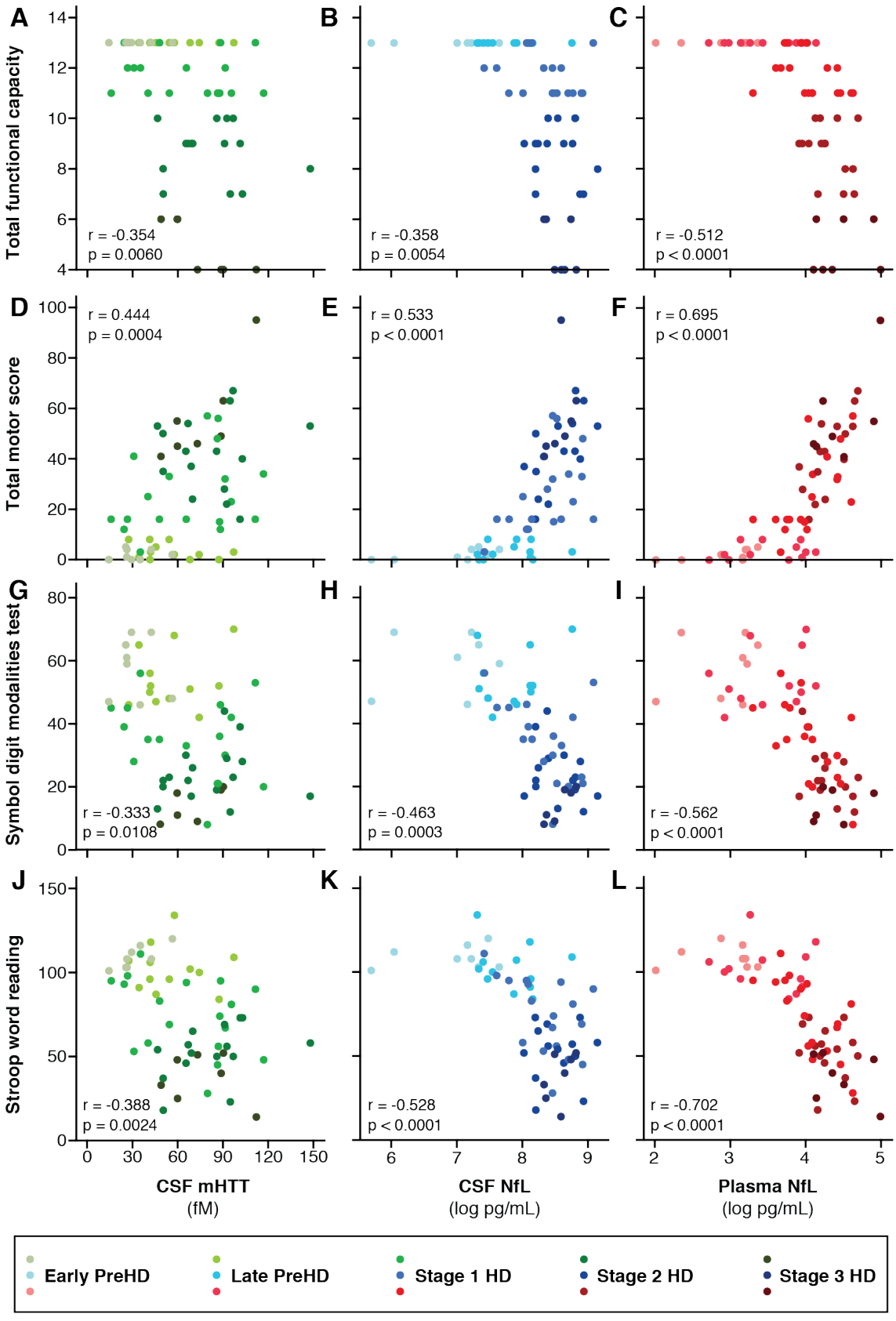

Figure 16 Association between the analytes and clinical measures within HD mutation carriers.

A, D, G, J) CSF mHTT; B, E, H, K) CSF NfL; C, F, I, L) plasma NfL; UHDRS clinical scores including A-C) functional, D-F) motor and G-L) cognitive measures. Scatter plots show unadjusted values. r and p values are age-adjusted, generated from Pearson's partial correlations including age as a covariate. NfL values are natural log transformed. UHDRS Unified Huntington's disease rating scale; PreHD, premanifest Huntington's disease; HD, Huntington's disease; CSF, cerebrospinal fluid; mHTT, mutant huntingtin; NfL, neurofilament light.

Table 12 Association between the biofluid analytes and UHDRS clinical scores.

For all HD mutation carriers. Values are Pearson's r, generated by partial correlations including age, or age and CAG repeat length, as covariates. CSF, cerebrospinal fluid; mHTT, mutant huntingtin; NfL, neurofilament light.

Measure (N=60)	**Adjusted for**	**CSF mHTT**		**CSF NfL**		**Plasma NfL**	
		r	**p-value**	**r**	**p-value**	**r**	**p-value**
Total functional capacity	Age	-0.354	0.0060	-0.358	0.0054	-0.512	<0.0001
	Age & CAG	-0.122	0.3618	-0.038	0.7785	-0.291	0.0267
Total motor score	Age	0.444	0.0004	0.533	<0.0001	0.695	<0.0001
	Age & CAG	0.208	0.1181	0.249	0.0594	0.525	<0.0001
Symbol digit modalities test	Age	-0.333	0.0108	-0.463	0.0003	-0.562	<0.0001
	Age & CAG	-0.061	0.6551	-0.140	0.2985	-0.329	0.0125
Stroop color naming	Age	-0.351	0.0064	-0.509	<0.0001	-0.650	<0.0001
	Age & CAG	-0.072	0.5931	-0.208	0.1166	-0.454	0.0003
Stroop word reading	Age	-0.388	0.0024	-0.528	<0.0001	-0.702	<0.0001
	Age & CAG	-0.108	0.4178	-0.219	0.0989	-0.525	<0.0001
Verbal fluency categorical	Age	-0.370	0.0040	-0.445	0.0004	-0.577	<0.0001
	Age & CAG	-0.097	0.4672	-0.103	0.4401	-0.340	0.0091

4.4.4 CSF NfL has stronger associations with brain volume than plasma NfL

64 out of the 80 participants (80%), opted to have the optional MRI scan, of whom 49 were HD mutation carriers. Those who opted to have the MRI scan had similar characteristics to those who did not (Table 13). Among HD mutation carriers, CSF mHTT was not significantly associated with brain volume. CSF NfL concentration was significantly associated with all MRI volumes: whole-brain volume, white-matter volume, grey-matter volume and caudate volume (Figure 17 and Table 14) and also survived additional adjustment for age and CAG repeat length. Plasma NfL was associated with whole-brain, grey-matter and caudate volume with both caudate and grey-matter associations remaining significant after age and CAG adjustment.

Table 13 Characteristics of participants who opted in for the optional MRI scan.

Intergroup differences were assessed using unpaired two-sample t-tests (with the exception of gender which was assessed using a 2 by 2 Pearson's chi-squared test). P-values are not adjusted for multiple comparisons. Values are mean ± SD, except where stated otherwise. PreHD, premanifest HD gene-expansion carriers; Manifest HD, manifest HD gene-expansion carriers; CSF, cerebrospinal fluid; mHTT, mutant Huntingtin; NfL, neurofilament light; CAG, CAG triplet repeat count; N/A, not applicable.

	MRI			No MRI			p-value		
	Control	**PreHD**	**Manifest HD**	**Control**	**PreHD**	**Manifest HD**	**Control**	**PreHD**	**Manifest HD**
n	15	16	33	5	4	7	N/A	N/A	N/A
Age	49.5 ± 11.0	42.0 ± 11.6	56.2 ± 9.1	54.5 ± 11.5	44.1 ± 9.5	55.5 ± 11.3	0.3907	0.7432	0.8663
Males (%)	8 (53)	9 (56)	18 (55)	2 (40)	1 (25)	4 (57)	0.606	0.264	0.900
CAG	N/A	42.3 ± 1.7	42.5 ± 1.8	N/A	41.0 ± 1.2	43.9 ± 3.5	N/A	0.1744	0.1413
Disease burden score	N/A	275.3 ± 66.8	387.3 ± 95.1	N/A	234.3 ± 12.4	434.4 ± 88.5	N/A	0.2464	0.2357
Total functional capacity	13.0 ± 0.0	13.0 ± 0.0	9.7 ± 2.7	13.0 ± 0.0	13.0 ± 0.0	8.0 ± 2.4	1.0000	1.0000	0.1322
Total motor score	1.7 ± 1.4	2.9 ± 3.0	34.4 ± 17.3	4.4 ± 3.8	2.5 ± 2.4	51.3 ± 23.8	0.0251	0.8181	0.0337
Symbol digit modalities test	51.5 ± 9.5	55.0 ± 9.7	28.5 ± 13.0	49.0 ± 13.7	57.8 ± 8.2	20.2 ± 7.7	0.6490	0.6109	0.1373
Stroop color naming	76.5 ± 11.7	81.6 ± 11.2	47.6 ± 16.4	73.8 ± 18.1	80.3 ± 3.9	36.7 ± 17.8	0.7038	0.8236	0.1251
Stroop word reading	100.7 ± 18.3	104.4 ± 12.9	62.4 ± 23.6	98.4 ± 15.8	107.5 ± 6.1	46.3 ± 20.0	0.8025	0.6537	0.1027
Verbal fluency categorical	23.8 ± 4.4	23.4 ± 3.1	15.1 ± 5.7	25.8 ± 3.1	22.8 ± 5.0	10.6 ± 5.3	0.3609	0.7295	0.0634
CSF mHTT (fM)	0.0 ± 0.0	50.9 ± 22.2	71.8 ± 29.6	0.0 ± 0.0	28.3 ± 4.5	82.8 ± 24.4	1.0000	0.0626	0.3657
CSF NfL (log pg/mL)	6.7 ± 0.6	7.5 ± 0.8	8.5 ± 0.4	6.7 ± 0.3	7.3 ± 0.3	8.5 ± 0.3	0.7537	0.5420	0.6938
Plasma NfL (log pg/mL)	2.8 ± 0.4	3.2 ± 0.6	4.2 ± 0.4	3.1 ± 0.2	3.2 ± 0.1	4.4 ± 0.4	0.1526	0.8621	0.1370

Table 14. Association between the analytes (CSF mHTT, CSF NfL and plasma NfL) and brain imaging.

All volumetric measures were calculated as a percentage of total intracranial volume. Values are Pearson's r generated by partial correlations including age, or age and CAG repeat length, as covariates. CSF, cerebrospinal fluid; mHTT, mutant huntingtin; NfL, neurofilament light.

Measure (N=49)	**Adjusted for**	**CSF mHTT**		**CSF NfL**		**Plasma NfL**	
		r	**p-value**	**r**	**p-value**	**r**	**p-value**
Whole-brain volume	Age	-0.234	0.1102	-0.479	0.0006	-0.406	0.0042
	Age & CAG	-0.082	0.5862	-0.452	0.0014	-0.285	0.0518
White-matter volume	Age	-0.142	0.3360	-0.354	0.0135	-0.205	0.1626
	Age & CAG	-0.053	0.7246	-0.351	0.0157	-0.122	0.4150
Grey-matter volume	Age	-0.266	0.0674	-0.507	0.0002	-0.477	0.0006
	Age & CAG	-0.151	0.3116	-0.398	0.0057	-0.404	0.0049
Caudate volume	Age	-0.211	0.1547	-0.539	0.0001	-0.718	<0.0001
	Age & CAG	-0.025	0.8682	-0.358	0.0144	-0.628	<0.0001

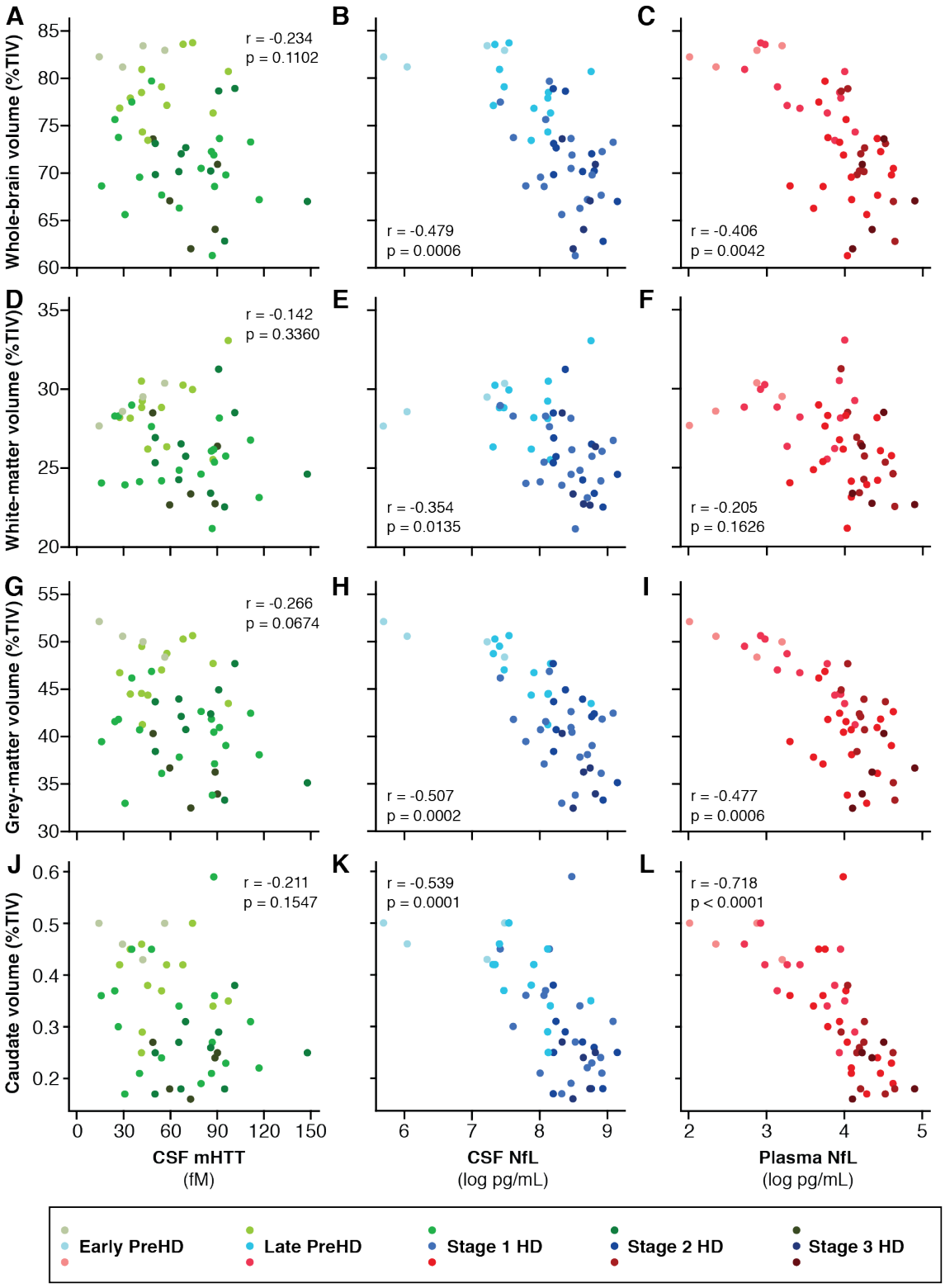

Figure 17 Association between the analytes and MRI volumes within HD mutation carriers.

A, D, G, J) CSF mHTT; B, E, H, K) CSF NfL; C, F, I, L) plasma NfL; MRI volumetric measures A-C) whole-brain, D-F) white-matter, G-I) grey-matter and J-L) caudate. All volumetric measures were calculated as a percentage of total intracranial volume. Scatter plots show unadjusted values. r and p values are age-adjusted, generated from Pearson's partial correlations including age as a covariate. NfL values are natural log transformed. PreHD, premanifest Huntington's disease; HD, Huntington's disease; CSF, cerebrospinal fluid; mHTT, mutant huntingtin; NfL, neurofilament light.

4.4.5 CSF mHTT, CSF NfL and plasma NfL are closely correlated

mHTT and NfL in CSF were strongly correlated in HD mutation carriers (Figure 18A; unadjusted: r=0.682, p<0.0001; age-adjusted: r=0.697, p<0.0001). CSF and plasma NfL were also highly correlated (Figure 18B; In the whole cohort, unadjusted: r=0.914, p<0.0001; age-adjusted: r=0.885, p<0.0001; In HD mutation carriers, unadjusted: r=0.878, p<0.0001; age-adjusted: r=0.794, p<0.0001). The mean concentration of CSF NfL was 33.7 times that in plasma. The CSF:plasma ratio for NfL in HD mutation carriers was significantly higher than controls (36.5 vs 25.5, respectively, p=0.0010), in keeping with our previous findings in the pilot CSF cohort from Chapter 3 (Byrne et al., 2017).

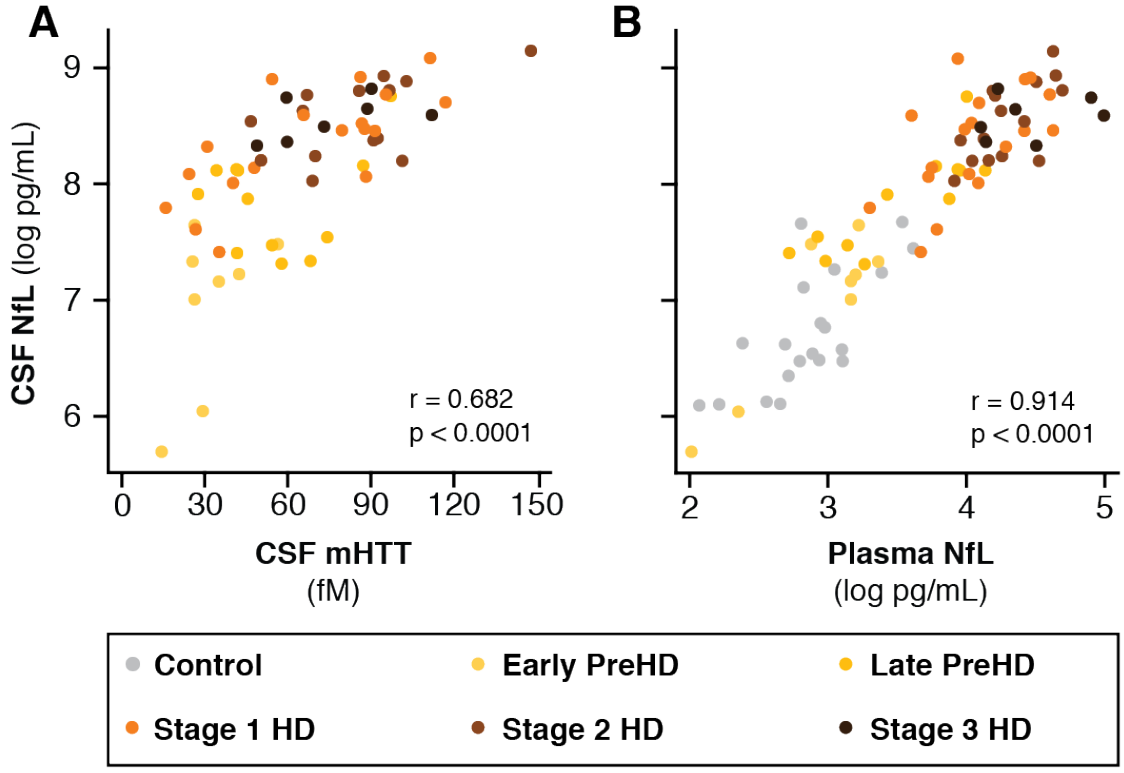

Figure 18 Association between the measured analytes.

A) CSF mHTT is correlated with CSF NfL. B) plasma NfL is correlated with CSF NfL. Scatter plots show unadjusted values. r and p values are unadjusted, generated from Pearson's correlations. NfL values are natural log transformed. PreHD, premanifest Huntington's disease; HD, Huntington's disease; CSF, cerebrospinal fluid; mHTT, mutant huntingtin; NfL, neurofilament light.

4.4.6 NfL has superior discriminatory ability for motor manifestation to mHTT

Receiver operating characteristic (ROC) curves were used to determine the sensitivity and specificity of each analyte in their ability to discriminate between HD mutation carriers and controls, and between manifest and premanifest HD. The area under a ROC curve (AUC) is an indication of a test's accuracy (i.e. discriminatory ability). Varying from 0.5 to 1 where 0.5 indicates a 50% probability of the test giving the correct answer (by chance), while 1 indicates a test that gives the correct answer every time (Lusted, 1971).

In distinguishing between controls and HD mutation carriers, CSF mHTT had essentially perfect accuracy (Figure 19A; AUC=1.000, 95% CI 1.000 - 1.000). CSF and plasma NfL both displayed excellent accuracy (Figure 19A; AUC=0.933, 95% CI 0.876 – 0.989 in CSF and AUC=0.914, 95% CI 0.852 – 0.976 in plasma). The accuracy of NfL was not statistically significantly different in CSF compared to plasma (p=0.364).

In distinguishing between premanifest and manifest HD (i.e. manifestation of motor symptoms), mHTT displayed fair accuracy (Figure 19B; AUC=0.775, 95% CI 0.650 – 0.900). NfL, however, had excellent accuracy in both CSF and plasma (Figure 19B; AUC=0.914, 95% CI 0.831 – 0.996 in CSF and AUC=0.931, 95% CI 0.869 – 0.993 in plasma). Again, the accuracy of NfL was not statistically significantly different between CSF and plasma (p=0.5800), but each was significantly superior to that of CSF mHTT (p=0.0039 for CSF NfL and p=0.0125 for plasma NfL).

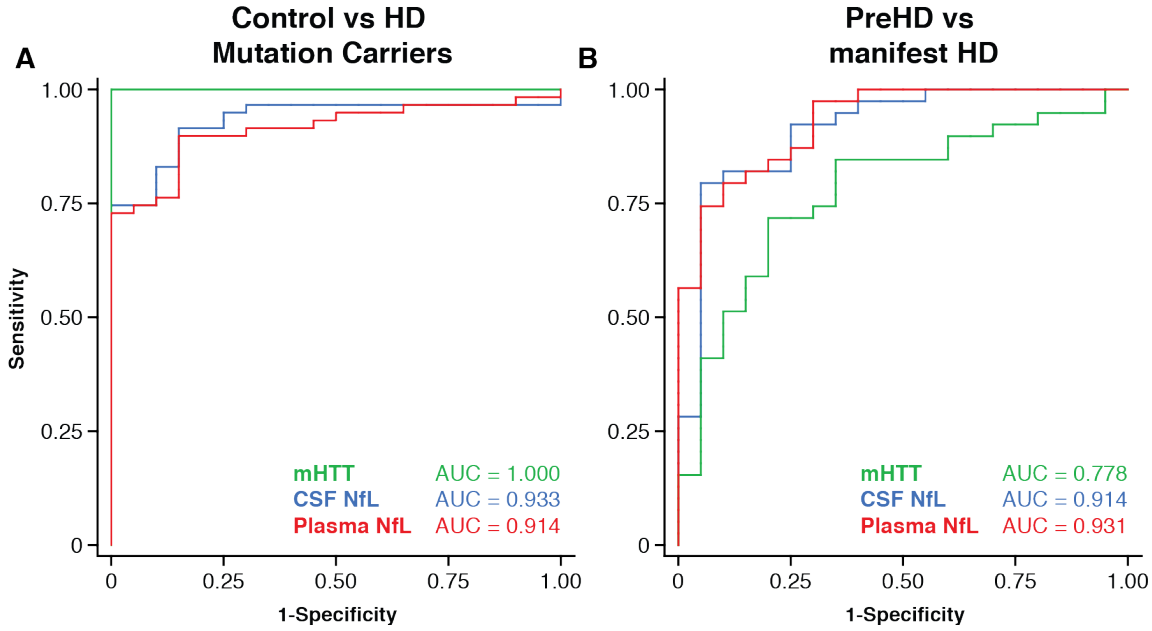

Figure 19 Receiver operating characteristics curves.

A) Discrimination between controls from HD mutation carriers. B) Discrimination between premanifest from manifest in HD mutation carriers. Analysis was performed using natural log transformed NfL values. PreHD, premanifest HD mutation carriers; AUC, area under the curve; CSF, cerebrospinal fluid; mHTT, mutant huntingtin; NfL, neurofilament light.

4.4.7 CSF mHTT, CSF NfL and plasma NfL are highly stable within individuals

To assess intra-individual stability of each analyte, 15 participants (18.8%; 2 controls, 3 premanifest HD and 10 manifest HD) underwent a second sampling visit 4-8 weeks after the first (mean interval 39.1 days), where CSF and blood where collected under the same conditions. They had similar characteristics to those who did not opt to do the repeat sampling (Table 15). The interclass correlation between the first and second sampling visits in this cohort was high for all analytes (CSF mHTT 0.937 (95%CI 0.83 – 0.98); CSF NfL 0.995 (95%CI 0.99 – 1.00); plasma NfL 0.954 (95%CI 0.87 – 0.98); Figure 20).

Table 15 Characteristics of participants who opted in for optional repeated sampling.

Intergroup differences were assessed using unpaired two-sample t-tests (with the exception of gender which was assessed using a 2 by 2 Pearson's chi-squared test). P-values are not adjusted for multiple comparisons. Values are mean ± SD, except where stated otherwise. PreHD, premanifest HD gene-expansion carriers; Manifest HD, manifest HD gene-expansion carriers; CAG, CAG triplet repeat count; N/A, not applicable.

	Optional sampling visit			**No optional sampling visit**			**p-value**		
	Control	**PreHD**	**Manifest HD**	**Control**	**PreHD**	**Manifest HD**	**Control**	**PreHD**	**Manifest HD**
n	2	3	10	18	17	30	N/A	N/A	N/A
Age	52.3 ± 2.4	37.1 ± 1.5	56.2 ± 8.2	50.5 ± 11.6	43.4 ± 11.8	56.0± 9.9	0.8332	0.3764	0.9655
Males (%)	2 (100)	1 (33)	3 (30)	8 (44)	9 (53)	19 (63)	0.136	0.531	0.067
CAG	N/A	42.7 ± 0.6	42.4 ± 1.6	N/A	41.9 ± 1.7	42.9 ± 2.4	N/A	0.4550	0.5647
Disease burden score	N/A	265.0 ± 15.5	378.7 ± 60.5	N/A	267.4 ± 67.2	401.1 ± 103.8	N/A	0.9524	0.5231
Total functional capacity	13.0 ± 0.0	13.0 ± 0.0	9.6 ± 3.5	13.0 ± 0.0	13.0 ± 0.0	9.3 ± 2.5	1.0000	1.0000	0.7905
Total motor score	2.0 ± 0.0	2.0 ± 2.0	35.2 ± 25.8	2.4 ± 2.6	2.9 ± 2.9	38.0 ± 17.2	0.8369	0.6053	0.6938
Symbol digit modalities test	46.0 ± 5.7	61.0 ± 6.2	32.2 ± 11.0	51.4 ± 10.7	54.6 ± 9.6	25.7 ± 12.8	0.4964	0.2835	0.1786
Stroop color naming	69.5 ± 9.2	86.0 ± 18.1	51.0 ± 17.5	76.5 ± 13.4	80.5 ± 8.7	43.9 ± 16.6	0.4872	0.3973	0.2530
Stroop word reading	91.5 ± 26.2	114.3 ± 17.1	68.1 ± 25.2	101.1 ± 16.9	103.4 ± 10.4	56.7 ± 22.8	0.4725	0.1419	0.1901
Verbal fluency categorical	20.5 ± 3.5	24.0 ± 4.4	15.7 ± 6.5	24.7 ± 4.0	23.2 ± 3.4	13.8 ± 5.6	0.1753	0.7115	0.3791
CSF mHTT (fM)	0.0 ± 0.0	41.9 ± 15.7	82.4 ± 32.5	0.0 ± 0.0	47.1 ± 23.1	70.8 ± 27.3	1.0000	0.7122	0.2751
CSF NfL (log pg/mL)	6.8 ± 0.5	7.5 ± 0.2	8.5 ± 0.4	6.7 ± 0.5	7.5 ± 0.8	8.4 ± 0.4	0.8512	0.9356	0.5200
Plasma NfL (log g/mL)	2.8 ± 0.0	3.1 ± 0.3	4.1 ± 0.5	2.9 ± 0.4	3.3 ± 0.6	4.2 ± 0.4	0.8466	0.5051	0.2912

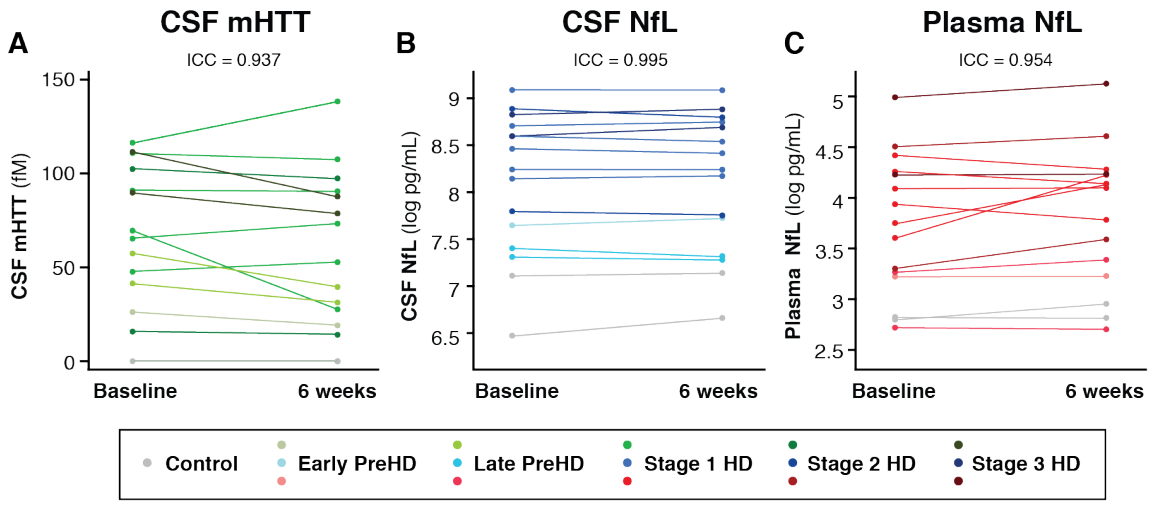

Figure 20 Stability of analyte measures over 6 (± two) weeks.

A) CSF mHTT, B) CSF NfL, C) plasma NfL. Baseline are values for each analyte in samples from the first sample collection and 6 weeks are values for each analyte in samples from the optional repeat sample collection. Lines linking between points indicate the samples from the same individual participant (n=15). NfL values are natural log transformed. ICC, interclass correlation; CSF, cerebrospinal fluid; mHTT, mutant huntingtin; NfL, neurofilament light.

4.4.8 Low sample size would be required to incorporate analytes into clinical trials

To inform the design of clinical trials that may use the lowering of mHTT or NfL as exploratory endpoints, we performed sample size calculations using the repeated measure data from the optional repeat sampling to infer between-subject variability in the change from baseline to 6 weeks and making an assumption that there would be no mean change from baseline to 6 weeks in a placebo group. We show the estimated sample sizes required per arm, for trials in HD mutation carriers for a range of treatment effect sizes (Figure 21). The sample sizes are less than those that would likely be required for the clinical endpoints of such trials (Long et al., 2017b).

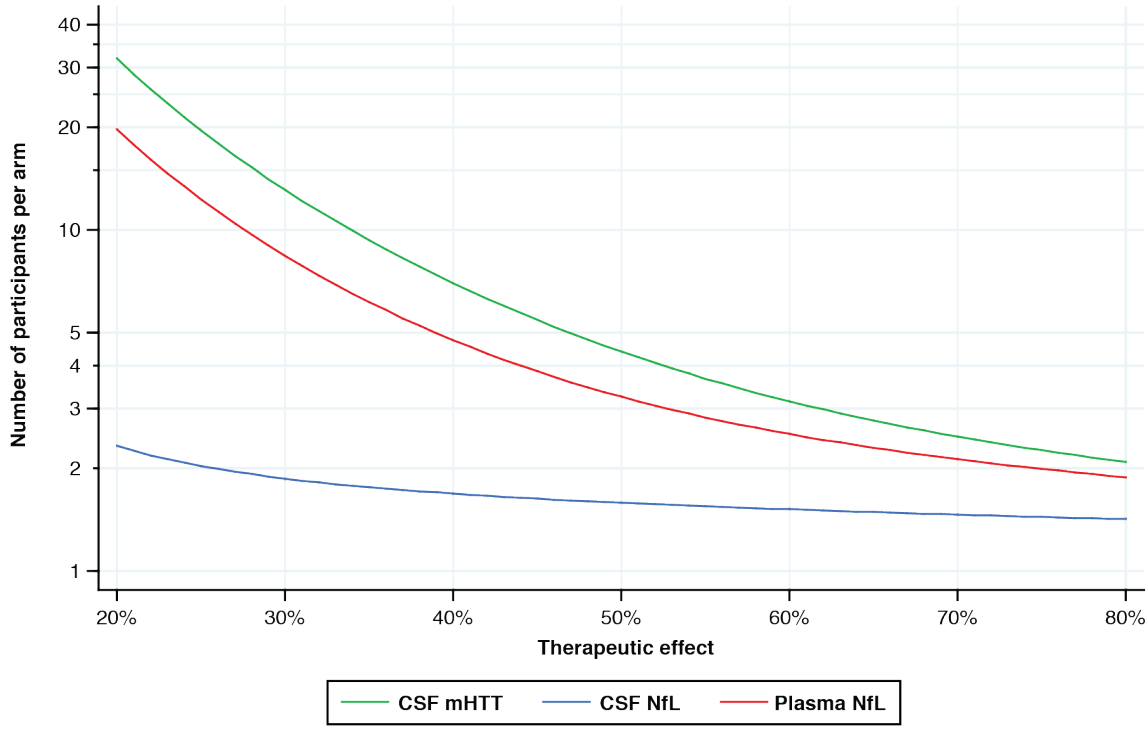

Figure 21 Sample size calculations for clinical trials.

Based on a trial in HD mutation carriers implementing the reduction in these analytes as an outcome measure. Therapeutic effect is based against an age-restricted control group mean, where 100% effect would indicate a reduction to the control mean value. CSF, cerebrospinal fluid; mHTT, mutant huntingtin; NfL, neurofilament light.

4.4.9 mHTT and NfL become detectably abnormal before clinical and brain volume measures

Adapting the previously published EBM (Wijeratne et al., 2018) to the HD-CSF cohort including all biomarkers of interest, the model outputted mHTT as the earliest detectable change, followed by plasma and CSF NfL (Figure 22A,B). This was followed by caudate volume, total motor score, whole-brain, white-matter and grey-matter volume, Symbol digit modalities test, Stroop word reading and Verbal fluency categorical. The model generated from EBM can be assessed by its ability to stage participants based on their individual data for all biomarkers combined. This model accurately characterized all control participants into stage 0, all preHD participants into "low-mid" stage and nearly all manifest HD patients into "mid-late" stages (Figure 22C). Having previously quantified plasma NfL in the baseline samples from TRACK-HD in Chapter 3 (Byrne et al., 2017), we added plasma NfL to the previously published TRACK-HD EBM which included only regional brain volume measures. Plasma NfL, again places early within the temporal sequence – its position between putamen and caudate volume (Figure 23A,B). Putamen volume was not a pre-specified imaging measure in HD-CSF because it is challenging

to quantify reliably and performs poorly as a longitudinal measure of progression. Figure 23C presents the adapted TRACK-HD EBM staging.

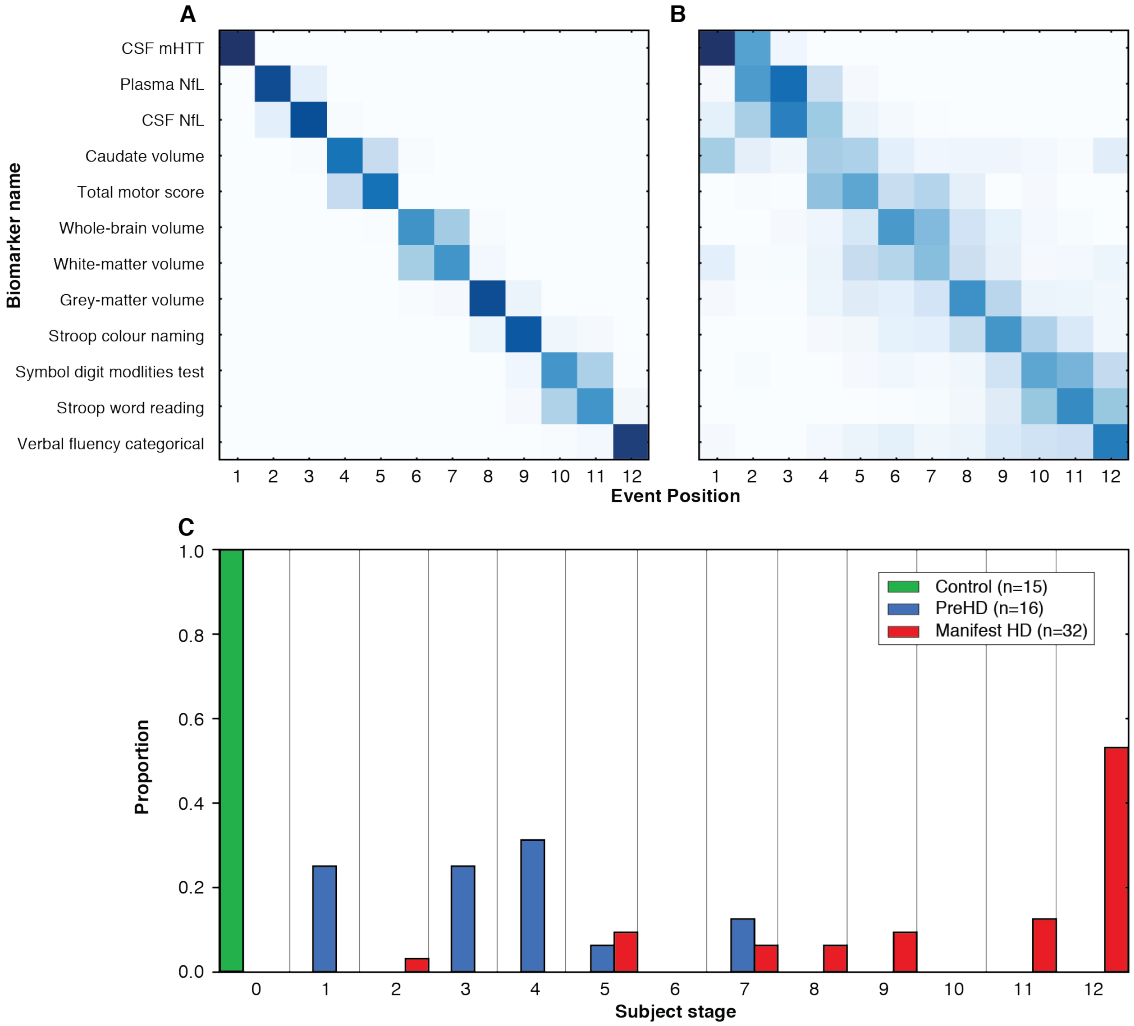

Figure 22 Event-based model in HD-CSF.

All three biofluid biomarkers become abnormal before caudate and global MRI brain volumes and clinical measures. A) The positional variance diagram produced from the event-based model (EBM), adapted from Wijeratne et al 2018 (Wijeratne et al., 2018) and applied to the 63 HD-CSF participants who had data for each of the selected biomarkers (Controls = 15; preHD = 16; manifest HD = 32). B) Re-estimation of the positional variance in A, using 100 bootstrap samples of the data providing internal validation of the model's findings. C) The distribution of HD-CSF participants staged using the HD-CSF EBM, based on their collective data for all 10 biomarkers. The positional variance diagrams represent the biomarker ordering or sequence of events which best fits the respective EBM. Darker diagonal squares represent higher certainty of the biomarker becoming abnormal at the corresponding event where multiple event boxes coloured indicating more uncertainty about its position. 1 indicates the earliest event. Proportion is with respect to each study group: control, preHD and Manifest HD. PreHD, premanifest HD mutation carriers; CSF, cerebrospinal fluid; mHTT, mutant huntingtin; NfL, neurofilament light.

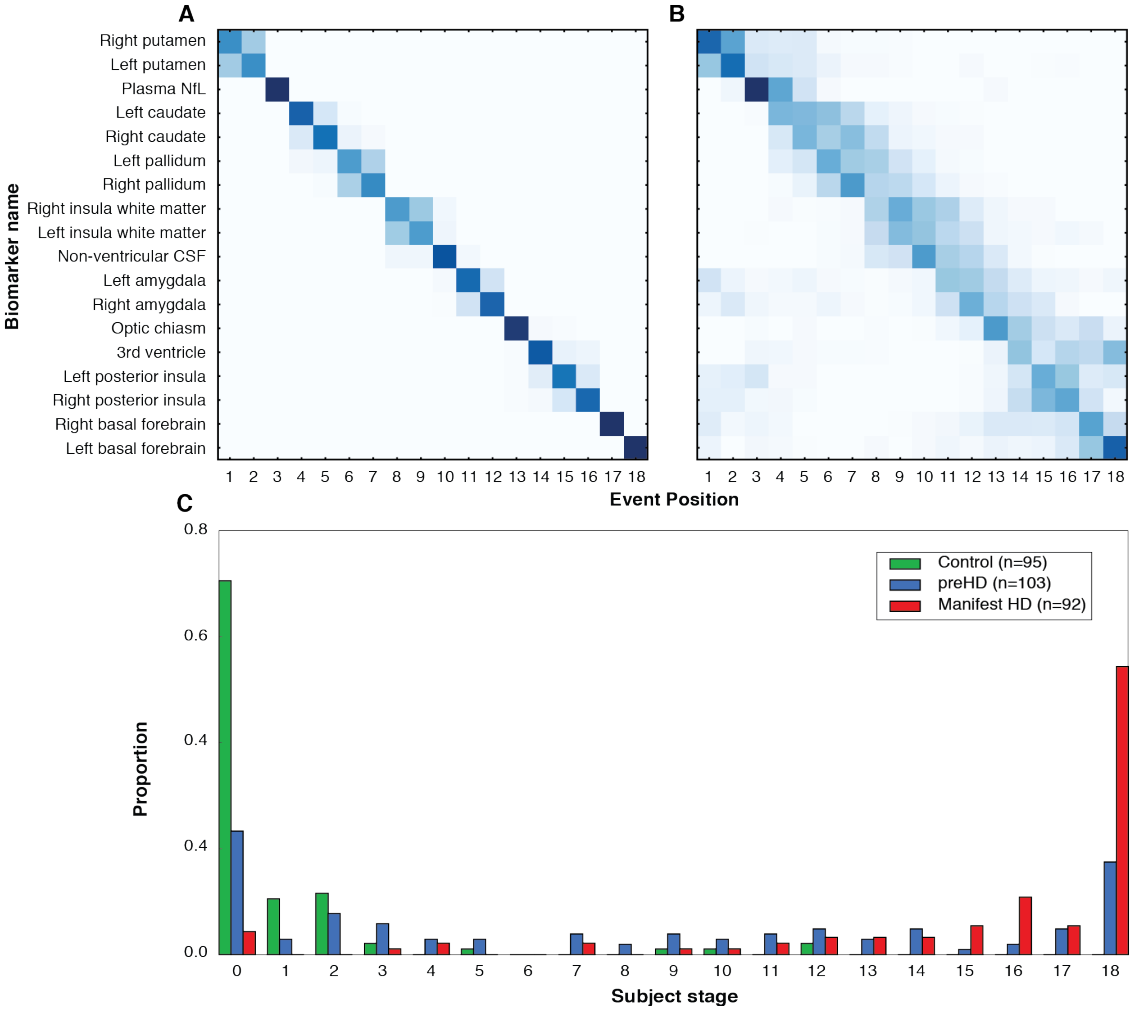

Figure 23 Event-based model in TRACK-HD.

All three biofluid biomarkers become abnormal before caudate and global MRI brain volumes and clinical measures. Plasma NfL was added to the previously published EBM (Wijeratne et al., 2018) using the TRACK-HD cohort where A) shows the positional variance diagram and B the re-estimation of the positional variance in A with 100 bootstrap samples of the data providing internal validation of the model's findings. C) The distribution of TRACK-HD participants staged using the adapted TRACK-HD EBM, based on their collective data for all 18 biomarkers. The positional variance diagrams represent the biomarker ordering or sequence of events which best fits the respective EBM. Darker diagonal squares represent higher certainty of the biomarker becoming abnormal at the corresponding event where multiple event boxes coloured indicating more uncertainty about its position. 1 indicates the earliest event. Proportion is with respect to each study group: control, preHD and Manifest HD. PreHD, premanifest HD mutation carriers; CSF, cerebrospinal fluid; mHTT, mutant huntingtin; NfL, neurofilament light.

4.5 Discussion

4.5.1 Summary

In this cross-sectional analysis of HD mutation carriers and healthy controls from the baseline of the 80-participant HD-CSF study – each having undergone rigorously standardized CSF and blood sample collection, phenotypic assessments and optional supporting MRI acquisition – we provide additional evidence to support two proteins, mHTT and NfL, as biofluid biomarkers for HD. We replicated previous findings that mHTT and NfL increase with worsening disease severity as well as clinical measures of function, motor and cognition (Byrne et al., 2017; Niemelä et al., 2017; Southwell et al., 2015; Wild et al., 2015). Plasma NfL level had the strongest associations with all clinical measures which survived adjustment for HD predictors, age and CAG repeat length. This is the first study in which brain imaging volumes have been examined for association with CSF mHTT or CSF NfL in HD mutation carriers. CSF NfL levels were significantly associated with all brain volume measures, and the associations remained significant after age and CAG adjustment. All three analytes were stable over 6 weeks and would require low sample numbers to incorporate them into clinical trials as exploratory endpoints. The EBM analysis results suggests that these biofluid biomarkers become abnormal very early in the pathological process of HD.

4.5.2 Unwrapping the meaning of biofluid mHTT and NfL alterations

We compared all three markers head-to-head, to investigate their relative associations with clinical, cognitive and imaging measures as well as their discriminatory ability. All associations between NfL, in CSF or plasma, and clinical and imaging measures were stronger than that for mHTT in CSF. This perhaps reflects that NfL, as a marker of axonal damage, has a more direct relationship with the development of clinical manifestations and brain atrophy. On the other hand, mHTT – being upstream to all subsequent pathological events in HD – may be a less direct predictor of clinical severity. However, as the pathogenic agent, quantifying it and studying the effect of reducing it are still of great importance.

The CSF concentrations of mHTT and NfL were closely associated. In turn, the levels of NfL were strongly associated between CSF and plasma, consistent with findings in smaller cohorts examining each association separately (Byrne et al., 2017; Wild et al., 2015). This is in keeping with the likely chain of events that links these biomarkers. mHTT is produced in neurons where it causes damage and ultimately death. Some mHTT is released with the NfL from damaged or dying neurons and enters the CSF, where it can be measured. This has been shown by the increase in CSF mHTT concentration after

experimentally inducing neuronal death with toxins in mice expressing mHTT (Southwell et al., 2015).

The signal obtained by the CSF mHTT immunoassay is influenced by more than simply the concentration of the mHTT. A higher signal read-out is generated by mHTT with longer polyglutamine length and also smaller N-terminal fragments of the protein (Fodale et al., 2017). This reflects the polyglutamine-dependent binding of the MW1 antibody which facilitates the mutant specific signal over non-expanded HTT. Somatic instability of the CAG repeat length is increasingly recognised as a potential driver of pathology in HD (Genetic Modifiers of Huntington's Disease (GeM-HD) Consortium, 2015; Hensman Moss et al., 2017). Further expansion of CAG repeat length in somatic tissue, in addition to varying levels of N-terminal HTT fragments and HTT aggregation, may contribute to the relatively large inter-subject variability in mHTT levels in the CSF. However, these caveats have little implication on CSF mHTT's utility as a pharmacodynamic marker in HTT-lowering trials which involves quantifying within-subject reductions of mHTT. The within-subject reduction in CSF mHTT concentration which occurred within a few months of treatment with the Ionis HTT-Rx ASO (Rodrigues and Wild, 2018; Tabrizi et al., 2019) is most likely due to a decrease in intracellular mHTT concentration without any immediate effect on neuronal death. If continued lowering mHTT in the CNS is neuroprotective we would expect a slowing in the rate of release of mHTT into the CSF from dying neurons. The multiple factors contributing to the concentration of mHTT in CSF mean that, although it will remain of critical importance to huntingtin-lowering trials, an mHTT-independent measure of neuronal damage will be an important means of establishing the effects of CSF mHTT reduction, as well as helping to dissect which factors (cellular mHTT concentration or neuronal damage) are contributing to the reduction in signal.

Neurofilament light in CSF and blood appears to be such a marker. NfL is produced throughout neurons with the bulk of it residing in axons. Its level rises after insults that produce reversible clinical syndromes, such as head injury and multiple sclerosis relapses (Disanto et al., 2017; Novakova et al., 2017; Shahim et al., 2016a, 2014), and irreversible ones such as stroke (Glushakova et al., 2016), indicating that the concentration of NfL reflects the current or recent level of both neuronal damage and/or death from any cause. Levels of NfL in blood and CSF have been reported to increase within two weeks post head trauma (Al Nimer et al., 2015; Shahim et al., 2016a) but upon resolution of the insult decreases in NfL back to a normal range tend to take several months. Our head-to-head findings show for the first time that while CSF mHTT and plasma NfL both reflect clinical state, CSF NfL was generally more closely associated with measures of brain volume in HD, and retained independent associations after CAG-

length adjustment indicating that it reflects historical brain volume loss beyond other known predictors, age and CAG count. This is in keeping with a biomarker that directly reflects ongoing neuronal injury.

The weaker associations of plasma NfL with global brain volume measures compared to CSF NfL, are perhaps unsurprising given that NfL in the periphery is a less direct reflection of neuronal injury. This does not mean that plasma NfL offers no insights into brain atrophy, either historically (brain volume) or prospectively (ongoing brain atrophy). Indeed, we have already shown in the large-scale, longitudinal TRACK-HD cohort that plasma NfL possesses independent prognostic value in predicting global and regional brain atrophy (Chapter 3), suggesting it is a dynamic marker of ongoing neuronal damage (Byrne et al., 2017; Johnson et al., 2018). Global measures of brain volume may not be as sensitive as regional measures such as caudate volume. The strong association between plasma NfL and caudate volume, even after age and CAG adjustment corroborates previous findings from the cross-sectional volumetric-based morphometry analysis (Johnson et al., 2018) and further implicating that plasma NfL has a robust relationship with historical caudate atrophy. Moreover, caudate atrophy is likely contributing to plasma NfL's association with grey-matter volume. The lack of association between CSF mHTT and brain volume may be attributed to the multiple factors contributing to the readout of the mHTT assay. Larger sample sizes would be needed to investigate whether a relationship does in fact exist.

CNS neuronal injury is widely accepted as the source of elevated NfL in blood plasma in neurodegenerative diseases including HD (Byrne et al., 2017; Gisslén et al., 2015; Hansson et al., 2017; Rohrer et al., 2016). While huntingtin-lowering therapeutics currently being tested are intrathecally administered, implying the ready availability of CSF for therapeutic monitoring, orally and intravenously administered therapeutics are under development (Wild and Tabrizi, 2017) for which a biomarker of neuronal rescue in a readily accessible biofluid would be desirable. Moreover, an accessible biomarker reflecting the current rate of neuronal injury could eventually be useful for guiding clinical decisions, such as when to escalate to more invasive CSF monitoring as a first step towards intrathecal treatment. Such uses will require substantial further investigation of the predictive power of NfL in individual patients.

Our ROC analysis revealed there was no statistically significant difference between CSF and plasma NfL in discriminating between disease groups. In its ability to distinguish between controls and HD mutation carriers, CSF mHTT was unsurprisingly superior to both CSF and plasma NfL, driven by the lack of mHTT signal that exists in healthy controls. However, NfL in either CSF or plasma surpassed mHTT in discriminating between preHD and manifest HD mutation carriers (i.e. motor manifestation). One

important caveat here is that while plasma and CSF NfL appear equivalent in tracking the natural history of HD over years of progression, we do not yet know how quickly either might respond to the rapid amelioration of pathology as may occur with sustained huntingtin lowering. It is likely that any such change would first be reflected in CSF before eventually being apparent in plasma. In boxers, serum NfL levels took three months to normalise after a boxing bout (Shahim et al., 2017), which may indicate the most rapid reduction in NfL that may be expected if a therapy truly alleviates neuronal pathology.

Niemela and colleagues, recently reported longitudinal CSF sampling in HD to analyse CSF biomarkers including CSF NfL (Niemelä et al., 2018). However, the follow-up interval between collections varied from one to four years and it was not supported by statistical analysis. To our knowledge, this is the first study of CSF in HD patients with longitudinal sampling over a short time period of four to eight weeks and the first in which the intra-individual stability of each analyte has been assessed. The very high ICC values of the three markers revealed them to be highly stable over four to eight weeks. This suggests that intra-individual variation in these biomarkers is likely to be a minimal source of noise in natural history and therapeutic studies. A proviso here is that each sampling visit in this study was conducted at around the same time of day after an overnight fast. We therefore cannot exclude the possibility that the level of any analyte may be affected by diet or time of day. This is worthy of dedicated study.

Our sample size calculations reveal that fewer than 35 participants per group would be sufficient to detect drug-related alterations in HD mutation carriers for all three markers, even at effect sizes as low as 20%. This is considerably smaller than the cohort sizes currently being enrolled in late phase efficacy trials (NCT03761849, 2019), indicating that NfL or mHTT quantification could be used to support interim or exploratory analyses without significant cost to the sample size requirement (Long et al., 2017b; Paulsen et al., 2006). An important caveat here is that assuming a variability based on within-subject change over 6 weeks may underestimate the variability over the time period of a late-phase efficacy trial. It may also not capture gradual increase due to aging.

We build upon the image-based EBM generated by Wijeratne and colleagues using the TRACK-HD cohort (Wijeratne et al., 2018) which outlined a fine-grained sequential pattern in brain atrophy and a system in which to stage HD mutation carriers based on changes in their brain MRI measures. The unique design of the HD-CSF study – having matched CSF and blood samples, clinical, cognitive and MR imaging data – permits us to explore biofluid biomarkers within this model head to head with neuroimaging modalities as well as the most widely used clinical rating scales. Here we present evidence suggesting that these three biofluid biomarkers, mHTT in CSF and NfL in CSF and plasma, are the earliest biomarkers to become detectably abnormal in HD. After

cross-validation, despite uncertainty increasing, the general pattern remains: CSF mHTT first, then plasma and CSF NfL are interchangeable with caudate volume, a block of total motor score interchangeable with whole-brain and white-matter volume, followed by grey-matter volume, then finally the cognitive scores for Symbol digit modalities test, Stroop word reading, Stroop Color naming and Verbal fluency. A method to stage HD mutation carriers using unbiased biomarkers could allow the field to move away from clinical rating scales to stage patients, overcoming issues with inter-rater variability, subjectivity and large floor/ceiling effects. We were able to further validate these findings for plasma NfL in the larger TRACK-HD cohort, showing plasma NfL is altered between putamen and caudate atrophy with high certainty after cross-validation. Having such a readily accessible measure equivalent to the earliest detectable pathological changes within the striatum, in blood, would be an invaluable tool for the future HD clinic. We hope these biofluid biomarkers will provide a means for stratifying premanifest HD mutation carriers, who have yet to develop overt clinical symptoms, for preventative studies.

4.5.3 Limitations

This study has some limitations that should be acknowledged. First, HD-CSF has relatively small PreHD and control groups as it was designed predominantly as a study of manifest HD. This has limited our ability to determine the earliest point of detection in alterations of both NfL and mHTT in HD mutation carriers. Second, we had no longitudinal data over a longer time interval (at the time of publishing the data in this chapter) to understand how these analytes vary with disease course and compare head-to-head the ability their rates of change to predict disease progression. We also could not assess the longitudinal efficacy of the event based model. However, these points are addressed in a longitudinal analysis performed using the samples and data from the HD-CSF 24-month follow up collection Chapter 5. Third, our study does not include any individuals with juvenile HD. It will be of interest to understand if these individuals display similar or different biomarker profiles. Fourth, for application in clinical decision-making, substantial further investigation of the predictive power of NfL in individual patients will be required. Fifth, sampling visits were conducted at around the same time after an over-night fast. We therefore could not investigate the possibility that these analytes may be affected by diet or time of day. This is worthy of dedicated study. Finally, signals from immunoassays are dependent on the reagents used that may vary between batches or sources. This means that results are most interpretable when used in a single run, within a cohort.

4.5.4 Future directions

Within the HD field there already exists a wealth of human cohorts involving more preHD mutation carriers that could be used to address some of the limitations of this study. Predict-HD followed over 1000 preHD and prodromal HD mutation carriers up to 10 years with blood collections annually and some CSF collections (Paulsen et al., 2014). TrackOn-HD, a follow on from the TRACK-HD study included roughly 200 preHD and prodromal HD with annual blood collection (Langbehn et al., 2019; McColgan et al., 2017). The Kids-HD and Kids-JHD cohorts studied children under the age of 18 that are at-risk for HD with blood samples available (van der Plas et al., 2019). These offer retrospective samples that are invaluable resources to answer crucial questions about how these analytes fluctuate over the lifespan of a HD mutation carrier, at least for plasma NfL. A recently completed study of young adult HD mutation carriers (n=60) and controls (n=60) has included both blood and CSF collections (Zeun et al., 2018). I anticipate the results from this study will help define a point where these biofluid biomarkers become detectably abnormal. Furthermore, the HDClarity study – which is set to be the largest ever collection of both CSF and blood (n=1200), spanning the whole range of HD stages and collecting longitudinally – will eventually supplement all these cohorts and allow a more robust comparison between the performance of CSF and plasma NfL (http://hdclarity.net/). An investigation of batch effects of these immunoassays and samples from the clinic will also be needed to fully understand the real life variability in these analytes and determine their predictive value at the individual level.

4.5.5 Conclusion

In conclusion, we have validated that mHTT in CSF and NfL in CSF and plasma are all increased in PreHD and further rise in manifest HD, and that each is associated with clinical severity. Parallel evaluation of CSF mHTT, CSF NfL, and plasma NfL in the HD-CSF cohort revealed that plasma NfL was most strongly associated with measures of clinical severity and that only NfL was associated with MRI brain volume. Through ROC analysis, we showed that NfL has greater clinical discriminatory ability than mHTT, within HD mutation carriers. All analytes were stable over short intervals, and the sample size numbers required for trials of drugs expected to alter these proteins are attainable within the numbers likely required to show clinical efficacy. Finally, we provide evidence through EBM that these biofluid biomarkers are among the earliest detectable changes as HD progresses. These results suggest that as our understanding grows further, analysis of mHTT and NfL might be useful for developing HD therapeutics and for clinical management.

4.6 Contributions and collaborations

I coordinated the HD-CSF study. I was involved in the final ethical approval of the study and attended the ethics review board meeting with the London - Camberwell St Giles Research Ethics Committee. I recruited all participants, managed all visit bookings, and oversaw sample and data management; I performed data collection including demographic and comorbidities information; I performed all cognitive assessments; I assisted with lumbar punctures; I transported samples for processing; I stored and managed the stock log of all samples; I was coordinated and took part in all meetings discussing study management and data analysis. CSF and blood samples were collected by Dr Filipe Rodrigues. CSF and blood samples were processed by the Fluid Biomarker Lab at UCL Dementia Research Institute. MRI protocol development and data acquisition was performed by Dr Enrico De Vita. MRI processing and segmentations were performed by Dr Rachael Scahill and Dr Eileanoir Johnson.

The project in this chapter was conceived by myself, Dr Wild and Dr Filipe Rodrigues. I coordinated the procurement of a materials transfer agreement and arranged the shipment of CSF samples to Evotec A.G. who performed mHTT quantification. I quantified NfL in both CSF and blood plasma in all the HD-CSF samples. The results were analysed jointly between myself and Dr Filipe Rodrigues. I initiated the analysis of the NfL data and Filipe completed the final analyses of all data. I was directly involved at each stage in the decision making of the analysis plan. I conceived the concept of using EBM to directly compare the biofluid biomarkers with imaging and clinical biomarkers. The EBM analysis was performed by Dr Peter Wijeratne. The sample size calculations were designed collaboratively between myself, Dr Filipe Rodrigues, Dr Edward Wild and Roche co-authors, and performed by a statistician from Roche (Dr Giuseppe Palermo). I was jointly involved in the interpretation of the results with Dr Filipe Rodrigues and Dr Edward Wild. I wrote the first draft of the manuscript and prepared all figures. I prepared the manuscript for submission including the decision to submit to Science Translational Medicine, collating all edits from co-authors and responding to reviewers.

Chapter 5 Longitudinal dynamics of mutant huntingtin and neurofilament light in Huntington's disease natural history: the HD-CSF cohort 24-month follow-up

Here I present the manuscript on the HD-CSF 24-month follow-up analysis of mHTT and NfL, to be submitted for publication. The format is based on the journals requirements and therefore varies from the rest of the thesis.

5.1 Introduction

Despite knowledge of its monogenetic cause, no treatments have been shown to slow neurodegeneration in Huntington's disease (HD; 1.1.4 Treatment and clinical monitoring; The Huntington's Disease Collaborative Research Group, 1993; Travessa et al., 2017). However, as previously mentioned (1.1.5 Current therapeutic candidates), multiple approaches aimed at lowering production of the causative mutant huntingtin protein (mHTT) are in human clinical trials (Rodrigues et al., 2019b; Rodrigues and Wild, 2018; Tabrizi et al., 2019). The ultimate goal – treating mutation carriers early, to prevent disease onset – will require prevention trials in premanifest HD mutation carriers (preHD).

Successful target engagement by the first targeted huntingtin-lowering therapeutic tested in HD patients – the antisense oligonucleotide RG6042 (formerly Ionis-HTTRx) – was demonstrated by dose-dependent mHTT reduction in cerebrospinal fluid (CSF) in a phase 1/2 trial (Tabrizi et al., 2019), quantified by ultrasensitive immunoassay (2.4.1 Ultrasensitive immunoassays; Wild et al., 2015). This notable success led to the first phase 3 trial of such a drug, whose primary outcomes are the Total Functional Capacity (TFC) score of the Unified Huntington's Disease Rating Scale (UHDRS) in the USA, and a composite UHDRS (cUHDRS) measure combining motor, functional, and cognitive scores in the EU (NCT02519036, 2015). I have highlighted already (1.1.5 Current therapeutic candidates) that such clinical rating scales quantify overt clinical manifestations, but lack the sensitivity to detect deterioration, or its therapeutic benefit, in preHD (Mestre et al., 2018d, 2018a, 2018b, 2016). Though clinically relevant, they are also far removed from the core disease mechanism: neuronal injury by the *HTT* gene product. Quantifying biochemical manifestations of neurodegeneration can inform our understanding of pathobiology and the development and testing of novel therapies.

Using ultrasensitive immunoassays (2.4.1 Ultrasensitive immunoassays) applied to CSF and blood in a well-characterised cohort of premanifest and manifest HD mutation carriers, and matched controls, we recently showed that mHTT – the toxic pathogenic protein – and neurofilament light (NfL) – an axonal protein indicative of neuronal injury – are among the earliest detectable changes in HD, and are strongly associated cross-sectionally with baseline measures of clinical severity and brain volume (Chapter 4; Byrne et al., 2018b). In the longitudinal TRACK-HD cohort, we showed that blood NfL independently predicts subsequent onset, clinical progression, and brain atrophy in HD (Chapter 3; Byrne et al., 2017).

One unexpected finding from the phase 1/2 ASO trial was a transient elevation of NfL in CSF around five months after first dose (Tabrizi et al., 2019). In the subsequent open-

label extension of this trial (NCT03342053, 2019), NfL levels rose again then fell in the context of ongoing huntingtin suppression, almost to baseline by month 9 (Ducray et al., 2019). While it remains unexplained mechanistically, this observation attests to the combined value of mHTT and NfL to highlight changes of note in the “undiscovered country” of huntingtin-lowering. It also calls for a more detailed understanding of how these markers change over time throughout the life of mutation carriers.

Here we present the mHTT and NfL findings from the two-year prospective longitudinal HD-CSF study (2.3 HD-CSF), in which an 80-participant cohort of HD mutation carriers and controls underwent clinical assessments, sampling of CSF and plasma, and MR imaging, under strictly standardised conditions. To our knowledge this is the first report of the longitudinal dynamics of CSF mHTT and NfL, studied and compared head-to-head in the natural history of HD. We assessed and compared the ability of the biomarkers at baseline, and their subsequent rates of change, to predict longitudinal progression in clinical and neuroimaging measures. Finally, we performed computational clinical trial simulations to provide insight into how they could be used and combined in the therapeutic context.

5.2 Methods

5.2.1 Study design and participants

HD-CSF was a prospective single-site study with standardised longitudinal collection of CSF, blood and phenotypic data (online protocol: http://hdresearch.ucl.ac.uk/wp-content/uploads/HDCSF-protocol-2015-10-19.pdf). Eighty participants were recruited. At baseline and follow-up timepoints, data and biosamples were collected within a 30-day window. Imaging was optional at both timepoints.

Manifest HD was defined as UHDRS diagnostic confidence level (DCL) of 4 and *HTT* CAG repeat count ≥36. PreHD participants had CAG≥40 and DCL<4. Controls were age- and gender-matched to mutation carriers, with no neurological symptoms/signs. Motor, cognitive and functional status were assessed using the UHDRS from the core Enroll-HD battery. We employed a calibrated iteration of the composite UHDRS (cUHDRS) as the primary multi-domain clinical outcome measure (Trundell et al., 2018).

5.2.2 Study assessments

Baseline assessments were conducted from February 2016 to February 2017 (Byrne et al., 2018b). 24-month (±3 months) follow-up was conducted from January 2018 to January 2019. At baseline, participants were invited to undergo an optional repeat sampling 4-8 weeks after baseline.

Participants were assessed with the UHDRS Total Motor Score, Total Functional Capacity, Symbol Digit Modalities Test, Stroop Word Reading, Stroop Color Naming and Verbal Fluency – Categorical. These were performed at either the screening or an associated Enroll-HD visit (https://www.enroll-hd.org) within the 2 months prior to screening. The cUHDRS was chosen as the primary outcome measure for the analysis of clinical progression as it has favourable signal-to-noise characteristics, encompasses clinical deterioration across multiple relevant domains and has regulatory acceptance as a meaningful measure of HD severity (NCT03761849) (Schobel et al., 2017).

5.2.3 Sample collection and processing

Sample collection and processing were as previously described (Byrne et al., 2018a). All collections were standardised for time of day after overnight fasting, and processed within 30 minutes of collection using standardised equipment. Blood was collected within 10 minutes of CSF and processed to plasma.

5.2.4 Analyte Quantification

CSF and plasma NfL were quantified in duplicate using the Neurology 4-plex B assay on the Simoa® HD-1 Analyzer (Quanterix, USA), per manufacturer's instructions. 4x dilution for blood samples was performed automatically by the HD-1 Analyser and CSF samples were manually diluted 100x in the sample diluent provided prior to loading onto the machine (as per manufacturer's instructions). The limit of detection (LoD) was 0.105pg/mL and lower limit of quantification (LLoQ) 0.500pg/mL. NfL was over the lower level of quantification (LLoQ) in all samples. The intra-assay coefficient of variance (CV) for CSF NfL and plasma NfL was 5.0% and 3.7% respectively. The inter-assay CVs for CSF NfL and plasma NfL were 2.7% and 8.4% respectively. We previously quantified NfL in the same baseline samples using an ELISA (NF-Light®, UmanDiagnostics, Sweden) in CSF and 1-plex Simoa® kit (NF-Light®, Quanterix) in plasma (Byrne et al., 2018b). In both biofluids, agreement between assays was good.

CSF mHTT was quantified in triplicate using the same 2B7-MW1 immunoassay as at baseline (SMC™ Erenna® platform, Merck, Germany) (Wild et al., 2015). The LoD was 8fM and LLoQ 25fM. All control samples were below limit of detection (LoD) of the assay except one subject's baseline re-measured sample. The control with detectable signal was excluded from the analysis due to biological implausibility. 27 (21%) samples were below the LLoQ and were included in subsequent analyses. The intra-assay CV for CSF mHTT were 14.1%. Haemoglobin contamination was quantified using a commercial ELISA (E88-134, Bethyl Laboratories, USA) by Evotec. Only 1 sample (2.186μg/mL) had haemoglobin just over the 2μg/mL recommended threshold (Fodale et al., 2017). We included the one sample which had haemoglobin slightly higher than the recommended threshold in the analysis.

Assays were run using same-batch reagents, blinded to clinical data.

5.2.5 MRI Acquisition

The MRI acquisition protocol was identical to that used at baseline (Byrne et al., 2018b). T1-weighted MRI data were acquired on a single 3T Siemens Prisma scanner using a protocol optimized for this study. The parameters were as follows: Images were acquired using a 3D magnetization-prepared 180 degrees radio-frequency pulses and rapid gradient-echo (MPRAGE) sequence with a repetition time (TR)=2000ms and echo time (TE)=2.05ms. The acquisition had an inversion time of 850ms, flip angle of 8 degrees, matrix size 256x240mm. 256 coronal partitions were collected to cover the entire brain with a slice thickness of 1.0 mm. Parallel imaging acceleration (GeneRalized

Autocalibrating Partial Parallel Acquisition [GRAPPA], acceleration factor [R]=2) was used and 3D distortion correction was applied to all images.

5.2.6 MRI Processing

Predefined regions-of-interest for volumetric analysis included the caudate, white matter, grey matter and whole brain. All baseline volumes were re-calculated at follow-up. Bias correction was performed on all scans prior to processing using the N3 procedure (Sled et al., 1998). All scans, segmentations and registrations underwent visual quality control blinded to group status to ensure successful processing. All T1-weighted scans passed visual quality control check for the presence of significant motion or other artefacts before processing; one scan failed quality control due to the presence of significant motion, meaning that 57 scans were processed. As described previously, a semi-automated segmentation procedure was performed via Medical Image Display Analysis Software (MIDAS)(Freeborough et al., 1997) to generate volumetric regions of the whole-brain and Total Intracranial Volume (TIV) at baseline (Byrne et al., 2018b). Changes in whole-brain and caudate were calculated via the Boundary Shift Integral method (Freeborough and Fox, 1997; Hobbs et al., 2009). The BSI is a semi-automated technique applied within MIDAS that quantifies change over time in regions of interest. For the whole-brain, baseline and follow-up scans were segmented with MIDAS via a morphological segmentor that uses the application of operator-driven thresholds and erosions and dilations to separate brain tissue from the scalp and CSF (Freeborough et al., 1997). The baseline and follow-up scans were then registered using 12 degrees-of-freedom and the BSI metrics were calculated for each participant (Fox and Freeborough, 1997). One scan failed registration and thus was excluded from the measures of whole-brain change.

Caudate volumes were generated using the automated MALP-EM software (Ledig et al., 2015). The caudate regions from this procedure underwent visual quality control and were used to calculate the caudate BSI (CBSI) based on a previously validated procedure (Hobbs et al., 2009). This procedure uses local rigid registrations to align the caudate region between baseline and follow-up scans, with a separate registration for left and right caudate. Measures of caudate change are then calculated between the two time points for each participant. No registrations failed quality control.

Baseline grey/white matter volumes were measured via voxel-based morphometry (Ashburner and Friston, 2000). To calculate grey and white matter change, a fluid-registration approach was applied (Christensen et al., 1996; Hobbs et al., 2010; Tabrizi et al., 2011). Baseline and follow-up scans were registered using fluid registration, which ran for 300 iterations (Freeborough and Fox, 1998). The result of this registration was a

voxel compression map (VCM) for each participant, representing the amount of contraction or expansion required within each voxel to map the follow-up scan to the baseline scan. Baseline grey and white matter regions, segmented as described in Byrne et al. (2018), were convolved with the VCM for each participant to calculate volume change within each tissue class for each participant. Registration failed for three datasets, resulting in the analysis of 55 scan pairs.

Cross-sectional data from the follow-up time point were used to replicate the baseline results. Follow-up whole-brain volume was measured via the semi-automated procedure described at baseline. Follow-up caudate volume was measured by the baseline volume minus the amount of atrophy measured via the CBSI, and follow-up grey and white matter volumes were calculated by subtracting the amount of atrophy from baseline volumes.

5.2.7 Event-based modelling

We used an event-based model (EBM; Fonteijn et al., 2012) to estimate the most likely sequence of biomarker changes and to stage participants at both baseline and follow-up. In brief, the EBM is a probabilistic model of observed data generated by an unknown sequence of biomarker events, where an event is defined as a biomarker transitioning from a normal to an abnormal state. The model learns the biomarker distributions of normality and abnormality directly from data, and hence estimates the most likely sequence of abnormality over the whole population. The EBM has been applied extensively to several progressive neurological diseases, including Alzheimer's disease, multiple sclerosis and HD (Eshaghi et al., 2017; Wijeratne et al., 2018; Young et al., 2014).

We recently developed an EBM for HD biofluid, neuroimaging and clinical biomarkers using baseline data from the HD-CSF cohort (Byrne et al., 2018b). Here we refit the model using baseline data from participants who are present at both baseline and follow-up, and use this model to both test the sequence of events estimated in Byrne et al., (2018b), and to stage participants at both time-points. Specifically, mixture models (Wijeratne et al., 2018) were fit to distributions of healthy control (HC) and manifest HD participants for each biomarker separately. All biomarkers were adjusted for age, sex, and total intracranial volume in the HC cohort at baseline. Following Wijeratne et al. 2018, the fitted mixture models and a uniform prior on the initial stage were used to estimate the maximum likelihood sequence of events, and its uncertainty estimated using Markov Chain Monte Carlo sampling of the posterior. Participants were then staged by their maximum likelihood position in the baseline sequence.

5.2.8 Statistical Analysis

As previously observed (Byrne et al., 2018b, 2017), NfL distributions were right-skewed, therefore log-transformed values were used for analytical purposes. Due to their known effects on HD, all models included age and CAG repeat count as covariates.

Cross-sectional analyses:

To validate previous findings and compare assays, we replicated the cross-sectional analyses from the study baseline (Byrne et al., 2018b), using re-measured baseline data and new 24-month follow-up data. To investigate intergroup differences, we applied generalised linear regression models estimated via ordinary least squares, with analyte concentration as the dependent variable, and group membership, and age as independent variables and then with group membership, age and CAG as independent variables. To study associations in HD mutation carriers between the analytes and clinical or imaging measures we used Pearson's partial correlations adjusted for age and for age and CAG. Bias-corrected and accelerated bootstrapped 95% confidence intervals were calculated for mean differences and correlation coefficients. To understand the discriminatory power of the studied analytes, we produced receiver operating characteristics (ROC) curves for each analyte to differentiate healthy controls from HD mutation carriers, and premanifest from manifest HD and compared areas under the curves (AUC), formally using the method suggested by DeLong and colleagues (DeLong et al., 1988).

Longitudinal modelling:

For modelling analyte trajectories over time generalised mixed effect models were performed, estimated via restricted maximum likelihood, with analyte concentration as the dependent variable. Independent models were developed for healthy controls and HD mutation carriers. Only HD mutation carriers were modelled for mHTT. For CSF mHTT in HD mutation carriers, the model had fixed effects for age and CAG, a random intercept per participant and a random slope for age. A similar model was used for healthy controls for NfL in CSF and plasma. HD mutation carriers were modelled with a second-order fixed effects for age and CAG and random slopes for age were included for both CSF and plasma NfL.

Rates of change simulation:

The longitudinal models above were used to estimate rate of change from simulated data. Model parameters, age and CAG distributions, and sample sizes were mimicked from the HD-CSF cohort. Each simulation was repeated 1,000 times and run

independently for each analyte for each participant subgroup (i.e. healthy controls, premanifest and manifest HD).

Change-point analysis:

Change-point analysis was applied to identify where the trajectory of mutation carriers was most likely to depart from healthy controls (assumed to have 0 fM CSF mHTT). We used an offline Bayesian change-point algorithm to estimate the most likely disease time at which a given biomarker changes from a normal to abnormal state. The algorithm was adapted from (Zhou et al., 2017) and estimates the marginal likelihood that the data over a segment of time is generated by a given underlying model. We explicitly model changes in both the mean and covariance and use a minimally informative prior. The change-point is then inferred by a change in likelihood of the underlying model (Figure 37. As we want to estimate the point of change from normality to abnormality, we use data from all groups (control, preHD, and HD) to fit the model over each time segment.

Prognostic value of baseline values versus rate of change:

Associations of the analytes' baseline values, and of their rates of change, with clinical and imaging changes, were assessed using Pearson's partial correlations adjusted for age, and for age and CAG. Rates of change were computed as the 24-month follow-up value minus the baseline value divided by the follow-up time in years. Bias-corrected and accelerated bootstrapped 95% confidence intervals (95%CI) were calculated for correlation coefficients and mean differences. To further explore clinical prognostic value we divided mutation carriers into nominally "fast" and "slow" progressors at the previously-described cUHDRS minimal clinically important difference for decline (absolute 1.2 point reduction) (Trundell et al., 2018). Intergroup differences were investigated with generalized linear regression estimated via ordinary least squares, with analyte concentration or rate of change as dependent variable, and group membership and age, and then group, age and CAG as independent variables.

Receiver operating characteristics (ROC) curves were produced and areas under the curves (AUC) compared for the ability of analytes' baseline values and rates of change to differentiate healthy controls from mutation carriers, and preHD from manifest HD using the method of DeLong (DeLong et al., 1988).

Clinical trial simulation:

We used the longitudinal trajectory models' parameters to run two-arm virtual clinical trials using Monte Carlo simulations, to assess the impact of duration and sample size on statistical power. We used 1,000 repetitions, a parallel design without attrition or placebo effect, a pseudo-control arm emulating the observed longitudinal trajectories,

and an intervention arm with constant 20% annualized reduction in the analyte of interest. Synthetic datasets were generated using mixed effect models matching the longitudinal models above. Main effects were estimated as inter-arm mean difference in the mean change from baseline, adjusted for CAG using generalized linear models estimated as above.

Data were analysed using StataMP 16 (StataCorp, USA).

5.3 Results

5.3.1 HD-CSF cohort

Seventy-four (92.5%) out of the eighty baseline participants came back for the 24-month follow-up assessments. Three (4%) out of the seventy-four opted out of doing the follow-up lumbar puncture but agreed to blood and phenotypic data collection. Participant disposition and study flow is presented in Figure 24. The full cohort characteristics are presented in Table 16.

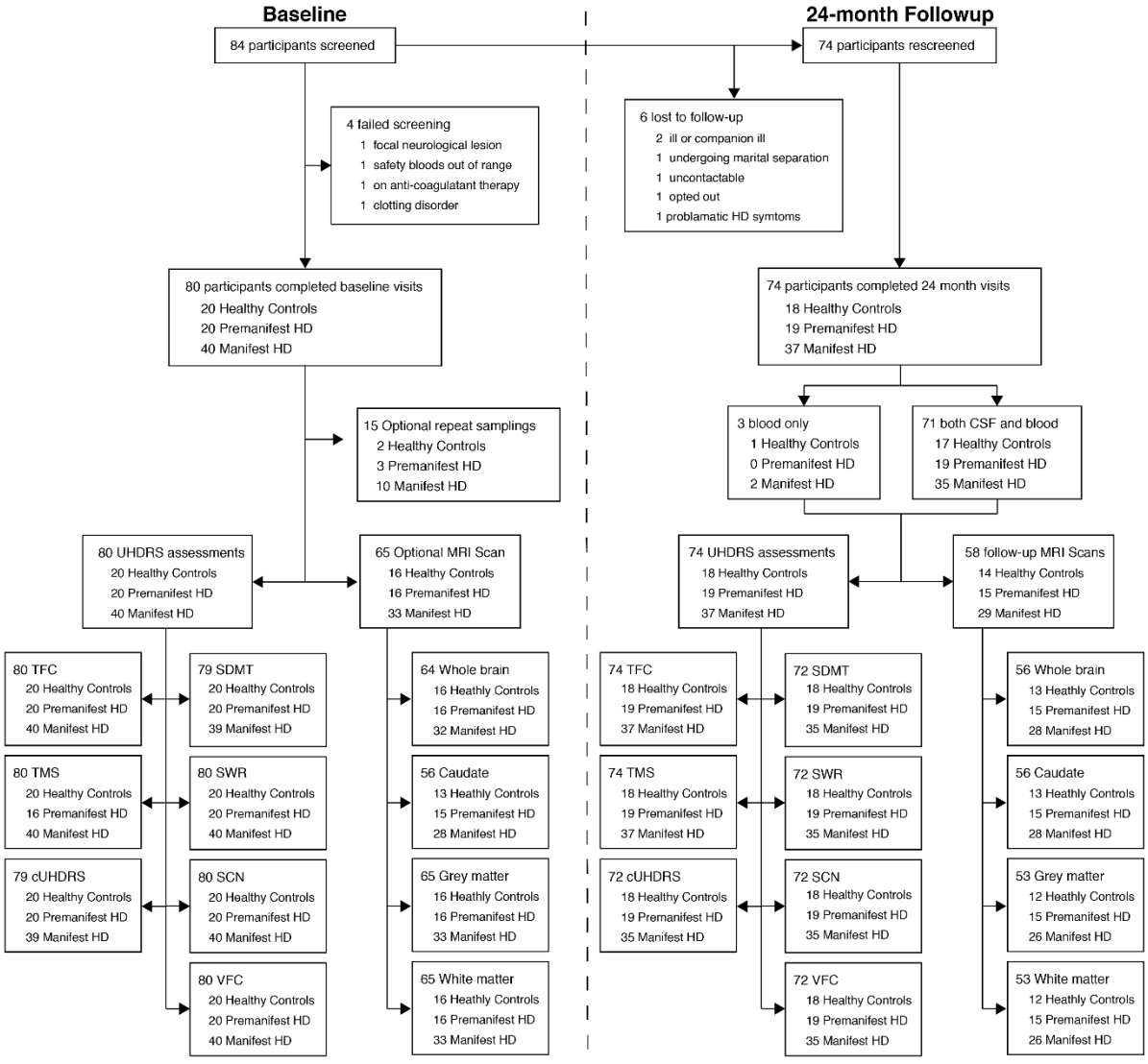

Figure 24 HD-CSF study participant disposition.

Baseline visit (n=80) was performed 24-months (± 3 months) before the follow-up visit (n=74). Optional repeat sampling visits occurred 6-8 weeks after baseline. MRI scans were optional at both baseline (n=65) and follow-up (n=56). At follow-up, 3 out of 74 opted to have blood sampling only. All participants who had sample collections had UHDRS assessments at baseline (80) and follow-up (n=74). Some participants were too advanced to perform all cognitive assessments at baseline (n=1) and follow-up (n=2).

Table 16 Full cohort characteristics at baseline and 24-month follow-up.

CAG, CAG repeat count; CAP, CAG age product score; DBS, Disease Burden Score; cUHDRS, composite Unified Huntington's Disease Rating Scale; mHTT, mutant huntingtin; N/A, not applicable; NfL, neurofilament light; r, Pearson's partial correlation coefficient; SD, standard deviation; SDMT, Symbol Digit Modalities Test; SCN, Stroop Color Naming; SWR, Stroop Word Reading; TFC, UHDRS Total Functional Capacity; TMS, UHDRS Total Motor Score; VFC, Verbal Fluency – Categorical.

Baseline characteristics													
		All Participants			**Controls**			**Premanifest HD**			**Manifest HD**		
		n	**Mean**	**SD**	**n**	**Mean**	**SD**	**n**	**Mean**	**SD**	**n**	**Mean**	**SD**
Demographic													
	Gender	80	F38/M42		20	F10/M10		20	F10/M10		40	F18/M22	
	Age	80	51.27	11.55	20	50.68	11.03	20	42.38	11.04	40	56.02	9.36
Clinical scores													
	CAG	60	42.50	2.03	N/A	N/A	N/A	20	42.00	1.62	40	42.75	2.18
	DBS	60	352.80	104.30	N/A	N/A	N/A	20	267.20	61.92	40	395.60	94.64
	CAP	60	447.50	116.10	N/A	N/A	N/A	20	345.20	73.90	40	498.7	98.41
	TFC	80	11.20	2.62	20	13.00	0.00	20	13.00	0.00	40	9.40	2.70
	TMS	80	20.05	22.34	20	2.35	2.43	20	2.80	2.80	40	37.52	19.43
	cUHDRS	79	14.12	4.509	20	17.40	1.49	20	17.98	1.10	39	10.46	3.57
Cognitive tests													
	SDMT	79	40.39	17.28	20	50.90	10.38	20	55.55	9.32	39	27.23	12.60
	VFC	80	19.04	6.84	20	24.30	4.12	20	23.30	3.42	40	14.28	5.83
	SCN	80	62.10	22.01	20	75.80	13.07	20	81.30	10.12	40	45.65	16.90
	SWR	80	81.08	29.22	20	100.20	17.36	20	105.00	11.75	40	59.55	23.63
Imaging volumes adjusted for total intracranial volume (mL)													
	Whole brain	64	1120.35	92.48	16	1188.00	60.59	16	1187.00	49.59	32	1053.00	71.02
	Caudate volume	56	5.17	1.74	13	7.02	0.79	15	6.07	1.19	28	3.82	1.09
	Grey matter	65	648.10	79.03	16	699.80	55.51	16	709.00	46.38	33	593.50	61.39
	White matter	65	407.25	41.38	16	436.20	34.40	16	430.40	28.14	33	382.00	34.00
Analytes													
	CSF mHTT (fM)	80	33.54	27.16	N/A	N/A	N/A	20	31.82	19.25	40	50.90	21.00
	CSF NfL (pg/mL)	80	1685.42	1264.58	20	410.10	228.50	20	1109.00	679.00	40	2611.00	1051.00
	Plasma NfL (pg/mL)	80	20.19	13.29	20	7.62	2.67	20	12.51	6.22	40	30.32	10.91
24-month follow-up characteristics													
		All Participants			**Controls**			**Premanifest HD**			**Manifest HD**		
		n	**Mean**	**SD**	**n**	**Mean**	**SD**	**n**	**Mean**	**SD**	**n**	**Mean**	**SD**
	Follow-up time (years)	74	1.90	0.14	18	1.89	0.12	19	1.89	0.12	37	1.90	0.16
Demographic													
	Gender	74	F36/M38		18	F8/M10		19	F10/M09		37	F18/M19	
	Age	74	53.32	11.66	18	53.30	10.30	19	44.10	11.29	37	58.07	9.68
Clinical scores													
	CAG	56	42.41	2.07	N/A	N/A	N/A	19	41.89	1.60	37	42.68	2.25
	DBS	56	360.50	108.40	N/A	N/A	N/A	19	272.90	57.55	37	405.60	100.80
	CAP	56	458.70	120.20	N/A	N/A	N/A	19	354.00	69.71	37	512.40	104.40
	TFC	74	10.49	3.45	18	13.00	0.00	19	12.89	0.32	37	8.03	3.40
	TMS	74	23.91	27.07	18	1.89	2.25	19	3.53	2.55	37	45.08	23.63
	cUHDRS	72	13.50	5.50	18	17.62	1.55	19	18.12	1.50	35	8.86	4.20
Cognitive tests													
	SDMT	72	40.10	20.02	18	52.56	11.05	19	58.58	10.05	35	23.66	13.09
	VerbFlu	72	18.94	8.19	18	24.94	5.09	19	24.79	5.01	35	12.69	5.95
	SCN	72	60.22	24.54	18	78.33	13.33	19	79.53	10.78	35	40.43	17.93
	SWR	72	77.92	33.39	18	101.40	15.95	19	104.50	19.00	35	51.43	24.55
Imaging volumes adjusted for total intracranial volume (mL)													
	Whole brain	56	1115.64	95.93	13	1199.00	52.22	15	1179.00	52.59	28	1043.00	71.26
	Caudate volume	56	4.98	1.81	13	7.00	0.71	15	5.86	1.18	28	3.57	1.13
	Grey matter	53	655.11	79.64	12	714.60	41.74	15	711.90	45.29	26	594.90	62.25
	White matter	53	401.36	41.54	12	432.20	30.62	15	423.10	23.46	26	374.60	37.17
Analytes													
	CSF mHTT (fM)	70	35.46	29.95	N/A	N/A	N/A	18	31.34	11.88	35	54.80	26.96
	CSF NfL (pg/mL)	71	2075.38	1859.97	17	581.10	448.70	19	1151.00	530.30	35	3303.00	1932.00
	Plasma NfL (pg/mL)	74	23.83	17.70	18	9.51	4.91	19	14.80	7.07	37	35.44	17.75

Disease groups were well-matched for gender but differed in HD clinical, cognitive and imaging measures (Byrne et al., 2018b). As expected, age differed significantly between groups due to the control group (50.68 years ± 11.0) being matched to all HD mutation carrier and manifest HD (56.02 years ± 9.36) being definitively more advanced in their disease course than preHD (42.38 years ± 11.04). As we showed in the baseline paper.

5.3.2 Technical validation of cross-sectional baseline results across assays

CSF mHTT, CSF NfL and plasma NfL were re-measured in baseline samples using the same methods used for the follow-up samples in order to perform the longitudinal analysis. Comparing the re-measured values with those previously published at baseline, we found that batch or storage effects did not affect our samples (Figure 25A-C).

For CSF mHTT the same assay was used (2B7-MW1 immunoassay) and measurements were strongly correlated (r=0.92, 95% CI 0.88 to 0.94; (Figure 25D) and the interclass correlation (ICC) between measurements were high (ICC=0.93, 95% CI 0.81 to 0.92). The mean difference between measurements was 19.29fM (95% CI -9.21 to 54.50). In baseline CSF, NfL measurements using the NF-Light® ELISA and Neurology 4-plex assay were strongly correlated (r=0.97, 95% CI 0.96 to 0.98; (Figure 25E)) and the ICC between measurements were high (ICC=0.96, 95% CI 0.89 to 0.95). The mean difference between measurements was 0.02 pg/mL (95% CI -0.44 to 0.92). In baseline plasma, NfL measurements using the NF-Light® Simoa singleplex assay and Neurology 4-plex assay were strongly correlated (r=0.99, 95% CI 0.97 to 0.99; (Figure 25F) and the ICC between measurements were high (ICC=0.83, 95% CI 0.58 to 0.79). The mean difference between measurements was 0.88 pg/mL (95% CI 0.32 to 1.46).

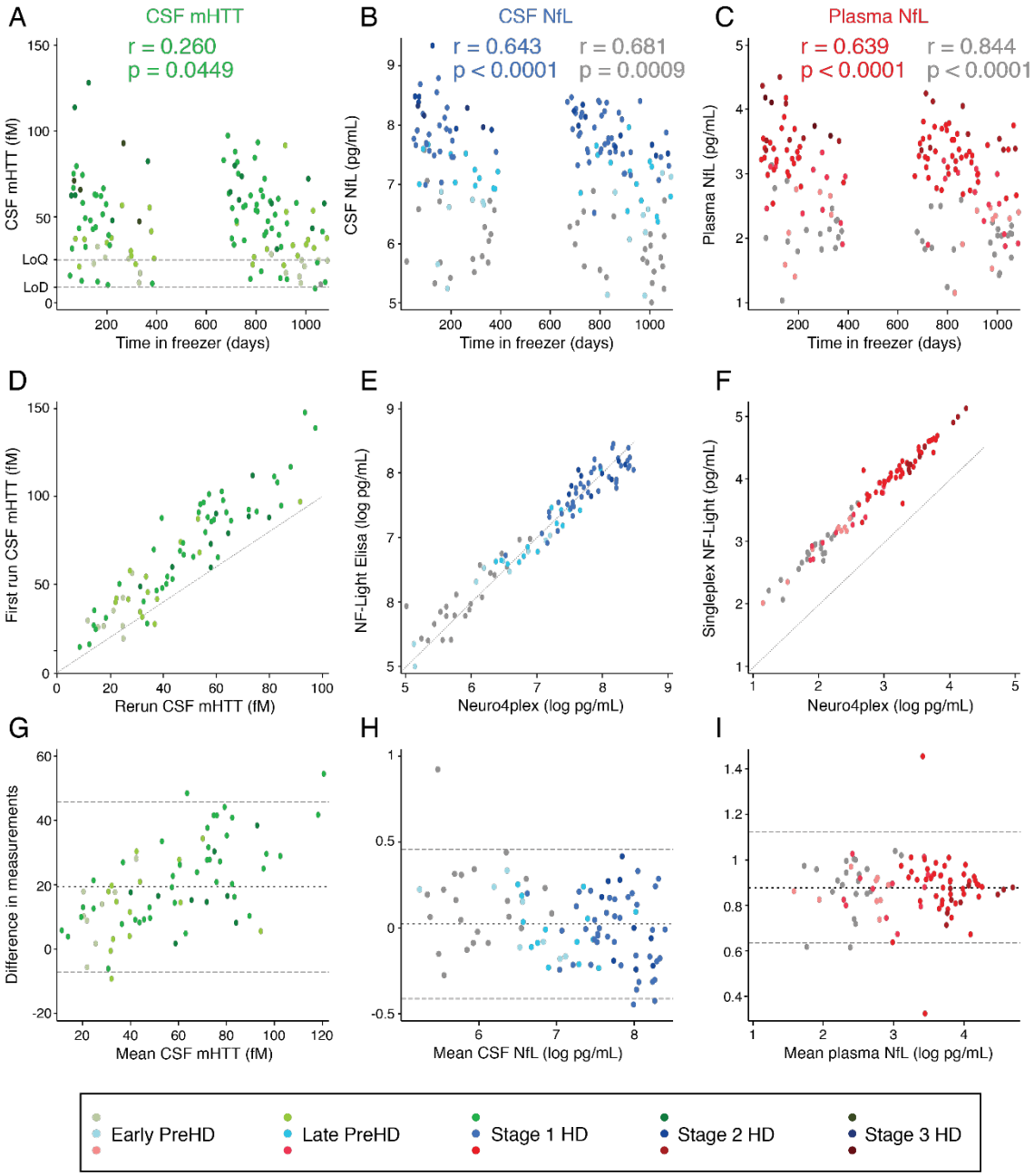

Figure 25 Comparison of re-measurement of baseline samples.

(A-C) There is no association with time in freezer and any analyte. (D-E) Associations between repeated baseline measurements for CSF mHTT (green; D, G), CSF NfL (blue; B, E) and plasma NfL (red; C, F) within controls (N=20 and HD mutation carriers (N=60). (G-I) Bland–Altman Plots for re-measurement of baseline samples. The difference between the two measurements is plotted against the mean of the two measurements. Mean difference is represented by the black solid horizontal line. The upper and lower 95% confidence intervals are designated with dotted horizontal lines. Each point represents one participant. NfL values are natural log transformed. ICC, intraclass correlation; PreHD, premanifest Huntington's disease; HD, Huntington's disease; CSF, cerebrospinal fluid; mHTT, mutant huntingtin; NfL, neurofilament light.

Confident that the re-measured values were consistent with baseline measures and could be used interchangeably, we went on to use the re-measured data to replicate our previously published cross-sectional findings (Chapter 4; Byrne et al., 2018b). This included each analytes' inter-group differences (Figure 26); associations with clinical and imaging measures (Figure 27, Figure 28); ROC curves and AUC analysis (Figure 29A,B);

correlations between analytes (Figure 29C,D) and the EBM (Figure 29E,F). All results for NfL were similar to that previously published. For CSF mHTT, the re-measured values had stronger associations with clinical measures and, where it previously lacked association with brain volume, the re-measured values now showed associations (Table 17).

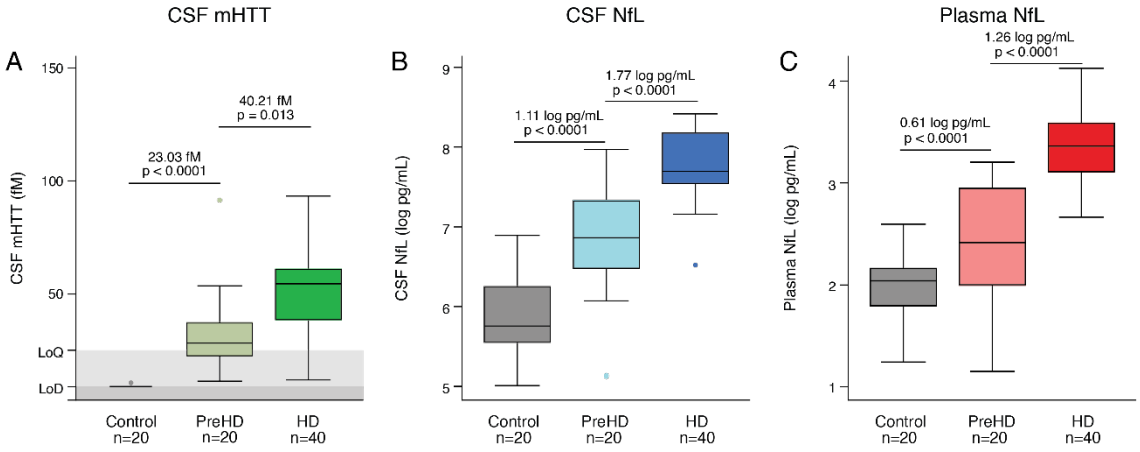

Figure 26 Cross-sectional disease group comparisons in re-measured baseline samples.

Concentration of (A) CSF mHTT, (B) CSF NfL, (C) plasma NfL in healthy controls, premanifest HD (PreHD) and manifest HD (HD) patients. NfL values are natural log transformed. P values were generated from multiple linear regression. PreHD, premanifest Huntington's disease; HD, Huntington's disease; CSF, cerebrospinal fluid; mHTT, mutant huntingtin; NfL, neurofilament light.

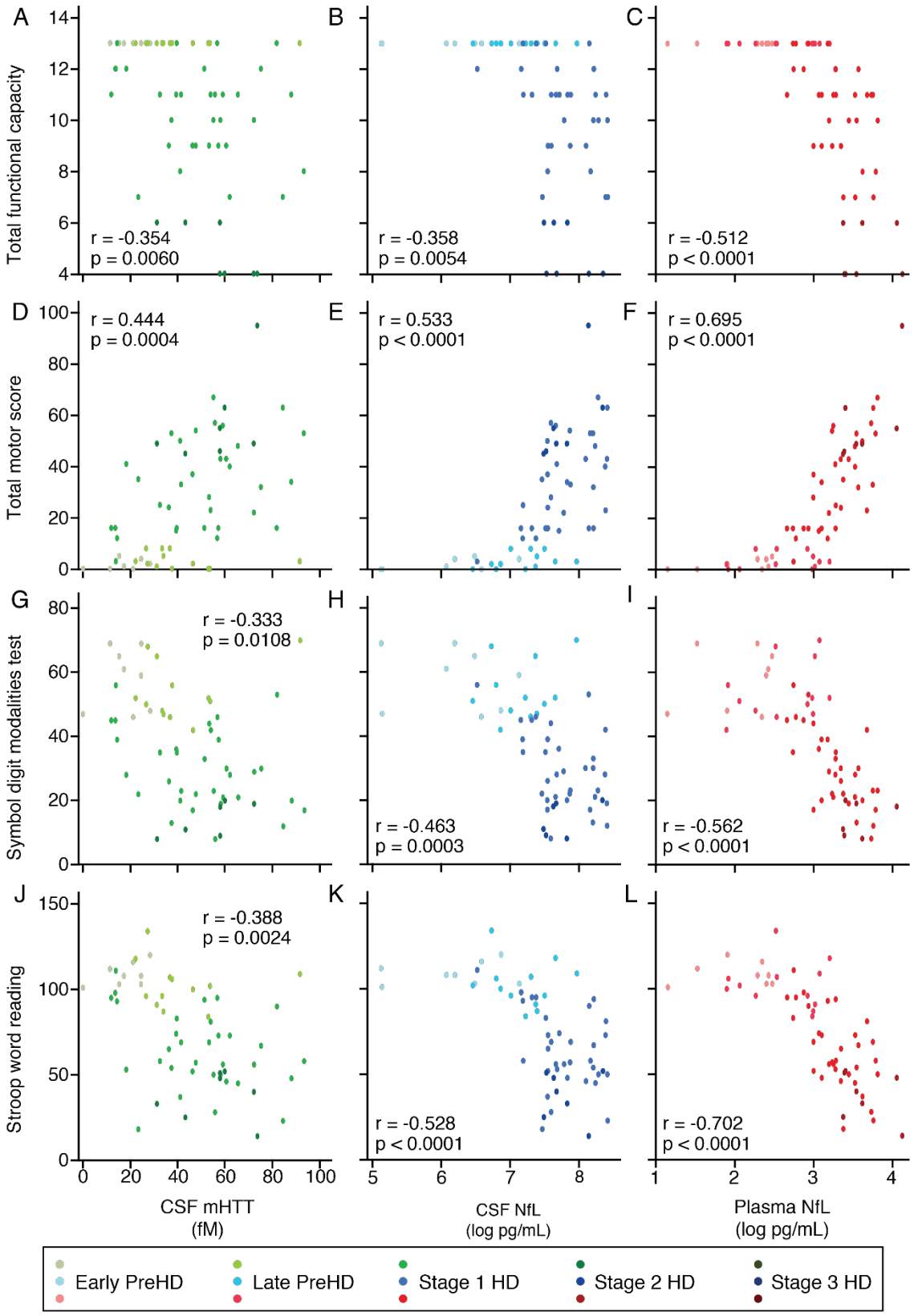

Figure 27 Cross-sectional clinical associations in re-measured baseline samples.

Association within HD mutation carriers (N=60) between CSF mHTT (green; A, D, G, J), CSF NfL (blue; B, E, H, K), plasma NfL (red; C, F, I, L) and UHDRS clinical scores including functional (A-C), motor (D-F) and cognitive (G-L) measures. Scatter plots show unadjusted values. r and p values are age-adjusted, generated from Pearson's partial correlations including age as a covariate. NfL values are natural log transformed. UHDRS Unified Huntington's disease rating scale; PreHD, premanifest Huntington's disease; HD, Huntington's disease; CSF, cerebrospinal fluid; mHTT, mutant huntingtin; NfL, neurofilament light.

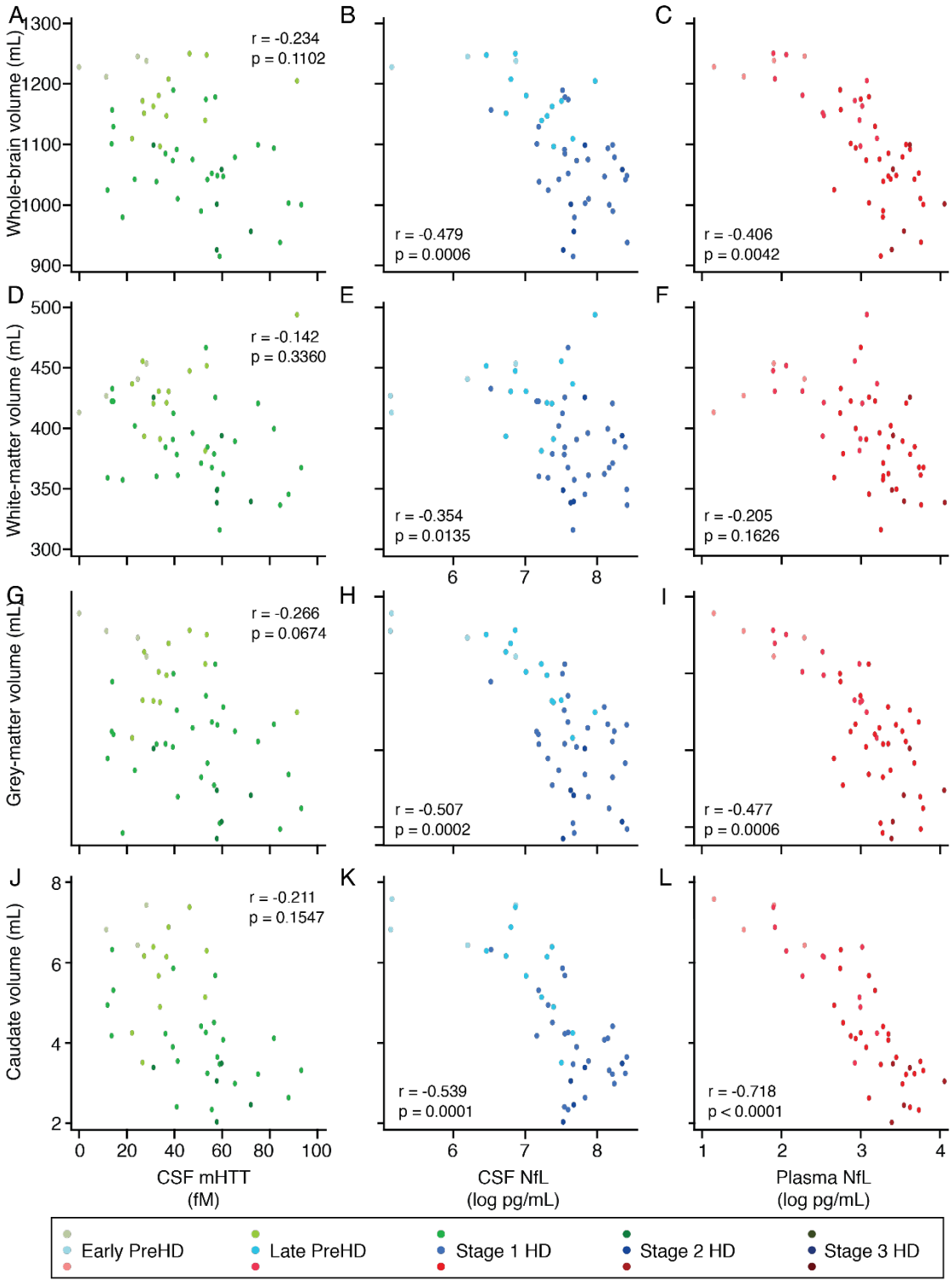

Figure 28 Cross-sectional associations in re-measured baseline samples between analyte concentrations and imaging measures.

Association within HD mutation carriers between the analytes CSF mHTT (green; A, D, G, J), CSF NfL (blue; B, E, H, K), plasma NfL (red; C, F, I, L) and MRI volumetric measures whole-brain (N=48; A-C), white-matter (N=49; D-F), grey-matter (N=49; G-I) and caudate (N=43; J-L). All volumetric measures were calculated as a percentage of total intracranial volume. Scatter plots show unadjusted values. r and p values are age-adjusted, generated from Pearson's partial correlations including age as a covariate. NfL values are natural log transformed. PreHD, premanifest Huntington's disease; HD, Huntington's disease; CSF, cerebrospinal fluid; mHTT, mutant huntingtin; NfL, neurofilament light.

Table 17 Re-measured baseline cross-sectional correlations between analytes and clinical and imaging measures.

(A) adjusted for age and (B) for age and CAG repeat count. 95% confidence intervals are bias-corrected accelerated. CSF, cerebrospinal fluid; cUHDRS, composite Unified Huntington's Disease Rating Scale; mHTT, mutant huntingtin; NfL, neurofilament light; r, Pearson's partial correlation coefficient; SDMT, Symbol Digit Modalities Test; SCN, Stroop Color Naming; SWR, Stroop Word Reading; TFC, UHDRS Total Functional Capacity; TMS, UHDRS Total Motor Score; VFC, Verbal Fluency – Categorical.

A

	CSF mHTT					**CSF NfL**					**Plasma NfL**				
	n	r	95% confidence interval		p-value	n	r	95% confidence interval		p-value	n	r	95% confidence interval		p-value
TFC	59	-0.36	-0.54	-0.13	0.001	60	-0.32	-0.49	-0.13	.001	60	-0.54	-0.70	-0.33	<0.001
TMS	59	0.47	0.18	0.63	<0.001	60	0.52	0.34	0.66	<0.001	60	0.71	0.55	0.81	<0.001
SDMT	58	-0.38	-0.60	0.00	0.008	59	-0.46	-0.65	-0.16	<0.001	59	-0.58	-0.73	-0.36	<0.001
SCN	59	-0.42	-0.61	-0.19	<0.001	60	-0.50	-0.66	-0.30	<0.001	60	-0.67	-0.78	-0.52	<0.001
VFC	59	-0.43	-0.62	-0.13	<0.001	60	-0.41	-0.59	-0.19	<0.001	60	-0.61	-0.75	-0.43	<0.001
SWR	59	-0.43	-0.63	-0.13	<0.001	60	-0.48	-0.64	-0.28	<0.001	60	-0.71	-0.81	-0.56	<0.001
cUHDRS	58	-0.43	-0.63	-0.12	0.001	59	-0.49	-0.67	-0.28	<0.001	59	-0.68	-0.79	-0.51	<0.001
Whole Brain	47	-0.31	-0.58	0.07	0.054	48	-0.35	-0.58	-0.09	.004	48	-0.51	-0.67	-0.29	<0.001
Grey Matter	48	-0.32	-0.57	0.06	0.043	49	-0.43	-0.59	-0.19	<0.001	49	-0.52	-0.66	-0.33	<0.001
White Matter	48	-0.23	-0.56	0.23	0.234	49	-0.10	-0.39	0.24	.528	49	-0.29	-0.53	0.00	0.033
Caudate	42	-0.54	-0.73	-0.31	<0.001	43	-0.58	-0.75	-0.38	<0.001	43	-0.79	-0.87	-0.64	<0.001

B

	CSF mHTT					**CSF NfL**					**Plasma NfL**				
	n	r	95% confidence interval		p-value	n	r	95% confidence interval		p-value	n	r	95% confidence interval		p-value
TFC	59	-0.07	-0.31	0.21	0.613	60	-0.01	-0.27	0.24	0.965	60	-0.32	-0.54	-0.07	.006
TMS	59	0.17	-0.10	0.39	0.159	60	0.25	0.00	0.53	0.074	60	0.54	0.28	0.74	<0.001
SDMT	58	-0.04	-0.33	0.38	0.834	59	-0.17	-0.47	0.14	0.295	59	-0.34	-0.62	-0.05	.019
SCN	59	-0.11	-.037	0.16	0.405	60	-0.22	-0.49	0.05	0.108	60	-0.47	-0.69	-0.20	<0.001
VFC	59	-0.12	-0.37	0.18	0.388	60	-0.08	-0.42	0.18	0.611	60	-0.37	-0.64	-0.09	.013
SWR	59	-0.10	-0.36	0.22	0.490	60	-0.18	-0.48	0.09	0.229	60	-0.53	-0.74	-0.29	<0.001
cUHDRS	58	-0.09	-.38	.25	0.578	59	-0.18	-0.47	0.12	0.237	59	-0.47	-0.70	-0.19	<0.001
Whole Brain	47	-0.10	-0.36	0.19	0.457	48	-0.19	-0.58	0.12	0.314	48	-0.41	-0.73	-0.10	.015
Grey Matter	48	-0.20	-0.42	0.01	0.062	49	-0.35	-0.71	-0.05	0.043	49	-0.46	-0.76	-0.17	.005
White Matter	48	-0.10	-0.40	0.35	0.587	49	0.01	-0.37	0.31	0.948	49	-0.22	-0.54	0.04	.131
Caudate	42	-0.25	-0.52	-0.02	0.052	43	-0.31	-0.54	-0.05	0.013	43	-0.65	-0.82	-0.42	<0.001

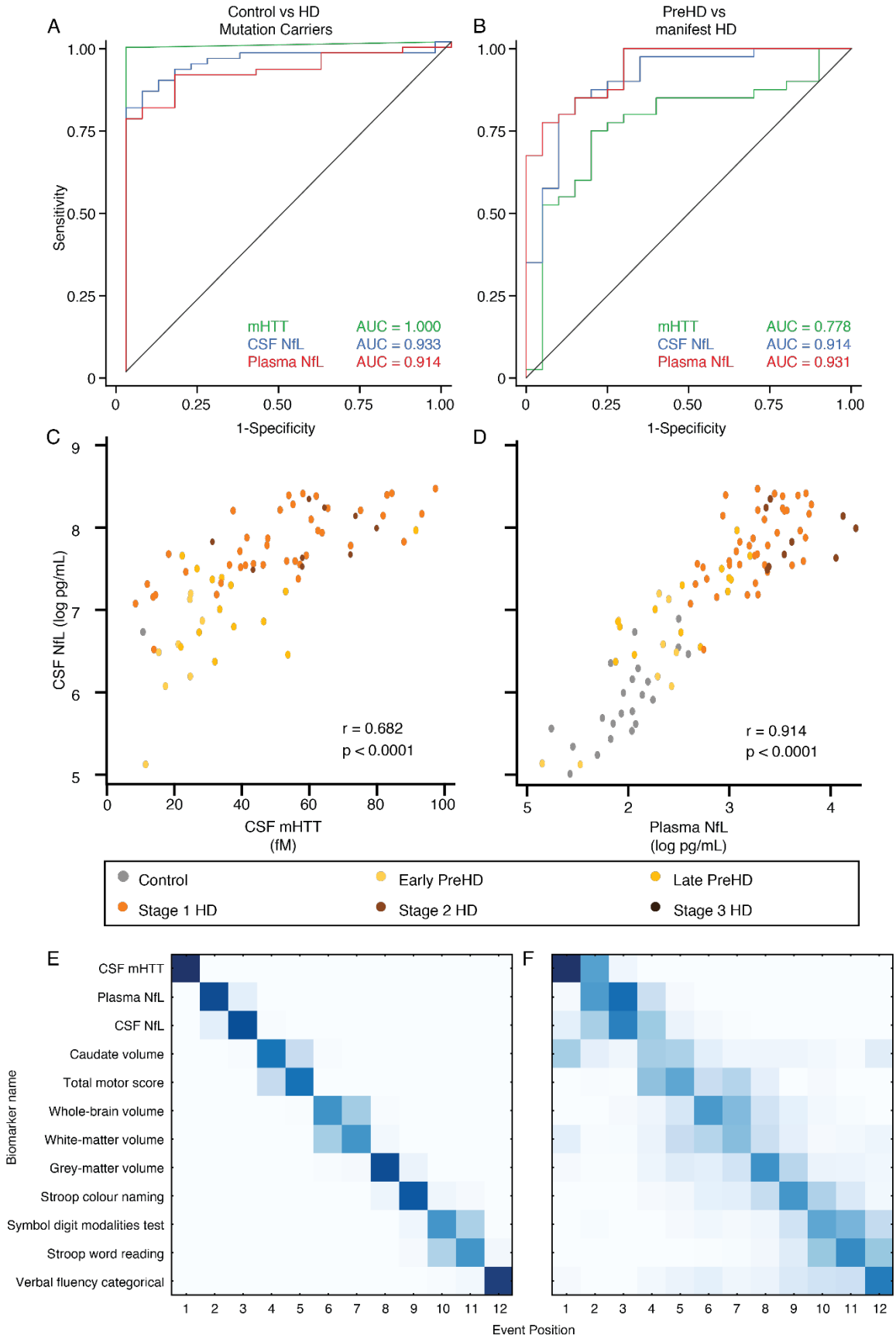

Figure 29 Receiver Operating Characteristics (ROC) analysis, analyte correlations and Event-Based Modelling (EBM) in re-measured baseline samples.

ROC curves for the (A) discrimination between controls (N=20) and HD mutation carriers (N=60) (95% CIs for AUCs: CSF mHTT 1.000 – 1.000; CSF NfL 0.894 – 0.994; Plasma NfL 0.855 – 0.977) and (B) discrimination between premanifest (N=20) and manifest HD mutation carriers (N=40) (95% CIs for AUCs: CSF mHTT 0.628 – 0.896; CSF NfL 0.819 – 0.988; Plasma NfL 0.887 – 0.996). Scatter plots showing correlation between CSF mHTT

and CSF NfL concentration (C, N=60) and between CSF NfL and Plasma NfL (D, N=80). Scatter plots show unadjusted values. r and p values are unadjusted, generated from Pearson's correlations. (E) Positional variance diagram produced from the, applied to the 63 HD-CSF participants who had data for all biomarkers (Controls 13; preHD 15; manifest HD 27). (F) Re-estimation of the positional variance in E, using 100 bootstrap samples of the data, providing internal validation of the model's findings. The positional variance diagrams represent the sequence of "events" (the individual measures going from normal to abnormal, identified by the EBM). Darker diagonal squares represent higher certainty of the biomarker becoming abnormal at the corresponding event where multiple event boxes coloured indicating more uncertainty about its position. 1 indicates the earliest event. NfL values were natural-log transformed. AUC, area under the curve; PreHD, premanifest HD mutation carriers; CSF, cerebrospinal fluid; mHTT, mutant huntingtin; NfL, neurofilament light.

5.3.3 Replication of cross-sectional results in follow-up data

We next used the samples and data from the 24-month follow-up to replicate our previously published cross-sectional findings (Chapter 4) and the re-measured baseline findings. This included each analytes inter-group differences (Figure 30) associations with clinical and imaging measures (Figure 31, Figure 32), ROC curves and AUC analysis (Figure 33A,B); correlations between analytes (Figure 33C,D) and EBM (Figure 33E,F). All results for NfL were similar to that previously published and to the re-measured baseline data. For CSF mHTT, we replicated the stronger associations with clinical measures and brain volumes that the re-measured baseline values showed (Table 17). Our data-driven event-based model for staging participants based on the totality of their baseline data was validated longitudinally, showing that at follow-up nearly all participants had an EBM stage greater than or equal to the baseline EBM (Figure 34).

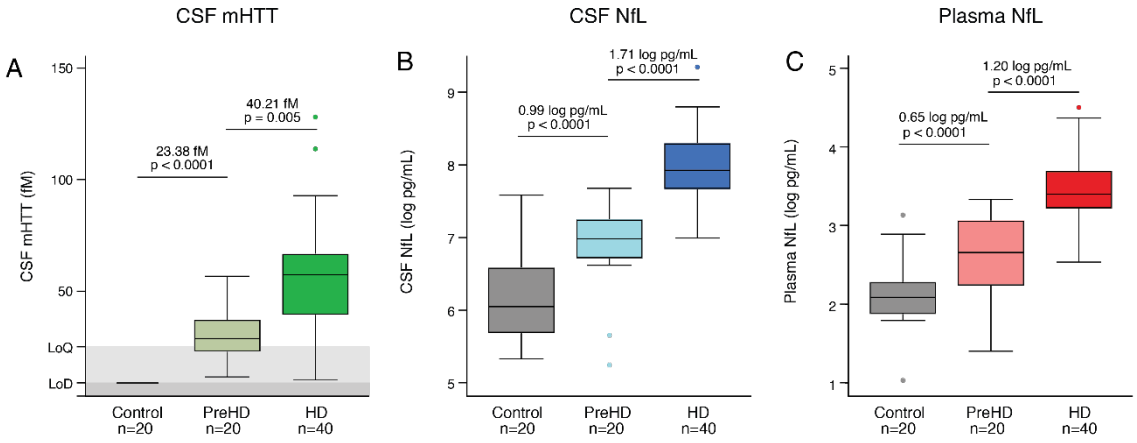

Figure 30 Cross-sectional disease group comparisons in 24-month follow-up samples.

Concentration of (A) CSF mHTT, (B) CSF NfL, (C) plasma NfL in healthy controls, premanifest HD (PreHD) and manifest HD (HD) patients. NfL values are natural log transformed. P values were generated from multiple linear regression. PreHD, premanifest Huntington's disease; HD, Huntington's disease; CSF, cerebrospinal fluid; mHTT, mutant huntingtin; NfL, neurofilament light.

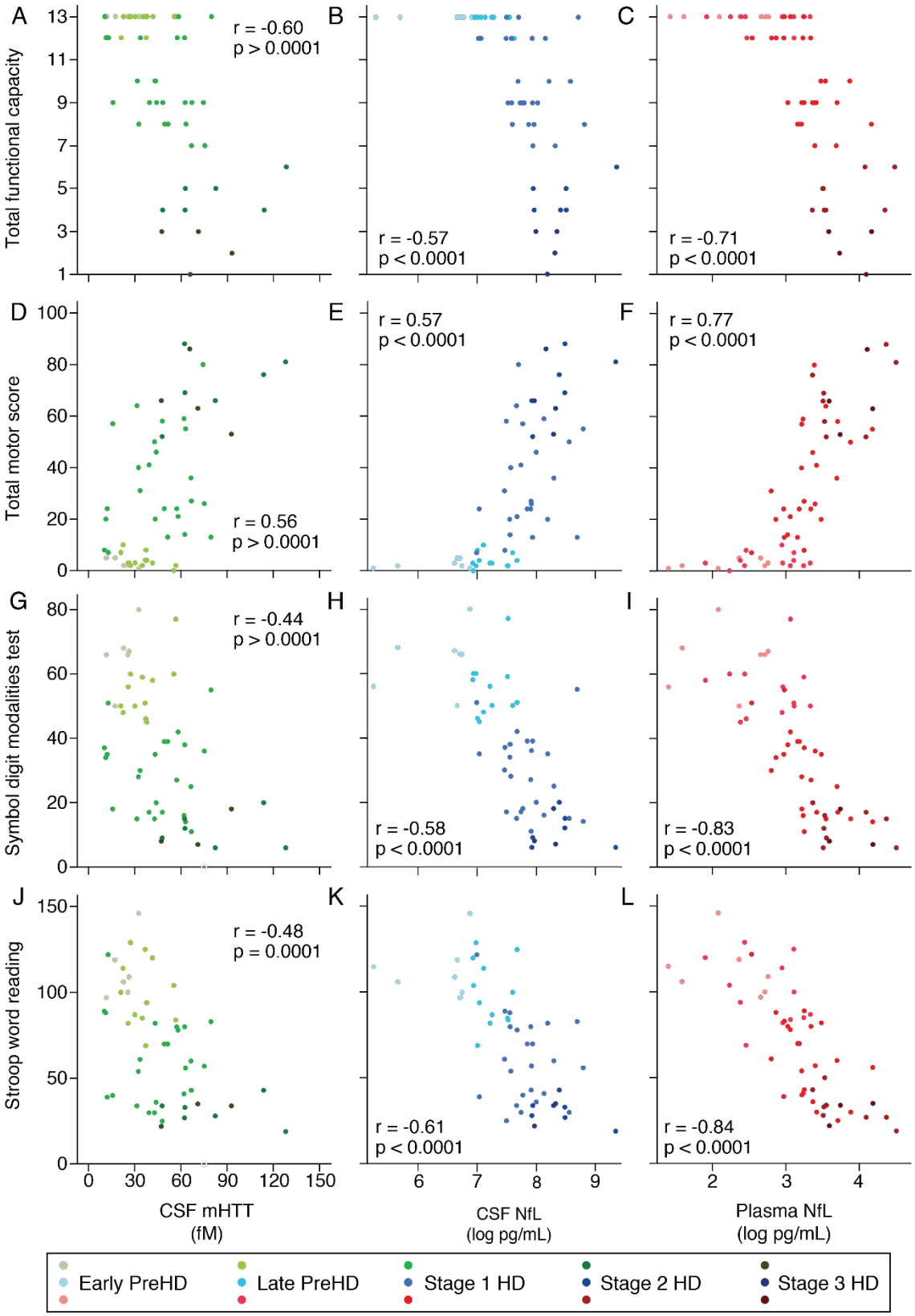

Figure 31 Cross-sectional clinical associations in 24-month follow-up samples.

Association within HD mutation carriers (N=60) between CSF mHTT (green; A, D, G, J), CSF NfL (blue; B, E, H, K), plasma NfL (red; C, F, I, L) and UHDRS clinical scores including functional (A-C), motor (D-F) and cognitive (G-L) measures. Scatter plots show unadjusted values. r and p values are age-adjusted, generated from Pearson's partial correlations including age as a covariate. NfL values are natural log transformed. UHDRS Unified Huntington's disease rating scale; PreHD, premanifest Huntington's disease; HD, Huntington's disease; CSF, cerebrospinal fluid; mHTT, mutant huntingtin; NfL, neurofilament light.

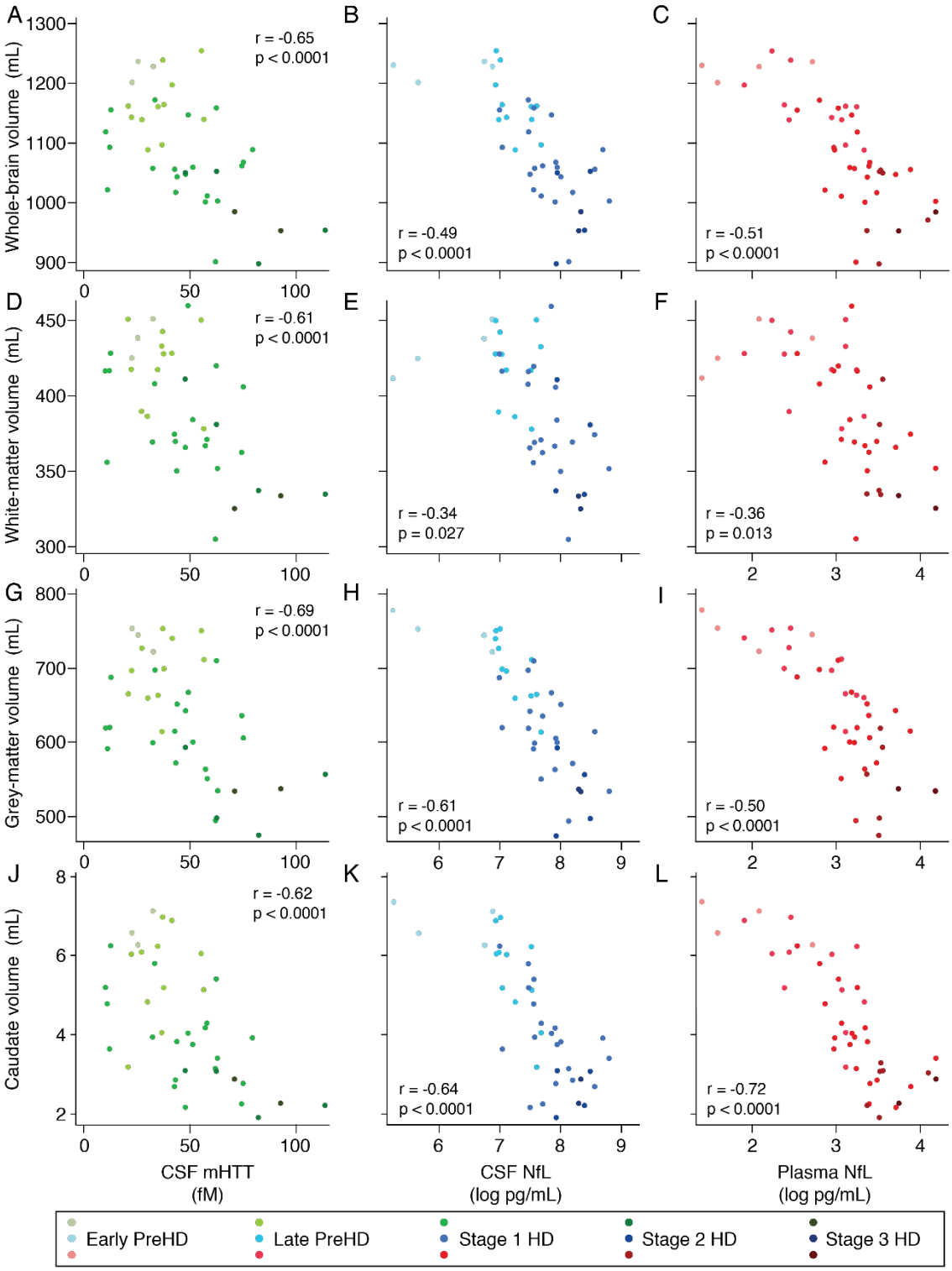

Figure 32 Cross-sectional associations in 24-month follow-up baseline samples between analyte concentrations and imaging measures.

Association within HD mutation carriers between the analytes CSF mHTT (green; A, D, G, J), CSF NfL (blue; B, E, H, K), plasma NfL (red; C, F, I, L) and MRI volumetric measures whole-brain (N=43; A-C), white-matter (N=41; D-F), grey-matter (N=41; G-I) and caudate (N=43; J-L). All volumetric measures were calculated as a percentage of total intracranial volume. Scatter plots show unadjusted values. r and p values are age-adjusted, generated from Pearson's partial correlations including age as a covariate. NfL values are natural log transformed. PreHD, premanifest Huntington's disease; HD, Huntington's disease; CSF, cerebrospinal fluid; mHTT, mutant huntingtin; NfL, neurofilament light.

Table 18 Follow-up cross-sectional correlations between analytes and clinical and imaging measures.

(A) adjusted for age and (B) age and CAG repeat count. 95% confidence intervals are bias-corrected accelerated. CSF, cerebrospinal fluid; cUHDRS, composite Unified Huntington's Disease Rating Scale; mHTT, mutant huntingtin; NfL, neurofilament light; r, Pearson's partial correlation coefficient; SDMT, Symbol Digit Modalities Test; SCN, Stroop Color Naming; SWR, Stroop Word Reading; TFC, UHDRS Total Functional Capacity; TMS, UHDRS Total Motor Score; VFC, Verbal Fluency – Categorical.

A

	CSF mHTT					CSF NfL					Plasma NfL				
	n	r	95% confidence interval		p-value	n	r	95% confidence interval		p-value	n	r	95% confidence interval		p-value
TFC	53	-0.60	-0.75	-0.40	<0.001	54	-0.57	-0.70	-0.39	<0.001	66	-0.66	-0.75	-0.55	<0.001
TMS	53	0.56	0.34	0.72	<0.001	54	0.57	0.34	0.72	<0.001	56	0.68	0.53	0.79	<0.001
SDMT	51	-0.44	-0.61	-0.20	<0.001	52	-0.58	-0.72	-0.33	<0.001	54	-0.66	-0.77	-0.49	<0.001
SCN	51	-0.45	-0.62	-0.22	<0.001	52	-0.63	-0.76	-0.41	<0.001	54	-0.71	-0.82	-0.57	<0.001
VFC	51	-0.52	-0.67	-0.28	<0.001	52	-0.57	-0.70	-0.41	<0.001	54	-0.62	-0.73	-0.45	<0.001
SWR	51	-0.48	-0.63	-0.26	<0.001	52	-0.61	-0.73	-0.42	<0.001	54	-0.74	-0.83	-0.61	<0.001
cUHDRS	51	-0.55	-0.71	-0.34	<0.001	52	-0.64	-0.76	-0.43	<0.001	54	-0.74	-0.82	-0.62	<0.001
Whole Brain	40	-0.65	-0.82	-0.38	<0.001	41	-0.49	-0.71	-0.25	<0.001	43	-0.51	-0.68	-0.27	<0.001
Grey Matter	39	-0.69	-0.82	-0.46	<0.001	40	-0.61	-0.78	-0.40	<0.001	41	-0.50	-0.66	-0.31	<0.001
White Matter	39	-0.61	-0.79	-0.35	<0.001	40	-0.34	-0.62	0.01	0.027	41	-0.36	-0.60	-0.02	0.013
Caudate	40	-0.62	-0.80	-0.41	<0.001	41	-0.64	-0.79	-0.46	<0.001	43	-0.72	-0.84	-0.54	<0.001

B

	CSF mHTT					CSF NfL					Plasma NfL				
	n	r	95% confidence interval		p-value	n	r	95% confidence interval		p-value	n	r	95% confidence interval		p-value
TFC	53	-0.36	-0.62	-0.06	0.011	54	-0.28	-0.53	0.02	0.052	56	-0.44	-0.63	-0.25	<0.001
TMS	53	0.29	0.03	0.58	0.034	54	0.28	-0.07	0.60	0.116	56	0.46	0.23	0.68	<0.001
SDMT	51	-0.11	-0.36	0.16	0.405	52	-0.29	-0.60	0.07	0.106	54	-0.43	-0.66	-0.17	0.001
SCN	51	-0.11	-0.30	0.11	0.306	52	-0.34	-0.64	-0.01	0.037	54	-0.50	-0.71	-0.23	<0.001
VFC	51	-0.25	-0.43	-0.03	0.014	52	-0.29	-0.63	-0.01	0.072	54	-0.38	-0.64	-0.12	0.005
SWR	51	-0.17	-0.35	0.05	0.101	52	-0.32	-0.61	-0.03	0.035	54	-0.56	-0.73	-0.36	<0.001
cUHDRS	51	-0.26	-0.52	0.02	0.052	52	-0.36	-0.66	-0.02	0.032	54	-0.54	-0.73	-0.34	<0.001
Whole Brain	40	-0.46	-0.73	-0.13	0.004	41	-0.23	-0.50	0.10	0.147	43	-0.29	-0.50	0.03	0.030
Grey Matter	39	-0.53	-0.73	-0.23	<0.001	40	-0.42	-0.66	-0.09	0.003	41	-0.29	-0.48	-0.05	0.007
White Matter	39	-0.48	-0.71	-0.15	0.001	40	-0.15	-0.42	0.14	0.304	41	-0.18	-0.42	0.13	0.198
Caudate	40	-0.37	-0.63	-0.09	0.008	41	-0.38	-0.61	-0.12	0.003	43	-0.55	-0.73	-0.28	<0.001

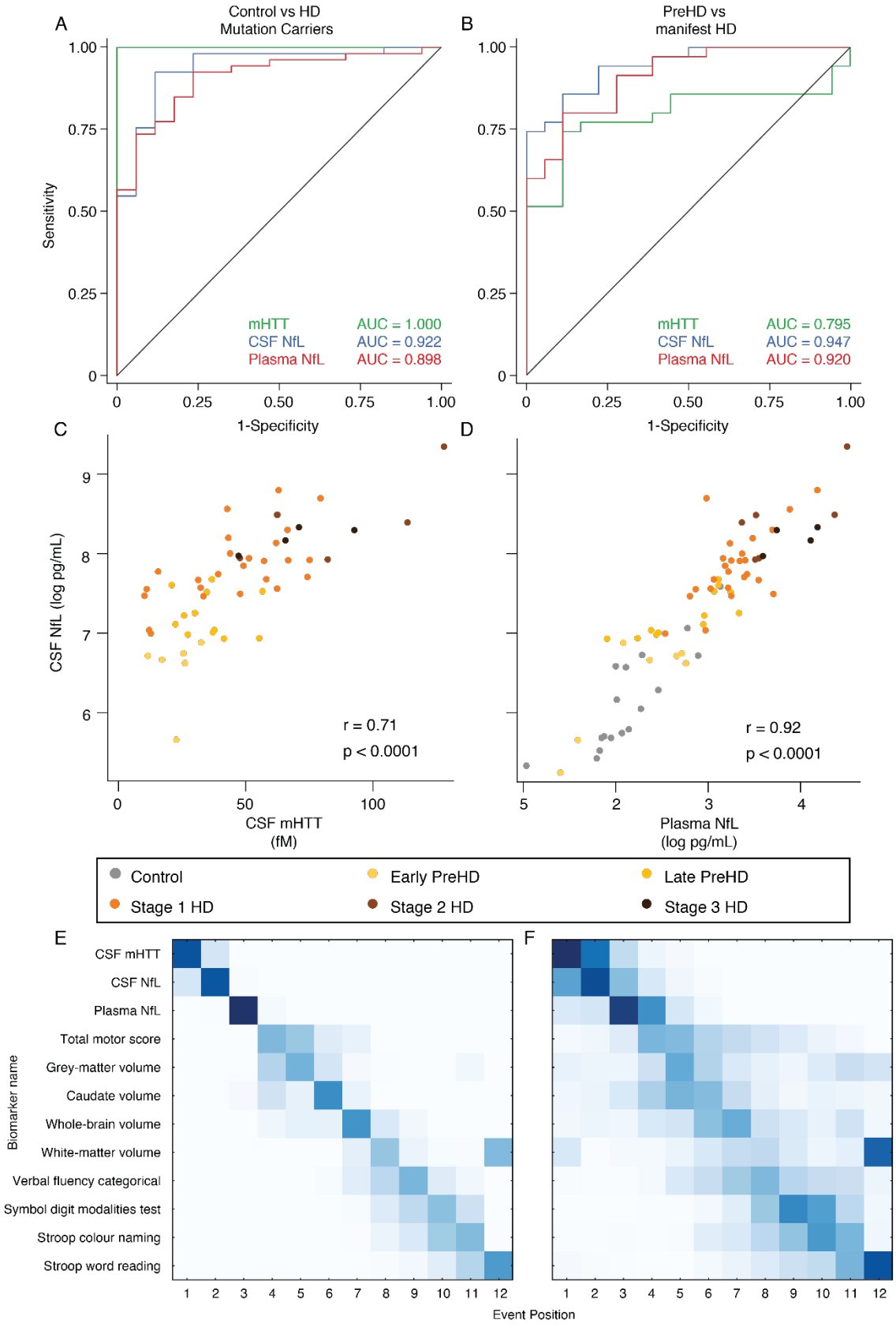

Figure 33 Receiver Operating Characteristics (ROC) analysis, analyte correlations and Event-Based Modelling (EBM) in 24-month follow-up samples.

ROC curves for the (A) discrimination between controls (N=17) and HD mutation carriers (N=54) (95% CIs for AUCs: CSF mHTT 1.000 – 1.000; CSF NfL 0.849 – 0.994; Plasma NfL 0.824 – 0.972) and (B) discrimination between premanifest (N=19) and manifest HD mutation carriers (N=35) (95% CIs for AUCs: CSF mHTT 0.672 – 0.919; CSF NfL 0.895 –1.000; Plasma NfL 0.852 – 0.989). Scatter plots showing correlation between CSF mHTT and CSF NfL concentration (C, N=54) and between CSF NfL and Plasma NfL (D, N=71). Scatter plots show

unadjusted values. r and p values are unadjusted, generated from Pearson's correlations. (E) Positional variance diagram produced from the, applied to the 63 HD-CSF participants who had data for all biomarkers (Controls 11; preHD 14; manifest HD 24). (F) Re-estimation of the positional variance in E, using 100 bootstrap samples of the data, providing internal validation of the model's findings. The positional variance diagrams represent the sequence of "events" (the individual measures going from normal to abnormal, identified by the EBM). Darker diagonal squares represent higher certainty of the biomarker becoming abnormal at the corresponding event where multiple event boxes coloured indicating more uncertainty about its position. 1 indicates the earliest event. NfL values were natural-log transformed. AUC, area under the curve; PreHD, premanifest HD mutation carriers; CSF, cerebrospinal fluid; mHTT, mutant huntingtin; NfL, neurofilament light.

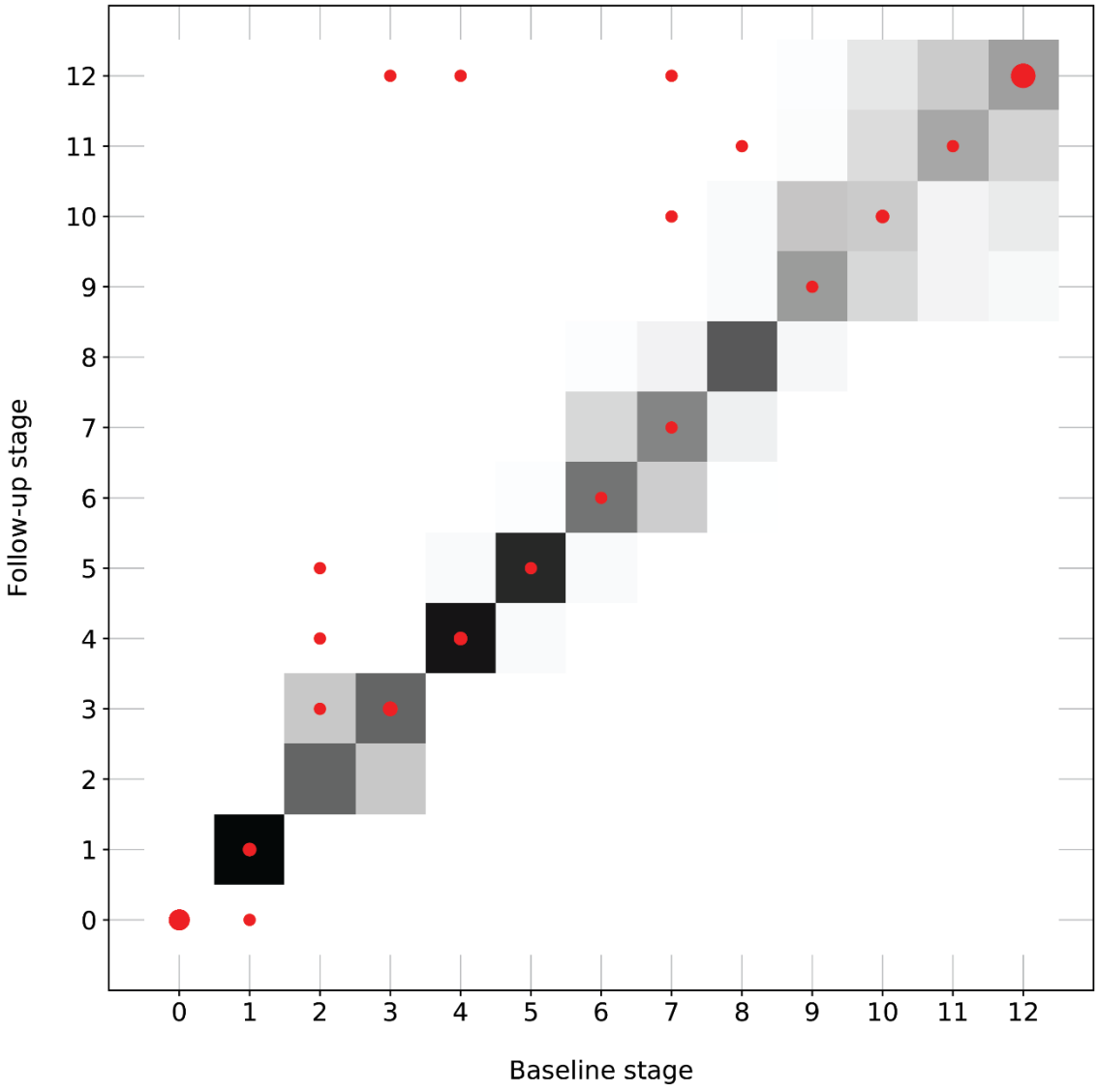

Figure 34 Longitudinal validation of EBM.

Predicted EBM stages in the HD-CSF cohort at baseline and follow-up. Marker radius scales with the number of participants at each point; the largest circle corresponds to N=10 at (12,12); smallest circles correspond to N=1. Greyscale indicates uncertainty in the event positioning (obtained from Markov Chaine Monte Carlo sampling of the posterior).

5.3.4 Longitudinal dynamics of mHTT and NfL

Longitudinal trajectories of each analyte within individuals are shown in Figure 35A-C. For NfL in CSF and plasma, there was little overlap in the trajectories of HD mutation

carriers and healthy controls. Mixed-effects models depict distinct patterns of longitudinal analyte dynamics (Figure 35D-F). CSF and plasma NfL showed a sigmoidal pattern over time in HD mutation carriers, initially accelerating then later slowing, compared to a slow linear rise with ageing in controls. CSF mHTT, on the other hand, rose linearly with age, albeit with more variability.

To explore the 'genetic dose-response relationship' between the causative gene mutation and each biofluid measure, we modelled their trajectories by CAG repeat length (Figure 35G-I; Figure 36). Using a change-point analysis, we estimated the disease burden score (a combination of age and CAG) at which each analyte in HD mutation carriers starts to deviate from controls. The DBS change-points for each analyte (CSF mHTT, 188.9; CSF NfL, 248.6; and Plasma NfL, 236.1; Figure 37) were used to annotate Figure 35G-I with the age of expected departure from controls, for each CAG length. Based on simulations, CSF NfL rose fastest in manifest HD by 98.85 pg/mL/year, in preHD by 79.16 pg/mL/year and in controls by 20.05 pg/mL/year; Figure 35J. Similar relative findings were seen for plasma NfL rates of change (controls 0.28, preHD 0.84, manifest HD 1.04 pg/mL/year; Figure 35J).

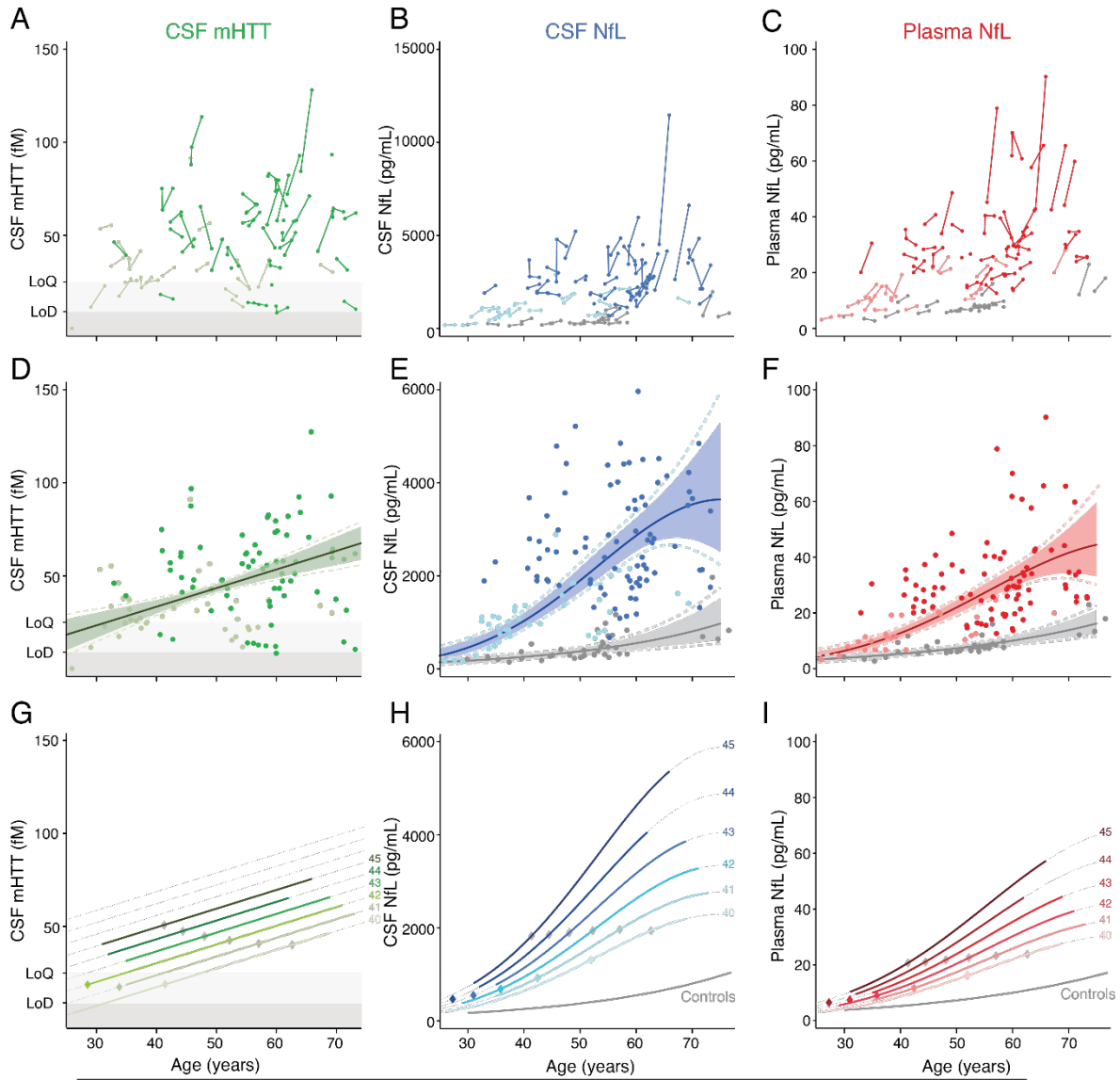

J

	fM/year [95% CI]	pg/mL/year [95% CI]	pg/mL/year [95% CI]
Healthy Controls	N/A	20.05 [18.57 to 21.53]	0.28 [0.27 to 0.29]
PreHD	1.03 [0.95 to 1.11]	79.16 [74.92 to 83.40]	0.84 [0.80 to 0.87]
Manifest HD	1.00 [0.95 to 1.05]	98.85 [93.01 to 104.70]	1.04 [1.00 to 1.08]

Figure 35 The longitudinal dynamics of mHTT and NfL over 24 months.

(A-C) Individual participant trajectories . Connected dots are measurements of the same participant. Disease groups are colour coded as per (J). (D-F) Modelled biomarker trajectories. Model (solid line), 95% (coloured area) and 99% (dashed line) bias-corrected accelerated confidence intervals were generated from generalized mixed effects models. For CSF mHTT, age was used as first-order fixed effect, while for HD mutation carriers for NfL there was a first- and second-order fixed effect for age. All models were adjusted for CAG repeat count and had a random intercept for participant, and corresponding random slopes for age. Dots represent the observed values. For ease of visual interpretation 2 individual datapoints (>6,000 pg/mL) were included in the model but excluded from figure (E). (G-I) Modelling genetic dose-response relationships to show associations between biomarkers, age and CAG repeat count. For all the analytes, the linear combinations of the interactions between age factors and CAG repeat were significant (CSF mHTT p=0.002; CSF NfL p=0.008; plasma NfL p=0.001). Solid lines were produced from our observations using the models above; dashed lines are predictions outside the range of our observations. Separate figures with individual datapoints for each individual CAG repeat count are provided in (Figure 36). Grey diamonds show the age of predicted age of onset for each CAG length (as per Langbehn et al 2004).(Langbehn et al., 2004) Coloured diamonds show the age at which gene expansion carriers trajectories are most likely to depart from healthy controls trajectories for each CAG repeat count, generated by threshold regression analysis. (J) Annualised rates of change and 95% confidence intervals. For each biomarker, estimates were computed as the average of the rate of change in 1,000 simulations per group of study participants (i.e. healthy controls, premanifest and manifest HD). For CSF mHTT, shaded rectangles mark the limits of detection (LoD, 8 fM) and quantification (LoQ, 25 fM) of the assay. CSF, cerebrospinal fluid; mHTT, mutant huntingtin; N/A, not applicable; NfL, neurofilament light.

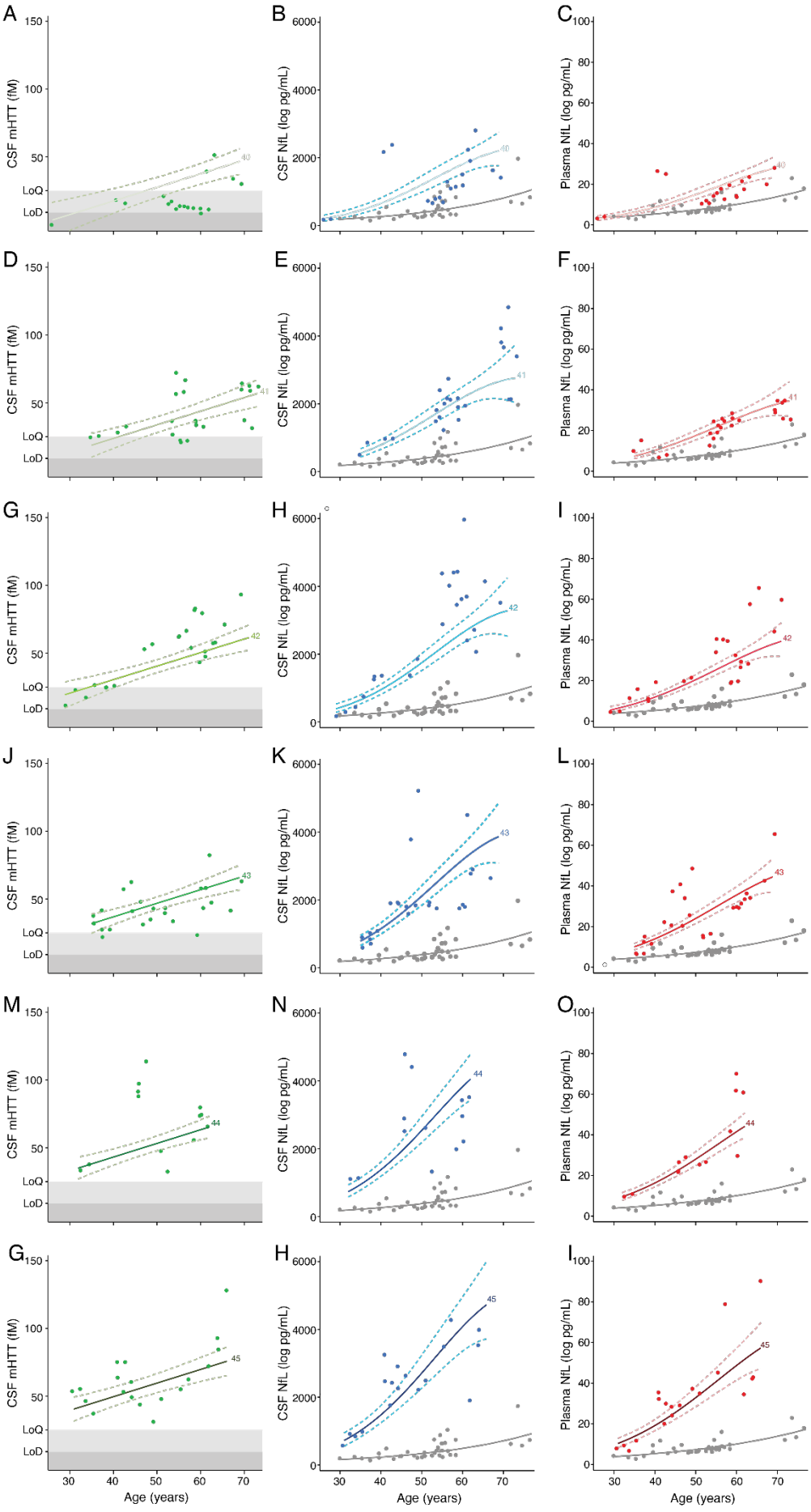

Figure 36 Modelling genetic dose-response relationships by individual CAG repeat length.

For all the analytes, the linear combinations of the interactions between age factors and CAG repeat were significant (CSF mHTT p=0.002; CSF NfL p=0.008; plasma NfL p=0.001). Solid lines were produced from our observations using the models from Figure 2. Dashed lines are 95% confidence intervals. Data points are individual patients' observed data.

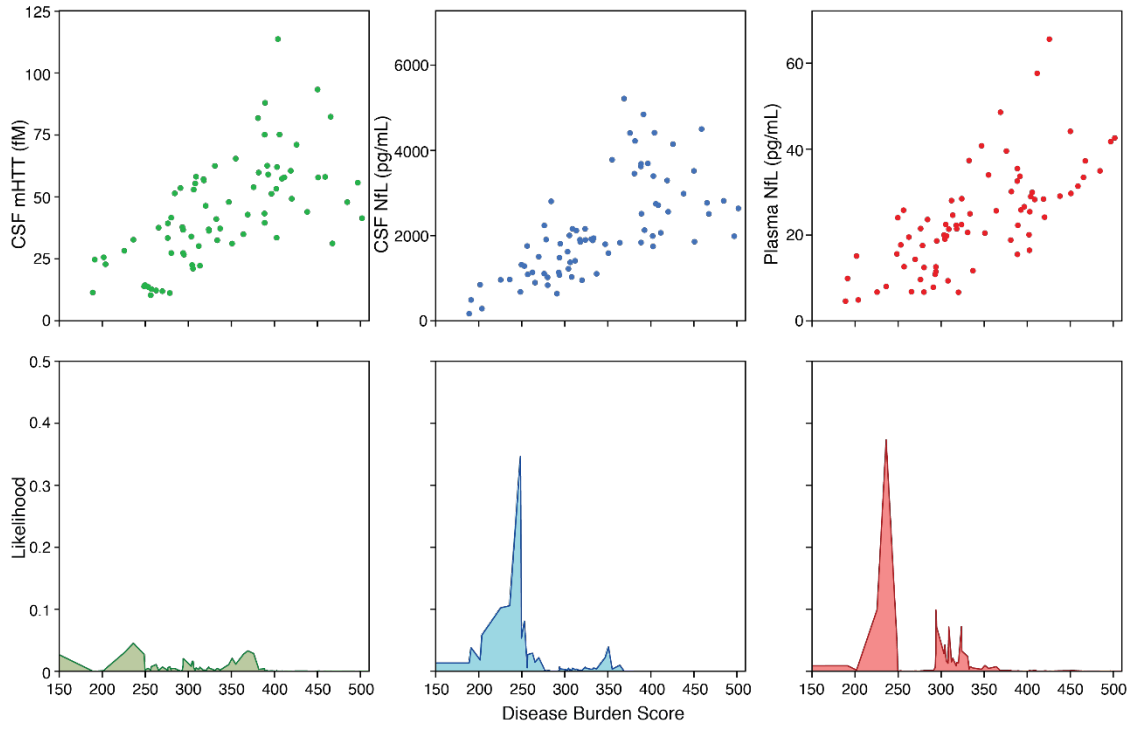

Figure 37 Change-point analysis for defining the point of deflection from controls in each analyte.

Top row: cross-sectional and follow-up data for all groups (non-GEC, preHD and HD) for each fluid biomarker as a function of disease burden score (DBS), where DBS = age x (CAG – 35.5). Bottom row: marginal likelihood of a change in the generating model as a function of DBS. We calculate the change-point as the maximum likelihood position over all DBS points.

5.3.5 Prognostic value for overall HD progression of baseline analyte versus its rate of change

We assessed the clinical associations of each analyte using the cUHDRS, a composite score derived from large natural history cohorts and combining motor, functional and cognitive symptoms to reflect overall HD clinical severity (Schobel et al., 2017). All three analytes had significant associations with cUHDRS cross-sectionally at both baseline and follow-up (Figure 38). To assess the prognostic value of each analyte for HD progression, we first examined whether their baseline values predicted subsequent change in cUHDRS. Significant associations with subsequent cUHDRS change were found for all three (CSF mHTT r=-0.31, 95%CI -0.57 to -0.03, p=0.026; CSF NfL r=-0.38, 95%CI -0.52 to -0.18, p<0.0001; plasma NfL r=-0.47, 95%CI -0.63 to -0.25, p<0.0001; Figure 39A-C). The association with baseline plasma NfL remained significant after adjustment for age and CAG (CSF mHTT r=-0.11, 95%CI -0.48 to 0.18, p=0.513; CSF

NfL r=-0.21, 95%CI -0.48 to 0.00, p=0.098; plasma NfL r=-0.33, 95%CI -0.58 to -0.08, p=0.011).

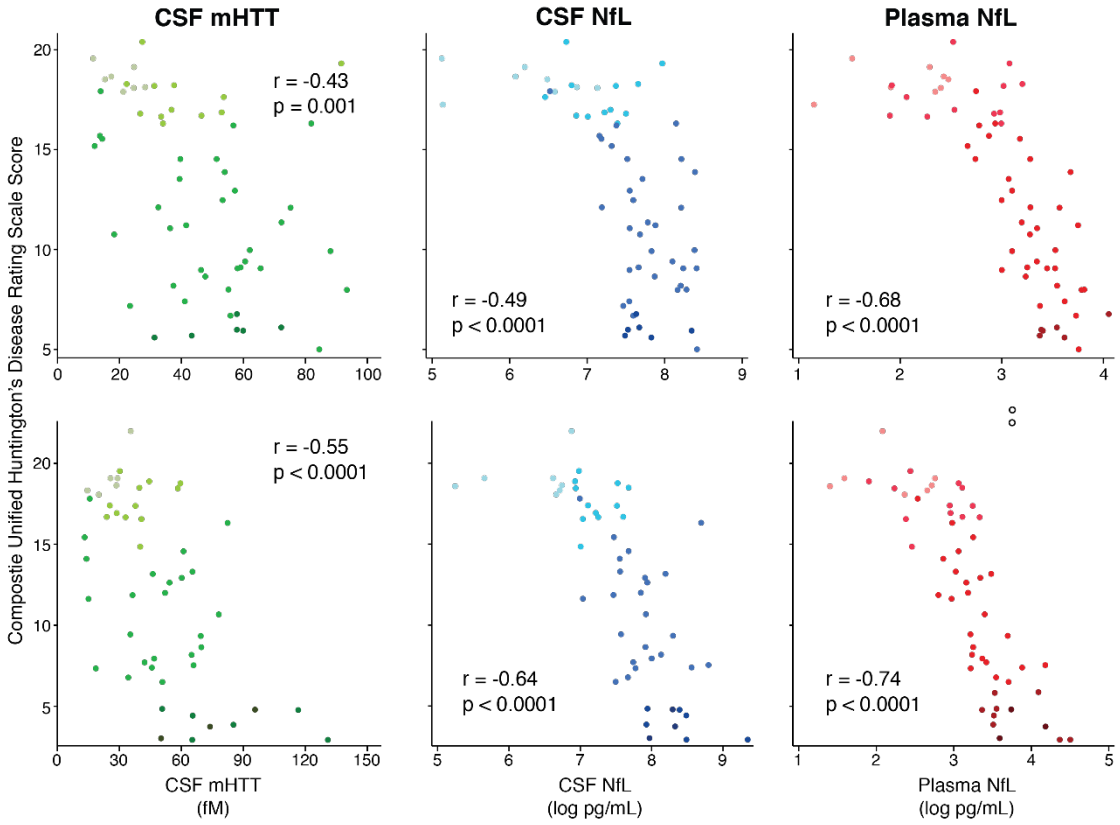

Figure 38 Cross-sectional associations with cUHDRS at baseline and 24-month follow-up.

Association within HD mutation carriers between CSF mHTT (green; A, D), CSF NfL (blue; B, E), plasma NfL (red; C, F) and cUHDRS score at baseline (A-C; N=58; N=59; N=59 respectively) and 24-month follow-up (D-F; N=51; N=52; N=54 respectively). Scatter plots show unadjusted values. r and p values are age-adjusted, generated from Pearson's partial correlations including age as a covariate. NfL values are natural log transformed. UHDRS Unified Huntington's disease rating scale; PreHD, premanifest Huntington's disease; HD, Huntington's disease; CSF, cerebrospinal fluid; mHTT, mutant huntingtin; NfL, neurofilament light.

Next we assessed whether the rate of change of each analyte gave any additional prognostic information, beyond that given by a single baseline measurement. The rates of change in CSF and plasma NfL were each loosely associated with the rate of change in cUHDRS (CSF mHTT r=-0.17, 95%CI -0.49 to 0.08, p=0.253; CSF NfL r=-0.20, 95%CI -0.43 to -0.01, p=0.049; plasma NfL r= -0.34, 95%CI -0.65 to -0.12, p=0.013; Figure 39D-F). These associations were weaker than those of the baseline values and none survived adjustment for age and CAG (CSF mHTT r=-0.09, 95%CI -0.46 to 0.15, p=0.539; CSF NfL r=-0.09, 95% CI -0.33 to 0.10, p= 0.401; plasma NfL r=-0.22, 95%CI -0.54 to -0.00, p=0.111).

In our analysis of fast and slow progressors (≥ or < 1.2 decline in cUHDRS respectively), baseline CSF mHTT, CSF NfL and plasma NfL were all significantly higher in faster progressors (mean differences: CSF mHTT 19.27 fM, 95%CI 10.74 to 27.80, p<0.0001; CSF NfL 1066.05 pg/mL, 95%CI 0. 532.62 to 1599.48, p<0.0001; plasma NfL 11.44 pg/mL 95%CI 6.45 to 16.43, p<0.0001; Figure 39G-I). Only plasma NfL remained

associated after adjustment for age and CAG (mean differences: CSF mHTT 7.38 fM, 95%CI -0.92 to 15.68, p=0.081; CSF NfL 449.75 pg/mL, 95%CI -61.52 to 961.02, p=0.087; plasma NfL 5.59 pg/mL, 95%CI 1.24 to 9.93, p=0.032).

We repeated this analysis using the rate of change in each analyte. Only the rate of change of plasma NfL was significantly higher in faster progressors (mean differences: CSF mHTT 0.67 fM/year, 95%CI -1.75 to 3.09, p=0.584; CSF NfL 230.23 pg/mL/year, 95%CI -29.32 to 489.78, p=0.082; plasma NfL 2.83 pg/mL/year, 95%CI 1.03 to 4.62, p=0.002; Figure 39J-L). This did not survive age and CAG adjustment (mean differences: CSF mHTT -1.04 fM/year, 95%CI -3.69 to 1.61, p=0.440; CSF NfL 27.07 pg/mL/year, 95%CI -253.56 to 307.70, p=0.849; plasma NfL 1.22 pg/mL/year 95%CI -0.71 to 3.15, p=0.210).

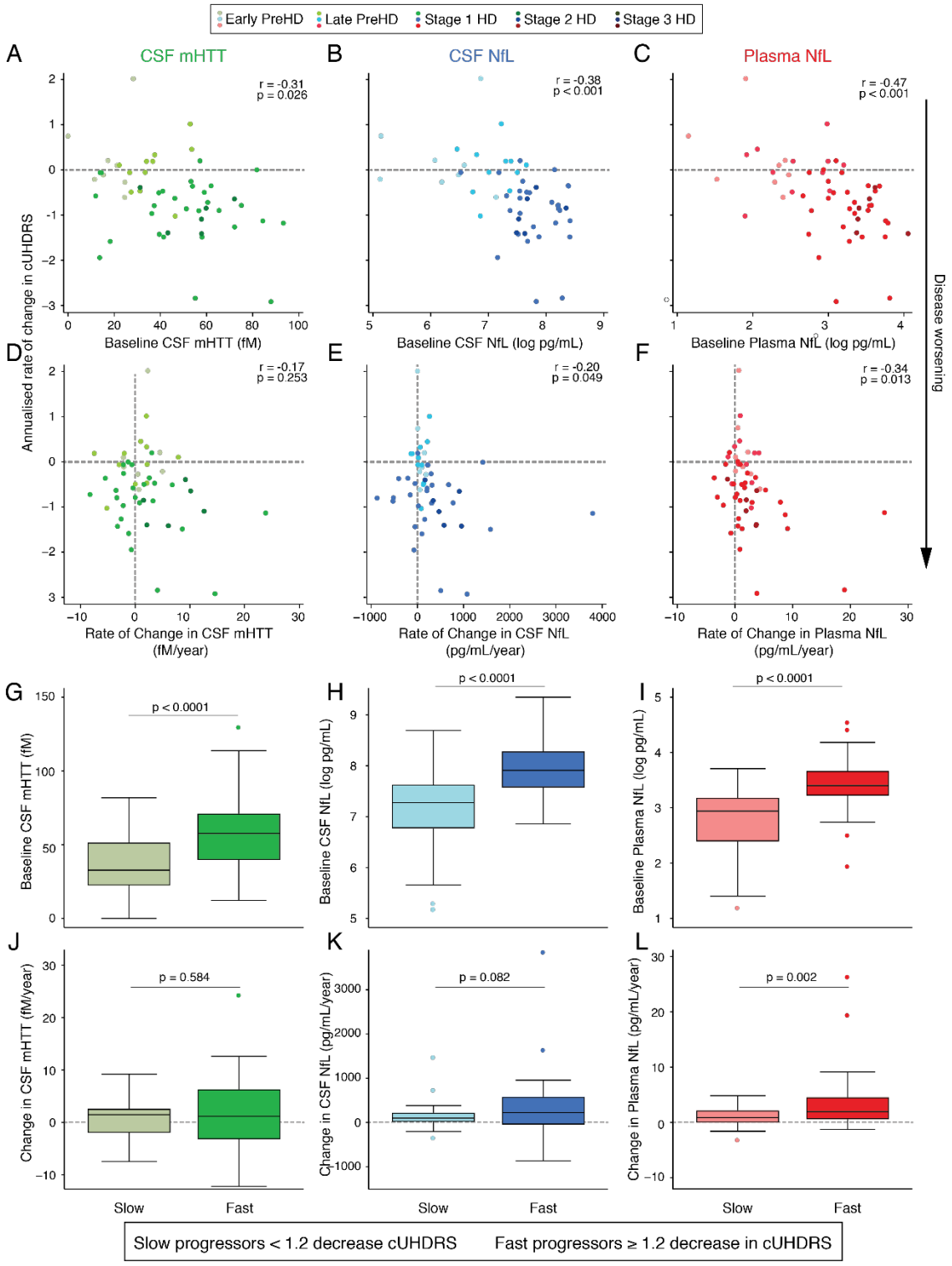

Figure 39 Longitudinal associations of mHTT and NfL with disease progression quantified by cUHDRS.

Associations between (A-C) baseline values or (D-F) annualised rate of change in each analyte and the annualised rate of change in the cUHDRS. Partial Pearson's correlation coefficient adjusted for age, and p-values are presented. Dashed horizontal lines mark no change in cUHDRS, with negative values representing deterioration. Dashed vertical lines mark no change in the biomarker. The baseline values (G-H) and annualised rate of change (I-L) for each biomarker compared between 'fast' (n=24) and 'slow' progressors (n=30), defined as participants with an absolute decrease in cUHDRS equal or superior to 1.2 over the follow-up period. The boxes show the median, and 25% and 75% percentiles, while whiskers are the lower and upper adjacent values (i.e. 1.5 times the interquartile range minus the 25% percentile or plus the 75% percentile). Dots are values under and above the adjacent values. CSF, cerebrospinal fluid; cUHDRS, composite Unified Huntington's Disease Rating Scale; mHTT, mutant huntingtin; NfL, neurofilament light.

5.3.6 *Prognostic value of biofluid clinical, imaging and cognitive measures*

Next we compared the prognostic power of each analyte, in terms of both its baseline value and its rate of change, to predict progression in individual clinical and MRI measures (Table 19, Figure 40A-B). Baseline measurements of all analytes had significant associations with subsequent decline in clinical and imaging measures (Table 19A, Figure 40A). Baseline CSF mHTT was associated with worsening in TFC (r=0.40, p=0.001) and the volumes of whole-brain (r=0.38, p=0.008), white-matter (r=0.64, p<0.0001), grey-matter (r=0.59, p<0.0001) and caudate (r=0.45, p=0.002), and very weak association with TMS or any cognitive measure (r<0.20, p>0.242). Baseline NfL, in both CSF and plasma, was associated with progression in all measures except TMS (CSF NfL: TFC r=0.39, p<0.0001; SDMT r=0.20, p=0.039 ; SWR r=0.22, SCN r=0.26, p=0.016; VFC r=0.23, whole-brain r=0.44, p<0.0001; white-matter r=0.58, p<0.0001; grey-matter r=0.37, p=0.002; caudate r=0.47, p<0.0001; Plasma NfL: TFC r=0.46, p<0.0001; SDMT r=0.32, p=0.009; SCN r=0.30, p=0.014; whole-brain r=0.56, p<0.0001; white-matter r=0.63, p<0.0001; grey-matter r=0.47, p<0.0001; caudate r=0.42, p<0.0001). After age and CAG adjustment (Table 19B, Figure 40B), associations remained significant between baseline CSF mHTT and subsequent change in white-matter (r=0.45 p<0.0001), grey-matter (r=0.46 p=0.0001) and caudate (r=0.29 p=0.074); between baseline CSF NfL and subsequent change in TFC (r=0.25, p=0.032), white-matter (r=0.37, p=0.009) and caudate (r=0.32, p=0.007); and between baseline plasma NfL and subsequent change in TFC (r=0.34, p=0.06), SDMT (r=0.29, p=0.023), whole-brain (r=0.45, p<0.0001), white-matter (r=0.46, p<0.0001) and grey-matter (r=0.30, p=0.023).

In contrast, the rate of change in each analyte had weaker associations with progression in any measure apart from change in TMS (mHTT r=0.46, p<0.0001; CSF NfL 0.32, p=0.012). These associations remained after adjustment for age and CAG (r=0.43, p=0.001; r=0.18, p=0.032 respectively).

Using a ROC curve analysis, we compared the discriminatory ability of each analyte's baseline value and rate of change, to distinguish between different clinical states: controls versus HD mutation carriers, and between premanifest versus manifest HD. For all three analytes, rate of change had poor ability to distinguish in either comparison; AUCs were around 0.5 (i.e. no better than chance). Baseline concentrations had excellent discriminatory ability with AUCs greater than 0.8 (Figure 40C,D). In each condition, and for each analyte, the AUC for the baseline measurement was significantly greater than that for its rate of change (Figure 40C,D).

Table 19 Longitudinal correlations.

(A) adjusted for age and (B) for age and CAG repeat count between baseline values or annualised rate of change (Δ) of each analyte and the annualised rate of change in clinical and imaging measures, each expressed such that higher positive values denote clinical worsening. 95% confidence intervals are bias-corrected accelerated. CSF, cerebrospinal fluid; cUHDRS, composite Unified Huntington's Disease Rating Scale; mHTT, mutant huntingtin; NfL, neurofilament light; r, Pearson's partial correlation coefficient; SDMT, Symbol Digit Modalities Test; SCN, Stroop Color Naming; SWR, Stroop Word Reading; TFC, UHDRS Total Functional Capacity; TMS, UHDRS Total Motor Score; VFC, Verbal Fluency – Categorical.

A

	Baseline CSF mHTT					**ΔCSF mHTT**				
	n	r	95% confidence interval		p-value	n	r	95% confidence interval		p-value
ΔTFC	55	0.40	0.18	0.62	0.001	53	0.26	0.01	0.60	0.085
ΔTMS	55	0.16	-0.18	0.54	0.403	53	0.46	0.19	0.68	<0.001
ΔSDMT	53	0.00	-0.24	0.23	0.980	51	-0.07	-0.24	0.11	0.426
ΔSCN	53	0.09	-0.20	0.30	0.471	51	0.03	-0.15	0.23	0.759
ΔVFC	53	0.16	-0.12	0.44	0.275	51	-0.09	-0.31	0.14	0.438
ΔSWR	53	0.15	-0.23	0.41	0.336	51	-0.13	-0.31	0.11	0.208
ΔcUHDRS	53	0.29	0.01	0.55	0.039	51	0.17	-0.07	0.50	0.234
ΔWhole Brain	40	0.38	0.04	0.64	0.010	39	0.00	-0.31	0.36	0.985
ΔCaudate	42	0.45	0.13	0.71	0.003	40	0.17	-0.15	0.57	0.361
ΔGrey Matter	40	0.59	0.38	0.79	<0.001	39	0.22	-0.21	0.59	0.284
ΔWhite Matter	40	0.64	0.39	0.79	<0.001	39	0.00	-0.42	0.42	0.994
	Baseline CSF NfL					**ΔCSF NfL**				
	n	r	95% confidence interval		p-value	n	r	95% confidence interval		p-value
ΔTFC	56	0.39	0.20	0.57	<0.001	54	0.18	-0.07	0.44	0.148
ΔTMS	56	0.10	-0.15	0.34	0.424	54	0.32	-0.02	0.50	0.014
ΔSDMT	54	0.20	0.00	0.39	0.035	52	0.08	-0.09	0.24	0.311
ΔSCN	54	0.26	0.03	0.46	0.013	52	0.04	-0.16	0.22	0.640
ΔVFC	54	0.23	-0.05	0.49	0.101	52	0.04	-0.16	0.24	0.688
ΔSWR	54	0.22	-0.07	0.43	0.071	52	-0.07	-0.21	0.13	0.456
ΔcUHDRS	54	0.38	0.18	0.53	<0.001	52	0.20	-0.01	0.43	0.055
ΔWhole Brain	41	0.44	0.12	0.65	<0.001	40	0.06	-0.32	0.45	0.756
ΔCaudate	43	0.47	0.25	0.66	<0.001	41	0.01	-0.33	0.48	0.947
ΔGrey Matter	41	0.37	0.10	0.57	0.002	40	0.33	-0.01	0.65	0.054
ΔWhite Matter	41	0.58	0.34	0.74	<0.001	40	0.14	-0.22	0.50	0.454
	Baseline Plasma NfL					**ΔPlasma NfL**				
	n	r	95% confidence interval		p-value	n	r	95% confidence interval		p-value
ΔTFC	56	0.46	0.23	0.62	<0.001	56	0.20	-0.08	0.62	0.257
ΔTMS	56	0.16	-0.12	0.36	0.194	56	0.24	-0.17	0.51	0.141
ΔSDMT	54	0.32	0.03	0.52	0.010	54	0.13	-0.02	0.26	0.088
ΔSCN	54	0.30	0.03	0.53	0.016	54	0.17	-0.04	0.50	0.196
ΔVFC	54	0.24	-0.04	0.48	0.087	54	0.02	-0.19	0.25	0.851
ΔSWR	54	0.24	-0.06	0.49	0.090	54	0.18	-0.10	0.41	0.176
ΔcUHDRS	54	0.47	0.24	0.62	<0.001	54	0.34	0.12	0.64	0.010
ΔWhole Brain	41	0.56	0.25	0.74	<0.001	41	0.10	-0.25	0.43	0.568
ΔCaudate	43	0.42	0.18	0.62	<0.001	43	0.05	-0.28	0.31	0.764
ΔGrey Matter	41	0.47	0.23	0.66	<0.001	41	0.12	-0.19	0.42	0.441
ΔWhite Matter	41	0.63	0.42	0.79	<0.001	41	0.03	-0.31	0.43	0.888

B

	Baseline CSF mHTT					ΔCSF mHTT				
	n	r	95% confidence interval		p-value	n	r	95% confidence interval		p-value
ΔTFC	55	0.26	-0.04	0.58	0.103	53	0.19	-0.10	0.55	0.258
ΔTMS	55	0.01	-0.32	0.51	0.943	53	0.43	0.19	0.66	0.001
ΔSDMT	53	-0.08	-0.29	0.26	0.538	51	-0.11	-0.28	0.07	0.217
ΔSCN	53	-0.10	-0.31	0.12	0.369	51	-0.05	-0.22	0.16	0.635
ΔVFC	53	0.07	-0.18	0.34	0.587	51	-0.14	-0.37	0.08	0.236
ΔSWR	53	0.04	-0.25	0.29	0.784	51	-0.20	-0.39	0.04	0.061
ΔcUHDRS	53	0.11	-0.17	0.48	0.502	51	0.09	-0.14	0.45	0.541
ΔWhole Brain	40	0.20	-0.24	0.53	0.300	39	-0.10	-0.42	0.21	0.514
ΔCaudate	42	0.29	-0.02	0.61	0.076	40	0.08	-0.23	0.50	0.678
ΔGrey Matter	40	0.46	0.19	0.69	<0.001	39	0.12	-0.30	0.48	0.532
ΔWhite Matter	40	0.45	0.16	0.66	<0.001	39	-0.17	-0.53	0.24	0.399
	Baseline CSF NfL					**ΔCSF NfL**				
	n	r	95% confidence interval		p-value	n	r	95% confidence interval		p-value
ΔTFC	56	0.25	-0.01	0.46	0.038	54	0.09	-0.19	0.40	0.548
ΔTMS	56	-0.05	-0.31	0.25	0.711	54	0.26	-0.04	0.47	0.033
ΔSDMT	54	0.15	-0.08	0.40	0.222	52	0.03	-0.11	0.25	0.709
ΔSCN	54	0.11	-0.10	0.34	0.348	52	-0.07	-0.23	0.17	0.491
ΔVFC	54	0.19	-0.12	0.43	0.168	52	0.00	-0.23	0.22	0.986
ΔSWR	54	0.09	-0.10	0.31	0.374	52	-0.17	-0.34	0.00	0.049
ΔcUHDRS	54	0.21	-0.01	0.48	0.098	52	0.09	-0.09	0.32	0.404
ΔWhole Brain	41	0.28	-0.04	0.56	0.068	40	-0.03	-0.41	0.39	0.893
ΔCaudate	43	0.32	0.04	0.53	0.009	41	-0.08	-0.41	0.38	0.688
ΔGrey Matter	41	0.15	-0.17	0.44	0.327	40	0.26	-0.16	0.59	0.164
ΔWhite Matter	41	0.37	0.06	0.62	0.008	40	0.02	-0.37	0.40	0.924
	Baseline Plasma NfL					**ΔPlasma NfL**				
	n	r	95% confidence interval		p-value	n	r	95% confidence interval		p-value
ΔTFC	56	0.34	0.09	0.56	0.005	56	0.10	-0.17	0.56	0.576
ΔTMS	56	0.02	-0.25	0.29	0.901	56	0.18	-0.19	0.44	0.228
ΔSDMT	54	0.29	-0.01	0.50	0.023	54	0.07	-0.08	0.25	0.371
ΔSCN	54	0.16	-0.08	0.43	0.218	54	0.05	-0.16	0.36	0.691
ΔVFC	54	0.20	-0.06	0.45	0.132	54	-0.04	-0.25	0.20	0.740
ΔSWR	54	0.12	-0.19	0.34	0.395	54	0.09	-0.20	0.33	0.505
ΔcUHDRS	54	0.33	0.07	0.57	0.010	54	0.22	0.00	0.52	0.108
ΔWhole Brain	41	0.45	0.16	0.66	<0.001	41	0.09	-0.26	0.51	0.636
ΔCaudate	43	0.24	-0.02	0.48	0.061	43	0.03	-0.33	0.33	0.844
ΔGrey Matter	41	0.30	0.02	0.54	0.019	41	0.12	-0.24	0.51	0.521
ΔWhite Matter	41	0.46	0.18	0.67	<0.001	41	0.02	-0.41	0.48	0.927

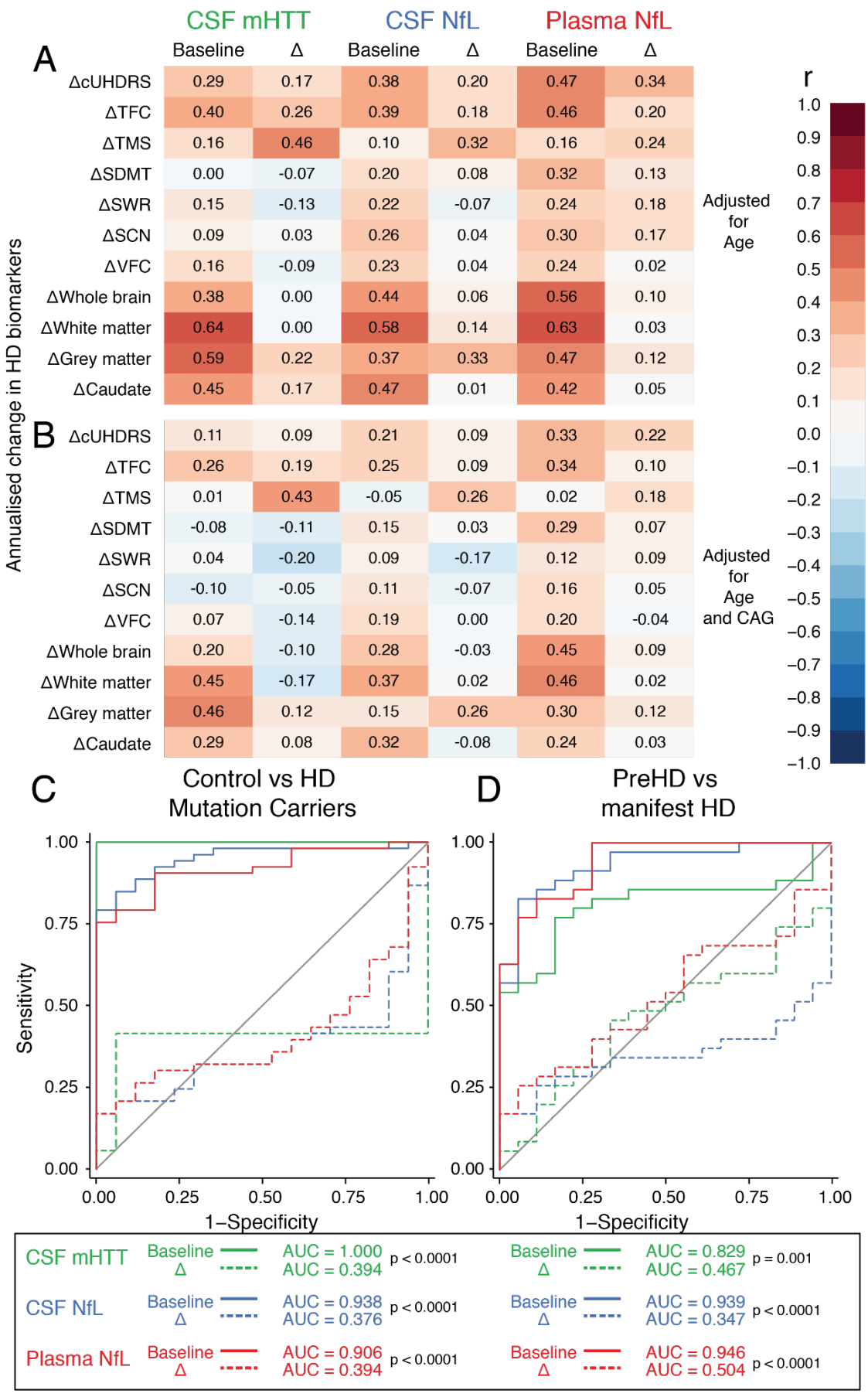

Figure 40 Comparison of prognostic abilities of mHTT and NfL for clinical and imaging measures, and disease state.

Matrices show the Pearson's partial correlation coefficients adjusted for (A) age only and (B) age and CAG repeat count for associations between baseline values or annualised rate of change (Δ) of each analyte and the annualised rate of change in clinical and imaging measures, each expressed such that higher positive values denote clinical worsening. Colour coding displays the magnitude and the direction of the association. Coeffiicients with corresponding confidence intervals and p-values for each combination are provided in Table 18. (C-D) ROC curves comparing the discriminatory ability of baseline values for each analyte and its annualised rate of change to distinguish (C) between healthy controls and HD mutation carriers and (D) between premanifest and manifest HD. p-values are for the comparison between the baseline AUC and rate of change AUC. AUC, area under the curve; CSF, cerebrospinal fluid; cUHDRS, composite Unified Huntington's Disease Rating Scale; mHTT, mutant huntingtin; NfL, neurofilament light; r, Pearson's partial correlation coefficient; SDMT, Symbol Digit Modalities Test; SCN, Stroop Color Naming; SWR, Stroop Word Reading; TFC, UHDRS Total Functional Capacity; TMS, UHDRS Total Motor Score; VFC, Verbal Fluency - Categorical; Δ, annualised rate of change.

5.3.7 Simulating clinical trials with biofluid biomarker surrogate endpoints

The data thus far suggests that these analytes indicate current clinical state and have prognostic value for clinical decline. We used longitudinal data from the HD-CSF cohort to run computationally simulated clinical trials using CSF mHTT, CSF NfL and plasma NfL as possible surrogates for clinical progression. These simulations assume that the intervention-induced change in the analyte emulate the change expected in clinical state by an intervention. Figure 41 depicts the relationships between statistical power, sample size and trial duration for such trials, using a nominal 20% drug effect per year. For longitudinal change in NfL, in CSF or plasma, fewer than 100 participants per arm are needed to show a slowing of progression over 9 months. More than 10,000 participants per arm would be required to achieve 80% power for a similar trial using the lowering of CSF mHTT over 24 months.

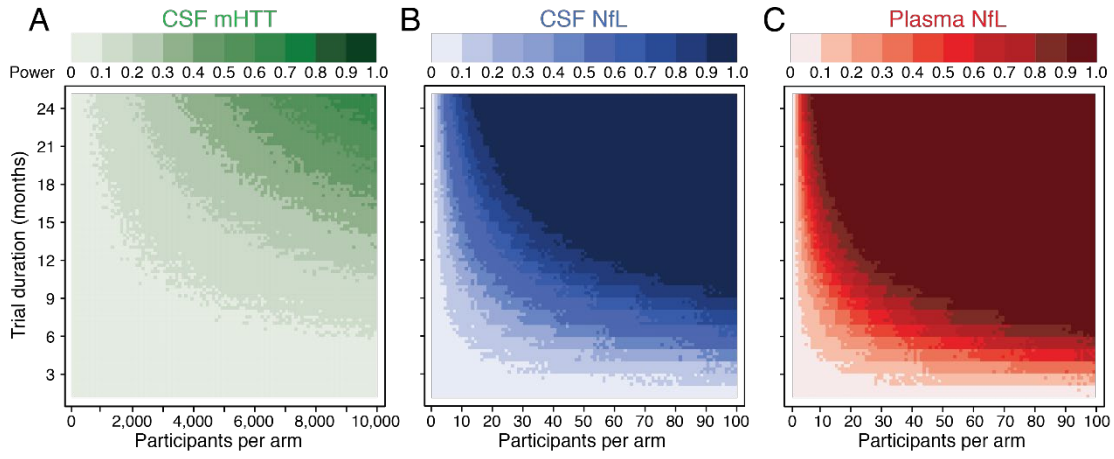

Figure 41 Statistical power, sample size and trial duration.

Monte Carlo simulations predicting the statistical power of each biomarker in the clinical trial context, contingent on sample size per arm and trial duration in months. 2-arm parallel design clinical triasl with no attrition or placebo effect with a constant effect size of 20% reduction in each analyte per year were simulated. Each pixel represents 1,000 simulated clinical trials, generated using generalised mixed effects models shaped to estimate the longitudinal trajectories of each biomarker (as in Figure 22). The main effect in each simulation repetition was calculated as the inter-arm mean difference in the mean change from baseline, using generalised linear models adjusted for CAG. Statistical power was calculated as the proportion of trial simulations with a p-value < 0.05 for the main effect. CSF; cerebrospinal fluid; mHTT; mutant huntingtin; NfL; neurofilament light.

5.4 Discussion

5.4.1 Summary

Here we present the 24-month analysis from HD-CSF, a longitudinal study of biofluid biomarkers in HD mutation carriers and matched controls, highly standardised with matching clinical and MRI data. For the first time to our knowledge, we have characterised and compared the longitudinal dynamics of mHTT and NfL in CSF, defining the trajectories of these biofluid biomarkers and the inflection points at which they depart from healthy controls in the natural history of HD. While rates of change in the analytes had some prognostic value, a single measurement at baseline of each analyte exhibited stronger ability to predict subsequent clinical decline, brain atrophy and disease state. Using clinical trial simulations, we show that NfL could be used as an outcome measure of neuronal protection and disease progression, to run trials over acceptably short periods.

5.4.2 A single measurement with more prognostic value

mHTT in CSF and NfL in CSF and plasma, all rose detectably within participants over 2 years. Over the whole course of the disease, mHTT rises rose linearly with age, whereas NfL rose in a more sigmoidal pattern. This was distinct from the trajectories in healthy controls, with little overlap. This suggests that monitoring these biomarkers against an age-relevant reference range derived from the healthy population could be clinically meaningful. The dynamics of both CSF mHTT and NfL are also CAG-dependent, revealing longitudinally the genetic dose-response relationships that we demonstrated previously for plasma NfL in the TRACK-HD cohort (Byrne et al., 2017). Change-point analysis identified the approximate age and analyte concentration at which HD mutation carriers became detectably different from controls, for a given CAG repeat length. Defining these points of deflection from the trajectories in healthy controls may help us move towards models based on CAG repeat length that could be used to enrich or stratify clinical trial participants and eventually be used to personalised treatment approaches (Leppert and Kuhle, 2019).

For the first time to our knowledge, we assessed the clinical prognostic potential of biofluid biomarkers against the cUHDRS – a composite measured derived from large cohort datasets to have high signal-to-noise ratio as a longitudinal measure of disease progression (Schobel et al., 2017). mHTT and NfL concentrations predicted change in cUHDRS, affirming their potential as biomarkers of HD progression. We show that both CSF mHTT and NfL each possess prognostic value for subsequent clinical decline and brain atrophy, as seen previously for plasma NfL in the TRACK-HD cohort.

That the rate of change in each analyte had lesser prognostic and discriminatory power than their baseline values may appear surprising. Longitudinal studies of NfL in other genetic neurodegenerative diseases including dominantly inherited Alzheimer's disease (AD) (Preische et al., 2019) and frontotemporal dementia (FTD) (van der Ende et al., 2019) have revealed that the rate of change in NfL was a stronger predictor of disease progression, with accelerated rate of change in those who converted from presymptomatic to symptomatic. The HD-CSF study was not designed to assess predictors of conversion from premanifest to manifest HD, but the rate of change in plasma NfL did show significant prognostic value in our comparison of fast versus slow progressors. NfL is an axonal protein but not specific to neuronal sub-populations or to a given disease pathology. It is likely that each disease exhibiting neuronal dysfunction will have a distinct longitudinal NfL profile. It is notable that HD has some of the highest elevated levels of CSF NfL compared to other neurological diseases studied to date, greater than levels in AD and FTD which progress more rapidly (Bridel et al., 2019). This may be one reason why rate of change does not appear to add significant prognostic potential to the baseline value.

Our computational clinical trial simulations offer a means to plan future clinical trials that would use the lowering of these biomarkers as disease progression endpoints. They suggest that a trial using plasma NfL with as few as 100 participants per arm run over six months would have over 90% power to show 20% slowing of disease progression. Using CSF NfL, the same trial would need to be run over nine months to achieve the same power. Because of a slower rate of increase, and more importantly, the inter-subject variability in the change over time, much larger participant numbers would be needed to show a deflection in the trajectory of mHTT by slowing disease progression alone. NfL is less variable and appears to be a better marker of HD progression and prognosis than mHTT. However, it is important to reiterate that mHTT retains its intrinsic value as a direct measure of the causative neurotoxin and as a means of assessing the on-target effects of huntingtin-lowering agents. To achieve this purpose, very small participant numbers are required, as shown by our previous cross-sectional power calculations and findings from the first human trial of such an agent (Byrne et al., 2018b; Tabrizi et al., 2019). Our novel finding that lower mHTT concentrations predict slower progression is potentially important in this respect.

5.4.3 Limitations

Despite being the largest longitudinal CSF collection with matched MRI data to our knowledge in HD, the sample number remains modest. We lack the granularity to make predictions of clinical outcome at the individual level. Larger sample numbers and greater follow-up durations may bring us closer to developing models that could inform clinical

prognosis. We are also limited to two longitudinal time points. The lack of associations between rate of change in analyte and the rate of clinical decline was likely driven by both sets of rates being derived from the same time period. Having additional time points would permit the comparison of rates of change in analyte with rates of clinical decline in the subsequent time period. For instance, change in NfL in year 1 may predict brain atrophy in year 2. Finally, the range of HD mutation carriers in this study does not cover the whole spectrum of HD. In particular, this study was not designed to detect the very earliest disease-related alterations, nor what happens in the later stages of disease.

5.4.4 Future perspective

Efforts are well underway to address these issues: HDClarity, a multi-national CSF collection initiative for HD has amassed over 600 CSF and plasma samples across the disease spectrum and is now accumulating longitudinal samples over repeated annual intervals (NCT02855476).

These insights into the longitudinal dynamics of mHTT and NfL shed light on the biology of HD in human mutation carriers and will be of immediate value in the design and conduct of disease-modifying clinical trials, especially as we enter the era of prevention trials where qualified surrogate endpoints will be fundamental (Food and Drug Administration, 2018). Looking ahead, some centres are already incorporating blood NfL measurement into shared clinical decision-making in neurological disease (Leppert and Kuhle, 2019). Continued study may reveal a role for mHTT and NfL in guiding decision-making for individuals living with HD.

5.5 Contributions and collaborations

I coordinated the HD-CSF study. I was involved in the final ethical approval of the study and attended the ethics review board meeting with the London - Camberwell St Giles Research Ethics Committee. I recruited all participants, managed all visit bookings, and oversaw sample and data management; I performed data collection including demographic and comorbidities information; I performed all cognitive assessments; I assisted with lumbar punctures; I transported samples for processing; I stored and managed the stock log of all samples; I coordinated and took part in all meetings discussing study management and data analysis. CSF and blood samples were collected by Dr Filipe Rodrigues. CSF and blood samples were processed by the Fluid Biomarker Lab at UCL Dementia Research Institute. MRI protocol development and data acquisition was performed by Dr Enrico De Vita. MRI processing and segmentations were performed by Dr Rachael Scahill and Dr Eileanoir Johnson.

The project in this chapter was conceived by myself, Dr Wild and Dr Filipe Rodrigues. I coordinated the procurement of a materials transfer agreement and arranged the shipment of CSF samples to Evotec A.G. who performed mHTT quantification. I quantified NfL in both CSF and blood plasma in all the HD-CSF samples at baseline and follow-up. The results were analysed jointly between myself and Dr Filipe Rodrigues. I was directly involved at each stage in the decision making of the analysis plan including developing the concept for using clinical trial simulations and power calculations to show how biofluid biomarkers may help to design more efficient trials. Filipe performed the statistical analyses, developing the longitudinal models and simulations. The EBM analysis and change-point analysis was performed by Dr Peter Wijeratne. I was jointly involved in the interpretation of the results with Dr Filipe Rodrigues and Dr Edward Wild. I wrote the first draft of the manuscript and prepared all figures. Dr Rodrigues and I prepared the manuscript for submission, collating all edits from co-authors and responding to reviewers.

Chapter 6 Cerebrospinal fluid neurogranin and TREM2 in Huntington's disease

This chapter is based on data previously published in Scientific Reports, of which I was joint first author (Byrne et al., 2018a). For the first time, we explored CSF neurogranin and TREM2 as potential biomarkers of HD.

6.1 Introduction

Studies in other neurodegenerative diseases have highlighted NfL as a compound of interest (1.2.2 Markers of neuronal damage). With neurodegenerative diseases all sharing the feature of progressive neuronal loss, one could extrapolate that there may be several shared biochemical processes up-stream of this. Therefore, biochemical markers for one disease, might have utility in HD. Inspired by recent findings in Alzheimer's disease (AD), we considered two such markers in CSF: neurogranin and TREM2.

I have discussed already how the *HTT* gene that causes HD (1.1.2 Genetics), does so by encoding a mutated form of the huntingtin protein (mHTT). Wild-type HTT has many intracellular functions and binding partners, and as such is involved in multiple signalling pathways (1.1.3 Pathobiology; Saudou and Humbert, 2016). mHTT has been implicated in the disruption of several of these pathways (Bates et al., 2015). Some overlap with those reported to be disrupted in Alzheimer's disease and other neurodegenerative diseases (Kinney et al., 2018; Li et al., 2018). These include disruption to synaptic maintenance (1.1.3 Neuropathology; Milnerwood and Raymond, 2010) and activation of the innate immune system (1.1.3 Neuropathology; Björkqvist et al., 2008; Dalrymple et al., 2007; Träger et al., 2014), which is thought to be mediated by a direct effect of mHTT on synaptic maintenance processes and within myeloid cells, respectively.

It has previously been shown that cytokines (Björkqvist et al., 2008; Dalrymple et al., 2007) and chemokines (Wild et al., 2011) were increased in plasma from HD mutation carriers and that the microglia-associated proteins, chitotriosidase and YKL40, were increased in HD mutation carriers' CSF (Rodrigues et al., 2016b). Further, YKL-40 was also associated with the severity of motor symptoms independent of the disease burden from exposure to the CAG repeat. Modulating the immune system has also been considered as a potential therapeutic target in HD (Björkqvist et al., 2009) and a phase II trial of the putative microglial-modulating agent (laquinimod) – an investigational medicinal product previously trialled in multiple sclerosis – was completed in 2018 (ClinicalTrials.gov, NCT02215616; Rodrigues and Wild, 2017).

Neurogranin is a postsynaptic protein that regulates the availability of calmodulin (Huang, 2004) – an important regulator of calcium-mediated signalling – and it has been proposed as a CSF biomarker of synaptic function (Blennow et al., 2010). Neurogranin is elevated in the CSF of AD disease patients (Tarawneh et al., 2016), but not in other neurodegenerative conditions such as frontotemporal dementia (FTD), Lewy body disease, Parkinson's disease (PD), progressive supranuclear palsy and multiple system atrophy (Wellington et al., 2016). I have already discussed in 1.1.3 Neuropathology the

evidence that synaptic dysfunction contributes to HD pathology (Sepers and Raymond, 2014; Smith et al., 2005). Further, a whole-brain gene expression study in post-mortem HD patient brains identified that *NRGN*, the gene encoding neurogranin, was amongst the most robustly downregulated genes in HD caudate compared to controls (Hodges et al., 2006). However, this differential expression did not appear in peripheral blood samples (Runne et al., 2007). It may be that the neurogranin phenotype in HD might only exist within the CNS. Neurogranin has yet to be quantified in CSF of HD patients.

Triggering receptor expressed on myeloid cells 2 (TREM2) is a protein primarily expressed in microglia within the CNS, but also in other myeloid cells including monocytes and macrophages. These cells are involved in the regulation of inflammatory pathways and their activation is thought to be inhibitory to the immune response (Sharif and Knapp, 2008). Missense mutations in TREM2 are associated with CNS diseases (Paloneva et al., 2002) and single-nucleotide polymorphisms in the gene encoding TREM2 have been reported as genetic modifiers of AD (Jonsson et al., 2013), amyotrophic lateral sclerosis (Cady et al., 2014), PD and FTD (Rayaprolu et al., 2013). Soluble TREM2 concentrations in CSF are elevated in other neurodegenerative diseases including AD (Heslegrave et al., 2016; Suárez-Calvet et al., 2019; Suárez - Calvet et al., 2016), and multiple sclerosis, however these could be normalised upon immunomodulatory treatment (Öhrfelt et al., 2016). While TREM2 has not been specifically linked to the pathobiology of HD, dysfunction of myeloid cells due to cell-autonomous expression of mHTT is a well-described feature of the disease (1.1.3 Neuropathology; Träger et al., 2014), and other microglial-associated proteins have shown disease-related alterations in HD patient CSF (Rodrigues et al., 2016b; Vinther-Jensen et al., 2014). The quantification of soluble TREM2 has not yet been completed in CSF from HD mutation carriers.

6.2 Aim

We set out to quantify neurogranin and soluble TREM2, two markers of AD, in CSF samples from HD mutation carriers and matched controls. We used the pilot CSF study to run an exploratory analysis of neurogranin. As we had previously shown disease-related alterations in the microglial-associated protein YKL-40 in HD patient CSF, we chose to use our larger 80 participant HD-CSF cohort to investigate TREM2 in HD mutation carriers. We aimed to determine if either analyte was altered in HD mutation carriers and associated with other measures of disease severity.

6.3 Methods

6.3.1 Participants and assessments

The pilot CSF study (see 2.3 Pilot CSF study) was used to study neurogranin and the HD-CSF study baseline samples and data were used to study TREM2 (see 2.3 HD-CSF). Ethical approval was given by the joint University College London/University College London Hospitals ethics committee (neurogranin cohort) and the London - Camberwell St Giles Research Ethics Committee (TREM2 cohort). All patients gave informed written consent before enrolment. For the neurogranin cohort, patient consent, inclusion and exclusion criteria, clinical assessment, CSF collection and storage were as previously published (Wild et al., 2015). In brief, samples were collected on ice after an overnight fast at the same time of day, centrifuged within 15 minutes, aliquoted and stored at -80°C using a standardised protocol and polypropylene plasticware. Inclusion and exclusion criteria, and methods of CSF collection were identical in the TREM2 cohort (Byrne et al., 2018a). Healthy controls were contemporaneously recruited, drawn from a population with a similar age to all HD mutation carriers, and clinically well, so the risk of incidental neurodegenerative diseases was very low. Clinical phenotype was assessed using the Unified Huntington's Disease Rating Scale (UHDRS) including total functional capacity and total motor score (Huntington Study Group, 1996). Manifest HD as opposed to premanifest HD was defined as UHDRS diagnostic confidence level of 4. Disease burden score, a function of age and CAG repeat length that predicts many features of HD onset and progression, was also used as an indicator of disease progression (Penney et al., 1997; Tabrizi et al., 2013). The TREM2 cohort had added optional MR imaging and the clinical assessment included the measures above, plus a cognitive battery consisting of Symbol Digit Modality Test, Categorical Verbal Fluency Test, Stroop Color Naming and Stroop Word Reading (full protocol available at http://hdclarity.net).

6.3.2 MRI acquisition

For the TREM2 cohort, T1-weighted MRI data were acquired on a 3T Siemens Prisma scanner using a protocol optimised for the HD-CSF study. Images were acquired using a 3D MPRAGE sequence with a TR=2000ms and TE=2.05ms. The protocol had an inversion time of 850ms, flip angle of 8 degrees, matrix size 256×240mm. A total of 256 coronal slices were collected to cover the entire brain with a slice thickness of 1.0mm with no gap. Parallel imaging acceleration was used (GRAPPA) and 3D distortion correction was applied to all images.

6.3.3 MRI Processing

Scans underwent visual quality control prior to processing. No scans were excluded due to the presence of significant motion or other artefacts. Bias correction was performed using the N3 procedure (Sled et al., 1998). Volumetric regions of the whole-brain, ventricles and total intracranial volume (TIV) were generated via MIDAS using semi-automated segmentation procedures as previously described (Freeborough et al., 1997; Scahill et al., 2003; Whitwell et al., 2001). SPM12 segment (MATLAB version 2012b) was used to measure the volumes of grey and white matter (Ashburner and Friston, 2005). Finally, to measure caudate volume the images were processed using MALP-EM (Ledig et al., 2015), a fully automated software that was recently validated in an HD cohort (Johnson et al., 2017). All segmentations underwent visual quality control to ensure accurate delineation of the regions. No scans failed processing. Brain volumes are expressed as a percentage of total intracranial volume, to account for overall head size.

6.3.4 CSF analyte quantification

CSF neurogranin was measured using an in-house ELISA and anti-Ng antibodies NG22 and NG2, as previously described (Wellington et al., 2016). All samples with the exception of six were above the limit of detection (LoD; i.e. 10.0 pg/mL) – four in the HD group and two samples in the control. Samples below the LoD were assigned the LoD concentration (i.e. 10.0 pg/mL). Concentrations of TREM2 were quantified with an in-house Meso Scale Discovery based ELISA, using an adapted protocol from Kleinberger et al., (2014). All samples were above the LoD (65.3 pg/mL). Haemoglobin concentration was measured using a commercial ELISA (E88-134, Bethyl Laboratories Inc.) to determine CSF contamination by blood. Quantification for each analyte was run on the same day for all samples using the same batch of reagents. Laboratory operators were blinded to clinical data.

6.3.5 Statistical analysis

Statistical analysis was performed with Stata 14 software (StataCorp, TX, USA). Significance level was defined as $p<0.05$. Both neurogranin and TREM2 concentrations were non-normally distributed; square-root transformation produced an acceptable normal distribution for TREM2, while non-parametric tests were used for neurogranin because of the smaller sample size.

Potentially confounding demographic variables (age, gender, haemoglobin i.e. blood contamination) were examined in preliminary analyses and those found significant were included as covariates for subsequent analyses.

For neurogranin, we used two-sample Wilcoxon rank-sum (Mann-Whitney) test or the exact Fisher test to assess intergroup differences. Two-group comparisons were tested using Wilcoxon rank-sum (Mann-Whitney) test, and associations were tested using Spearman rank-order correlation.

For TREM2, we used unpaired two-sample t-test/ANOVA or the Pearson's chi-squared test to assess intergroup differences in demographics. Group comparisons were tested using unpaired two-sample t-test/ANOVA for unadjusted comparisons or multiple linear regression for adjusted comparisons. Correlations were tested using Pearson's correlation and partial correlations for covariate adjustment. Where necessary, multiple comparisons were corrected for using the Bonferroni method.

For both analyses, a post-hoc power calculation for equivalence was computed assuming 1% type I errors (Jones et al., 1996) to provide an estimation of the statistical power of the data set. This was completed to robustly prove that analyte levels in healthy controls and HD mutation carriers were not different. We also performed sample size calculations for theoretical experiments to demonstrate that the level of each analyte was higher in HD mutation carriers than in controls, assuming 5% type I errors and 20% type II errors.

6.4 Results

6.4.1 Neurogranin

The neurogranin cohort consisted of 32 participants: 12 healthy controls and 20 HD mutation carriers. The HD group contained 17 manifest and 3 premanifest HD mutation carriers pooled together. Details of the cohort characteristics are presented in Table 20. There was no significant difference in age (p=0.243) or gender (p=0.452) distribution between the HD group and healthy controls.

Table 20 Characteristics of the neurogranin cohort.

Values are median (interquartile range). HD, HD mutation carriers; CAG, CAG repeat count; DBS, disease burden score.

Group (n)	Control (12)	HD (20)
Age	40 (25)	54 (13)
Sex F/M	3/9	9/11
CAG	N/A	44 (4)
DBS	N/A	401 (127)
Total functional capacity	N/A	11 (3)
UHDRS total motor score	N/A	26 (24)
CSF Neurogranin pg/mL	40.5 (100.5)	43.5 (72.5)

Medians and interquartile ranges (IQR) of CSF neurogranin are shown in Table 20. Assessing for potential confounding factors using healthy controls, CSF neurogranin concentration did not differ between genders (p=0.984); was not associated with age in healthy controls (rho=-0.15, p=0.412); and concentration of CSF haemoglobin was not associated with CSF neurogranin (rho=-0.25, p=0.585).

CSF neurogranin concentration was not significantly different between healthy controls and HD mutation carriers (Figure 42A; p=1.000). There was no significant correlation between CSF neurogranin levels and disease burden score (Figure 42B; rho=0.42, p=0.0660), UHDRS total functional capacity score (Figure 42C; rho=0.12, p=0.626) or UHDRS total motor score (Figure 42D; rho=-0.04, p=0.867).

We ran a post-hoc power calculation due to the low sample numbers, lack of previous data and as the results were negative. This showed that this dataset had 98% power to determine that CSF neurogranin levels are equivalent between healthy controls and HD mutation carriers. A sample size calculation indicated that 14,661 samples per group would be needed to establish with 80% power at p=0.05 that neurogranin levels are in fact higher in HD mutation carriers than in controls. Therefore, the analysis was not repeated in the larger TREM2 cohort.

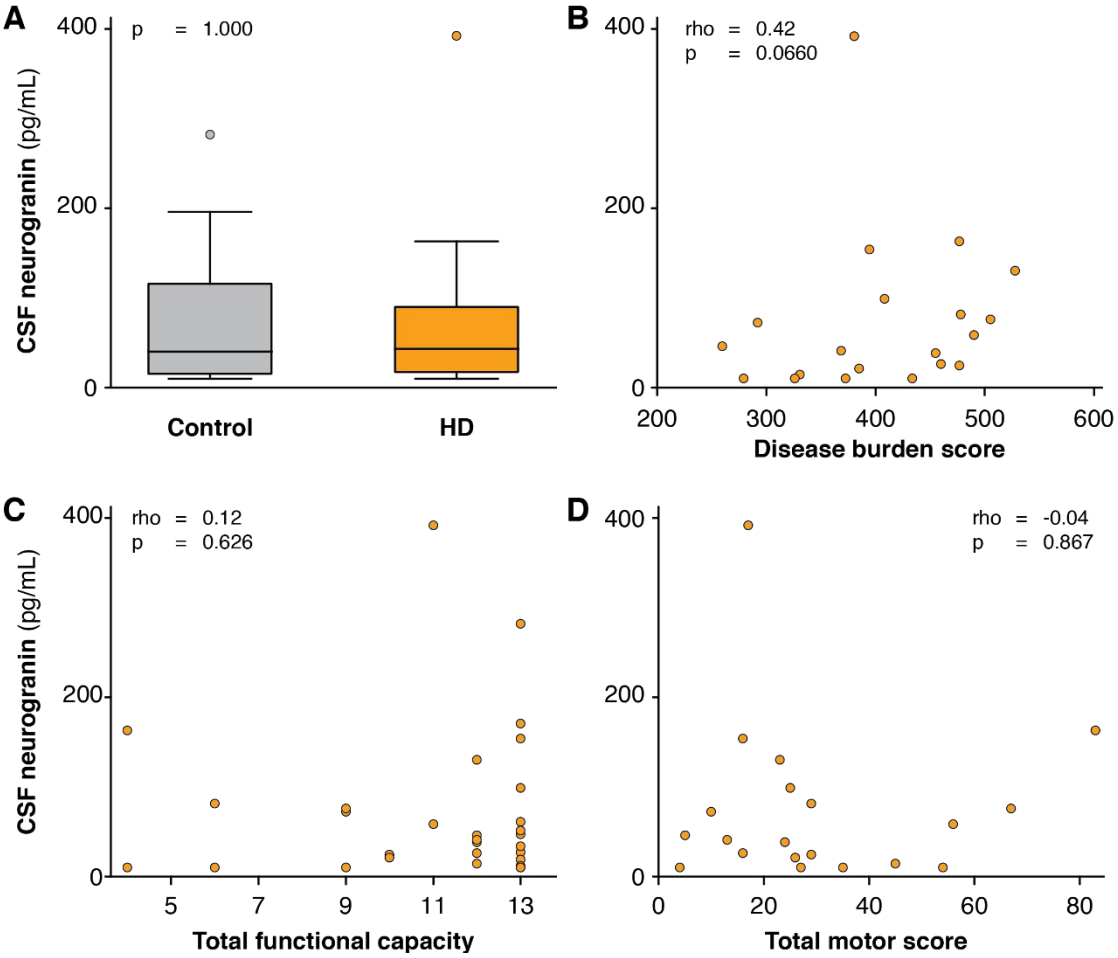

Figure 42 CSF neurogranin levels in HD mutation carriers within the pilot CSF study cohort.

(A) Inter-group comparison between healthy controls (n = 12) and HD mutation carriers (n = 20) using Wilcoxon rank-sum (Mann-Whitney) test. (B–D) Relationship between CSF neurogranin concentration and (B) disease burden score; (C) UHDRS total functional capacity score and (D) UHDRS total motor score. rho and corresponding p-values were generated using Spearman rank-order correlations.

6.4.2 TREM2

The TREM2 cohort consisted of 80 independent CSF samples collected from 20 healthy controls, 20 premanifest and 40 manifest HD patients from early to moderate stage disease. The cohort's demographics and clinical characteristics are presented in Table 21. The premanifest HD group was significantly younger than the control and manifest HD groups (ANOVA $p<0.0001$; control versus premanifest HD, $p=0.012$; premanifest versus manifest HD $p<0.0001$; $p=0.0244$ and $p<0.0001$ after Bonferroni adjustment for two comparisons), emphasising the need to adjust inter-group comparison analyses for age. There were no inter-group differences in gender ($p=0.905$).

Table 21 Clinical characteristics of the TREM2 cohort.

Values are mean ± SD. CAG, CAG repeat count; DBS, disease burden score; TFC, total functional capacity; TMS, total motor score; CSF, cerebrospinal fluid (mean ± SD of square-root transformed values).

Group (n)	**Control** (20)	**Premanifest HD** (20)	**Manifest HD** (40)
Age	50.7 ± 11.0	42.4 ± 11.0	56.0 ± 9.37
Sex F/M	10/10	10/10	18/22
CAG	N/A	42.0 ± 1.62	42.8 ± 2.18
Disease burden score	N/A	267.1 ± 61.2	395.3 ± 19.3
Total functional capacity	13 ± 0	13 ± 0	9.4 ± 2.70
Total motor score	2.35 ± 2.43	2.80 ± 2.80	37.3 ± 19.3
CSF TREM2 (√pg/mL)	77.5 ± 12.5	75.4 ± 11.6	87.6 ± 16.7

CSF TREM2 concentrations were strongly associated with age overall (Figure 43; r=0.609, p<0.0001) as well as within the control and HD mutation carrier groups (r=0.625, p=0.00320 for control; r=0.610, p<0.0001 for HD mutation carriers), so subsequent analyses included age as a covariate. There was no evidence for an effect of gender on TREM2 concentration in controls or HD mutation carriers (p=0.403 and p=0.808 respectively). The concentration of CSF haemoglobin, used to evaluate any effect of blood contamination, was not significantly associated with the concentration of CSF TREM2 (r=0.043 p=0.741 in all participants; r=0.357 p=0.122 in controls; r=-0.040 p=0.812 in HD mutation carriers).

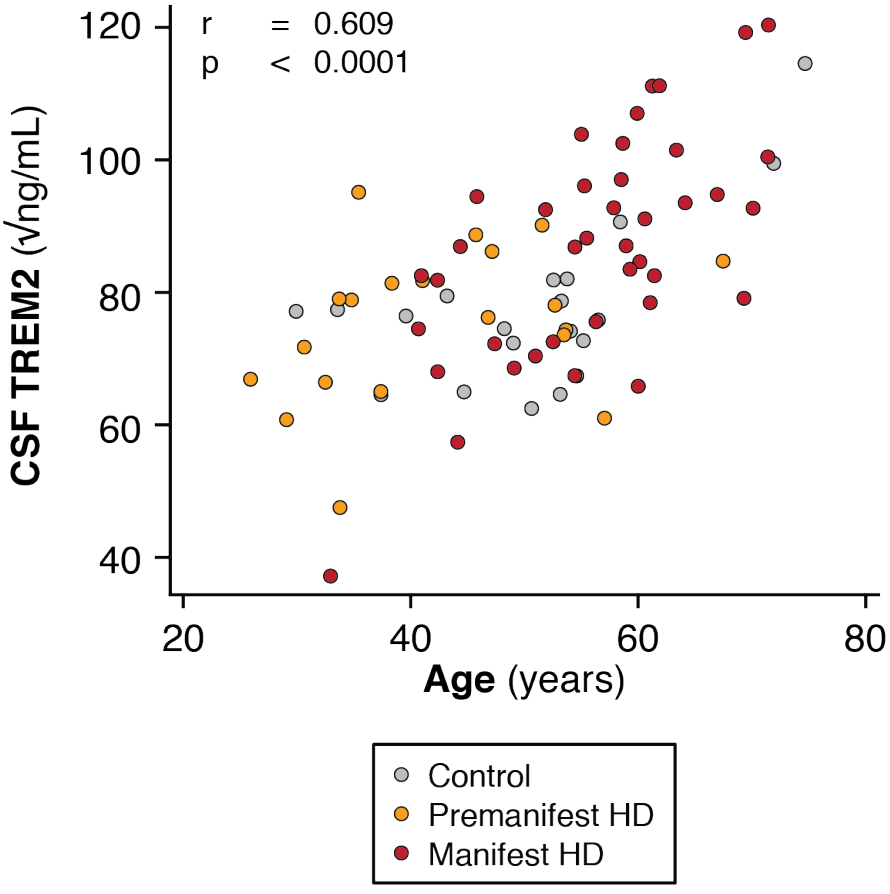

Figure 43 CSF TREM2 is associated with age in healthy controls and HD mutation carriers.

r and p generated from Pearson's correlation.

In the unadjusted dataset, CSF TREM2 was significantly higher in manifest HD compared to premanifest HD (p=0.00578) and controls (p=0.0243; Figure 44A). However, with age included as a covariate, these differences were no longer significant (p=0.152 and p=0.889 respectively), suggesting that this finding, along with an association with disease burden score (r=0.317 , p=0.0155), was an artefact of the tendency of TREM2 to increase with age, as supported by the older age of the manifest HD group (Figure 44B).

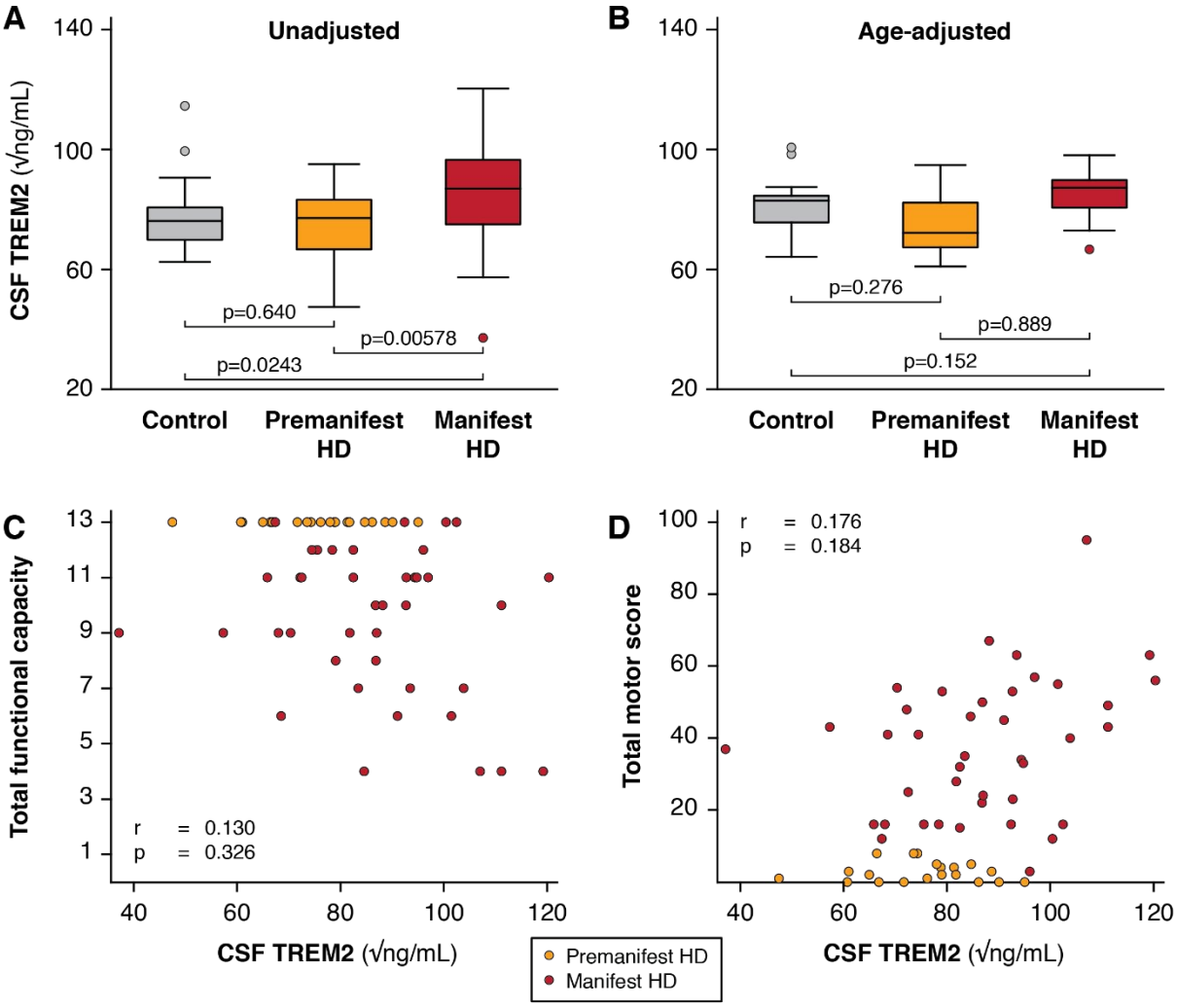

Figure 44 CSF TREM2 is not associated with disease stage or clinical measures in HD mutation carriers.

(A) Group comparisons from ANOVA of CSF TREM2 concentration between controls, premanifest HD and manifest HD before age-adjustment. (B) Group comparisons from multiple linear regression of CSF TREM2 concentration between controls, premanifest HD and manifest HD after age-adjustment. Relationship between CSF TREM2 and (C) UHDRS total functional capacity and (D) UHDRS total motor score. Scatter plots of unadjusted data points with r and p values that are age adjusted using partial correlations.

Predictably, these comparisons remained non-significant after Bonferroni multiplicity correction (Table 22). With age as a covariate, TREM2 concentration was not significantly different in HD mutation carriers overall than in controls (77.5 v 83.4 √pg/mL, p=0.133). There was no significant association among HD mutation carriers between

age-adjusted CSF TREM2 concentration and TFC, TMS (Figure 44C-D), SDMT, Stroop word reading, verbal fluency, Stroop color naming, and volumes of whole brain, caudate, grey matter, white matter, and lateral ventricles (Table 22).

Table 22 Relationships between CSF TREM2 and clinical, cognitive and MRI brain volume measures.

All volumetric measures were calculated as a percentage of total intracranial volume. r and p values generated using Pearson's partial correlations with adjustment for age.

Variable	r	p-value
UHDRS Total functional capacity	-0.1300	0.326
UHDRS Total motor score	0.176	0.184
Symbol-digit modality test	-0.030	0.823
Stroop word reading	-0.112	0.398
Stroop color naming	-0.0369	0.782
Verbal fluency test	-0.142	0.285
Volume of whole brain	0.0656	0.658
Volume of caudate	-0.0042	0.978
Volume of grey matter	0.0235	0.874
Volume of white matter	-0.0830	0.575
Volume of lateral ventricles	0.230	0.116

This sample had 88% power to demonstrate that CSF TREM2 levels are equivalent between healthy controls and HD mutation carriers. A sample size calculation indicated that 3,288 samples per group would be needed to establish with 80% power at p=0.05 that a significant CSF TREM2 increase does in fact exist in HD mutation carriers versus controls, after adjustment for age.

6.4.3 A post-hoc analysis of blood contamination

After publishing the preceding results in this chapter, data on the albumin concentration in CSF and blood plasma from all HD-CSF participants became available. TREM2 was not associated with the CSF to blood albumin ratio (r=-0.108 p= 0.538 in controls) but was associated with CSF albumin only (r= 0.379 p= 0.021 in controls). After re-analysis the lack of significant difference between groups remained after adjustment for age and CSF albumin (F=1.450, p= 0.2401).

6.5 Discussion

6.5.1 Summary

In two adequately-powered sample sets, we have shown that neither neurogranin, a putative marker of synaptic dysfunction, nor TREM2, a marker of microglial function, have an altered concentration in CSF in HD mutation carriers. An apparent increase in CSF TREM2 concentration in manifest HD was determined to be an artefact of its tendency to increase with age, rather than a mutation-driven effect. Sample size calculations revealed that an implausibly large number of samples would be required to show a significant difference between controls and HD mutation carriers.

6.5.2 Interpretation

Although neurogranin is a marker of synaptic dysfunction, the fact that neurogranin concentration was not altered in HD mutation carriers' CSF – nor blood as previously reported in Runne *et al* (2007) – does not necessarily indicate that synaptic dysfunction is absent from HD pathology. Since publishing these results, evidence for synaptic dysfunction in HD has been increasing with several studies involving both human data and mouse models (Smith-Dijak, Sepers and Raymond, 2019). A recent gene enrichment analysis using a combination of published studies reporting gene perturbation with mHTT-driven endpoints and HTT interactome databases, revealed that there is an enrichment for genes involved in exosome synaptic functions and homeostatic synaptic plasticity (Wang et al., 2017). McColgan and colleagues have provided further 'omics'-driven evidence of synaptic dysfunction within the neuropathological process in HD, using a combination of structural connectivity and transcriptomic studies in HD mutation carriers (McColgan et al., 2018). They reported that the white-matter connections most vulnerable in HD were associated with gene expression profiles enriched for synaptic genes and metabolic genes. It may be that synaptic disruption is localised to regions more pathologically effected in the HD brain creating a dilution effect when quantified in the CSF, which bathes and is in contact with the whole brain. Further, the process may be transient through the course of HD, adding further noise to the measurements from CSF.

Using the same logic, the increase seen in CSF TREM2, which did not survive age adjustment, could also be an artefact of a dilution effect in CSF, where the generalised neuroinflammation occurring with aging (Di Benedetto et al., 2017) outweighs any localised microglial activation in HD. Indeed, the same age response was also seen with CSF YKL-40 in HD (Rodrigues et al., 2016b; Vinther-Jensen et al., 2014). However, YKL-40 survived age-adjustment suggesting that it has a stronger relationship with HD-specific pathology. YKL-40, unlike TREM2, is also expressed in astrocytes under

neuroinflammatory conditions (Bonneh-Barkay et al., 2012). Therefore, astrocytes may be contributing to the increased CSF YKL-40 in HD and not solely microglia as previously thought.

6.5.3 Outside of HD

The neurogranin results presented here are consistent with increasing evidence that suggests that CSF-derived neurogranin is a specific biomarker for AD and beta amyloid pathology (Portelius et al., 2018; Wellington et al., 2018, 2016; Yilmaz et al., 2019). However, a marked increase in neurogranin has recently been reported in sporadic creutzfeldt-Jakob disease (CJD) compared to controls, and even when compared to AD patients (Blennow et al., 2019). Blennow and colleagues reported that in healthy control brains, neurogranin concentration was greater within neurons from the cortex and hippocampus; in AD, these are key brain regions that are known to degenerate in AD (Alafuzoff et al., 2008) and in CJD, cortical neuroaxonal damage is a prominent feature (Llorens et al., 2015). Further, the concentrations of neurogranin in brain lysate in AD and CJD inversely correlate that in CSF. Altogether, this suggests that an increase in CSF neurogranin could reflect a more regional and cell-specific neuronal loss with subsequent release of neurogranin, than simply synaptic loss as previously thought. For this reason and in light of previously mentioned data alluding to the involvement of synaptic dysfunction in HD, it seems unlikely that the lack of disease relevant changes in CSF neurogranin reflects on synaptic dysfunction within HD pathology.

Several genetic variants of TREM2 have been reported as risk factors for neurodegenerative diseases including AD, FTD and ALS (Cady et al., 2014; Hou et al., 2019; Jonsson et al., 2013; Kleinberger et al., 2014; Rayaprolu et al., 2013; Suárez - Calvet et al., 2016). Like CSF neurogranin, soluble TREM2 in the CSF has mostly been investigated and found to be altered in AD pathology (Gispert et al., 2016; Henjum et al., 2016; Heslegrave et al., 2016; Piccio et al., 2016; Suárez-Calvet et al., 2019; Suárez - Calvet et al., 2016). It appears to have a transient increase in AD that occurs after amyloid pathology and before tau pathology begins in AD (Suárez-Calvet et al., 2019, 2016). In FTD and patients with delirium, CSF TREM2 was found to be increased in cases where an amyloid pathology was present (Henjum et al., 2018; Woollacott et al., 2018). This suggests that permeabilisation of TREM2 is more closely influenced by derangements in beta amyloid. With little evidence indicating amyloid pathology in HD, this could be why we failed to find HD related changes in CSF TREM2.

6.5.4 Limitations

It could be that the alterations in both TREM2 and neurogranin are transient in the CSF and only occur at a particular stage in the pathology of HD. Despite the fact that our HD mutation carriers span a wide range of disease from early premanifest to moderate stage disease, we were not powered to stratify them into more discrete groups to compare this. However, disease burden score – a unidirectional measure of exposure to effects of the HD mutation, which increases linearly with disease stage, – correlated with TREM2, suggesting any increase in TREM2 occurs in parallel to the disease process.

TREM2 is expressed in all monocytes, therefore it is important to rule out blood contamination of samples. At the time of publishing the results from this chapter, haemoglobin was the only measure of blood contamination we had available. It is likely that haemoglobin is not the best measure for blood contamination. However, the post hoc analysis investigating other surrogate measures of blood contamination indicated that there remained no significant group difference after adjustment.

6.5.5 Future perspective

Even though HDClarity has amassed a CSF collection from several hundred participants, the sample sizes necessary to demonstrate alterations of these substances in CSF in HD are likely a prohibitively factor against further study. However, it will be important to elucidate the involvement of astrocytes versus microglia as well as synaptic processes in HD pathology. Human induced pluripotent stem cells (iPSC) differentiated into HD microglial cells and astrocytes could be useful in determining the relative contributions from astrocytes and microglial to secreted neurogranin (Bonneh-Barkay et al., 2012). Co-culturing iPSC-derived cortical and medium spiny neurons could also be used to recapitulate corticostriatal synapses *in vitro,* to further investigate mechanisms of synaptic loss and dysfunction in HD affected brain regions (Virlogeux et al., 2018).

Despite the evidence presented here that suggests these biomarkers do not track with HD progression, neurogranin and TREM2 may have their own utility as pharmacodynamic markers in trials aiming to ameliorate these pathways. For example, a drug designed to specifically target and improve synaptic function, might be expected to alter CSF neurogranin concentration. As such, concentrations of neurogranin or TREM2 could be considered as exploratory outcomes within clinical trial frameworks.

6.5.6 Conclusion

While they do not challenge findings from other conditions, these results suggest that neither neurogranin nor TREM2 is likely to be of value as a biomarker for disease progression in HD. Further work is needed to better understand the underlying mechanism of synaptic dysfunction and neuroinflammation in HD.

6.6 Contributions and collaborations

I coordinated the HD-CSF study. I was involved in the final ethical approval of the study and attended the ethics review board meeting with the London - Camberwell St Giles Research Ethics Committee. I recruited all participants, managed all visit bookings, and oversaw sample and data management; I performed data collection including demographic and comorbidities information; I performed all cognitive assessments; I assisted with lumbar punctures; I transported samples for processing; I stored and managed the stock log of all samples; I coordinated and took part in all meetings discussing study management and data analysis. CSF and blood samples were collected by Dr Filipe Rodrigues. CSF and blood samples were processed by the Fluid Biomarker Lab at UCL Dementia Research Institute. MRI protocol development and data acquisition was performed by Dr Enrico De Vita. MRI processing and segmentations were performed by Dr Rachael Scahill and Dr Eileanoir Johnson.

The project in this chapter was conceived by myself, Dr Wild and Prof. Henrik Zetterberg. Neurogranin was quantified in Prof. Zetterberg's lab in Gothenburg. I coordinated the procurement of a materials transfer agreement and arranged the shipment of CSF samples to Gothenburg. I shipped the Pilot CSF study CSF samples to Gothenburg – which had previously been collected by Dr Wild and were stored at the Institute of Neurology. The TREM2 protocol was shared with me by Prof. Henrik Zetterberg and Dr Amanda Heslegrave who were setting up the MSD assay in the Fluid Biomarker Lab at UCL Dementia Research Institute. I helped with initial testing and optimising the protocol. I quantified TREM2 in all the HD-CSF samples. The results were analysed jointly between myself and Dr Filipe Rodrigues. I was directly involved at each stage in the decision making of the analysis plan and Filipe performed the statistical analyses. I was jointly involved in the interpretation of the results with Dr Filipe Rodrigues and Dr Edward Wild. Filipe wrote the first draft of the manuscript and prepared all figures. I reviewed and edited subsequent versions. Dr Rodrigues and I prepared the manuscript for submission, collating all edits from co-authors and responding to reviewers.

Chapter 7 Discussion

7.1 Thesis synopsis

7.1.1 NfL: The first blood-based biomarker of HD progression

Using the large and well characterised TRACK-HD cohort, we demonstrated that NfL in blood plasma was elevated in HD mutation carriers and that this increase began over 10 years from predicted onset, continued to increase with disease severity and was associated with well-established clinical and brain volume measures. Plasma NfL has a striking CAG-dependent genetic dose relationship, with higher CAG leading to earlier and steeper increases in NfL with age. Notably, a single measurement at baseline predicted subsequent clinical decline and brain atrophy, as well as onset age of motor symptoms. The strong correlation between plasma and CSF levels were supportive of the CNS origin of plasma levels. This is the first time a blood-based marker has been shown to possess such prognostic value in HD.

Using an independent cohort, HD-CSF, we were able to replicate these findings for plasma NfL both in its cross-sectional associations using both baseline and 24-month follow-up sample collections, and its CAG dependent longitudinal trajectories over time in HD mutation carriers. We also confirmed the result that baseline values were associated with subsequent disease progression, particularly with brain atrophy. Further to this, we showed that rate of change in NfL had less prognostic value than the single measurement at baseline. CSF and plasma levels of NfL were highly correlated in both cohorts, and at least within HD-CSF, plasma NfL appears to be as good as, if not better than CSF NfL for prognostic use.

7.1.2 mHTT and NfL: the dynamic duo

The primary aim of HD-CSF was to determine the longitudinal characteristics of mHTT in CSF in order to inform ongoing huntingtin-lowering clinical trials. When plasma NfL emerged as a robust biomarker for disease progression, it became imperative to assess NfL in parallel to mHTT. As with plasma NfL, we were able to replicate the observed increases in CSF mHTT and NfL with disease severity previously shown in other cohorts (Constantinescu *et al.*, 2009; Wild *et al.*, 2015; Vinther-Jensen *et al.*, 2016). Compared to CSF mHTT and CSF NfL, plasma NfL had the strongest associations with clinical and cognitive measures. All three were stable over the short interval of six weeks meaning fewer participants would be needed to detect effective drug-induced within-subject change. Cross-sectionally in the HD-CSF baseline, NfL in both CSF and blood had stronger associations with brain volumes than CSF mHTT. However, in the 24-month follow-up – with the same subjects being two years more advanced along their HD trajectories – CSF mHTT had the strongest associations with brain volume. Baseline values for each CSF mHTT, CSF NfL and plasma NfL all predicted subsequent brain

atrophy. The clinical trial simulations of using lowering of these markers in terms of progression suggested that NfL could potentially be used to run shorter trials with much lower participant numbers to achieve the same power and effect size as mHTT. NfL appears to be the stronger biomarker of disease progression, and combined with the pharmacodynamic ability of mHTT, makes a potentially powerful toolkit for huntingtin-lowering trials.

7.1.3 The earliest detection of Huntington's disease pathology?

The event-based modelling method revealed that these three biofluid biomarkers were detectably altered earlier than all other clinical, cognitive and imaging measures that were investigated in HD-CSF. It is important to note that like all models, this technique has its own caveats. The ordering is generated by using the values for controls and manifest HD patients to define normal and abnormal for each biomarker. mHTT is not present in healthy controls, thus the zero levels for these controls create a bias suggesting it is the earliest to change in HD mutation carriers. However, since the aim is to capture the earliest detection of pathology rather than emulate the genetic test, then NfL could be a powerful candidate for a marker because it enables detection of such subtle alterations. To develop this further, additional measurements are needed in a cohort of HD mutation carriers who are much further from onset than those in previous studies.

7.1.4 Characterising longitudinal dynamics of mHTT and NfL

The longitudinal dynamics of NfL in CSF and plasma were both distinct from controls with little overlap at any age. CSF mHTT - perhaps unsurprising given that controls do not produce mHTT - also had a distinct trajectory from controls but with greater inter-subject variability. All three displayed a CAG dependent dose response, as was previously found for plasma NfL in TRACK-HD.

7.1.5 Neurogranin and TREM2 are not HD biomarkers

Our discovery of the prognostic potential of NfL for HD was inspired by prior study of NfL in other diseases, such as Multiple sclerosis and other neurodegenerative diseases. With the same reasoning, we hoped that Neurogranin and TREM2 could be 'borrowed' from the Alzheimer's disease field and provide utility as a biofluid biomarker for HD. Unfortunately, neither showed disease related differences in our hands. This is not to say that there is no synaptic dysfunction or microglial activation in HD. Both processes are highly dynamic, and to interpret changes from them is difficult using cross-sectional data. Further, the processes might be localised in the brain and the signal then diluted in the CSF.

7.1.6 HD-CSF is a high quality biofluid resource for the HD community

The HD-CSF is the first prospectively designed longitudinal CSF collection with standardisation procedures in HD, matched blood collection and phenotypic data. This is a unique resource for the HD community that allows the interrogation of CSF biomarkers alongside MRI modalities. As highlighted in this thesis, the dataset has already brought new insights into mHTT, NfL, neurogranin and TREM2. A bank of precious samples and data remains and will be used in the future to propagate biofluid biomarker discovery.

7.1.7 What are the impact of these results for HD?

This thesis has provided novel insights into mHTT and NfL and their role as biomarkers for HD. The main findings in the context of other literature are summarised in Table 23. These combined findings demonstrate that mHTT and NfL are robust biomarkers for disease progression. However, a strong relationship with natural history does not guarantee a biomarker will show a good response to successful treatment. We know from studies in diseases that possess disease modifying therapies such as Multiple Sclerosis and Spinal muscular atrophy (SMA), that NfL levels reduce with effective treatments (Kuhle *et al.*, 2015; Winter *et al.*, 2019). Whether CSF mHTT reduction would bring about slowing of disease progression remains to be seen, but it has already been proven as a pharmacodynamic marker of huntingtin-lowering (Tabrizi *et al.*, 2019).

Other groups have also reported on NfL in HD CSF since the start of this thesis, with consistent increases in HD mutation carriers observed compared to controls (Niemelä *et al.*, 2017, 2018; Szejko *et al.*, 2018). Niemelä and colleagues compared NfL directly with total Tau in CSF. Interestingly, despite both being thought to be markers of neuronal injury, NfL had the strongest associations with clinical features of HD. This poses the question of whether NfL is more closely intertwined in the pathogenesis of HD than is currently thought, and thus is not simply a pure marker of neuronal damage. There was a transient increase of CSF NfL after 4 months of dosing at the two highest ASO doses in the phase 1b/2a trial and subsequent open label extension (Tabrizi *et al.*, 2019). Although this could suggest the undesirable occurrence of neuroinflammation, an alternative explanation could be interactions of mHTT and NfL: a transcriptional analysis of HD brains showed that NfL was the second most down-regulated protein in HD versus controls (Hodges *et al.*, 2006). mHTT may have a direct effect of levels of NfL, and so, lowering it may lead to increase in NfL.

Table 23 Summary of what this thesis adds to our previous understanding of the performance of mHTT and NfL as biomarkers for HD.

Chapters from this thesis reporting these findings are indicated; entries in bold were first reported as a result of this thesis work. Citations refer to the first published work in which each finding was reported; HD, Huntington's disease; C, healthy controls;

Cross-sectional data	**CSF mHTT**	**CSF NfL**	**Plasma NfL**
Higher in HD v C	Yes (Wild et al., 2015) Chapters 4, 5	Yes (Constantinescu et al., 2009) Chapters 3, 4, 5	**Yes (Byrne et al., 2017)** **Chapters 3, 4, 5**
Rises with disease stage	Yes (Wild et al., 2015) Chapters 4, 5	Yes (Vinther-Jensen et al., 2016) Chapters 4, 5	**Yes (Byrne et al., 2017)** **Chapters 3, 4, 5**
Baseline level associated with clinical severity	Yes (Wild et al., 2015) Chapters 4, 5	**Yes (Byrne et al., 2018b)** **Chapters 4, 5**	**Yes (Byrne et al., 2017)** **Chapters 3, 4, 5**
Baseline level associated with brain volume	**Yes** **Chapter 5**	**Yes (Byrne et al., 2018b)** **Chapters 4, 5**	**Yes (Byrne et al., 2017)** **Chapters 3, 4, 5**
Longitudinal data			
Baseline level predicts onset	?	?	**Yes (Byrne et al., 2017)** **Chapter 3**
Baseline level predicts clinical progression	**Yes** **Chapter 5**	**Yes** **Chapter 5**	**Yes (Byrne et al., 2017)** **Chapters 3, 5**
Baseline level predicts brain atrophy	**Yes** **Chapter 5**	**Yes** **Chapter 5**	**Yes (Byrne et al., 2017)** **Chapters 3, 5**
Change predicts clinical progression	**Yes**(TMS only) **Chapter 5**	**Yes** **Chapter 5**	**Yes** **Chapter 5**
Change predicts clinical atrophy	**Yes** **Chapter 5**	**Yes** **Chapter 5**	**Yes** **Chapter 5**

7.2 Lessons learned

7.2.1 Importance of confounders

Many biological processes alter with age, including disease-specific processes. It is important to distinguish whether these processes are due to the disease or healthy aging. We showed in chapter 6, an association with both disease burden and disease group differences in CSF TREM2 prior to adjusting for age. Consistent with a generalised neuroinflammation with ageing, these associations were lost after adjusting for age, showing they are unlikely to be disease-related. In comparison, the NfL and mHTT show alterations with disease progression and prognostic ability over and above normal aging.

Blood contamination is another important consideration when investigating markers in CSF, which are highly expressed peripherally in blood. Many inflammatory markers, including soluble TREM2, have higher concentrations in blood compared to CSF (Bekris *et al.*, 2018). Blood contamination in CSF could, therefore, confound any signal specific to the CNS.

Outside of this thesis, we have also explored Brain-derived neurotrophic factor (BDNF; unpublished work) in HD-CSF. We found an association with the time in freezer in blood measurements of BDNF and not CSF. Although this effect was not present when we investigated it in mHTT and NfL in Chapter 5, it suggests that time in the freezer is another factor that may need to considered as a potential confounder, particularly when studying previously collected samples retrospectively and longitudinal sampling over years.

7.2.2 Interpreting what is measured in biofluids

In general, there is a lack of information in the literature reported on immunoassays both commercially and those developed in-house. Very few are fully validated for the protein they are said to measure in terms of the specific species or isoforms that they bind to.

This has been made apparent with the mHTT immunoassay which despite being technically validated, has a lot of variability between HD carriers (Fodale *et al.*, 2017). The mHTT assay signal is a composite of many contributing factors. The nature of the MW1 antibody binding to multiple polyglutamines is essential for the mutant vs wild-type signal because mHTT has a much longer polyglutamine length than wild-type. MW1 acts as the detector antibody in the immunocomplex sandwich and in the presence of mHTT, it is thought that multiple MW1 detector will bind to protein, generating the higher signal. Fodale and colleagues also showed that the size of the mHTT protein impacts the signal, with smaller protein fragments generating higher signal than the large full length protein. In the clinical setting, where patients have varying CAG repeats and the possibility of

varying lengths within in their own brains, this is perhaps why there is greater variability between HD mutation carriers.

7.3 A changing landscape for HD

7.3.1 Huntingtin lowering programs

When the work described in this thesis began, only one targeted huntingtin-lowering therapeutic candidate was being tested in the clinic (now known under several names: Ionis-$HTT_{RX;}$ ISIS 443139, RG6042, RO7234292). After the announcement of the top line results from the Ionis phase 1b/2a trial – safety profile and a dose-dependent lowering of mHTT in CSF – in December 2017, Roche exercised their option to license the drug. Since then the program has expanded extensively, from an open-label extension of the original trial, to a phase 3 efficacy trial (GENERATION HD1), a pharmacokinetics and pharmacodynamics trial (GEN-PEAK), a natural history study and an overarching open-label extension that participants can enter after completing earlier trials (GEN-EXTEND). GEN-EXTEND will continue to collect data for long-term safety of continued administration until the drug is licensed or the program is cut.

As of December 2019, several other candidates are now being tested in the clinic including two allele-specific ASOs from Wave Life sciences (NCT03225833, 2017; NCT03225846, 2017), and the first virally administrated gene therapy for HD from UniQure (NCT04120493, 2019). Many others are in the pipeline (Wild and Tabrizi, 2017). Each candidate comes with their own potential caveats including titratability, penetrability into affected regions of the brain, routes of administration and the longevity of expected effect. Whether any will be truly disease-modifying of HD progression the fields remains unknown. However, the momentum that has been building in the field is tangible and generating hope for researchers and HD family members alike.

7.3.2 Genetic modifiers of HD

Following on from the GWAS published in 2015 by the GeM-HD consortium, several other GWA studies have been published with more evidence supporting the involvement DNA Repair pathway genes in the modification of disease onset and progression (Hensman Moss *et al.*, 2017; Lee *et al.*, 2019; Wright *et al.*, 2019). DNA damage and repair has since become a major focus of HD research and other CAG repeat diseases (Massey and Jones, 2018).

The two separate GWAS that were published in 2019, also found rare but potent hits on chromosome 4 around the *HTT* CAG repeat itself (Lee *et al.*, 2019; Wright *et al.*, 2019). These related to presence or lack of CAA interruptions within the CAG tract. The canonical polyCAG tract sequence has a penultimate CAA interruption. Individuals missing this CAA interruption had a significantly earlier age of onset than expected for their CAG length whereas those with additional CAA interruptions had delayed onset.

The mechanism of disease modification of both DNA repair genes and HTT CAA interruptions is thought to be acting on the somatic instability of the CAG repeat (Lee *et al.*, 2019). The concept of somatic CAG repeat instability (variation and higher CAG expansions in more affected tissues) driving disease was introduced many years ago (Telenius, Kremer and Goldberg, 1994; Kennedy and Shelbourne, 2000; Kennedy *et al.*, 2003; Wheeler, 2003; Shelbourne *et al.*, 2007; Swami *et al.*, 2009) but in light of these GWAS results, interest in it has been reinvigorated.

7.3.3 Clinical characterisation

In the clinic, defining diagnosis and age of onset of HD generates much inconsistency and variability which may bias how disease modifiers are defined and characterised. This diagnosis has relied heavily on the motor phenotype which can present less prominently in some individuals who are already functionally affected by the disease. To suggest those who present first with a more cognitive or neuropsychiatric phenotype and have functional decline are not manifest is potentially detrimental to research that assesses disease progression.

The HD field is now acknowledging this with an effort to further subcategorise HD mutation carriers into not only manifest or premanifest HD, but with the additional prodromal HD category for genetically confirmed individuals presenting some symptoms but not sufficient enough for a clinician to be certain of the onset of disease (Table 1) (Ross *et al.*, 2019) However, this proposed reconfiguration remains under discussion and has yet to be integrated into standard clinical care. With prevention trials potentially on the horizon, the importance of characterising this prodromal phase grows. Using this new format of clinical characterisation may help stratify HD mutation carriers prior to clinical diagnosis in biomarker research.

Table 24 The criteria for diagnoses of HD mutation carriers.

Adapted from (Ross et al., 2019). DCL, diagnostic confidence level.

Diagnosis	Motor	Cognitive	Potential Treatment
(1) Presymptomatic HD	DCL 0–2	Normal	(1) Disease modifying
(2) Prodromal HD (either A or B)	A) DCL 2 B) DCL 3	(A) + Minor or major neurocognitive changes (B) With normal (unchanged) cognition	(2A or B) Symptomatic or disease modifying
(3) Manifest HD (either A or B)	A) DCL 3 B) DCL 4	(A) + Minor or major neurocognitive changes (B) With normal (unchanged) cognition	(3A or B) Symptomatic or disease modifying

7.3.4 Biofluid biomarkers for HD

There has been a handful of published studies since the beginning of this thesis reporting on biofluid biomarkers for HD, two of which involved CSF. Reed and colleagues were able to successfully quantify free microRNAs from HD CSF from the Predict-HD study (Reed *et al.*, 2018). They found 6 microRNAs were upregulated in HD CSF compared but these did not correlate with the microRNAs they previously shown to be dysregulated in HD brains. This may be due to unknown mechanisms of how microRNAs enter in CSF, or simply that HD brains are from individuals much later in their disease than the prodromal the individuals who gave their CSF. The potential importance of the adaptive immune system has also emerged, with a report on sCD27 showing it increases with disease stage and also early in preHD (Niemelä *et al.*, 2018). This promising finding will need further investigation. However, it might be important to note that the majority of controls and a few preHD samples had levels below the assays limit of detection. A more sensitive assay may be needed to elucidate this further.

Studies in blood have included a longitudinal collection that investigated plasma cytokine levels and found IL-6 and IL8 to have weak associations with cognitive dysfunction but not neuropsychiatric symptoms (Bouwens *et al.*, 2016), TNF-α and IL-10 to increase over 2 years and IL-6 and IL-8 to be associated with total functional capacity (Bouwens *et al.*, 2017). In light of the GWAS results and the connection to DNA repair genes in HD modification, it is perhaps interesting that DNA damage signatures appear to be present in peripheral blood mononuclear cells (Castaldo *et al.*, 2018). This is a promising result

and could mean that quantifying telomere length and double-strand breaks may be a useful readout for testing drugs aimed at reducing DNA damage.

7.3.5 Technological advancement

The advancement of certain technologies has now made ultrasensitive detection of biochemical markers possible. The results from this thesis would not have been attainable without development towards single molecule counting and single molecule array platforms. I anticipate the unearthing of many more sensitive and pathologically relevant biochemical biomarkers which were previously undetectable will be achieved by harnessing these platforms and their subsequent iteration.

Outside of immunoassays, further technological advancements are being made that may expedite biomarker research in HD. The dawn of 7 Tesla MRI has arrived which will bring about the highest resolution images of the human brains than ever before (Kraff *et al.*, 2015). The first huntingtin PET-ligands will enter first in human studies next year (NCT03810898, 2019). This could provide a much more explicit pharmacodynamics marker of huntingtin-lowering, giving spatial clarity to the effectiveness in deeper brain regions.

7.4 Future directions

7.4.1 THE INfLUX:HD CONSORTIUM

With the striking ability of NfL to act as a biomarker of HD progression, the first priority should be to generate as much data on the dynamics of this protein throughout the entire natural history of HD. This will be essential to building its case for regulatory approval of its use as a clinical trial endpoint. I have received funding to continue this work at postdoctoral level, and have begun amassing samples and data from HD human and animal model cohorts in which I will quantify NfL in blood (and CSF if available) and fully characterise it for its clinical utility. The aim of the project, called Influx-HD, is to generate a model for expected NfL trajectories for a given CAG repeat length, with the hope they will inform clinical trial enrichment or stratification for prevention trials, and eventually go/no-go decision making on when to initiate potentially invasive disease modifying treatments (in hope that they will indeed become a reality).

I have already received samples from the Kids-HD and Kids-JHD cohorts and will investigate NfL in children at-risk for HD as well those with Juvenile HD. Having a blood biomarker for Juvenile HD could be crucial for facilitating clinical trials in this rare and understudied population. Predict-HD, which followed over 1000 premanifest and prodromal HD mutation carriers up to 10 years, offers a rich dataset of longitudinal phenotypic data. I will quantify NfL in all blood plasma samples as well as the subset of CSF samples available. HDClarity, is set to be the largest and longest longitudinal biofluid collection in HD with a target of 1200 participants spanning the whole spectrum of HD and annual longitudinal sampling, to be continued indefinitely.

Another aspect of Influx-HD is to assess the translatability of NfL to HD animal models. I plan to identify which HD animal models have an NfL phenotype and therefore might be more optimal for preclinical therapeutic development of drugs targeting neuronal protection.

7.4.2 Developing better mHTT assays

It is evident from chapters 4 and 5 that our current means of quantifying mHTT may not be sensitive enough for prevention trials. Further, the concentrations extrapolated from it must be interpreted with extreme caution as we cannot infer if the difference in signal truly comes from raw concentration or polyglutamine length or protein size. We not only need more sensitive mHTT assays but we need sensitive assays for all HTT species.

Assay development and sensitivity will always be constrained by the availability of the antibodies with high affinity and specificity that you want to assay. Huntingtin antibodies have been poorly characterised. During my postdoctoral fellowship, I will carry out a placement at the Structural Genomic Consortium to perform an extensive assessment of all HTT antibodies currently available, defining their binding affinities and determining their precise epitopes. I plan to take the best antibodies forward for the development of ultrasensitive immunoassays for huntingtin species.

7.4.3 Future candidates and targets

With the multiple independent findings from GWAS studies supporting the involvement of DNA handling and repair as a modifier for HD and the mechanism thought to be acting through somatic instability of the CAG repeat, I anticipate molecules that modulate these genes will be tested as therapeutic candidates for HD. There currently is no means to assess somatic instability within the brain *in vivo* nor at the protein level. The low concentration of mHTT DNA and RNA in CSF will make quantifying CAG length variation extremely difficult. One possible option could be extracting exosomes – membrane bound extracellular vesicles containing various molecular constituents from their original cell – from CSF with the hope that they will hold a more concentrated source to perform DNA and RNA sequencing. As already mentioned within this thesis, NfL is not disease-specific and is elevated in many neurodegenerative diseases (Bridel *et al.*, 2019). It would be valuable to have other biomarkers related to a neuronal population more specific to regions of the brain which degenerate in HD. For instance, DARPP32 for medium spiny striatal neurons, or TCIP2 for cortical pyramidal neurons. These have yet to be explored any biofluids for HD (Rodrigues, Byrne and Wild, 2018).

7.4.4 Conclusion

In closing, I have provided evidence for the application of mHTT and NfL as highly sensitive and unbiased biomarkers of HD progression. This work has established a framework for the assessment of prospective biomarkers for HD and set a precedent for future candidates. I feel privileged to have had the opportunity to help assemble and work on the highest quality datasets to bring mHTT and NfL closer to full validation. These advancements in biofluid biomarkers have arrived in a timely matter with the acceleration of huntingtin-lowering therapeutic programs. I anticipate it will be early administration and a combination of huntingtin-lowering therapies that will make the biggest impact to the ultimate goal, to stop this cruel and relentless disease in its tracks.

References

Al Nimer, F., Thelin, E., Nyström, H., Dring, A.M., Svenningsson, A., Piehl, F., Nelson, D.W., Bellander, B.-M., 2015. Comparative Assessment of the Prognostic Value of Biomarkers in Traumatic Brain Injury Reveals an Independent Role for Serum Levels of Neurofilament Light. PLoS One 10, e0132177. https://doi.org/10.1371/journal.pone.0132177

Alafuzoff, I., Arzberger, T., Al-Sarraj, S., Bodi, I., Bogdanovic, N., Braak, H., Bugiani, O., Del-Tredici, K., Ferrer, I., Gelpi, E., Giaccone, G., Graeber, M.B., Ince, P., Kamphorst, W., King, A., Korkolopoulou, P., Kovács, G.G., Larionov, S., Meyronet, D., Monoranu, C., Parchi, P., Patsouris, E., Roggendorf, W., Seilhean, D., Tagliavini, F., Stadelmann, C., Streichenberger, N., Thal, D.R., Wharton, S.B., Kretzschmar, H., 2008. Staging of Neurofibrillary Pathology in Alzheimer's Disease: A Study of the BrainNet Europe Consortium. Brain Pathol. 18, 484–496. https://doi.org/10.1111/j.1750-3639.2008.00147.x

Amor, S., van der Star, B.J., Bosca, I., Raffel, J., Gnanapavan, S., Watchorn, J., Kuhle, J., Giovannoni, G., Baker, D., Malaspina, A., Puentes, F., 2014. Neurofilament light antibodies in serum reflect response to natalizumab treatment in multiple sclerosis. Mult. Scler. J. 20, 1355–1362. https://doi.org/10.1177/1352458514521887

Andersen, A.D., Binzer, M., Stenager, E., Gramsbergen, J.B., 2017. Cerebrospinal fluid biomarkers for Parkinson's disease - a systematic review. Acta Neurol. Scand. 135, 34–56. https://doi.org/10.1111/ane.12590

Andrew, S.E., Goldberg, Y.P., Kremer, B., Telenius, H., Theilmann, J., Adam, S., Starr, E., Squitieri, F., Lin, B., Kalchman, M.A., Graham, R.K., Hayden, M.R., 1993. The relationship between trinucleotide (CAG) repeat length and clinical features of Huntington's disease. Nat. Genet. 4, 398–403. https://doi.org/10.1038/ng0893-398

Aronson, N.N., Blanchard, C.J., Madura, J.D., 1997. Homology modeling of glycosyl hydrolase family 18 enzymes and proteins. J. Chem. Inf. Comput. Sci. 37, 999–1005.

Ashburner, J., Friston, K.J., 2005. Unified segmentation. Neuroimage 26, 839–851. https://doi.org/10.1016/j.neuroimage.2005.02.018

Ashburner, J., Friston, K.J., 2000. Voxel-Based Morphometry—The Methods. Neuroimage 11, 805–821. https://doi.org/10.1006/nimg.2000.0582

Bates, G., Tabrizi, S.J., Jones, L., 2014. Huntington's Disease, 4th ed. Oxford University

Press.

Bates, G.P., Dorsey, R., Gusella, J.F., Hayden, M.R., Kay, C., Leavitt, B.R., Nance, M., Ross, C. a., Scahill, R.I., Wetzel, R., Wild, E.J., Tabrizi, S.J., 2015. Huntington disease. Nat. Rev. Dis. Prim. 15005. https://doi.org/10.1038/nrdp.2015.5

Biglan, K.M., Zhang, Y., Long, J.D., Geschwind, M., Kang, G.A., Killoran, A., Lu, W., McCusker, E., Mills, J.A., Raymond, L.A., Testa, C., Wojcieszek, J., Paulsen, J.S., 2013. Refining the diagnosis of Huntington disease: the PREDICT-HD study. Front. Aging Neurosci. 5, 12. https://doi.org/10.3389/fnagi.2013.00012

Bjerke, M., Engelborghs, S., 2018. Cerebrospinal Fluid Biomarkers for Early and Differential Alzheimer's Disease Diagnosis. J. Alzheimer's Dis. https://doi.org/10.3233/JAD-170680

Björkqvist, M., Wild, E.J., Tabrizi, S.J., 2009. Harnessing Immune Alterations in Neurodegenerative Diseases. Neuron 64, 21–24. https://doi.org/10.1016/J.NEURON.2009.09.034

Björkqvist, M., Wild, E.J., Thiele, J., Silvestroni, A., Andre, R., Lahiri, N., Raibon, E., Lee, R. V, Benn, C.L., Soulet, D., Magnusson, A., Woodman, B., Landles, C., Pouladi, M.A., Hayden, M.R., Khalili-Shirazi, A., Lowdell, M.W., Brundin, P., Bates, G.P., Leavitt, B.R., Möller, T., Tabrizi, S.J., 2008. A novel pathogenic pathway of immune activation detectable before clinical onset in Huntington's disease. J. Exp. Med. 205, 1869–77. https://doi.org/10.1084/jem.20080178

Blennow, K., Diaz-Lucena, D., Zetterberg, H., Villar-Pique, A., Karch, A., Vidal, E., Hermann, P., Schmitz, M., Ferrer Abizanda, I., Zerr, I., Llorens, F., 2019. CSF neurogranin as a neuronal damage marker in CJD: a comparative study with AD. J. Neurol. Neurosurg. Psychiatry jnnp-2018-320155. https://doi.org/10.1136/jnnp-2018-320155

Blennow, K., Hampel, H., Weiner, M., Zetterberg, H., 2010. Cerebrospinal fluid and plasma biomarkers in Alzheimer disease. Nat. Publ. Gr. 6, 131–144. https://doi.org/10.1038/nrneurol.2010.4

Bohár, Z., Toldi, J., Fülöp, F., Vécsei, L., 2015. Changing the face of kynurenines and neurotoxicity: therapeutic considerations. Int. J. Mol. Sci. 16, 9772–93. https://doi.org/10.3390/ijms16059772

Bonneh-Barkay, D., Bissel, S.J., Kofler, J., Starkey, A., Wang, G., Wiley, C.A., 2012. Astrocyte and Macrophage Regulation of YKL-40 Expression and Cellular Response in Neuroinflammation. Brain Pathol. 22, 530–546.

https://doi.org/10.1111/j.1750-3639.2011.00550.x

Borowsky, B., Warner, J., Leavitt, B.R., Tabrizi, S.J., Roos, R.A.C., Durr, A., Becker, C., Sampaio, C., Tobin, A.J., Schulman, H., 2013. 8OHdG is not a biomarker for Huntington disease state or progression. Neurology 80, 1934–41. https://doi.org/10.1212/WNL.0b013e318293e1a1

Bridel, C., Van Wieringen, W.N., Zetterberg, H., Tijms, B.M., Teunissen, C.E., Alvarez-Cermeño, J.C., Andreasson, U., Axelsson, M., Bäckström, D.C., Bartos, A., Bjerke, M., Blennow, K., Boxer, A., Brundin, L., Burman, J., Christensen, T., Fialová, L., Forsgren, L., Frederiksen, J.L., Gisslén, M., Gray, E., Gunnarsson, M., Hall, S., Hansson, O., Herbert, M.K., Jakobsson, J., Jessen-Krut, J., Janelidze, S., Johannsson, G., Jonsson, M., Kappos, L., Khademi, M., Khalil, M., Kuhle, J., Landén, M., Leinonen, V., Logroscino, G., Lu, C.H., Lycke, J., Magdalinou, N.K., Malaspina, A., Mattsson, N., Meeter, L.H., Mehta, S.R., Modvig, S., Olsson, T., Paterson, R.W., Pérez-Santiago, J., Piehl, F., Pijnenburg, Y.A.L., Pyykkö, O.T., Ragnarsson, O., Rojas, J.C., Romme Christensen, J., Sandberg, L., Scherling, C.S., Schott, J.M., Sellebjerg, F.T., Simone, I.L., Skillbäck, T., Stilund, M., Sundström, P., Svenningsson, A., Tortelli, R., Tortorella, C., Trentini, A., Troiano, M., Turner, M.R., Van Swieten, J.C., Vågberg, M., Verbeek, M.M., Villar, L.M., Visser, P.J., Wallin, A., Weiss, A., Wikkelsø, C., Wild, E.J., 2019. Diagnostic Value of Cerebrospinal Fluid Neurofilament Light Protein in Neurology: A Systematic Review and Meta-analysis. JAMA Neurol. 76, 1035–1048. https://doi.org/10.1001/jamaneurol.2019.1534

Burchell, J.T., Panegyres, P.K., 2017. New cerebrospinal fluid biomarkers in Alzheimer's disease. Future Neurol. 12, 53–56. https://doi.org/10.2217/fnl-2017-0009

Byrne, L.M., Rodrigues, F.B., Blennow, K., Durr, A., Leavitt, B.R., Roos, R.A.C., Scahill, R.I., Tabrizi, S.J., Zetterberg, H., Langbehn, D., Wild, E.J., 2017. Neurofilament light protein in blood as a potential biomarker of neurodegeneration in Huntington's disease: a retrospective cohort analysis. Lancet Neurol. 16, 601–9. https://doi.org/10.1016/S1474-4422(17)30124-2

Byrne, L.M., Rodrigues, F.B., Johnson, E.B., De Vita, E., Blennow, K., Scahill, R., Zetterberg, H., Heslegrave, A., Wild, E.J., 2018a. Cerebrospinal fluid neurogranin and TREM2 in Huntington's disease. Sci. Rep. 8, 4260. https://doi.org/10.1038/s41598-018-21788-x

Byrne, L.M., Rodrigues, F.B., Johnson, E.B., Wijeratne, P.A., De Vita, E., Alexander, D.C., Palermo, G., Czech, C., Schobel, S., Scahill, R.I., Heslegrave, A., Zetterberg,

H., Wild, E.J., 2018b. Evaluation of mutant huntingtin and neurofilament proteins as potential markers in Huntington's disease. Sci. Transl. Med. 10, eaat7108. https://doi.org/10.1126/scitranslmed.aat7108

Byrne, L.M.L.M., Wild, E.J.E.J., 2016. Cerebrospinal Fluid Biomarkers for Huntington's Disease. J. Huntingtons. Dis. 5, 1–13. https://doi.org/10.3233/JHD-160196

Cady, J., Koval, E.D., Benitez, B.A., Zaidman, C., Jockel-Balsarotti, J., Allred, P., Baloh, R.H., Ravits, J., Simpson, E., Appel, S.H., Pestronk, A., Goate, A.M., Miller, T.M., Cruchaga, C., Harms, M.B., 2014. *TREM2* Variant p.R47H as a Risk Factor for Sporadic Amyotrophic Lateral Sclerosis. JAMA Neurol. 71, 449. https://doi.org/10.1001/jamaneurol.2013.6237

Califf, R.M., 2018. Biomarker definitions and their applications. Exp. Biol. Med. 243, 213–221. https://doi.org/10.1177/1535370217750088

Callaghan, J., Stopford, C., Arran, N., Boisse, M.-F., Coleman, A., Santos, R.D., Dumas, E.M., Hart, E.P., Justo, D., Owen, G., Read, J., Say, M.J., Durr, A., Leavitt, B.R., Roos, R.A.C., Tabrizi, S.J., Bachoud-Levi, A.-C., Bourdet, C., van Duijn, E., Craufurd, D., 2015. Reliability and factor structure of the Short Problem Behaviors Assessment for Huntington's disease (PBA-s) in the TRACK-HD and REGISTRY studies. J. Neuropsychiatry Clin. Neurosci. 27, 59–64. https://doi.org/10.1176/appi.neuropsych.13070169

Christensen, G.E., Rabbitt, R.D., Miller, M.I., 1996. Deformable templates using large deformation kinematics. IEEE Trans. Image Process. 5, 1435–1447. https://doi.org/10.1109/83.536892

Constantinescu, R., Romer, M., Oakes, D., Rosengren, L., Kieburtz, K., 2009. Levels of the light subunit of neurofilament triplet protein in cerebrospinal fluid in Huntington's disease. Parkinsonism Relat. Disord. 15, 245–8. https://doi.org/10.1016/j.parkreldis.2008.05.012

Constantinescu, R., Romer, M., Zetterberg, H., Rosengren, L., Kieburtz, K., 2011. Increased levels of total tau protein in the cerebrospinal fluid in Huntington's disease. Parkinsonism Relat. Disord. 17, 714–5. https://doi.org/10.1016/j.parkreldis.2011.06.010

Craufurd, D., Thompson, J.C., Snowden, J.S., 2001. Behavioral changes in Huntington disease. Neuropsychiatry, Neuropsychol. Behav. Neurol. 14, 219–226.

Cummings, D.M., André, V.M., Uzgil, B.O., Gee, S.M., Fisher, Y.E., Cepeda, C., Levine, M.S., 2009. Alterations in cortical excitation and inhibition in genetic mouse models

of Huntington's disease. J. Neurosci. 29, 10371–10386. https://doi.org/10.1523/JNEUROSCI.1592-09.2009

Cummings, D.M., Milnerwood, A.J., Dallérac, G.M., Vatsavayai, S.C., Hirst, M.C., Murphy, K.P.S.J., 2007. Abnormal cortical synaptic plasticity in a mouse model of Huntington's disease. Brain Res. Bull. 72, 103–107. https://doi.org/10.1016/j.brainresbull.2006.10.016

Cummings, D.M., Milnerwood, A.J., Dallérac, G.M., Waights, V., Brown, J.Y., Vatsavayai, S.C., Hirst, M.C., Murphy, K.P.S.J., 2006. Aberrant cortical synaptic plasticity and dopaminergic dysfunction in a mouse model of huntington's disease. Hum. Mol. Genet. 15, 2856–2868. https://doi.org/10.1093/hmg/ddl224

Dallérac, G.M., Vatsavayai, S.C., Cummings, D.M., Milnerwood, A.J., Peddie, C.J., Evans, K.A., Walters, S.W., Rezaie, P., Hirst, M.C., Murphy, K.P.S.J., 2011. Impaired Long-Term Potentiation in the Prefrontal Cortex of Huntington's Disease Mouse Models: Rescue by D₁ Dopamine Receptor Activation. Neurodegener. Dis. 8, 230–239. https://doi.org/10.1159/000322540

Dalrymple, A., Wild, E.J., Joubert, R., Sathasivam, K., Björkqvist, M., Petersén, A., Jackson, G.S., Isaacs, J.D., Kristiansen, M., Bates, G.P., Leavitt, B.R., Keir, G., Ward, M., Tabrizi, S.J., 2007. Proteomic profiling of plasma in Huntington's disease reveals neuroinflammatory activation and biomarker candidates. J. Proteome Res. 6, 2833–2840. https://doi.org/10.1021/pr0700753

Davies, S.W., Turmaine, M., Cozens, B.A., DiFiglia, M., Sharp, A.H., Ross, C.A., Scherzinger, E., Wanker, E.E., Mangiarini, L., Bates, G.P., 1997. Formation of neuronal intranuclear inclusions underlies the neurological dysfunction in mice transgenic for the HD mutation. Cell 90, 537–548. https://doi.org/10.1016/S0092-8674(00)80513-9

De La Monte, S.M., Vonsattel, J.P., Richardson, E.P., 1988. Morphometric demonstration of atrophic changes in the ceRebral cortex, white matter, and neostriatum in huntington's disease. J. Neuropathol. Exp. Neurol. 47, 516–525. https://doi.org/10.1097/00005072-198809000-00003

DeLong, E.R., DeLong, D.M., Clarke-Pearson, D.L., 1988. Comparing the Areas under Two or More Correlated Receiver Operating Characteristic Curves: A Nonparametric Approach. Biometrics 44, 837. https://doi.org/10.2307/2531595

Di Benedetto, S., Müller, L., Wenger, E., Düzel, S., Pawelec, G., 2017. Contribution of neuroinflammation and immunity to brain aging and the mitigating effects of physical and cognitive interventions. Neurosci. Biobehav. Rev. 75, 114–128.

https://doi.org/10.1016/j.neubiorev.2017.01.044

DiFiglia, M., Sapp, E., Chase, K.O., Davies, S.W., Bates, G.P., Vonsattel, J.P., Aronin, N., 1997. Aggregation of huntingtin in neuronal intranuclear inclusions and dystrophic neurites in brain. Science (80-.). 277, 1990–1993. https://doi.org/10.1126/science.277.5334.1990

Disanto, G., Barro, C., Benkert, P., Naegelin, Y., Schädelin, S., Giardiello, A., Zecca, C., Blennow, K., Zetterberg, H., Leppert, D., Kappos, L., Gobbi, C., Kuhle, J., 2017. Serum Neurofilament light: A biomarker of neuronal damage in multiple sclerosis. Ann. Neurol. 81, 857–870. https://doi.org/10.1002/ana.24954

Dorsey, E.R., Beck, C.A., Darwin, K., Nichols, P., Brocht, A.F.D., Biglan, K.M., Shoulson, I., 2013. Natural history of Huntington disease. JAMA Neurol. 70, 1520–1530. https://doi.org/10.1001/jamaneurol.2013.4408

Ducray, P.S., Frances, N., Smart, K., Norris, D., Kordasiewicz, H., Guenther, A., Wild, E., Schobel, S., 2019. Translational Pharmacokinetic/Pharmacodynamic (PK/PD) Modeling Strategy to Support RG6042 Dose Selection in Huntington's Disease (HD) (S16.005). Neurology 92.

Dunlap, C.B., 1927. Pathologic changes in huntington's chorea: With special reference to the corpus striatum. Arch. Neurol. Psychiatry 18, 867–943. https://doi.org/10.1001/archneurpsyc.1927.02210060002001

Duyao, M., Ambrose, C., Myers, R., Novelletto, A., Persichetti, F., Frontali, M., Folstein, S., Ross, C., Franz, M., Abbott, M., Gray, J., Conneally, P., Young, A., Penney, J., Hollingsworth, Z., Shoulson, I., Lazzarini, A., Falek, A., Koroshetz, W., Sax, D., Bird, E., Vonsattel, J., Bonilla, E., Alvir, J., Conde, J.B., Cha, J.H., Dure, L., Gomez, F., Ramos, M., Sanchez-Ramos, J., Snodgrass, S., De-Young, M., Wexler, N., Moscowitz, C., Penchaszadeh, G., Macfarlane, H., Anderson, M., Jenkins, B., Srinidhi, J., Barnes, G., Gusella, J., Macdonald, M., 1993. Trinucleotide repeat length instability and age of onset in Huntington's disease. Nat. Genet. 4, 387–392. https://doi.org/10.1038/ng0893-387

EMA, 2008. OVERVIEW OF COMMENTS RECEIVED ON DRAFT GUIDANCE DOCUMENT ON QUALIFICATION OF BIOMARKERS.

Engvall, E., Perlmann, P., 1972. Enzyme-linked immunosorbent assay, Elisa. J. Immunol. 109, 129–35.

Engvall, E., Perlmann, P., 1971. Enzyme-linked immunosorbent assay (ELISA) quantitative assay of immunoglobulin G. Immunochemistry 8, 871–874.

https://doi.org/10.1016/0019-2791(71)90454-X

Enna, S.J., Stern, L.Z., Wastek, G.J., Yamamura, H.I., 1977. Cerebrospinal fluid gamma-aminobutyric acid variations in neurological disorders. Arch. Neurol. 34, 683–5.

Eshaghi, A., Marinescu, R. V., Young, A.L., Firth, N.C., Prados, F., Cardoso, M.J., Tur, C., Angelis, F. De, Cawley, N., Brownlee, W., Stefano, N. De, Stromillo, M.L., Battaglini, M., Ruggieri, S., Gasperini, C., Filippi, M., Rocca, M.A., Rovira, A., Sastre-Garriga, J., Geurts, J., Vrenken, H., Wottschel, V., Leurs, C.E., Uitdehaag, B., Pirpamer, L., Enzinger, C., Ourselin, S., Wheeler-Kingshott, C.A.G., Chard, D., Thompson, A.J., Barkhof, F., Alexander, D.C., Ciccarelli, O., 2017. Progression of regional grey matter atrophy in multiple sclerosis. bioRxiv 190116. https://doi.org/10.1101/190116

Evans, S.J.W., Douglas, I., Rawlins, M.D., Wexler, N.S., Tabrizi, S.J., Smeeth, L., 2013. Prevalence of adult Huntington's disease in the UK based on diagnoses recorded in general practice records. J. Neurol. Neurosurg. Psychiatry 84, 1156–1160. https://doi.org/10.1136/jnnp-2012-304636

Ewers, M., Mattsson, N., Minthon, L., Molinuevo, J.L., Antonell, A., Popp, J., Jessen, F., Herukka, S.K., Soininen, H., Maetzler, W., Leyhe, T., Bürger, K., Taniguchi, M., Urakami, K., Lista, S., Dubois, B., Blennow, K., Hampel, H., 2015. CSF biomarkers for the differential diagnosis of Alzheimer's disease: A large-scale international multicenter study. Alzheimer's Dement. 11, 1306–1315. https://doi.org/10.1016/j.jalz.2014.12.006

Fang, Q., Strand, A., Law, W., Faca, V.M., Fitzgibbon, M.P., Hamel, N., Houle, B., Liu, X., May, D.H., Poschmann, G., Roy, L., Stühler, K., Ying, W., Zhang, J., Zheng, Z., Bergeron, J.J.M., Hanash, S., He, F., Leavitt, B.R., Meyer, H.E., Qian, X., McIntosh, M.W., 2009. Brain-specific proteins decline in the cerebrospinal fluid of humans with Huntington disease. Mol. Cell. Proteomics 8, 451–66. https://doi.org/10.1074/mcp.M800231-MCP200

FDA-NIH Biomarker Working Group, 2016. BEST (Biomarkers, EndpointS, and other Tools) Resource, BEST (Biomarkers, EndpointS, and other Tools) Resource. Food and Drug Administration (US)/National Institutes of Health (US).

Ferrante, R.J., Kowall, N.W., Beal, M.F., Martin, J.B., Bird, E.D., Richardson, E.P., 1987. Morphologic and histochemical characteristics of a spared subset of striatal neurons in huntington's disease. J. Neuropathol. Exp. Neurol. 46, 12–27. https://doi.org/10.1097/00005072-198701000-00002

Fodale, V., Boggio, R., Daldin, M., Cariulo, C., Spiezia, M.C.M.C., Byrne, L.M.L.M.,

Leavitt, B.R.B.R., Wild, E.J.E.J., Macdonald, D., Weiss, A., Bresciani, A., 2017. Validation of Ultrasensitive Mutant Huntingtin Detection in Human Cerebrospinal Fluid by Single Molecule Counting Immunoassay. J. Huntingtons. Dis. 6, 349–361. https://doi.org/10.3233/JHD-170269

Fonteijn, H.M., Modat, M., Clarkson, M.J., Barnes, J., Lehmann, M., Hobbs, N.Z., Scahill, R.I., Tabrizi, S.J., Ourselin, S., Fox, N.C., Alexander, D.C., 2012. An event-based model for disease progression and its application in familial Alzheimer's disease and Huntington's disease. Neuroimage 60, 1880–1889. https://doi.org/10.1016/J.NEUROIMAGE.2012.01.062

Food and Drug Administration, 2018. Biomarker Qualification: Evidentiary Framework Guidance for Industry and FDA Staff DRAFT GUIDANCE.

Fox, N.C., Freeborough, P.A., 1997. Brain atrophy progression measured from registered serial MRI: validation and application to Alzheimer's disease. J Magn Reson. 7, 1069–1075.

Freeborough, P.A., Fox, N.C., 1998. Modeling brain deformations in Alzheimer disease by fluid registration of serial 3D MR images. J. Comput. Assist. Tomogr. 22, 838–43.

Freeborough, P.A., Fox, N.C., 1997. The boundary shift integral: An accurate and robust measure of cerebral volume changes from registered repeat MRI. IEEE Trans. Med. Imaging 16, 623–629. https://doi.org/10.1109/42.640753

Freeborough, P.A., Fox, N.C., Kitney, R.I., 1997. Interactive algorithms for the segmentation and quantitation of 3-D MRI brain scans. Comput. Methods Programs Biomed. 53, 15–25.

Gaiottino, J., Norgren, N., Dobson, R., Topping, J., Nissim, A., Malaspina, A., Bestwick, J.P., Monsch, A.U., Regeniter, A., Lindberg, R.L., Kappos, L., Leppert, D., Petzold, A., Giovannoni, G., Kuhle, J., 2013. Increased neurofilament light chain blood levels in neurodegenerative neurological diseases. PLoS One 8, e75091. https://doi.org/10.1371/journal.pone.0075091

Genetic Modifiers of Huntington's Disease (GeM-HD) Consortium, G.M. of H.D. (GeM-H., 2015. Identification of Genetic Factors that Modify Clinical Onset of Huntington's Disease. Cell 162, 516–26. https://doi.org/10.1016/j.cell.2015.07.003

Gispert, J.D., Suárez-Calvet, M., Monté, G.C., Tucholka, A., Falcon, C., Rojas, S., Rami, L., Sánchez-Valle, R., Lladó, A., Kleinberger, G., Haass, C., Molinuevo, J.L., 2016. Cerebrospinal fluid sTREM2 levels are associated with gray matter volume

increases and reduced diffusivity in early Alzheimer's disease. Alzheimers. Dement. 12, 1259–1272. https://doi.org/10.1016/j.jalz.2016.06.005

Gisslén, M., Price, R.W., Andreasson, U., Norgren, N., Nilsson, S., Hagberg, L., Fuchs, D., Spudich, S., Blennow, K., Zetterberg, H., 2015. Plasma Concentration of the Neurofilament Light Protein (NFL) is a Biomarker of CNS Injury in HIV Infection: A Cross-Sectional Study. EBioMedicine 3, 135–140. https://doi.org/10.1016/j.ebiom.2015.11.036

Glushakova, O., Glushakov, A., Miller, E., Valadka, A., Hayes, R., 2016. Biomarkers for acute diagnosis and management of stroke in neurointensive care units. Brain Circ. 2, 28. https://doi.org/10.4103/2394-8108.178546

Gmitterová, K., Gawinecka, J., Llorens, F., Varges, D., Valkovič, P., Zerr, I., 2018. Cerebrospinal fluid markers analysis in the differential diagnosis of dementia with Lewy bodies and Parkinson's disease dementia. Eur. Arch. Psychiatry Clin. Neurosci. https://doi.org/10.1007/s00406-018-0928-9

Gusella, J.F., MacDonald, M.E., 2009. Huntington's disease: The case for genetic modifiers. Genome Med. https://doi.org/10.1186/gm80

Hansson, O., Janelidze, S., Hall, S., Magdalinou, N., Lees, A.J., Andreasson, U., Norgren, N., Linder, J., Forsgren, L., Constantinescu, R., Zetterberg, H., Blennow, K., 2017. Blood-based NfL. Neurology 88, 930–937. https://doi.org/10.1212/WNL.0000000000003680

Hedreen, J.C., Folstein, S.E., 1995. Early Loss of Neostriatal Striosome Neurons in Huntington's Disease. J. Neuropathol. Exp. Neurol. 54, 105–120. https://doi.org/10.1097/00005072-199501000-00013

Henjum, K., Almdahl, I.S., Årskog, V., Minthon, L., Hansson, O., Fladby, T., Nilsson, L.N.G., 2016. Cerebrospinal fluid soluble TREM2 in aging and Alzheimer's disease. Alzheimers. Res. Ther. 8, 17. https://doi.org/10.1186/s13195-016-0182-1

Henjum, K., Quist-Paulsen, E., Zetterberg, H., Blennow, K., G Nilsson, L.N., Otto Watne, L., 2018. CSF sTREM2 in delirium—relation to Alzheimer's disease CSF biomarkers Aβ42, t-tau and p-tau. J. Neuroinflammation 15. https://doi.org/10.1186/s12974-018-1331-1

Hensman Moss, D.J., Pardiñas, A.F., Langbehn, D., Lo, K., Leavitt, B.R., Roos, R., Durr, A., Mead, S., TRACK-HD investigators, T., REGISTRY investigators, T., Holmans, P., Jones, L., Tabrizi, S.J., 2017. Identification of genetic variants associated with Huntington's disease progression: a genome-wide association study. Lancet.

Neurol. 16, 701–711. https://doi.org/10.1016/S1474-4422(17)30161-8

Heslegrave, A., Heywood, W., Paterson, R., Magdalinou, N., Svensson, J., Johansson, P., Öhrfelt, A., Blennow, K., Hardy, J., Schott, J., Mills, K., Zetterberg, H., 2016. Increased cerebrospinal fluid soluble TREM2 concentration in Alzheimer's disease. Mol. Neurodegener. 11, 3. https://doi.org/10.1186/s13024-016-0071-x

Heyes, M.P., Saito, K., S., C.J., Davis, L.E., Demitrack, M.A., Der, M., Dilling, L.A., Elia, J., Kruesi, M.J.P., Lackner, A., Larsen, S.A., Lee, K., Leornard, H.L., Markey, S.P., Martin, A., Milstein, S.P., Mouradian, M.M., Pranzatelli, M.R., Quearry, B.J., Salazar, A., Smith, M., Strauss, S.E., Sunderland, T., Swedo, S.W.A., Tourtellotte, W.W., Crowley, J.S., Lee, L.E., Markey, M.A., Quearry, M., Demitrack, L.A., Elia, J., Kruesi, M.J.P., Leonard, A., Swedo, S.W.A., Martin, K., Sunderland, H.L., Milstein, S.P., Der, A., Mouradian, S., Strauss, M.M., Davis, M.R., Lackner, B.J., Smith, A., Larsen, M., Pranzatelli, S.E., Alazar, T., Tourtellotte, S.W., Dilling, W.W., Heyes, W.W., 1992. Quinolinc acid and kynurenine pathway metabolism in inflammatory and non-inflammatory neurological disease. Brain 115, 1249–1273. https://doi.org/10.1093/brain/115.5.1249

Heyes, M.P., Swartz, K.J., Markey, S.P., Beal, M.F., 1991. Regional brain and cerebrospinal fluid quinolinic acid concentrations in Huntington's disease. Neurosci. Lett. 122, 265–269. https://doi.org/10.1016/0304-3940(91)90874-S

Hobbs, N.Z., Henley, S.M.D., Ridgway, G.R., Wild, E.J., Barker, R.A., Scahill, R.I., Barnes, J., Fox, N.C., Tabrizi, S.J., 2010. The progression of regional atrophy in premanifest and early Huntington's disease: a longitudinal voxel-based morphometry study. J. Neurol. Neurosurg. Psychiatry 81, 756–763. https://doi.org/10.1136/jnnp.2009.190702

Hobbs, N.Z., Henley, S.M.D., Wild, E.J., Leung, K.K., Frost, C., Barker, R.A., Scahill, R.I., Barnes, J., Tabrizi, S.J., Fox, N.C., 2009. Automated quantification of caudate atrophy by local registration of serial MRI: Evaluation and application in Huntington's disease. Neuroimage 47, 1659–1665. https://doi.org/10.1016/j.neuroimage.2009.06.003

Hodges, A., Strand, A.D., Aragaki, A.K., Kuhn, A., Sengstag, T., Hughes, G., Elliston, L.A., Hartog, C., Goldstein, D.R., Thu, D., Hollingsworth, Z.R., Collin, F., Synek, B., Holmans, P.A., Young, A.B., Wexler, N.S., Delorenzi, M., Kooperberg, C., Augood, S.J., Faull, R.L.M., Olson, J.M., Jones, L., Luthi-Carter, R., 2006. Regional and cellular gene expression changes in human Huntington's disease brain. Hum. Mol. Genet. 15, 965–977. https://doi.org/10.1093/hmg/ddl013

Hou, X.-H., Bi, Y.-L., Tan, M.-S., Xu, W., Li, J.-Q., Shen, X.-N., Dou, K.-X., Tan, C.-C., Tan, L., Yu, J.-T., 2019. Genome-wide association study identifies Alzheimer's risk variant in MS4A6A influencing cerebrospinal fluid sTREM2 levels. Neurobiol. Aging. https://doi.org/10.1016/J.NEUROBIOLAGING.2019.05.008

Huang, K.-P., 2004. Neurogranin/RC3 Enhances Long-Term Potentiation and Learning by Promoting Calcium-Mediated Signaling. J. Neurosci. 24, 10660–10669. https://doi.org/10.1523/JNEUROSCI.2213-04.2004

Huang, Y.-C., Wu, Y.-R., Tseng, M.-Y., Chen, Y.-C., Hsieh, S.-Y., Chen, C.-M., 2011. Increased prothrombin, apolipoprotein A-IV, and haptoglobin in the cerebrospinal fluid of patients with Huntington's disease. PLoS One 6, e15809. https://doi.org/10.1371/journal.pone.0015809

Huntington Study Group, 1996. Unified Huntington's Disease Rating Scale: Reliability and Consistency. Mov. Disord. 11, 136–142. https://doi.org/10.1002/mds.870110204

Ionis Pharmaceuticals, 2017. Ionis Pharmaceuticals Licenses IONIS-HTT Rx to Partner Following Successful Phase 1/2a Study in Patients with Huntington's Disease [WWW Document]. URL http://ir.ionispharma.com/news-releases/news-release-details/ionis-pharmaceuticals-licenses-ionis-htt-rx-partner-following (accessed 12.19.17).

Jeitner, T.M., Bogdanov, M.B., Matson, W.R., Daikhin, Y., Yudkoff, M., Folk, J.E., Steinman, L., Browne, S.E., Beal, M.F., Blass, J.P.P., Cooper, A.J.L., 2001. Nε-(γ-l-Glutamyl)-l-lysine (GGEL) is increased in cerebrospinal fluid of patients with Huntington's disease. J. Neurochem. 79, 1109–1112. https://doi.org/10.1046/j.1471-4159.2001.00673.x

Johnson, E.B., Byrne, L.M., Gregory, S., Rodrigues, F.B., Blennow, K., Durr, A., Leavitt, B.R., Roos, R.A., Zetterberg, H., Tabrizi, S.J., Scahill, R.I., Wild, E.J., 2018. Neurofilament light protein in blood predicts regional atrophy in Huntington disease. Neurology 90, e717–e723. https://doi.org/10.1212/WNL.0000000000005005

Johnson, E.B., Gregory, S., Johnson, H.J., Durr, A., Leavitt, B.R., Roos, R.A., Rees, G., Tabrizi, S.J., Scahill, R.I., 2017. Recommendations for the Use of Automated Gray Matter Segmentation Tools: Evidence from Huntington's Disease. Front. Neurol. 8, 519. https://doi.org/10.3389/fneur.2017.00519

Jones, B., Jarvis, P., Lewis, J.A., Ebbutt, A.F., 1996. Trials to assess equivalence: the importance of rigorous methods. BMJ 313, 36–9. https://doi.org/10.1136/bmj.313.7048.36

Jonsson, T., Stefansson, H., Steinberg, S., Jonsdottir, I., Jonsson, P. V., Snaedal, J., Bjornsson, S., Huttenlocher, J., Levey, A.I., Lah, J.J., Rujescu, D., Hampel, H., Giegling, I., Andreassen, O.A., Engedal, K., Ulstein, I., Djurovic, S., Ibrahim-Verbaas, C., Hofman, A., Ikram, M.A., van Duijn, C.M., Thorsteinsdottir, U., Kong, A., Stefansson, K., 2013. Variant of TREM2 Associated with the Risk of Alzheimer's Disease. N. Engl. J. Med. 368, 107–116. https://doi.org/10.1056/NEJMoa1211103

Kennedy, L., Evans, E., Chen, C.-M., Craven, L., Detloff, P.J., Ennis, M., Shelbourne, P.F., 2003. Dramatic tissue-specific mutation length increases are an early molecular event in Huntington disease pathogenesis. Hum. Mol. Genet. 12, 3359–67. https://doi.org/10.1093/hmg/ddg352

Keshavan, A., Heslegrave, A., Zetterberg, H., Schott, J.M., 2018. Stability of blood-based biomarkers of Alzheimer's disease over multiple freeze-thaw cycles. Alzheimer's Dement. Diagnosis, Assess. Dis. Monit. 10, 448–451. https://doi.org/10.1016/J.DADM.2018.06.001

Kinney, J.W., Bemiller, S.M., Murtishaw, A.S., Leisgang, A.M., Salazar, A.M., Lamb, B.T., 2018. Inflammation as a central mechanism in Alzheimer's disease. Alzheimer's Dement. Transl. Res. Clin. Interv. https://doi.org/10.1016/j.trci.2018.06.014

Kleinberger, G., Yamanishi, Y., Suárez-Calvet, M., Czirr, E., Lohmann, E., Cuyvers, E., Struyfs, H., Pettkus, N., Wenninger-Weinzierl, A., Mazaheri, F., Tahirovic, S., Lleó, A., Alcolea, D., Fortea, J., Willem, M., Lammich, S., Molinuevo, J.L., Sánchez-Valle, R., Antonell, A., Ramirez, A., Heneka, M.T., Sleegers, K., van der Zee, J., Martin, J.-J., Engelborghs, S., Demirtas-Tatlidede, A., Zetterberg, H., Van Broeckhoven, C., Gurvit, H., Wyss-Coray, T., Hardy, J., Colonna, M., Haass, C., 2014. TREM2 mutations implicated in neurodegeneration impair cell surface transport and phagocytosis. Sci. Transl. Med. 6, 243ra86. https://doi.org/10.1126/scitranslmed.3009093

Kolodziejczyk, K., Parsons, M.P., Southwell, A.L., Hayden, M.R., Raymond, L.A., 2014. Striatal synaptic dysfunction and hippocampal plasticity deficits in the Hu97/18 mouse model of huntington disease. PLoS One 9. https://doi.org/10.1371/journal.pone.0094562

Kuhle, J., Barro, C., Andreasson, U., Derfuss, T., Lindberg, R., Sandelius, Å., Liman, V., Norgren, N., Blennow, K., Zetterberg, H., 2016. Comparison of three analytical platforms for quantification of the neurofilament light chain in blood samples: ELISA, electrochemiluminescence immunoassay and Simoa. Clin. Chem. Lab. Med. 0.

https://doi.org/10.1515/cclm-2015-1195

Kuhle, J., Disanto, G., Lorscheider, J., Stites, T., Chen, Y., Dahlke, F., Francis, G., Shrinivasan, A., Radue, E.-W., Giovannoni, G., Kappos, L., 2015. Fingolimod and CSF neurofilament light chain levels in relapsing-remitting multiple sclerosis. Neurology 84, 1639–43. https://doi.org/10.1212/WNL.0000000000001491

Langbehn, D., Brinkman, R., Falush, D., Paulsen, J., Hayden, M., 2004. A new model for prediction of the age of onset and penetrance for Huntington's disease based on CAG length. Clin. Genet. 65, 267–277. https://doi.org/10.1111/j.1399-0004.2004.00241.x

Langbehn, D.R., Hayden, M.R., Paulsen, J.S., 2010. CAG-repeat length and the age of onset in Huntington disease (HD): A review and validation study of statistical approaches. Am. J. Med. Genet. Part B Neuropsychiatr. Genet. 153B, 397–408. https://doi.org/10.1002/ajmg.b.30992

Langbehn, D.R., Stout, J.C., Gregory, S., Mills, J.A., Durr, A., Leavitt, B.R., Roos, R.A.C., Long, J.D., Owen, G., Johnson, H.J., Borowsky, B., Craufurd, D., Reilmann, R., Bernhard Landwehrmeyer, G., Scahill, R.I., Tabrizi, S.J., 2019. Association of CAG Repeats with Long-term Progression in Huntington Disease. JAMA Neurol. 76, 1375–1385. https://doi.org/10.1001/jamaneurol.2019.2368

Ledig, C., Heckemann, R.A., Hammers, A., Lopez, J.C., Newcombe, V.F.J., Makropoulos, A., Lötjönen, J., Menon, D.K., Rueckert, D., 2015. Robust whole-brain segmentation: Application to traumatic brain injury. Med. Image Anal. 21, 40–58. https://doi.org/10.1016/j.media.2014.12.003

Lee, J.M., Wheeler, V.C., Chao, M.J., Vonsattel, J.P.G., Pinto, R.M., Lucente, D., Abu-Elneel, K., Ramos, E.M., Mysore, J.S., Gillis, T., MacDonald, M.E., Gusella, J.F., Harold, D., Stone, T.C., Escott-Price, V., Han, J., Vedernikov, A., Holmans, P., Jones, L., Kwak, S., Mahmoudi, M., Orth, M., Landwehrmeyer, G.B., Paulsen, J.S., Dorsey, E.R., Shoulson, I., Myers, R.H., 2015. Identification of Genetic Factors that Modify Clinical Onset of Huntington's Disease. Cell 162, 516–526. https://doi.org/10.1016/j.cell.2015.07.003

Leppert, D., Kuhle, J., 2019. Blood neurofilament light chain at the doorstep of clinical application. Neurol. Neuroimmunol. NeuroInflammation. https://doi.org/10.1212/NXI.0000000000000599

Lewczuk, P., Beck, G., Esselmann, H., Bruckmoser, R., Zimmermann, R., Fiszer, M., Bibl, M., Maler, J.M., Kornhuber, J., Wiltfang, J., 2005. Effect of Sample Collection Tubes on Cerebrospinal Fluid Concentrations of Tau Proteins and Amyloid β

Peptides. Clin. Chem. 52, 331–332. https://doi.org/10.1373/clinchem.2005.061754

Li, K., Wei, Q., Liu, F.F., Hu, F., Xie, A. ji, Zhu, L.Q., Liu, D., 2018. Synaptic Dysfunction in Alzheimer's Disease: Aβ, Tau, and Epigenetic Alterations. Mol. Neurobiol. 55, 3021–3032. https://doi.org/10.1007/s12035-017-0533-3

Liu, J.P., Zeitlin, S.O., 2017. Is huntingtin dispensable in the adult brain? J. Huntingtons. Dis. https://doi.org/10.3233/JHD-170235

Llorens, F., Kruse, N., Schmitz, M., Shafiq, M., da Cunha, J.E.G., Gotzman, N., Zafar, S., Thune, K., de Oliveira, J.R.M., Mollenhauer, B., Zerr, I., 2015. Quantification of CSF biomarkers using an electrochemiluminescence-based detection system in the differential diagnosis of AD and sCJD. J. Neurol. https://doi.org/10.1007/s00415-015-7837-x

Long, J.D., Langbehn, D.R., Tabrizi, S.J., Landwehrmeyer, B.G., Paulsen, J.S., Warner, J., Sampaio, C., 2017a. Validation of a prognostic index for Huntington's disease. Mov. Disord. 32, 256–263. https://doi.org/10.1002/mds.26838

Long, J.D., Mills, J.A., Leavitt, B.R., Durr, A., Roos, R.A., Stout, J.C., Reilmann, R., Landwehrmeyer, B., Gregory, S., Scahill, R.I., Langbehn, D.R., Tabrizi, S.J., 2017b. Survival End Points for Huntington Disease Trials Prior to a Motor Diagnosis. JAMA Neurol. 74, 1352. https://doi.org/10.1001/jamaneurol.2017.2107

Lu, C.-H., Macdonald-Wallis, C., Gray, E., Pearce, N., Petzold, A., Norgren, N., Giovannoni, G., Fratta, P., Sidle, K., Fish, M., Orrell, R., Howard, R., Talbot, K., Greensmith, L., Kuhle, J., Turner, M.R., Malaspina, A., 2015. Neurofilament light chain: A prognostic biomarker in amyotrophic lateral sclerosis. Neurology 84, 2247–57. https://doi.org/10.1212/WNL.0000000000001642

Lusted, L.B., 1971. Signal detectability and medical decision-making. Science 171, 1217–9. https://doi.org/10.1126/SCIENCE.171.3977.1217

Magdalinou, N., Lees, A.J., Zetterberg, H., 2014. Cerebrospinal fluid biomarkers in parkinsonian conditions: An update and future directions. J. Neurol. Neurosurg. Psychiatry. https://doi.org/10.1136/jnnp-2013-307539

Manyam, B. V, Giacobini, E., Colliver, J.A., 1990. Cerebrospinal fluid acetylcholinesterase and choline measurements in Huntington's disease. J. Neurol. 237, 281–4.

McColgan, P., Gregory, S., Seunarine, K.K., Razi, A., Papoutsi, Marina, Johnson, E., Durr, A., Roos, R.A.C., Leavitt, B.R., Holmans, P., Scahill, R.I., Clark, C.A., Rees, G., Tabrizi, S.J., Coleman, A., Decolongon, J., Fan, M., Petkau, T., Jauffret, C.,

Justo, D., Lehericy, S., Nigaud, K., Valabrègue, R., Schoonderbeek, A., 't Hart, E.P., Moss, D.J.H., Ghosh, R., Crawford, H., Papoutsi, M., Berna, C., Mahaleskshmi, D., Reilmann, R., Weber, N., Labuschagne, I., Stout, J., Landwehrmeyer, B., Orth, M., Mayer, I., Johnson, H., Crawfurd, D., 2018. Brain Regions Showing White Matter Loss in Huntington's Disease Are Enriched for Synaptic and Metabolic Genes. Biol. Psychiatry 83, 456–465. https://doi.org/10.1016/J.BIOPSYCH.2017.10.019

McColgan, P., Seunarine, K.K., Gregory, S., Razi, A., Papoutsi, M., Long, J.D., Mills, J.A., Johnson, E., Durr, A., Roos, R.A., Leavitt, B.R., Stout, J.C., Scahill, R.I., Clark, C.A., Rees, G., Tabrizi, S.J., Investigators, T.T.O.H., 2017. Topological length of white matter connections predicts their rate of atrophy in premanifest Huntington's disease. JCI insight 2. https://doi.org/10.1172/jci.insight.92641

McColgan, P., Tabrizi, S.J., 2018. Huntington's disease: a clinical review. Eur. J. Neurol. 25, 24–34. https://doi.org/10.1111/ene.13413

McCusker, E., Loy, C.T., 2014. The many facets of unawareness in Huntington disease. Tremor and Other Hyperkinetic Movements. https://doi.org/10.7916/D8FJ2FD3

McGeer, P.L., Itagaki, S., McGeer, E.G., 1988. Expression of the histocompatibility glycoprotein HLA-DR in neurological disease. Acta Neuropathol. 76, 550–557. https://doi.org/10.1007/BF00689592

Meeter, L.H., Dopper, E.G., Jiskoot, L.C., Sanchez-Valle, R., Graff, C., Benussi, L., Ghidoni, R., Pijnenburg, Y.A., Borroni, B., Galimberti, D., Laforce, R.J., Masellis, M., Vandenberghe, R., Ber, I. Le, Otto, M., van Minkelen, R., Papma, J.M., Rombouts, S.A., Balasa, M., Öijerstedt, L., Jelic, V., Dick, K.M., Cash, D.M., Harding, S.R., Jorge Cardoso, M., Ourselin, S., Rossor, M.N., Padovani, A., Scarpini, E., Fenoglio, C., Tartaglia, M.C., Lamari, F., Barro, C., Kuhle, J., Rohrer, J.D., Teunissen, C.E., van Swieten, J.C., 2016. Neurofilament light chain: a biomarker for genetic frontotemporal dementia. Ann. Clin. Transl. Neurol. 3, 623–636. https://doi.org/10.1002/acn3.325

Meßmer, K., Reynolds, G.P., 1998. Increased peripheral benzodiazepine binding sites in the brain of patients with Huntington's disease. Neurosci. Lett. 241, 53–56. https://doi.org/10.1016/S0304-3940(97)00967-1

Mestre, T., Ferreira, J., Coelho, M.M., Rosa, M., Sampaio, C., 2009a. Therapeutic interventions for symptomatic treatment in Huntington's disease. Cochrane Database Syst. Rev. https://doi.org/10.1002/14651858.CD006456.pub2

Mestre, T., Ferreira, J., Coelho, M.M., Rosa, M., Sampaio, C., 2009b. Therapeutic interventions for symptomatic treatment in Huntington's disease. Cochrane

Database Syst. Rev. https://doi.org/10.1002/14651858.CD006456.pub2

Mestre, T., Ferreira, J., Coelho, M.M., Rosa, M., Sampaio, C., 2009c. Therapeutic interventions for disease progression in Huntington's disease. Cochrane Database Syst. Rev. https://doi.org/10.1002/14651858.CD006455.pub2

Mestre, T.A., Bachoud-Lévi, A.-C., Marinus, J., Stout, J.C., Paulsen, J.S., Como, P., Duff, K., Sampaio, C., Goetz, C.G., Cubo, E., Stebbins, G.T., Martinez-Martin, P., 2018a. Rating scales for cognition in Huntington's disease: Critique and recommendations. Mov. Disord. 33, 187–195. https://doi.org/10.1002/mds.27227

Mestre, T.A., Busse, M., Davis, A.M., Quinn, L., Rodrigues, F.B., Burgunder, J.-M., Carlozzi, N.E., Walker, F., Ho, A.K., Sampaio, C., Goetz, C.G., Cubo, E., Martinez-Martin, P., Stebbins, G.T., 2018b. Rating Scales and Performance-based Measures For Assessment of Functional Ability In Huntington's Disease: Critique And Recommendations. Mov. Disord. Clin. Pract. https://doi.org/10.1002/mdc3.12617

Mestre, T.A., Carlozzi, N.E., Ho, A.K., Burgunder, J.-M., Walker, F., Davis, A.M., Busse, M., Quinn, L., Rodrigues, F.B., Sampaio, C., Goetz, C.G., Cubo, E., Martinez-Martin, P., Stebbins, G.T., Members of the MDS Committee on Rating Scales Development, 2018c. Quality of life in Huntington's disease: Critique and recommendations for measures assessing patient health-related quality of life and caregiver quality of life. Mov. Disord. https://doi.org/10.1002/mds.27317

Mestre, T.A., Forjaz, M.J., Mahlknecht, P., Cardoso, F., Ferreira, J.J., Reilmann, R., Sampaio, C., Goetz, C.G., Cubo, E., Martinez-Martin, P., Stebbins, G.T., 2018d. Rating Scales for Motor Symptoms and Signs in Huntington's Disease: Critique and Recommendations. Mov. Disord. Clin. Pract. https://doi.org/10.1002/mdc3.12571

Mestre, T.A., van Duijn, E., Davis, A.M., Bachoud-Lévi, A.-C., Busse, M., Anderson, K.E., Ferreira, J.J., Mahlknecht, P., Tumas, V., Sampaio, C., Goetz, C.G., Cubo, E., Stebbins, G.T., Martinez-Martin, P., 2016. Rating scales for behavioral symptoms in Huntington's disease: Critique and recommendations. Mov. Disord. 31, 1466–1478. https://doi.org/10.1002/mds.26675

Milnerwood, A.J., Cummings, D.M., Dallérac, G.M., Brown, J.Y., Vatsavayai, S.C., Hirst, M.C., Rezaie, P., Murphy, K.P.S.J., 2006. Early development of aberrant synaptic plasticity in a mouse model of Huntington's disease. Hum. Mol. Genet. 15, 1690–1703. https://doi.org/10.1093/hmg/ddl092

Milnerwood, A.J., Raymond, L.A., 2010. Early synaptic pathophysiology in neurodegeneration: insights from Huntington's disease. Trends Neurosci. 33, 513–23. https://doi.org/10.1016/j.tins.2010.08.002

Myers, R.H., Vonsattel, J.P., Paskevich, P.A., Kiely, D.K., Stevens, T.J., Cupples, L.A., Richardson, E.P., Bird, E.D., 1991. Decreased Neuronal and Increased Oligodendroglial Densities in Huntington's Disease Caudate Nucleus. J. Neuropathol. Exp. Neurol. 50, 729–742. https://doi.org/10.1097/00005072-199111000-00005

Nance, M.A., Myers, R.H., 2001. Juvenile onset Huntington's disease?clinical and research perspectives. Ment. Retard. Dev. Disabil. Res. Rev. 7, 153–157. https://doi.org/10.1002/mrdd.1022

Nance, M.A., Seltzer, W., Ashizawa, T., Bennett, R., McIntosh, N., Myers, R.H., Potter, N.T., Shea, D.K., 1998. Laboratory Guidelines for Huntington Disease Genetic Testing. Am. J. Hum. Genet. 62, 1243–1247. https://doi.org/10.1086/301846

NCT02215616, 2016. A Clinical Study in Subjects With Huntington's Disease to Assess the Efficacy and Safety of Three Oral Doses of Laquinimod - Full Text View - ClinicalTrials.gov [WWW Document]. ClinicalTrials.gov. URL https://clinicaltrials.gov/ct2/show/NCT02215616?term=legato&rank=1 (accessed 3.1.16).

NCT02519036, 2015. Safety, Tolerability, Pharmacokinetics, and Pharmacodynamics of ISIS 443139 in Participants With Early Manifest Huntington's Disease [WWW Document]. ClinicalTrials.gov. URL https://clinicaltrials.gov/ct2/show/NCT02519036 (accessed 3.1.16).

NCT03225833, 2017. clinicaltrials.gov/NCT03225833 [WWW Document]. URL https://clinicaltrials.gov/ct2/show/NCT03225833

NCT03342053, 2019. An Open-Label Extension Study to Evaluate the Safety, Tolerability, Pharmacokinetics, and Pharmacodynamics of RO7234292 (ISIS 443139) in Huntington's Disease Patients Who Participated in Prior Investigational Studies of RO7234292 (ISIS 443139) [WWW Document]. clinicaltrials.gov. URL https://clinicaltrials.gov/ct2/show/NCT03342053

NCT03761849, 2019. A Study to Evaluate the Efficacy and Safety of Intrathecally Administered RO7234292 (RG6042) in Patients With Manifest Huntington's Disease [WWW Document]. ClinicalTrials.gov. URL https://clinicaltrials.gov/ct2/show/NCT03761849

NCT03810898, 2019. iMagemHTT: FIH Evaluation of Novel Mutant Huntingtin PET Radioligands [^{11}C]CHDI-00485180-R and [^{11}C]CHDI-00485626 [WWW Document]. ClinicalTrials.gov. URL https://clinicaltrials.gov/ct2/show/NCT03810898 (accessed 12.15.19).

NCT04120493, 2019. clinicaltrials.gov/NCT04120493 [WWW Document]. URL https://clinicaltrials.gov/ct2/show/NCT04120493

Neselius, S., Brisby, H., Theodorsson, A., Blennow, K., Zetterberg, H., Marcusson, J., 2012. CSF-biomarkers in Olympic boxing: diagnosis and effects of repetitive head trauma. PLoS One 7, e33606. https://doi.org/10.1371/journal.pone.0033606

Niemelä, V., Burman, J., Blennow, K., Zetterberg, H., Larsson, A., Sundblom, J., 2018. Cerebrospinal fluid sCD27 levels indicate active T cell-mediated inflammation in premanifest Huntington's disease. PLoS One 13, e0193492. https://doi.org/10.1371/journal.pone.0193492

Niemelä, V., Landtblom, A.-M., Blennow, K., Sundblom, J., 2017. Tau or neurofilament light—Which is the more suitable biomarker for Huntington's disease? PLoS One 12, e0172762. https://doi.org/10.1371/journal.pone.0172762

Novak, M.J.U., Tabrizi, S.J., 2010. Huntington's disease. BMJ. https://doi.org/10.1136/bmj.c3109

Novakova, L., Zetterberg, H., Sundström, P., Axelsson, M., Khademi, M., Gunnarsson, M., Malmeström, C., Svenningsson, A., Olsson, T., Piehl, F., Blennow, K., Lycke, J., 2017. Monitoring disease activity in multiple sclerosis using serum neurofilament light protein. Neurology 89, 2230–2237. https://doi.org/10.1212/WNL.0000000000004683

Öhrfelt, A., Axelsson, M., Malmeström, C., Novakova, L., Heslegrave, A., Blennow, K., Lycke, J., Zetterberg, H., 2016. Soluble TREM-2 in cerebrospinal fluid from patients with multiple sclerosis treated with natalizumab or mitoxantrone. Mult. Scler. J. 22, 1587–1595. https://doi.org/10.1177/1352458515624558

Orth, M., Schippling, S., Schneider, S.A., Bhatia, K.P., Talelli, P., Tabrizi, S.J., Rothwell, J.C., 2010. Abnormal motor cortex plasticity in premanifest and very early manifest Huntington disease. J. Neurol. Neurosurg. Psychiatry 81, 267–270. https://doi.org/10.1136/jnnp.2009.171926

Oxtoby, N.P., Young, A.L., Cash, D.M., Benzinger, T.L.S., Fagan, A.M., Morris, J.C., Bateman, R.J., Fox, N.C., Schott, J.M., Alexander, D.C., 2018. Data-driven models of dominantly-inherited Alzheimer's disease progression. Brain. https://doi.org/10.1093/brain/awy050

Paganetti, P., Weiss, A., Trapp, M., Hammerl, I., Bleckmann, D., Bodner, R.A., Coven-Easter, S., Housman, D.E., Parker, C.N., 2009. Development of a method for the high-throughput quantification of cellular proteins. ChemBioChem 10, 1678–1688.

https://doi.org/10.1002/cbic.200900131

Paloneva, J., Manninen, T., Christman, G., Hovanes, K., Mandelin, J., Adolfsson, R., Bianchin, M., Bird, T., Miranda, R., Salmaggi, A., Tranebjærg, L., Konttinen, Y., Peltonen, L., 2002. Mutations in Two Genes Encoding Different Subunits of a Receptor Signaling Complex Result in an Identical Disease Phenotype. Am. J. Hum. Genet. 71, 656–662. https://doi.org/10.1086/342259

Papoutsi, M., Labuschagne, I., Tabrizi, S.J., Stout, J.C., 2014. The cognitive burden in Huntington's disease: Pathology, phenotype, and mechanisms of compensation. Mov. Disord. 29, 673–683. https://doi.org/10.1002/mds.25864

Paulsen, J.S., Hayden, M., Stout, J.C., Langbehn, D.R., Aylward, E., Ross, C.A., Guttman, M., Nance, M., Kieburtz, K., Oakes, D., Shoulson, I., Kayson, E., Johnson, S., Penziner, E., 2006. Preparing for Preventive Clinical Trials. Arch. Neurol. 63, 883. https://doi.org/10.1001/archneur.63.6.883

Paulsen, J.S., Langbehn, D.R., Stout, J.C., Aylward, E., Ross, C.A., Nance, M., Guttman, M., Johnson, S., MacDonald, M., Beglinger, L.J., Duff, K., Kayson, E., Biglan, K., Shoulson, I., Oakes, D., Hayden, M., Predict-HD Investigators and Coordinators of the Huntington Study Group, T.P.-H.I. and C. of the H.S., 2008. Detection of Huntington's disease decades before diagnosis: the Predict-HD study. J. Neurol. Neurosurg. Psychiatry 79, 874–80. https://doi.org/10.1136/jnnp.2007.128728

Paulsen, J.S., Long, J.D., Ross, C.A., Harrington, D.L., Erwin, C.J., Williams, J.K., Westervelt, H.J., Johnson, H.J., Aylward, E.H., Zhang, Y., Bockholt, H.J., Barker, R.A., 2014. Prediction of manifest huntington's disease with clinical and imaging measures: A prospective observational study. Lancet Neurol. 13, 1193–1201. https://doi.org/10.1016/S1474-4422(14)70238-8

Pavese, N., Gerhard, A., Tai, Y.F., Ho, A.K., Turkheimer, F., Barker, R.A., Brooks, D.J., Piccini, P., 2006. Microglial activation correlates with severity in Huntington disease: A clinical and PET study. Neurology 66, 1638–1643. https://doi.org/10.1212/01.wnl.0000222734.56412.17

Pawlowski, M., Meuth, S.G., Duning, T., 2017. Cerebrospinal Fluid Biomarkers in Alzheimer's Disease—From Brain Starch to Bench and Bedside. Diagnostics 7, 42. https://doi.org/10.3390/diagnostics7030042

Penney, J.B., Vonsattel, J.P., MacDonald, M.E., Gusella, J.F., Myers, R.H., 1997. CAG repeat number governs the development rate of pathology in Huntington's disease. Ann. Neurol. 41, 689–92. https://doi.org/10.1002/ana.410410521

Perret-Liaudet, A., Pelpel, M., Tholance, Y., Dumont, B., Vanderstichele, H., Zorzi, W., ElMoualij, B., Schraen, S., Moreaud, O., Gabelle, A., Thouvenot, E., Thomas-Anterion, C., Touchon, J., Krolak-Salmon, P., Kovacs, G.G., Coudreuse, A., Quadrio, I., Lehmann, S., 2012. Cerebrospinal Fluid Collection Tubes: A Critical Issue for Alzheimer Disease Diagnosis. Clin. Chem. 58, 787–789. https://doi.org/10.1373/clinchem.2011.178368

Piccio, L., Deming, Y., Del-Águila, J.L., Ghezzi, L., Holtzman, D.M., Fagan, A.M., Fenoglio, C., Galimberti, D., Borroni, B., Cruchaga, C., 2016. Cerebrospinal fluid soluble TREM2 is higher in Alzheimer disease and associated with mutation status. Acta Neuropathol. 131, 925–933. https://doi.org/10.1007/s00401-016-1533-5

Plotkin, J.L., Day, M., Peterson, J.D., Xie, Z., Kress, G.J., Rafalovich, I., Kondapalli, J., Gertler, T.S., Flajolet, M., Greengard, P., Stavarache, M., Kaplitt, M.G., Rosinski, J., Chan, C.S., Surmeier, D.J., 2014. Impaired TrkB receptor signaling underlies corticostriatal dysfunction in Huntington's disease. Neuron 83, 178–188. https://doi.org/10.1016/j.neuron.2014.05.032

Plotkin, J.L., Surmeier, D.J., 2015. Corticostriatal synaptic adaptations in Huntington's disease. Curr. Opin. Neurobiol. https://doi.org/10.1016/j.conb.2015.01.020

Portelius, E., Olsson, B., Höglund, K., Cullen, N.C., Kvartsberg, H., Andreasson, U., Zetterberg, H., Sandelius, Å., Shaw, L.M., Lee, V.M.Y., Irwin, D.J., Grossman, M., Weintraub, D., Chen-Plotkin, A., Wolk, D.A., McCluskey, L., Elman, L., McBride, J., Toledo, J.B., Trojanowski, J.Q., Blennow, K., 2018. Cerebrospinal fluid neurogranin concentration in neurodegeneration: relation to clinical phenotypes and neuropathology. Acta Neuropathol. 136, 363–376. https://doi.org/10.1007/s00401-018-1851-x

Preische, O., Schultz, S.A., Apel, A., Kuhle, J., Kaeser, S.A., Barro, C., Gräber, S., Kuder-Buletta, E., LaFougere, C., Laske, C., Vöglein, J., Levin, J., Masters, C.L., Martins, R., Schofield, P.R., Rossor, M.N., Graff-Radford, N.R., Salloway, S., Ghetti, B., Ringman, J.M., Noble, J.M., Chhatwal, J., Goate, A.M., Benzinger, T.L.S., Morris, J.C., Bateman, R.J., Wang, G., Fagan, A.M., McDade, E.M., Gordon, B.A., Jucker, M., 2019. Serum neurofilament dynamics predicts neurodegeneration and clinical progression in presymptomatic Alzheimer's disease. Nat. Med. 25, 277–283. https://doi.org/10.1038/s41591-018-0304-3

Rayaprolu, S., Mullen, B., Baker, M., Lynch, T., Finger, E., Seeley, W.W., Hatanpaa, K.J., Lomen-Hoerth, C., Kertesz, A., Bigio, E.H., Lippa, C., Josephs, K.A., Knopman, D.S., White, C.L., Caselli, R., Mackenzie, I.R., Miller, B.L., Boczarska-

Jedynak, M., Opala, G., Krygowska-Wajs, A., Barcikowska, M., Younkin, S.G., Petersen, R.C., Ertekin-Taner, N., Uitti, R.J., Meschia, J.F., Boylan, K.B., Boeve, B.F., Graff-Radford, N.R., Wszolek, Z.K., Dickson, D.W., Rademakers, R., Ross, O.A., 2013. TREM2 in neurodegeneration: evidence for association of the p.R47H variant with frontotemporal dementia and Parkinson's disease. Mol. Neurodegener. 8, 19. https://doi.org/10.1186/1750-1326-8-19

Reiber, H., 2003. Proteins in cerebrospinal fluid and blood: barriers, CSF flow rate and source-related dynamics. Restor. Neurol. Neurosci. 21, 79–96.

Reilmann, R., Leavitt, B.R., Ross, C.A., 2014. Diagnostic criteria for Huntington's disease based on natural history. Mov. Disord. 29, 1335–1341. https://doi.org/10.1002/mds.26011

Reiner, A., Albin, R.L., Anderson, K.D., D'Amato, C.J., Penney, J.B., Young, A.B., 1988. Differential loss of striatal projection neurons in Huntington disease. Proc. Natl. Acad. Sci. U. S. A. 85, 5733–5737. https://doi.org/10.1073/pnas.85.15.5733

Rodrigues, F.B., Abreu, D., Damásio, J., Goncalves, N., Correia-Guedes, L., Coelho, M., Ferreira, J.J., 2017. Survival, Mortality, Causes and Places of Death in a European Huntington's Disease Prospective Cohort. Mov. Disord. Clin. Pract. 4, 737–742. https://doi.org/10.1002/mdc3.12502

Rodrigues, F.B., Byrne, L.M., McColgan, P., Robertson, N., Tabrizi, S.J., Leavitt, B.R., Zetterberg, H., Wild, E.J., 2016a. Cerebrospinal fluid total tau concentration predicts clinical phenotype in Huntington's disease. J. Neurochem. 139, 22–25. https://doi.org/10.1111/jnc.13719

Rodrigues, F.B., Byrne, L.M., McColgan, P., Robertson, N., Tabrizi, S.J., Zetterberg, H., Wild, E.J., 2016b. Cerebrospinal Fluid Inflammatory Biomarkers Reflect Clinical Severity in Huntington's Disease. PLoS One 11, e0163479. https://doi.org/10.1371/journal.pone.0163479

Rodrigues, F.B., Byrne, L.M., Wild, E.J., 2018. Biofluid biomarkers in Huntington's diseas, Methods in Molecular Biology. https://doi.org/10.1007/978-1-4939-7825-0_17

Rodrigues, F.B., Ferreira, J.J., Wild, E.J., 2019a. Huntington's disease clinical trials corner: June 2019. J. Huntingtons. Dis. 8, 363–371. https://doi.org/10.3233/JHD-199003

Rodrigues, F.B., Quinn, L., Wild, E.J., 2019b. Huntington's Disease Clinical Trials Corner: January 2019. J. Huntingtons. Dis. https://doi.org/10.3233/JHD-190001

Rodrigues, F.B., Wild, E.J., 2018. Huntington's Disease Clinical Trials Corner: February 2018. J. Huntingtons. Dis. 7, 89–98. https://doi.org/10.3233/JHD-189001

Rodrigues, F.B., Wild, E.J., 2017. Clinical Trials Corner: September 2017. J. Huntingtons. Dis. 6, 255–263. https://doi.org/10.3233/JHD-170262

Rohrer, J.D., Woollacott, I.O.C., Dick, K.M., Brotherhood, E., Gordon, E., Fellows, A., Toombs, J., Druyeh, R., Cardoso, M.J., Ourselin, S., Nicholas, J.M., Norgren, N., Mead, S., Andreasson, U., Blennow, K., Schott, J.M., Fox, N.C., Warren, J.D., Zetterberg, H., 2016. Serum neurofilament light chain protein is a measure of disease intensity in frontotemporal dementia. Neurology 87, 1329–36. https://doi.org/10.1212/WNL.0000000000003154

Rojas, J.C., Karydas, A., Bang, J., Tsai, R.M., Blennow, K., Liman, V., Kramer, J.H., Rosen, H., Miller, B.L., Zetterberg, H., Boxer, A.L., 2016. Plasma neurofilament light chain predicts progression in progressive supranuclear palsy. Ann. Clin. Transl. Neurol. 3, 216–225. https://doi.org/10.1002/acn3.290

Rosengren, L.E., Karlsson, J.E., Karlsson, J.O., Persson, L.I., Wikkelsø, C., 1996. Patients with amyotrophic lateral sclerosis and other neurodegenerative diseases have increased levels of neurofilament protein in CSF. J. Neurochem. 67, 2013–2018.

Ross, C. a, Aylward, E.H., Wild, E.J., Langbehn, D.R., Long, J.D., Warner, J.H., Scahill, R.I., Leavitt, B.R., Stout, J.C., Paulsen, J.S., Reilmann, R., Unschuld, P.G., Wexler, A., Margolis, R.L., Tabrizi, S.J., 2014. Huntington disease: natural history, biomarkers and prospects for therapeutics. Nat. Rev. Neurol. 10, 204–216. https://doi.org/10.1038/nrneurol.2014.24

Rubinsztein, D.C., Leggo, J., Coles, R., Almqvist, E., Biancalana, V. V., Cassiman, J.J., Chotai, K., Connarty, M., Craufurd, D., Curtis, A., Curtis, D., Davidson, M.J., Differ, A.M., Dode, C., Dodge, A., Frontali, M., Ranen, N.G., Stine, O.C., Sherr, M., 1996. Phenotypic characterization of individuals with 30-40 CAG repeats in the Huntington disease (HD) gene reveals HD cases with 36 repeats and apparently normal elderly individuals with 36-39 repeats. Am. J. Hum. Genet. 59, 16–22.

Runne, H., Kuhn, A., Wild, E.J., Pratyaksha, W., Kristiansen, M., Isaacs, J.D., Régulier, E., Delorenzi, M., Tabrizi, S.J., Luthi-Carter, R., 2007. Analysis of potential transcriptomic biomarkers for Huntington's disease in peripheral blood. Proc. Natl. Acad. Sci. U. S. A. 104, 14424–9. https://doi.org/10.1073/pnas.0703652104

Sapp, E., Kegel, K.B., Aronin, N., Hashikawa, T., Uchiyama, Y., Tohyama, K., Bhide, P.G., Vonsattel, J.P., Difiglia, M., 2001. Early and Progressive Accumulation of

Reactive Microglia in the Huntington Disease Brain. J. Neuropathol. Exp. Neurol. 60, 161–172. https://doi.org/10.1093/jnen/60.2.161

Sathyasaikumar, K. V, Stachowski, E.K., Amori, L., Guidetti, P., Muchowski, P.J., Schwarcz, R., 2010. Dysfunctional kynurenine pathway metabolism in the R6/2 mouse model of Huntington's disease. J. Neurochem. 113, 1416–25. https://doi.org/10.1111/j.1471-4159.2010.06675.x

Saudou, F., Humbert, S., 2016. The Biology of Huntingtin. Neuron 89, 910–926. https://doi.org/10.1016/j.neuron.2016.02.003

Scahill, R.I., Frost, C., Jenkins, R., Whitwell, J.L., Rossor, M.N., Fox, N.C., 2003. A Longitudinal Study of Brain Volume Changes in Normal Aging Using Serial Registered Magnetic Resonance Imaging. Arch. Neurol. 60, 989. https://doi.org/10.1001/archneur.60.7.989

Scahill, R.I., Wild, E.J., Tabrizi, S.J., 2012. Biomarkers for Huntington ' s disease : an update. Expert Opin. Med. Diagn. 6, 371–375.

Scarpina, F., Tagini, S., 2017. The stroop color and word test. Front. Psychol. https://doi.org/10.3389/fpsyg.2017.00557

Schippling, S., Schneider, S.A., Bhatia, K.P., Münchau, A., Rothwell, J.C., Tabrizi, S.J., Orth, M., 2009. Abnormal Motor Cortex Excitability in Preclinical and Very Early Huntington's Disease. Biol. Psychiatry 65, 959–965. https://doi.org/10.1016/j.biopsych.2008.12.026

Schobel, S.A., Palermo, G., Auinger, P., Long, J.D., Ma, S., Khwaja, O.S., Trundell, D., Cudkowicz, M., Hersch, S., Sampaio, C., Dorsey, E.R., Leavitt, B.R., Kieburtz, K.D., Sevigny, J.J., Langbehn, D.R., Tabrizi, S.J., 2017. Motor, cognitive, and functional declines contribute to a single progressive factor in early HD. Neurology 89, 2495–2502. https://doi.org/10.1212/WNL.0000000000004743

Schwarcz, R., Tamminga, C.A., Kurlan, R., Shoulson, I., 1988. Cerebrospinal fluid levels of quinolinic acid in Huntington's disease and schizophrenia. Ann. Neurol. 24, 580–2. https://doi.org/10.1002/ana.410240417

Sepers, M.D., Raymond, L.A., 2014. Mechanisms of synaptic dysfunction and excitotoxicity in Huntington's disease. Drug Discov. Today 19, 990–996. https://doi.org/10.1016/j.drudis.2014.02.006

Sepers, M.D., Smith-Dijak, A., LeDue, J., Kolodziejczyk, K., Mackie, K., Raymond, L.A., 2018. Endocannabinoid-specific impairment in synaptic plasticity in striatum of huntington's disease mouse model. J. Neurosci. 38, 544–554.

https://doi.org/10.1523/JNEUROSCI.1739-17.2017

Shahim, P., Gren, M., Liman, V., Andreasson, U., Norgren, N., Tegner, Y., Mattsson, N., Andreasen, N., Öst, M., Zetterberg, H., Nellgård, B., Blennow, K., 2016a. Serum neurofilament light protein predicts clinical outcome in traumatic brain injury. Sci. Rep. 6, 36791. https://doi.org/10.1038/srep36791

Shahim, P., Tegner, Y., Gustafsson, B., Gren, M., Ärlig, J., Olsson, M., Lehto, N., Engström, Å., Höglund, K., Portelius, E., Zetterberg, H., Blennow, K., 2016b. Neurochemical Aftermath of Repetitive Mild Traumatic Brain Injury. JAMA Neurol. 73, 1308–1315. https://doi.org/10.1001/jamaneurol.2016.2038

Shahim, P., Tegner, Y., Wilson, D.H., Randall, J., Skillbäck, T., Pazooki, D., Kallberg, B., Blennow, K., Zetterberg, H., 2014. Blood biomarkers for brain injury in concussed professional ice hockey players. JAMA Neurol. 71, 684–92. https://doi.org/10.1001/jamaneurol.2014.367

Shahim, P., Zetterberg, H., Tegner, Y., Blennow, K., 2017. Serum neurofilament light as a biomarker for mild traumatic brain injury in contact sports. Neurology 88, 1788–1794. https://doi.org/10.1212/WNL.0000000000003912

Shao, Z., Janse, E., Visser, K., Meyer, A.S., 2014. What do verbal fluency tasks measure? Predictors of verbal fluency performance in older adults. Front. Psychol. 5. https://doi.org/10.3389/fpsyg.2014.00772

Sharif, O., Knapp, S., 2008. From expression to signaling: Roles of TREM-1 and TREM-2 in innate immunity and bacterial infection. Immunobiology 213, 701–713. https://doi.org/10.1016/J.IMBIO.2008.07.008

Shirasaki, D.I., Greiner, E.R., Al-Ramahi, I., Gray, M., Boontheung, P., Geschwind, D.H., Botas, J., Coppola, G., Horvath, S., Loo, J.A., Yang, X.W., 2012. Network organization of the huntingtin proteomic interactome in mammalian brain. Neuron 75, 41–57. https://doi.org/10.1016/j.neuron.2012.05.024

Shoulson, I., Fahn, S., 1979. Huntington disease: Clinical care and evaluation. Neurology 29, 1–1. https://doi.org/10.1212/WNL.29.1.1

Singhrao, S.., Neal, J.., Morgan, B.., Gasque, P., 1999. Increased Complement Biosynthesis By Microglia and Complement Activation on Neurons in Huntington's Disease. Exp. Neurol. 159, 362–376. https://doi.org/10.1006/exnr.1999.7170

Sled, J.G., Zijdenbos, A.P., Evans, A.C., 1998. A nonparametric method for automatic correction of intensity nonuniformity in MRI data. IEEE Trans. Med. Imaging 17, 87–97. https://doi.org/10.1109/42.668698

Smith-Dijak, A.I., Sepers, M.D., Raymond, L.A., 2019. Alterations in synaptic function and plasticity in Huntington disease. J. Neurochem. jnc.14723. https://doi.org/10.1111/jnc.14723

Smith, A., 1973. How to calculate standard scores for the Symbol Modalities Test.

Smith, R., Brundin, P., Li, J.-Y., 2005. Synaptic dysfunction in Huntington's disease: a new perspective. Cell. Mol. Life Sci. 62, 1901–1912. https://doi.org/10.1007/s00018-005-5084-5

Snell, R.G., Macmillan, J.C., Cheadle, J.P., Fenton, I., Lazarou, L.P., Davies, P., Macdonald, M.E., Gusella, J.F., Harper, P.S., Shaw, D.J., 1993. Relationship between trinucleotide repeat expansion and phenotypic variation in Huntington's disease. Nat. Genet. 4, 393–397. https://doi.org/10.1038/ng0893-393

Southwell, A.L., Smith, S.E.P., Davis, T.R., Caron, N.S., Villanueva, E.B., Xie, Y., Collins, J. a., Li Ye, M., Sturrock, A., Leavitt, B.R., Schrum, A.G., Hayden, M.R., 2015. Ultrasensitive measurement of huntingtin protein in cerebrospinal fluid demonstrates increase with Huntington disease stage and decrease following brain huntingtin suppression. Sci. Rep. 5, 12166. https://doi.org/10.1038/srep12166

Soylu-Kucharz, R., Sandelius, Å., Sjögren, M., Blennow, K., Wild, E.J., Zetterberg, H., Björkqvist, M., 2017. Neurofilament light protein in CSF and blood is associated with neurodegeneration and disease severity in Huntington's disease R6/2 mice. Sci. Rep. 7, 14114. https://doi.org/10.1038/s41598-017-14179-1

Steinacker, P., Semler, E., Anderl-straub, S., Diehl-schmid, J., Foerstl, H., Fliessbach, K., Volk, A.E., Lauer, M., Danek, A., Ludolph, A.C., Otto, M., 2017. Neurofilament as a blood marker for diagnosis and monitoring of primary progressive aphasias.

Suárez-Calvet, M., Araque Caballero, M.Á., Kleinberger, G., Bateman, R.J., Fagan, A.M., Morris, J.C., Levin, J., Danek, A., Ewers, M., Haass, C., Dominantly Inherited Alzheimer Network, for the D.I.A., 2016. Early changes in CSF sTREM2 in dominantly inherited Alzheimer's disease occur after amyloid deposition and neuronal injury. Sci. Transl. Med. 8, 369ra178. https://doi.org/10.1126/scitranslmed.aag1767

Suárez-Calvet, M., Morenas-Rodríguez, E., Kleinberger, G., Schlepckow, K., Ángel Araque Caballero, M., Franzmeier, N., Capell, A., Fellerer, K., Nuscher, B., Eren, E., Levin, J., Deming, Y., Piccio, L., Karch, C.M., Cruchaga, C., Shaw, L.M., Trojanowski, J.Q., Weiner, M., Ewers, M., Haass, C., Araque Caballero, M.Á., Franzmeier, N., Capell, A., Fellerer, K., Nuscher, B., Eren, E., Levin, J., Deming, Y., Piccio, L., Karch, C.M., Cruchaga, C., Shaw, L.M., Trojanowski, J.Q., Weiner, M.,

Ewers, M., Haass, C., 2019. Early increase of CSF sTREM2 in Alzheimer's disease is associated with tau related-neurodegeneration but not with amyloid-β pathology. Mol. Neurodegener. 14, 1. https://doi.org/10.1186/s13024-018-0301-5

Suárez-Calvet, M., Kleinberger, G., Araque Caballero, M.Á., Brendel, M., Rominger, A., Alcolea, D., Fortea, J., Lleó, A., Blesa, R., Gispert, J.D., Sánchez-Valle, R., Antonell, A., Rami, L., Molinuevo, J.L.J., Brosseron, F., Traschütz, A., Heneka, M.T.M., Struyfs, H., Engelborghs, S., Sleegers, K., Van Broeckhoven, C., Zetterberg, H., Nellgård, B., Blennow, K., Crispin, A., Ewers, M., Haass, C., Suárez-Calvet, M., Kleinberger, G., Araque Caballero, M.Á., Brendel, M., Rominger, A., Alcolea, D., Fortea, J., Lleó, A., Blesa, R., Gispert, J.D., Sánchez-Valle, R., Antonell, A., Rami, L., Molinuevo, J.L.J., Brosseron, F., Traschütz, A., Heneka, M.T.M., Struyfs, H., Engelborghs, S., Sleegers, K., Van Broeckhoven, C., Zetterberg, H., Nellgård, B., Blennow, K., Crispin, A., Ewers, M., Haass, C., Albert, M., DeKosky, S., Dickson, D., Dubois, B., Feldman, H., Fox, N., Gamst, A., Holtzman, D., Jagust, W., Petersen, R., Alcolea, D., Carmona-Iragui, M., Suárez-Calvet, M., Sánchez-Saudinós, M., Sala, I., Antón-Aguirre, S., Blesa, R., Clarimón, J., Fortea, J., Lleó, A., Antonell, A., Fortea, J., Rami, L., Bosch, B., Balasa, M., Sánchez-Valle, R., Iranzo, A., Molinuevo, J.L.J., Lladó, A., Blennow, K., Hampel, H., Weiner, M., Zetterberg, H., Borroni, B., Ferrari, F., Galimberti, D., Nacmias, B., Barone, C., Bagnoli, S., Fenoglio, C., Piaceri, I., Archetti, S., Bonvicini, C., Bouchon, A., Hernández-Munain, C., Cella, M., Colonna, M., Braak, H., Braak, E., Brosseron, F., Krauthausen, M., Kummer, M., Heneka, M.T.M., Clark, C., Xie, S., Chittams, J., Ewbank, D., Peskind, E., Galasko, D., Morris, J., McKeel, D., Farlow, M., Weitlauf, S., Craig-Schapiro, R., Kuhn, M., Xiong, C., Pickering, E., Liu, J., Misko, T., Perrin, R., Bales, K., Soares, H., Fagan, A., Cuyvers, E., Bettens, K., Philtjens, S., Langenhove, T. Van, Gijselinck, I., Zee, J. van der, Engelborghs, S., Vandenbulcke, M., Dongen, J. Van, Geerts, N., Galimberti, D., Fenoglio, C., Lovati, C., Venturelli, E., Guidi, I., Corrà, B., Scalabrini, D., Clerici, F., Mariani, C., Bresolin, N., Galimberti, D., Schoonenboom, N., Scheltens, P., Fenoglio, C., Bouwman, F., Venturelli, E., Guidi, I., Blankenstein, M., Bresolin, N., Scarpini, E., Guerreiro, R., Wojtas, A., Bras, J., Carrasquillo, M., Rogaeva, E., Majounie, E., Cruchaga, C., Sassi, C., Kauwe, J., Younkin, S., Guerreiro, R., Lohmann, E., Brás, J., Gibbs, J., Rohrer, J., Gurunlian, N., Dursun, B., Bilgic, B., Hanagasi, H., Gurvit, H., Heneka, M.T.M., Carson, M., Khoury, J. El, Landreth, G., Brosseron, F., Feinstein, D., Jacobs, A., Wyss-Coray, T., Vitorica, J., Ransohoff, R., Heslegrave, A., Heywood, W., Paterson, R., Magdalinou, N., Svensson, J., Johansson, P., Öhrfelt, A., Blennow, K., Hardy, J., Schott, J., Hsieh, C., Koike, M., Spusta, S., Niemi, E., Yenari, M., Nakamura, M., Seaman, W., Hulette, C., Welsh-Bohmer, K., Murray, M., Saunders, A., Mash, D.,

McIntyre, L., Jack, C., Knopman, D., Weigand, S., Wiste, H., Vemuri, P., Lowe, V., Kantarci, K., Gunter, J., Senjem, M., Ivnik, R., Jay, T., Miller, C., Cheng, P., Graham, L., Bemiller, S., Broihier, M., Xu, G., Margevicius, D., Karlo, J., Sousa, G., Jonsson, T., Stefansson, H., Steinberg, S., Jonsdottir, I., Jonsson, P., Snaedal, J., Bjornsson, S., Huttenlocher, J., Levey, A., Lah, J., Kiialainen, A., Hovanes, K., Paloneva, J., Kopra, O., Peltonen, L., Kleinberger, G., Yamanishi, Y., Suárez-Calvet, M., Czirr, E., Lohmann, E., Cuyvers, E., Struyfs, H., Pettkus, N., Wenninger-Weinzierl, A., Mazaheri, F., Klesney-Tait, J., Turnbull, I., Colonna, M., Liu, B., Le, K., Park, M., Wang, S., Belanger, A., Dubey, S., Frost, J., Holton, P., Reiser, V., Jones, P., Matarin, M., Salih, D., Yasvoina, M., Cummings, D., Guelfi, S., Liu, W., Solim, M.N., Moens, T., Paublete, R., Ali, S., Mattsson, N., Andreasson, U., Persson, S., Arai, H., Batish, S., Bernardini, S., Bocchio-Chiavetto, L., Blankenstein, M., Carrillo, M., Chalbot, S., McKhann, G., Knopman, D., Chertkow, H., Hyman, B., Jack, C., Kawas, C., Klunk, W., Koroshetz, W., Manly, J., Mayeux, R., Molinuevo, J.L.J., Blennow, K., Dubois, B., Engelborghs, S., Lewczuk, P., Perret-Liaudet, A., Teunissen, C., Parnetti, L., Morris, J., Storandt, M., McKeel, D., Rubin, E., Price, J., Grant, E., Berg, L., Mosher, K., Wyss-Coray, T., Motta, M., Imbesi, R., Rosa, M. Di, Stivala, F., Malaguarnera, L., Paloneva, J., Manninen, T., Christman, G., Hovanes, K., Mandelin, J., Adolfsson, R., Bianchin, M., Bird, T., Miranda, R., Salmaggi, A., Paloneva, J., Mandelin, J., Kiialainen, A., Bohling, T., Prudlo, J., Hakola, P., Haltia, M., Konttinen, Y., Peltonen, L., Piccio, L., Buonsanti, C., Cella, M., Tassi, I., Schmidt, R., Fenoglio, C., Rinker, J., Naismith, R., Panina-Bordignon, P., Passini, N., Piccio, L., Deming, Y., Del-Águila, J., Ghezzi, L., Holtzman, D., Fagan, A., Fenoglio, C., Galimberti, D., Borroni, B., Cruchaga, C., Price, J., Morris, J., Rayaprolu, S., Mullen, B., Baker, M., Lynch, T., Finger, E., Seeley, W., Hatanpaa, K., Lomen-Hoerth, C., Kertesz, A., Bigio, E., Schmid, C., Sautkulis, L., Danielson, P., Cooper, J., Hasel, K., Hilbush, B., Sutcliffe, J., Carson, M., Shaw, L., Vanderstichele, H., Knapik-Czajka, M., Clark, C., Aisen, P., Petersen, R., Blennow, K., Soares, H., Simon, A., Lewczuk, P., Sperling, R., Aisen, P., Beckett, L., Bennett, D., Craft, S., Fagan, A., Iwatsubo, T., Jack, C., Kaye, J., Montine, T., Streit, W., Xue, Q., Tischer, J., Bechmann, I., Takahashi, K., Rochford, C., Neumann, H., Tanzi, R., Mussele, S. Van der, Fransen, E., Struyfs, H., Luyckx, J., Mariën, P., Saerens, J., Somers, N., Goeman, J., Deyn, P. De, Engelborghs, S., Vanderstichele, H., Bibl, M., Engelborghs, S., Bastard, N. Le, Lewczuk, P., Molinuevo, J.L.J., Parnetti, L., Perret-Liaudet, A., Shaw, L., Teunissen, C., Wang, Y., Cella, M., Mallinson, K., Ulrich, J., Young, K., Robinette, M., Gilfillan, S., Krishnan, G., Sudhakar, S., Zinselmeyer, B., Winblad, B., Palmer, K., Kivipelto, M., Jelic, V., Fratiglioni, L., Wahlund, L., Nordberg, A., Bäckman, L., Albert, M.,

Almkvist, O., Wunderlich, P., Glebov, K., Kemmerling, N., Tien, N., Neumann, H., Walter, J., 2016. sTREM2 cerebrospinal fluid levels are a potential biomarker for microglia activity in early-stage Alzheimer's disease and associate with neuronal injury markers. EMBO Mol. Med. 8, 466–76. https://doi.org/10.15252/emmm.201506123

Tabrizi, S.J., Langbehn, D.R., Leavitt, B.R., Roos, R.A., Durr, A., Craufurd, D., Kennard, C., Hicks, S.L., Fox, N.C., Scahill, R.I., Borowsky, B., Tobin, A.J., Rosas, H.D., Johnson, H., Reilmann, R., Landwehrmeyer, B., Stout, J.C., 2009. Biological and clinical manifestations of Huntington's disease in the longitudinal TRACK-HD study: cross-sectional analysis of baseline data. Lancet Neurol. 8, 791–801. https://doi.org/10.1016/S1474-4422(09)70170-X

Tabrizi, S.J., Leavitt, B.R., Landwehrmeyer, G.B., Wild, E.J., Saft, C., Barker, R.A., Blair, N.F., Craufurd, D., Priller, J., Rickards, H., Rosser, A., Kordasiewicz, H.B., Czech, C., Swayze, E.E., Norris, D.A., Baumann, T., Gerlach, I., Schobel, S.A., Paz, E., Smith, A. V., Bennett, C.F., Lane, R.M., 2019. Targeting Huntingtin Expression in Patients with Huntington's Disease. N. Engl. J. Med. NEJMoa1900907. https://doi.org/10.1056/NEJMoa1900907

Tabrizi, S.J., Reilmann, R., Roos, R.A.C., Durr, A., Leavitt, B., Owen, G., Jones, R., Johnson, H., Craufurd, D., Hicks, S.L., Kennard, C., Landwehrmeyer, B., Stout, J.C., Borowsky, B., Scahill, R.I., Frost, C., Langbehn, D.R., 2012. Potential endpoints for clinical trials in premanifest and early Huntington's disease in the TRACK-HD study: analysis of 24 month observational data. Lancet. Neurol. 11, 42–53. https://doi.org/10.1016/S1474-4422(11)70263-0

Tabrizi, S.J., Scahill, R.I., Durr, A., Roos, R.A.C., Leavitt, B.R., Jones, R., Landwehrmeyer, G.B., Fox, N.C., Johnson, H., Hicks, S.L., Kennard, C., Craufurd, D., Frost, C., Langbehn, D.R., Reilmann, R., Stout, J.C., 2011. Biological and clinical changes in premanifest and early stage Huntington's disease in the TRACK-HD study: The 12-month longitudinal analysis. Lancet Neurol. 10, 31–42. https://doi.org/10.1016/S1474-4422(10)70276-3

Tabrizi, S.J., Scahill, R.I., Owen, G., Durr, A., Leavitt, B.R., Roos, R.A., Borowsky, B., Landwehrmeyer, B., Frost, C., Johnson, H., Craufurd, D., Reilmann, R., Stout, J.C., Langbehn, D.R., 2013. Predictors of phenotypic progression and disease onset in premanifest and early-stage Huntington's disease in the TRACK-HD study: analysis of 36-month observational data. Lancet Neurol. 12, 637–649. https://doi.org/10.1016/S1474-4422(13)70088-7

Tai, Y.F., Pavese, N., Gerhard, A., Tabrizi, S.J., Barker, R.A., Brooks, D.J., Piccini, P., 2007. Microglial activation in presymptomatic Huntington's disease gene carriers. Brain 130, 1759–1766. https://doi.org/10.1093/brain/awm044

Tan, Z., Dai, W., van Erp, T.G.M., Overman, J., Demuro, A., Digman, M. a, Hatami, A., Albay, R., Sontag, E.M., Potkin, K.T., Ling, S., Macciardi, F., Bunney, W.E., Long, J.D., Paulsen, J.S., Ringman, J.M., Parker, I., Glabe, C., Thompson, L.M., Chiu, W., Potkin, S.G., 2015. Huntington's disease cerebrospinal fluid seeds aggregation of mutant huntingtin. Mol. Psychiatry 1–8. https://doi.org/10.1038/mp.2015.81

Tarawneh, R., D'Angelo, G., Crimmins, D., Herries, E., Griest, T., Fagan, A.M., Zipfel, G.J., Ladenson, J.H., Morris, J.C., Holtzman, D.M., 2016. Diagnostic and Prognostic Utility of the Synaptic Marker Neurogranin in Alzheimer Disease. JAMA Neurol. 73, 561. https://doi.org/10.1001/jamaneurol.2016.0086

Teixeira, A.L., Cruz De Souza, L., Rocha, N.P., Furr-Stimming, E., Lauterbach, E.C., 2016. Revisiting the neuropsychiatry of Huntington's disease. Dement Neuropsychol 10, 261–266. https://doi.org/10.1590/S1980-5764-2016DN1004002

Telenius, H., Kremer, B., Goldberg, Y., 1994. Somatic and gonadal mosaicism of the Huntington disease gene CAG repeat in brain and sperm. Nat. Genet. 6, 409–414. https://doi.org/10.1038/ng0494-409

Terrence, C.F., Delaney, J.F., Alberts, M.C., 1977. Computed tomography for Huntington's disease. Neuroradiology 13, 173–175. https://doi.org/10.1007/BF00344209

The Huntington's Disease Collaborative Research Group, 1993. A novel gene containing a trinucleotide repeat that is expanded and unstable on Huntington's disease chromosomes. The Huntington's Disease Collaborative Research Group. Cell 72, 971–83.

The U.S.-Venezuela Collaborative, Wexler, N.S., Lorimer, J., Porter, J., Gomez, F., Moskowitz, C., Shackell, E., Marder, K., Penchaszadeh, G., Roberts, S.A., Gayan, J., Brocklebank, D., Cherny, S.S., Cardon, L.R., Gray, J., Dlouhy, S.R., Wiktorski, S., Hodes, M.E., Conneally, P.M., Penney, J.B., Gusella, J., Cha, J.-H., Irizarry, M., Rosas, D., Hersch, S., Hollingsworth, Z., MacDonald, M., Young, A.B., Andresen, J.M., Housman, D.E., de Young, M.M., Bonilla, E., Stillings, T., Negrette, A., Snodgrass, S.R., Martinez-Jaurrieta, M.D., Ramos-Arroyo, M.A., Bickham, J., Ramos, J.S., Marshall, F., Shoulson, I., Rey, G.J., Feigin, A., Arnheim, N., Acevedo-Cruz, A., Acosta, L., Alvir, J., Fischbeck, K., Thompson, L.M., Young, A., Dure, L., O'Brien, C.J., Paulsen, J., Brickman, A., Krch, D., Peery, S., Hogarth, P., Higgins,

D.S., Landwehrmeyer, B., 2004. Venezuelan kindreds reveal that genetic and environmental factors modulate Huntington's disease age of onset. Proc. Natl. Acad. Sci. 101, 3498–3503. https://doi.org/10.1073/pnas.0308679101

Toombs, J., Paterson, R.W., Lunn, M.P., Nicholas, J.M., Fox, N.C., Chapman, M.D., Schott, J.M., Zetterberg, H., 2013. Identification of an important potential confound in CSF AD studies: Aliquot volume. Clin. Chem. Lab. Med. 51, 2311–2317. https://doi.org/10.1515/cclm-2013-0293

Träger, U., Andre, R., Lahiri, N., Magnusson-Lind, A., Weiss, A., Grueninger, S., McKinnon, C., Sirinathsinghji, E., Kahlon, S., Pfister, E.L., Moser, R., Hummerich, H., Antoniou, M., Bates, G.P., Luthi-Carter, R., Lowdell, M.W., Björkqvist, M., Ostroff, G.R., Aronin, N., Tabrizi, S.J., 2014. HTT-lowering reverses Huntington's disease immune dysfunction caused by NFκB pathway dysregulation. Brain 137, 819–833. https://doi.org/10.1093/brain/awt355

Travessa, A.M., Rodrigues, F.B., Mestre, T.A., Ferreira, J.J., 2017. Fifteen Years of Clinical Trials in Huntington's Disease: A Very Low Clinical Drug Development Success Rate. J. Huntingtons. Dis. 6, 157–163. https://doi.org/10.3233/JHD-170245

Trundell, D., Palermo, G., Schobel, S., Long, J.D., Leavitt, B.R., Tabrizi, S.J., 2018. Validity, reliability, ability to detect change and meaningful within-patient change of the cUHDRS, in: Huntington Study Group 2018.

Turrigiano, G.G., 2017. The dialectic of hebb and homeostasis. Philos. Trans. R. Soc. B Biol. Sci. 372. https://doi.org/10.1098/rstb.2016.0258

van der Ende, E.L., Meeter, L.H., Poos, J.M., Panman, J.L., Jiskoot, L.C., Dopper, E.G.P., Papma, J.M., de Jong, F.J., Verberk, I.M.W., Teunissen, C., Rizopoulos, D., Heller, C., Convery, R.S., Moore, K.M., Bocchetta, M., Neason, M., Cash, D.M., Borroni, B., Galimberti, D., Sanchez-Valle, R., Laforce, R., Moreno, F., Synofzik, M., Graff, C., Masellis, M., Carmela Tartaglia, M., Rowe, J.B., Vandenberghe, R., Finger, E., Tagliavini, F., de Mendonça, A., Santana, I., Butler, C., Ducharme, S., Gerhard, A., Danek, A., Levin, J., Otto, M., Frisoni, G.B., Cappa, S., Pijnenburg, Y.A.L., Rohrer, J.D., van Swieten, J.C., 2019. Serum neurofilament light chain in genetic frontotemporal dementia: a longitudinal, multicentre cohort study. Lancet Neurol. 18, 1103–1111. https://doi.org/10.1016/S1474-4422(19)30354-0

van der Plas, E., Langbehn, D.R., Conrad, A.L., Koscik, T.R., Tereshchenko, A., Epping, E.A., Magnotta, V.A., Nopoulos, P.C., 2019. Abnormal brain development in child and adolescent carriers of mutant huntingtin. Neurology

10.1212/WNL.0000000000008066. https://doi.org/10.1212/wnl.0000000000008066

Van Duijn, E., Craufurd, D., Hubers, A.A.M., Giltay, E.J., Bonelli, R., Rickards, H., Anderson, K.E., Van Walsem, M.R., Van Der Mast, R.C., Orth, M., Landwehrmeyer, G.B., 2014. Neuropsychiatric symptoms in a European Huntington's disease cohort (REGISTRY). J. Neurol. Neurosurg. Psychiatry 85, 1411–1418. https://doi.org/10.1136/jnnp-2013-307343

Vécsei, L., Szalárdy, L., Fülöp, F., Toldi, J., 2013. Kynurenines in the CNS: recent advances and new questions. Nat. Rev. Drug Discov. 12, 64–82. https://doi.org/10.1038/nrd3793

Veldman, M.B., Yang, X.W., 2018. Molecular insights into cortico-striatal miscommunications in Huntington's disease. Curr. Opin. Neurobiol. https://doi.org/10.1016/j.conb.2017.10.019

Vinther-Jensen, T., Börnsen, L., Budtz-Jørgensen, E., Ammitzbøll, C., Larsen, I.U., Hjermind, L.E., Sellebjerg, F., Nielsen, J.E., 2016. Selected CSF biomarkers indicate no evidence of early neuroinflammation in Huntington disease. Neurol. - Neuroimmunol. Neuroinflammation 3, e287. https://doi.org/10.1212/NXI.0000000000000287

Vinther-Jensen, T., Budtz-Jørgensen, E., Simonsen, A.H., Nielsen, J.E., Hjermind, L.E., 2014. YKL-40 in cerebrospinal fluid in Huntington's disease--a role in pathology or a nonspecific response to inflammation? Parkinsonism Relat. Disord. 20, 1301–3. https://doi.org/10.1016/j.parkreldis.2014.08.011

Virlogeux, A., Moutaux, E., Christaller, W., Genoux, A., Bruyère, J., Fino, E., Charlot, B., Cazorla, M., Saudou, F., 2018. Reconstituting Corticostriatal Network on-a-Chip Reveals the Contribution of the Presynaptic Compartment to Huntington's Disease. CellReports 22, 110–122. https://doi.org/10.1016/j.celrep.2017.12.013

Vonsattel, J.P., Myers, R.H., Stevens, T.J., Ferrante, R.J., Bird, E.D., Richardson, E.P., 1985. Neuropathological classification of huntington's disease. J. Neuropathol. Exp. Neurol. 44, 559–577. https://doi.org/10.1097/00005072-198511000-00003

Vranová, H.P., Hényková, E., Kaiserová, M., Menšíková, K., Vaštík, M., Mareš, J., Hluštík, P., Zapletalová, J., Strnad, M., Stejskal, D., Kaňovský, P., 2014. Tau protein, beta-amyloid$_{1-42}$ and clusterin CSF levels in the differential diagnosis of Parkinsonian syndrome with dementia. J. Neurol. Sci. 343, 120–4. https://doi.org/10.1016/j.jns.2014.05.052

Waldö, M.L., Santillo, A.F., Passant, U., Zetterberg, H., Rosengren, L., Nilsson, C., Englund, E., 2013. Cerebrospinal fluid neurofilament light chain protein levels in subtypes of frontotemporal dementia. BMC Neurol. 13. https://doi.org/10.1186/1471-2377-13-54

Wang, J.K.T.T., Langfelder, P., Horvath, S., Palazzolo, M.J., 2017. Exosomes and homeostatic synaptic plasticity are linked to each other and to Huntington's, Parkinson's, and other neurodegenerative diseases by database-enabled analyses of comprehensively curated datasets. Front. Neurosci. 11, 149. https://doi.org/10.3389/fnins.2017.00149

Watt, A.J., Desai, N.S., 2010. Homeostatic plasticity and STDP: Keeping a neuron's cool in a fluctuating world. Front. Synaptic Neurosci. https://doi.org/10.3389/fnsyn.2010.00005

Weiss, A., Abramowski, D., Bibel, M., Bodner, R., Chopra, V., Difiglia, M., Fox, J., Kegel, K., Klein, C., Grueninger, S., Hersch, S., Housman, D., Régulier, E., Rosas, H.D., Stefani, M., Zeitlin, S., Bilbe, G., Paganetti, P., 2009. Single-step detection of mutant huntingtin in animal and human tissues: A bioassay for Huntington's disease. https://doi.org/10.1016/j.ab.2009.08.001

Weiss, A., Träger, U., Wild, E.J., Grueninger, S., Farmer, R., Landles, C., Scahill, R.I., Lahiri, N., Haider, S., Macdonald, D., Frost, C., Bates, G.P., Bilbe, G., Kuhn, R., Andre, R., Tabrizi, S.J., 2012. Mutant huntingtin fragmentation in immune cells tracks Huntington's disease progression. J. Clin. Invest. 122, 3731–6. https://doi.org/10.1172/JCI64565

Wellington, H., Paterson, R.W., Portelius, E., Törnqvist, U., Magdalinou, N., Fox, N.C., Blennow, K., Schott, J.M., Zetterberg, H., 2016. Increased CSF neurogranin concentration is specific to Alzheimer disease. Neurology 86, 829–35. https://doi.org/10.1212/WNL.0000000000002423

Wellington, H., Paterson, R.W., Suárez-González, A., Poole, T., Frost, C., Sjöbom, U., Slattery, C.F., Magdalinou, N.K., Lehmann, M., Portelius, E., Fox, N.C., Blennow, K., Zetterberg, H., Schott, J.M., 2018. CSF neurogranin or tau distinguish typical and atypical Alzheimer disease. Ann. Clin. Transl. Neurol. 5, 162–171. https://doi.org/10.1002/acn3.518

Whitwell, J.L., Crum, W.R., Watt, H.C., Fox, N.C., 2001. Normalization of cerebral volumes by use of intracranial volume: implications for longitudinal quantitative MR imaging. AJNR. Am. J. Neuroradiol. 22, 1483–9.

Wijeratne, P.A., Young, A.L., Oxtoby, N.P., Marinescu, R. V, Firth, N.C., Johnson, E.B.,

Mohan, A., Sampaio, C., Scahill, R.I., Tabrizi, S.J., Alexander, D.C., 2018. An image-based model of brain volume biomarker changes in Huntington's disease. Ann. Clin. Transl. Neurol. https://doi.org/10.1002/acn3.558

Wild, E., Magnusson, A., Lahiri, N., Krus, U., Orth, M., Tabrizi, S.J., Björkqvist, M., 2011. Abnormal peripheral chemokine profile in Huntington's disease. PLoS Curr. 3, RRN1231. https://doi.org/10.1371/currents.RRN1231

Wild, E.J., Boggio, R., Langbehn, D., Robertson, N., Haider, S., Miller, J.R.C., Zetterberg, H., Leavitt, B.R., Kuhn, R., Tabrizi, S.J., Macdonald, D., Weiss, A., 2015. Quantification of mutant huntingtin protein in cerebrospinal fluid from Huntington's disease patients 125, 1–8. https://doi.org/10.1172/JCI80743DS1

Wild, E.J., Tabrizi, S.J., 2017. Therapies targeting DNA and RNA in Huntington's disease. Lancet. Neurol. 16, 837–847. https://doi.org/10.1016/S1474-4422(17)30280-6

Wild, E.J., Tabrizi, S.J., 2014. Targets for future clinical trials in Huntington's disease: What's in the pipeline? Mov. Disord. 29, 1434–1445. https://doi.org/10.1002/mds.26007

Winder, J.Y., Roos, R.A.C., Burgunder, J.-M., Marinus, J., Reilmann, R., 2018. Interrater Reliability of the Unified Huntington's Disease Rating Scale-Total Motor Score Certification. Mov. Disord. Clin. Pract. 5, 290–295. https://doi.org/10.1002/mdc3.12618

Woollacott, I.O.C., Nicholas, J.M., Heslegrave, A., Heller, C., Foiani, M.S., Dick, K.M., Russell, L.L., Paterson, R.W., Keshavan, A., Fox, N.C., Warren, J.D., Schott, J.M., Zetterberg, H., Rohrer, J.D., 2018. Cerebrospinal fluid soluble TREM2 levels in frontotemporal dementia differ by genetic and pathological subgroup. Alzheimer Res. Ther. 10. https://doi.org/10.1186/s13195-018-0405-8

Yalow, R.S., Berson, S.A., 1960. IMMUNOASSAY OF ENDOGENOUS PLASMA INSULIN IN MAN. J. Clin. Invest.

Yilmaz, A., Fuchs, D., Price, R.W., Spudich, S., Blennow, K., Zetterberg, H., Gisslén, M., 2019. Cerebrospinal Fluid Concentrations of the Synaptic Marker Neurogranin in Neuro-HIV and Other Neurological Disorders. Curr. HIV/AIDS Rep. 16, 76–81. https://doi.org/10.1007/s11904-019-00420-1

Young, A.L., Oxtoby, N.P., Daga, P., Cash, D.M., Fox, N., Ourselin, S., Schott, J.M., Alexander, D.C., 2014. Adata-driven model of biomarker changes in sporadic Alzheimer's disease. Alzheimer's Dement. 10, P172.

https://doi.org/10.1016/j.jalz.2014.04.180

Zeitlin, S., Liu, J.P., Chapman, D.L., Papaioannou, V.E., Efstratiadis, A., 1995. Increased apoptosis and early embryonic lethality in mice nullizygous for the Huntington's disease gene homologue. Nat. Genet. 11, 155–163. https://doi.org/10.1038/ng1095-155

Zeun, P., Lowe, J., Osborne-Crowley, K., O'Callaghan, C., Johnson, E., Gregory, S., Nair, A., Fayer, K., Rodrigues, F., Estevez-Fraga, C., Wild, E., Zhang, G., Sampaio, C., Robbins, T., Rees, G., Scahill, R., Sahakian, B., Tabrizi, S.J., 2018. F59 Huntington's disease young adult study (HD-YAS). J. Neurol. Neurosurg. & Psychiatry 89, A60 LP-A61. https://doi.org/10.1136/jnnp-2018-EHDN.160

Zhou, W., Zhang, J., Ye, F., Xu, G., Su, H., Su, Y., Zhang, X., 2017. Plasma neurofilament light chain levels in Alzheimer's disease. Neurosci. Lett. 650, 60–64. https://doi.org/10.1016/j.neulet.2017.04.027

Appendix

Clinical Study Protocol

HD-CSF: Studying cerebrospinal fluid to understand key CNS pathobiological targets in Huntington's disease

PRINCIPAL INVESTIGATOR: Edward Wild, MA MB BChir PhD MRCP

UCL Institute of Neurology
Box 104
National Hospital for Neurology & Neurosurgery
Queen Square, London
WC1N 3BG, UK

Phone: + 44 207 611 0125
Fax: + 44 207 611 0129

e.wild@ucl.ac.uk

SPONSOR: University College London

ORIGINAL VERSION DATE: 19 October 2015

This Clinical Study Protocol is approved by:

[redacted]

Signatur[redacted]ate: 19 OCT 2015 .

Edward Wild, MA MB BChir PhD MRCP
Principal Investigator

Synopsis

Study Title: HD-CSF: Studying cerebrospinal fluid to understand key CNS pathobiological targets in Huntington's disease

Short Study Title: HD-CSF

Funding Source: Medical Research Council Clinician Scientist Fellowship MR/M008592/1

Study Location: University College London Institute of Neurology / National Hospital for Neurology & Neurosurgery

Number of Participants planned: 80

Principal Investigator:

Dr. Edward Wild
MRC Clinician Scientist, UCL Institute of Neurology;
Honorary Consultant Neurologist, National Hospital for Neurology & Neurosurgery, Queen Square
London WC1N 3BG, UK

Study period:

Estimated date first subject enrolled: Q4 2015
Estimated date last subject completed: April 30th, 2019

Objectives:

Primary: The primary objective of this study is to generate a high quality cerebrospinal fluid (CSF) sample collection and evaluate biomarkers and pathways that contribute to the development of Huntington's disease (HD).

Secondary:

- To generate a high quality plasma sample collection matching the CSF collections, which will also be used to evaluate biomarkers and pathways of relevance to HD research and development.
- To collect phenotypic and clinical data for each participant.

Study Design:

HD-CSF is a longitudinal observational study. At baseline participants will attend a Screening Visit and Sampling Visit (collectively referred to as Core Baseline activities) and may attend an optional third visit (optional Repeat Sampling Visit). At follow-up 24 months later the screening Visit, sampling (collectively referred to as Core Follow-up activities) and optional Repeat Sampling Visit will be repeated. During the Screening Visit, medical history, and clinical and phenotypic data including an optional MRI scan will be obtained. Participants who meet the eligibility requirements of the study and are willing to continue in the study, will return for a Sampling Visit. During that visit, biosamples will be collected following an overnight fast: blood will be obtained via venepuncture and CSF will be obtained via lumbar puncture. Some participants may be

invited to return for a Repeat Sampling Visit approximately 4-8 weeks later. Participant cohorts are as follows:

1. Healthy controls, n= 20
2. Pre-manifest HD, n=20
3. Early to moderate manifest HD, n = 40

Diagnosis and main criteria for inclusion:

Healthy controls as well as Huntington's disease gene expansion carriers (HDGECs) will be enrolled. The latter will include two groups: pre-manifest HD and early to moderate HD.

Inclusion Criteria:

1. All eligible participants
   a. Are 18-75 years of age, inclusive; and
   b. Are capable of providing informed consent. A legal representative will be used only in the event of communication difficulties to verify that the person has understood and consented; and
   c. Are capable of complying with study procedures, including fasting, blood sampling and lumbar puncture; and
   d. Are participating in the Enroll-HD study
2. For the **Healthy Control** group, subjects eligible are persons who meet the following criteria:
   a. Have no known family history of HD; or
   b. Have known family history of HD but have been tested for the huntingtin gene glutamine codon (CAG) expansion and are not at genetic risk for HD (CAG < 36).
3. For the **Pre-manifest HD** group, participants eligible are persons who meet the following criteria:
   a. Do not have clinical diagnostic motor features of HD, defined as Unified Huntington's Disease Rating Scale (UHDRS) Diagnostic Confidence Score < 4; and
   b. Have CAG expansion ≥ 40; and
4. For the **Early to moderate HD** group, participants eligible are persons who meet the following criteria:
   a. Have clinical diagnostic motor features of HD, defined as UHDRS Diagnostic Confidence Score = 4; and
   b. Have CAG expansion ≥ 36; and
   c. Have Stage I, II or III HD, defined as UHDRS Total Functional Capacity (TFC) scores between 4 and 13 inclusive.

Exclusion Criteria:

1. For all groups, participants are ineligible if they meet any of the following exclusion criteria:
   a. Current use of investigational drugs or participation in a clinical drug trial within 30 days prior to Sampling Visit; or
   b. Current intoxication, drug or alcohol abuse or dependence; or
   c. If using any antidepressant, psychoactive, psychotropic or other medications or nutraceuticals used to treat HD, the use of inappropriate (e.g., non-therapeutically

high) or unstable dose within 30 days prior to Sampling Visit; or

d. Significant medical, neurological or psychiatric co-morbidity likely, in the judgment of the Principal Investigator, to impair participant's ability to complete essential study procedures; or
e. Needle phobia, frequent headache, significant lower spinal deformity or major surgery; or
f. Antiplatelet or anticoagulant therapy within the 14 days prior to sampling visit, including but not limited to: aspirin, clopidogrel, dipyridamole, warfarin, dabigatran, rivaroxaban and apixaban; or
g. Clotting or bruising disorder; or
h. Screening blood test results outside the clinical laboratory's normal range for the following: white cell count, neutrophil count, lymphocyte count, hemoglobin (Hb), platelets, prothrombin time (PT) or activated partial thromboplastin time (APTT); or
i. Screening blood test results for C-reactive protein (CRP)>2× upper limit of normal; or
j. Predictable non-compliance as assessed by the Principal Investigator; or
k. Inability or unwillingness to undertake any of the essential study procedures; or
l. Exclusion during history or physical examination, final decision to be made by the Principal Investigator; including but not limited to:
    i any reason to suspect abnormal bleeding tendency, e.g. easy bruising, petechial rash; or
    ii any reason to suspect new focal neurological lesion, e.g. new headache, optic disc swelling, asymmetric focal long tract signs; or
    iii any other reason that, in the clinical judgment of the operator or the Principal Investigator, it is felt that lumbar puncture is unsafe.

Participants are ineligible for the optional MRI component if they meet any of the following criteria:

a. Contraindication to MRI, including, but not limited to, MR-incompatible pacemakers, recent metallic implants, foreign body in the eye or other indications, as assessed by a standard pre-MRI questionnaire; or
b. Pregnant (as confirmed by urine pregnancy test); or
c. Claustrophobia, or any other condition that would make the subject incapable of undergoing an MRI.

Sample Size:

Power calculations were based on a 12-subject CSF analysis of mutant huntingtin using a novel single molecule counting immunoassay[1]. Detecting cross-sectional differences between control and HD requires very small numbers (<5 per group for >90% power at 5% significance). 20 subjects per group gives >90% power to detect predicted longitudinal change in mutant huntingtin over two years.

Table of Contents

List of Abbreviations and Definitions of Terms

Abbreviation	Definition
AE	Adverse Event
APTT	Activated partial thromboplastin time
CAG	Cytosine-arginine-glutamine codon whose count in the HTT gene determines the genetic diagnosis of HD
CRP	C-reactive protein
CSF	Cerebrospinal fluid
eCRF	electronic Case Report Form
GCP	Good Clinical Practice
Hb	Hemoglobin
HD	Huntington's disease
HDGEC	Huntington's disease gene expansion carrier
HTT	huntingtin protein
ICH Guidelines	International Conference on Harmonisation Guidance for Industry
IRB	Institutional Review Board
KMO	kynurenine mono-oxygenase
KP	kynurenine pathway
PT	Prothrombin time
REC	Regional Ethics Committee
SAE	Serious Adverse Event
TFC	Total Functional Capacity
TMS	Total Motor Score
UHDRS	Unified Huntington's Disease Rating Scale

1. Introduction

1.1 Background and Rationale

Huntington's disease (HD) is an autosomal dominant genetic disease, which typically manifests beginning in adulthood in the form of movement symptoms, cognitive decline, and psychiatric changes.[2] Currently the only approved treatment for HD is tetrabenazine, but several clinical trials are expected to launch shortly to explore novel therapeutic approaches to treating this disease. In preparation for such trials, biomarkers are needed to evaluate: (1) how well these novel therapeutics reach their intended target and have a biological effect (pharmacodynamic markers); (2) the effectiveness of these novel therapeutics at improving clinical signs and symptoms (efficacy biomarkers); and (3) the state of disease patients are in throughout the trial (disease progression biomarkers). Cerebrospinal fluid (CSF) is an ideal fluid compartment for assessing HD biomarkers, particularly pharmacodynamics markers, due to its proximity to the brain.

Evidence from preclinical animal studies as well as post-mortem human brain studies suggests that the kynurenine pathway (KP) may be abnormally regulated in HD.[3] Thus, this enzymatic pathway may be a target for therapeutic intervention. However, the KP has not been extensively investigated in HD patients and premanifest HD gene expansion carriers (HDGECs). To further investigate the potential dysregulation of the pathway, and inter-participant variability of the dysregulation, we propose to measure levels of some of the key KP metabolites in CSF and plasma from HD patients, premanifest HDGECs and healthy controls. The results of this study will serve not only to support the biological rationale for pursuing this line of treatment for HD, but will also set the ground work for the use of particular metabolites as pharmacodynamic biomarkers in future clinical trials of therapeutics modulating the KP, such as inhibitors of kynurenine mono-oxygenase (KMO).

Several therapeutic approaches focused on lowering huntingtin protein (HTT) in the brain are currently pursued, and studies in animals suggest this is a promising approach.[4] However, one of the key tools needed to pursue such approaches in humans is the ability to demonstrate that the intervention did lower HTT levels in the brain. Fortunately, assays have been developed that can detect HTT in CSF.[1] We propose to further the development and validation of CSF HTT assays by measuring HTT levels in CSF and plasma from HD patients, premanifest HDGECs and healthy controls. This will also help to understand to what extent CSF mHTT level predicts disease progression in HD and could be used to guide future treatment decisions. The results of these studies will lead to the establishment of the best practices for measuring HTT in CSF from patients before and after HTT lowering therapies.

Several CSF and plasma HD biomarker discovery programs have resulted in the generation of many substances potentially differentially expressed in HD.[2,5] While promising, these need to be replicated in a new sample set and with more quantitative assays. The samples and data generate by HD-CSF will be used to conduct biochemical analyses to understand the pathobiology of HD and possible biomarkers in CSF and plasma.

1.2 Rationale for Current Study

With promising new therapeutic trials expected to begin in the next few years, exploration of potential biomarkers needs to be accelerated now. There is currently no high quality repository of CSF from well-characterised HDGECs spanning the disease spectrum. The

current study will provide such a repository in order to expedite the research into biomarkers for HD. We also need to understand to what extent proposed CSF and plasma biomarkers can predict the progression of HD to help design future trials and guide clinical decision-making in HD.

2. Study Objectives

The overall objective of this study is to generate a high quality CSF sample collection and use it to identify and validate biomarkers for HD clinical development. In one usage, the sample collection will be assayed to determine if the KP is dysregulated in premanifest and early HD in comparison to healthy controls, and to evaluate the variability in KP metabolite levels within each participant group. This information will help assess the potential for KMO inhibitors as therapies for HD and guide the use of such assays as pharmacodynamic biomarkers in clinical trials. The sample collection will also enable the further development and validation of assays to measure HTT in CSF, which may be an attractive pharmacodynamic biomarker for HTT lowering clinical trials. Last, the sample collection will enable the continued evaluation of a number of potential novel biomarkers of disease progression and, potentially, efficacy in HD.

2.1 Primary Objective

The primary objective of this study is to generate a high quality CSF sample collection and use it to evaluate biomarkers and pathways that will enable the development of novel treatments for HD.

2.2 Secondary Objective(s)

The secondary objectives of this study are:

- To generate a high quality plasma sample collection matching the CSF collections, which will also be used to evaluate biomarkers and pathways of relevance to HD research and development.
- To collect phenotypic and clinical data for each participant.

3. Study Design

3.1 Overall Study Design

This is a longitudinal observational study.

Recruitment: Participants will be recruited from the Huntington's Disease Multidisciplinary Clinic at the UCLH National Hospital for Neurology and Neurosurgery, from the database of partipants in the Enroll-HD study.

Study Visits: There are two time points, core baseline and core follow-up activities. At baseline, participants will attend two study visits: a **Screening Visit** and a **Sampling Visit**. During the **Screening Visit**, which may coincide with an Enroll-HD visit, medical history, clinical and phenotypic data (including a screening blood sample and an optional MRI scan) will be obtained. These data will determine participant eligibility for participation in the study and will be used in the analysis of biomarker data. Participants meeting the eligibility requirements of the study and willing to continue in the study, will return for a **Sampling Visit** within 30 days of the Screening Visit. During that visit, biosamples will be collected following an overnight fast: blood will be obtained via venepuncture and CSF will be obtained via lumbar puncture. Participants will be contacted by telephone approximately 24-72 hours after the Sampling Visit for safety and

adverse event monitoring. The Screening Visit, Sampling Visit and Telephone Call are all part of the Core Baseline activities. Some participants may be invited to return for an optional **Repeat Sampling Visit** 4-8 weeks following the Sampling visit.

Core Follow-up visits will occur 24 months (+/- 3 months) after Core Baseline visits and will take exactly the same format as the Core Baseline visits.

HD-CSF is designed to use the standardised phenotypic data from Enroll-HD. Where possible, routine, planned Enroll-HD visits will be used to plan recruitment into HD-CSF. However, where such scheduling may jeopardise a potential participant's inclusion in HD-CSF, assessments equivalent to an Enroll-HD Core visit may be performed at the HD-CSF screening visit.

Biosample Preparation: Samples will be processed and stored as described in Sections 10.1, 10.2 and 10.3 until ready for analysis.

Laboratory analyses: Samples will either be analysed locally or be shipped to collaborators authorised by the Principal Investigator, for investigations into biomarkers and pathogenic mechanisms in HD including, but not limited to, evaluation of the kynurenine pathway, measurement of huntingtin protein and other HD pathobiology, biomarker discovery or validation studies.

Statistical analysis: Statistical advice has been provided by the UCL/UCLH Biostatistics Unit. For each set of laboratory analyses conducted, a statistical analysis plan will be finalised before samples are sent to the laboratory conducting the studies. In brief, a two-stage approach will be used with linear regression models comparing change in molecular markers between clinical groups and for primary and secondary outcomes, with those found to be associated with disease progression then being examined for associations with measures of phenotypic change using a similar model.

3.2 Safety

The procedures for performing lumbar punctures and venous blood draws have been designed to maximize participant safety.

Study-related risks are explained in the informed consent document. In particular, the following risks may be associated with lumbar puncture: pain; headache (approximately 5%), infection, bleeding and nerve root damage. Most headaches resolve spontaneously but occasionally a headache may be persistent; in rare cases this may necessitate treatment, which may include a second procedure (a blood patch), carried out in a clinical setting.

See Appendix A –Principal Investigator Obligations for additional information.

4. Study Population

Three participant cohorts will be included in the study:

1. Healthy controls, n= 20
2. Pre-manifest HD, n=20
3. Early to moderate HD, n=40

4.1 Diagnosis and Main Selection Criteria

A total of 80 participants, aged between 18 and 75 years, inclusive, will be enrolled in the study. Eligible participants include healthy controls, people who are in the pre-manifest stage of HD, and people diagnosed with early or moderate HD.

4.1.1 Inclusion Criteria

1. **All eligible participants**:
   a. Are male or female, 18-75 years of age, inclusive; and
   b. Are capable of providing informed consent. A legal representative will be used only in the event of communication difficulties to verify that the person has understood and consented; and
   c. Are capable of complying with study procedures, including fasting, blood sampling and lumbar puncture; and
   d. Are participating in the Enroll-HD study;
   e. No contraindication to MRI scan
2. For the **Healthy Control** group, subjects eligible are persons who meet the following criteria:
   a. Have no known family history of HD; or
   b. Have a known family history of HD but have been tested for the huntingtin gene glutamine codon (CAG) expansion and are **not** at genetic risk for HD (CAG < 36)*.

3. For the **Pre-manifest HD** group, participants eligible are persons who meet the following criteria:

   a. Do not have clinical diagnostic motor features of HD, defined as Unified Huntington's Disease Rating Scale (UHDRS) Diagnostic Confidence Score < 4; and
   b. Have CAG expansion ≥ 40*; and

4. For the Early to moderate HD group, participants eligible are persons who meet the following criteria:

   d. Have clinical diagnostic motor features of HD, defined as UHDRS Diagnostic Confidence Score = 4; and
   e. Have CAG expansion ≥ 36*; and
   f. Have Stage I, II or III HD, defined as UHDRS Total Functional Capacity (TFC) scores between 4 and 13 inclusive.

*Genetic test results must be recorded in a documented report from an accredited genetics laboratory in the medical notes.

4.1.2 Exclusion Criteria

1. For all groups, participants are ineligible if they meet any of the following exclusion criteria:

   a. Use of investigational drugs or participation in a clinical drug trial within 30 days prior to Sampling Visit; or

   b. Current intoxication, drug or alcohol abuse or dependence; or

c. If using any antidepressant, psychoactive, psychotropic or other medications or nutraceuticals used to treat HD, the use of inappropriate (e.g., non-therapeutically high) or unstable dose within 30 days prior to the Sampling Visit; or

d. Significant medical, neurological or psychiatric co-morbidity likely, in the judgment of the Principal Investigator, to impair participant's ability to complete essential study procedures; or

e. Needle phobia, frequent headache, significant lower spinal deformity or major surgery; or

f. Antiplatelet or anticoagulant therapy within 14 days prior to Sampling Visit, including but not limited to: aspirin, clopidogrel, dipyridamole, warfarin, dabigatran, rivaroxaban and apixaban; or

g. Clotting or bruising disorder; or

h. Screening blood test results outside the clinical laboratory's normal range for the following: white cell count, neutrophil count, lymphocyte count, hemoglobin (Hb), platelets, Prothrombin time (PT) and activated partial thromboplastin time (APTT); or

i. Screening blood test results for C-reactive protein (CRP) >2× upper limit of normal; or

j. Predictable non-compliance as assessed by the Principal Investigator; or

k. Inability or unwillingness to undertake any of the essential study procedures; or

l. Exclusion during history or physical examination, final decision to be made by the Principal Investigator; including but not limited to:

   i any reason to suspect abnormal bleeding tendency, e.g. easy bruising, petechial rash; or

   ii any reason to suspect new focal neurological lesion, e.g. new headache, optic disc swelling, asymmetric focal long tract signs; or

   iii any other reason that, in the clinical judgment of the operator or the Principal Investigator (including clinically relevant abnormalities on the optional MRI scan), it is felt that lumbar puncture is unsafe.

2. Participants are ineligible for the optional MRI component if they meet any of the following criteria:

   a. Contraindication to MRI, including, but not limited to, MR-incompatible pacemakers, recent metallic implants, foreign body in the eye or other indications, as assessed by a standard pre-MRI questionnaire; or

   b. Pregnant (as confirmed by urine pregnancy test); or

   c. Claustrophobia, or any other condition that would make the subject incapable of undergoing an MRI.

4.2 Criteria for Termination of the Study

If the study is prematurely terminated or suspended for any reason, the Principal Investigator/institution will promptly inform the study participants and should assure appropriate follow-up for them. The Principal Investigator will also inform the appropriate Regional Ethics Committee and Trust Joint Research Office.

5. Study Procedures

All procedures are performed at baseline and follow-up (24 months +/- 3 months)

Visit Number	**1**	**2**		**3**	
	CORE BASELINE ACTIVITIES			**OPTIONAL BASELINE ACTIVITIES**	
Visit Type	**Screening**	**Sampling**	**Telephone Follow-Up**	**Optional Repeat Sampling**	**Telephone Follow-Up[3]**
Days	-30 to -1	Day 0	Day 1 to 3	Day 28 - 56	+1-3 Days After Optional Sampling Visit
Informed Consent	✓			✓	
Inclusion/Exclusion Criteria review	✓	✓		✓	
Confirm Enroll-HD core assessments completed within last two months; **if not, complete Enroll-HD core assessments**	✓				
UHDRS motor assessment, diagnostic confidence score, total functional capacity and Independence Scale (if applicable	✓				
Short Problem behaviours assessment (PBA-S) (if applicable)	✓				
Symbol-digit modality test (if applicable)	✓				
Stroop word reading (if applicable)	✓				
Stroop colour naming (if applicable)	✓				
Categorical verbal fluency (if applicable)	✓				
Brief Physical Exam	✓	✓		✓	
Medical History update	✓	✓		✓	
Prior/Concomitant Medication update	✓	✓	✓	✓	✓
Standard Neurological Examination	✓	✓		✓	
Total Motor Score (TMS)		✓		✓	
Vital Signs (BP, pulse, body temp)		✓		✓	
Safety Laboratory Assessments	✓				
Optional MRI scan	✓				
Adverse Events	✓	✓	✓	✓	✓
Final Eligibility Check		✓		✓	
Lumbar CSF Collection		✓		✓	
Venous Blood Draw[2]		✓		✓	
CSF and Blood Sample Processing		✓		✓	
CSF QC Processing		✓		✓	

Visit Number	4	5		6	
	CORE FOLLOWUP ACTIVITIES			OPTIONAL FOLLOWUP ACTIVITIES	
Visit Type	**Screening**	**Sampling**	**Telephone FollowUp**	**Optional Repeat Sampling**	**Telephone FollowUp[3]**
Time window	Upto 30 days before follow-up sampling	21 to 27 months after baseline sampling	Follow-up sampling + 1-3 days	28 – 56 days after follow-up sampling	+1-3 Days After follow-up optional Sampling Visit
Informed Consent	✓			✓	
Inclusion/Exclusion Criteria review	✓	✓		✓	
Confirm Enroll-HD core assessments completed within last two months; **if not, complete Enroll-HD core assessments**	✓				
UHDRS motor assessment, diagnostic confidence score, total functional capacity and Independence Scale (if applicable)	✓				
Short Problem behaviours assessment (PBA-S) (if applicable)	✓				
Symbol-digit modality test (if applicable)	✓				
Stroop word reading (if applicable)	✓				
Stroop colour naming (if applicable)	✓				
Categorical verbal fluency (if applicable)	✓				
Brief Physical Exam	✓	✓		✓	
Medical History update	✓	✓		✓	
Prior/Concomitant Medication update	✓	✓	✓	✓	✓
Standard Neurological Examination	✓	✓		✓	
Total Motor Score (TMS)		✓		✓	
Vital Signs (BP, pulse, body temp)		✓		✓	
Safety Laboratory Assessments	✓				
Optional MRI scan	✓				
Adverse Events	✓	✓	✓	✓	✓
Final Eligibility Check		✓		✓	
Lumbar CSF Collection		✓		✓	
Venous Blood Draw[2]		✓		✓	
CSF and Blood Sample Processing		✓		✓	
CSF QC Processing		✓		✓	

[1]Confirm and record continued consent. [2]Obtain venous blood sample immediately after CSF collection is complete. [3]For selected subjects only.

5.1 Description of Study Assessments

HD-CSF is a longitudinal study with two assessment blocks – baseline and follow-up. Follow-up activities occur 24 months (+/- 3 months) after baseline.

Each block contains three core activities: a screening visit, a sampling visit and a telephone follow-up. Each block also has two optional activities: an optional repeat sampling visit and a corresponding telephone follow-up.

The Screening and Sampling Visits within each block should be no more than 30 days apart. The screening visit may occur with an Enroll-HD visit. The optional Repeat Sampling Visit will occur within 4-8 weeks of the first sampling visit.

Optional repeat sampling visits will be offered to all subjects and booked after the baseline sampling visit for those who wish to proceed. Optional MRI scans will be offered to all subjects at the baseline and follow-up screening visits.

Information regarding occurrence of adverse events (AEs) will be captured throughout the study. Duration (start and stop dates and times), severity/grade, outcome, treatment and relation to study procedures will be recorded on the electronic case report form (eCRF).

5.1.1 Screening Visit

- The study will be described in detail to prospective participants then informed consent will be obtained at baseline and reconfirmed at follow-up.
- If Enroll-HD study core assessments have not been performed within the last two months, these will be carried out during the Screening Visit according to the procedures in the Enroll-HD Protocol and study materials. The Enroll core assessments currently include:
    - Height and weight measurement
    - UHDRS motor assessment, diagnostic confidence score, total functional capacity and Independence Scale. (*The UHDRS is a standardised rating scale for assessing clinical features of Huntington's disease. The motor assessment is a brief directed neurological examination and includes a diagnostic confidence score of 1-4 that reflects the assessor's certainty that the person has manifest HD. The TFC and IS both quantify the degree to which a person's functioning is affected by HD.)*
    - Short Problem behaviours assessment (PBA-S). *(The PBA assesses behavioural symptoms of HD in a standardised way using a semi-structured questionnaire)*
    - Symbol-digit modality test *(This is a paper-based cognitive test that involves matching symbols to numbers. It is sensitive to change in early HD.)*
    - Stroop word reading *(This is a paper-based cognitive test that involves reading words. It is sensitive to change in early HD.)*
    - Stroop colour naming *(This is a paper-based cognitive test that involves naming the colours of written words. It is sensitive to change in early HD.)*

    - Categorical verbal fluency *(This is a cognitive test in which the participant is asked to name as many items within a particular category as possible within a time limit. It is sensitive to change in early HD.)*

- Medical history update since the last Enroll-HD study visit, including medication history and co-morbidities, is obtained.
- Demographic information update since the last Enroll-HD study visit.
- A standard neurological examination is performed as below, as well as a brief general physical examination. Evidence of possible bleeding tendency such as bruises or petechial rash should be noted.
    - Cranial nerves
        - visual acuity
        - visual fields to confrontation
        - fundoscopy (including appearance of discs and presence / absence of venous pulsations)
        - smooth pursuit and saccadic eye movements
        - facial sensation
        - jaw power
        - facial symmetry and power
        - bedside auditory acuity
        - palatal elevation
        - pharyngeal sensation
        - cough
        - Sternocleidomastoid muscle and trapezius power
    - Upper and lower limbs
        - Tone
        - Proximal and distal power
        - Reflexes (-, +/-, +, ++, +++)
        - Pinprick sensation
        - Plantar responses
        - Coordination
- Up to 15 ml of venous blood is drawn according to local clinical standards and procedures, and routine blood tests performed by UCLH clinical laboratory.
    - Biochemistry panel
    - Full blood count
    - Clotting profiles: PT and APTT
    - CRP
- An optional MRI brain scan, lasting up to 45 minutes, is obtained. This will consist of localiser, 2 T1 volumetric sequences and a diffusion tensor imaging sequence.

If the blood count or clotting profiles are outside normal range, or if CRP is greater than 2× the upper limits of normal the subject will not be booked for a sampling visit. The Principal Investigator will act on any abnormalities according to clinical judgment.

The MRI scan is not intended or sufficient to establish the safety or otherwise of lumbar puncture, which is determined on clinical grounds. Scans will be briefly reviewed for any major abnormalities by the study radiographer and, if necessary, escalated to the Principal Investigator for review and further action including postponing the sampling visit if the PI has concerns about the safety of lumbar puncture on reviewing the scan.

If participants do not fulfil all inclusion criteria, they may be rescheduled to repeat some or all of the screening assessments above within the one-month screening window.

If these assessments confirm all the eligibility requirements are met for the study, a date will be given via a telephone call for the sampling visit.

5.1.2 Sampling Visit

- The sampling visit is scheduled in such a way to allow for the lumbar puncture to be performed between 8:00 and 10:30 am local time. All participants will be asked to fast from midnight the night before their appointment, but are permitted to drink water freely. Compliance with instructions to fast is recorded. If participant did not fast, they will be sent home, and the procedure rescheduled.
- Participant continued consent to participate is confirmed and recorded.
- The results of the routine laboratory examination are reviewed and recorded.
- Medical and concomitant medication history is updated.
- Measurement of vital signs.
- The check-list ‘Inclusion and Exclusion Criteria – Sampling Visit’ is completed. Any changes to medical history and medication are noted.
- The neurological examination and brief physical exam are repeated for safety.
- The Total Motor Score (TMS) of the UHDRS is performed.
- Lumbar CSF Collection is performed. (See Section 6.1 for full details)
- Venous blood sampling is performed immediately after CSF collection is complete. (See Section 6.2 for complete instructions)
- CSF, Serum and Plasma samples are processed as per Sections 7.1, 7.2 and 7.3
- Samples are stored per Section 8.

5.1.2.1 Participant Discharge

Participants are observed for potential complications for at least an hour and discharged once appropriate. Any AEs are recorded.

Participant is discharged by nurses with instructions for over-the-counter pain medication and hydration in the event of headache.

5.1.3 Follow-up Telephone Call

Participants will be contacted 24 to 72 hours following the Sampling Visit to collect any AE and/or concomitant medication data.

5.1.4 Optional Sampling

- This visit is optional. Participant continued consent to participate is confirmed and recorded.

- This visit should be scheduled 4 - 8 weeks following the initial Sampling Visit.
- All procedures are identical to the sampling visit including sample collection, processing and storage; participant discharge and follow-up telephone call.

6. Sample Collection Procedures

6.1 Lumbar CSF Collection

1. Ensure that all equipment is on hand and that ice is available for CSF collection and transportation of samples to the lab.
2. Ensure availability and settings of centrifuges for appropriate temperatures and timely processing of CSF and blood samples.
3. Pre-cool CSF collection tubes on ice.
4. Prepare a sterile field containing all equipment needed, label tubes.
5. Place participant into lateral decubitus position with pillow between knees.
6. Identify L4/5 or L3/4 space using surface markings.
7. Disinfect skin using pre-filled antiseptic sponge.
8. Inject up to 5ml of 2% lidocaine for local anaesthesia. Use the 25g needle and inject lidocaine to raise a skin wheal. Then inject lidocaine more deeply.
9. Obtain CSF using a 22G spinal needle. If the participant is thin, do not insert the deep infiltration needle all the way. Use only about 2/3 of its length (to prevent entering the subarachnoid space with anything other than the pencil-point spinal needle).
10. If CSF cannot be obtained, up to three needles may be used.
11. An adjacent space may be used (with further lidocaine, max. total 10 ml, if needed).
12. If necessary, CSF space may be located by sitting patient up, but once CSF is seen, it is recommended to have patient lie back in lateral decubitus position for 30 seconds before collection begins. Document positions of patient during puncture and collection in the eCRF.
13. Document the space used for lumbar puncture, the number of attempts and volume of lidocaine used in the eCRF.
14. Omit pressure measurement for all participants (because polypropylene spinal manometers are not available).
15. CSF is collected in 50ml tubes placed on ice in the Styrofoam cup.
16. Collect the first 1 ml of CSF into the supplied tube labelled ‘CSF’. If the first 1 ml (approx. 15 drops) is not macroscopically bloody, continue sampling CSF in the same tube up to 20 ml, keeping the tube in the ice cup. If the first 1 ml is macroscopically bloody, stop collecting CSF by reinserting the stylet partially, discard the tube, and collect a second 1 ml in a new pre-cooled ‘CSF’ tube, and examine it visually for blood contamination. If it is free of blood, continue collecting CSF up to 19 ml. If the second separately collected ml of CSF is also macroscopically bloody, discard the tube, and continue to collect 18 ml of CSF in

a third pre-cooled ‘CSF’ tube. Stop collecting CSF when sampling time exceeds 20 minutes. Document these details in the eCRF.

17. Place cap on tube and leave on crushed ice until further processing.
18. Reinsert the stylet before withdrawing the needle.
19. Cover the puncture site with sterile dressing.
20. Record time of CSF collection.
21. Participants can mobilise or remain lying for an hour at their discretion.
22. Transport samples immediately to biomarker laboratory for processing.

6.2 Venous Blood Collection

Venous blood is drawn immediately after CSF collection is complete, recording the time. The following samples are acquired:

- 1 × 8.5 ml serum tube.
- 4 × 10 ml blood in lithium heparin tubes. Gently invert each tube 10 times immediately after collection, and place on ice.
- If venepuncture with vacuum tubes proves challenging, a needle and syringe may be used and the blood transferred immediately into the vacuum tubes, observing safety precautions.

7. Sample Processing Procedures

7.1 CSF Sample Processing

1. All CSF processing should be done on ice, beginning within 15 minutes of completion of collection.
2. Agitate the entire CSF sample for 10 seconds to homogenise CSF.
3. Use 200 µl of the CSF to determine white blood cell count and erythrocyte count per µl according to local GLP-approved laboratory practice. This should be done in triplicate within 60 minutes of collection and all values recorded in the eCRF.
4. Centrifuge the 50 ml tube containing residual CSF at 400 × g for 10 min at 4°C to remove cells while preserving cell integrity for potential future use.
5. Pipette supernatant into a single tube labelled “CSF supernatant” and agitate for 10 seconds to homogenise CSF
6. Aliquot the CSF into 300 µl aliquots, using supplied pipette tips and cryovials labelled “CSF”.
7. Gently resuspend pellet in 300µL of supplied preservative solution and transfer to the cryovial labelled “Cells from CSF”.
8. Freeze CSF aliquots and resuspended cells on dry ice and store at -80°C.
9. Record time of freezing

7.2 Serum Sample Processing

1. Spin serum tube at 2000×g at room temperature for 10 min immediately upon arrival in the biomarker laboratory

2. Transfer 1500 µl of the supernatant into each of 2 separate 2 ml cryovials labeled “serum”, freeze on dry ice and store in -80°C.
3. Record time of freezing

7.3 Plasma Sample Processing

1. Spin lithium heparin tubes at 1300×g for 10 min at 4°C immediately on arrival.
2. Discard any tubes whose plasma is pink due to hemolysis.
3. Combine the supernatant in one tube labelled “plasma” and mix by inverting 10 times. Store on crushed ice.
4. Divide lithium heparin plasma into 300 µl aliquots using supplied pipette tips and cryovials labeled ‘plasma’.
5. Freeze samples on dry ice and store at -80°C.
6. Record time of freezing.

8. Sample storage

- Store samples in a -80°C freezer.
- Log samples in eCRF.

9. Sample Quality Control

The following quality control measures will be carried out to identify and flag samples subject to potential confounders:

- Microscopic erythrocyte count in CSF is performed locally in triplicate and recorded on eCRF. Cut-off for flagging: > 1000 cells/µl.
- Microscopic leukocyte count in CSF is performed locally in triplicate and recorded on eCRF. Cut-off for flagging: ≥ 5 cells/µl.

10. Analysis

10.1 CSF and plasma samples

CSF and plasma samples will be analysed locally at UCL Institute of Neurology or by collaborators authorised by the Principal Investigator. This may include collaborators outside the EU from academic or commercial entities for the purpose of research (1) to better understand HD or other diseases being studied, (2) that furthers the development of treatments for HD or other diseases or (3) that furthers biomedical research. Any shared samples will be coded and linked-anonymised.

Analyses of huntingtin protein and the kynurenine pathway are specifically planned. Specifically, the levels of the following KP metabolites will be measured in CSF and plasma: kynurenine, kynurenic acid, 3-OH-kynurenine, quinolinic acid and anthranilic acid. In addition, the plasma levels of tryptophan will be determined, which will allow for an additional control for lack of compliance with the stipulation of an overnight fast.

Additional measurements, including but not limited to other KP metabolites or precursors, the levels of soluble HTT, and other putative biomarkers may also be measured at appropriate laboratories.

The primary outcome measurements are of unknown clinical significance. The detailed analysis may include measurements of potential clinical significance in relation to conditions other than HD, such as oligoclonal bands. However, patients with other neurological diagnoses or unexpected examination findings will be excluded. Therefore any abnormal results, obtained on a linked-anonymised basis, will remain of indeterminate clinical significance and will not be fed back to the participant.

A portion of each participant's samples will be shared alongside phenotypic data with CHDI Foundation to augment the collection of CSF and plasma for the complementary HDClarity project (global Chief Investigator: Dr Edward Wild). This shares the aims of HD-CSF in investigating huntingtin protein, the kynurenine pathway and other biomarkers and pathways of relevance to HD.

10.2 MRI data processing

Whole-brain, caudate and white-matter atrophy rates will be calculated using the robust, reproducible methods developed in TRACK-HD, which compared many potential clinical, imaging, cognitive and other biomarkers head-to-head and produced a toolkit for longitudinal clinical trials in HD[6-9]. Baseline regions will be segmented using MIDAS software and volume change estimated using the boundary shift integral (BSI) method. White matter will be quantified using voxel-based morphometry. Additional analyses may be conducted locally or by authorized collaborators.

10.3 Statistical analysis

Statistical design advice was received from UCL/UCLH Biostatistics Unit. Each biochemical analysis will require its own statistical plan which will be prepared before the analysis is conducted. Broadly, linear regression models, adjusted for age and gender, will compare inter-group cross-sectional differences in primary outcomes (CSF mHTT concentration and CSF ratio of 3HK:KYN) and associations with disease burden score across all groups. Longitudinal analysis will compare rates of change between and across groups. Significantly altered primary outcomes will be taken forward to a second-level analysis and regressed against secondary outcomes (CSF and plasma levels of individual KP metabolites (kynurenine, KA, 3HK, QA) and clinical/ cognitive/ MRI measures. This will identify mHTT species and KP metabolites that predict specific neurobiological or mechanistic features of HD. Multiplicity correction and bootstrapping for non-normally distributed variables will be used where appropriate.

11. Adverse Event Reporting and Documentation

11.1 Adverse Events

An adverse event (AE) is any untoward medical occurrence during a clinical investigation and that does not necessarily have a causal relationship with study treatments or procedures. An AE is therefore any unfavourable and unintended sign (including an abnormal laboratory finding), symptom or disease temporally associated with the administration of study procedures.

The Principal Investigator or appointed delegate(s) will probe, via discussion with the participant, for the occurrence of AEs during each participant visit, after the screening visit, and record the information in the site's source documents. AEs will be recorded in the patient eCRF. AEs will be described by duration (start and stop dates and times), severity, outcome, treatment and relation to study procedures if applicable, or if unrelated, the cause.

11.1.1 AE Severity Grading

The severity of an AE will be graded on a 5-point scale (Common Terminology Criteria for Adverse Events v3.0 (CTCAE); http://ctep.cancer.gov/protocolDevelopment/electronic_applications/ctc.htm) defined as follows:

Grade 1	Mild AE
Grade 2	Moderate AE
Grade 3	Severe AE
Grade 4	Life-threatening or disabling AE
Grade 5	Death related to AE

11.1.2 AE Relationship to study procedures

The relationship of an AE to the study procedures will be evaluated according to the following guidelines:

Probable: This category applies to AEs which are considered with a high degree of certainty to be related to the study procedure. An AE may be considered probably related to the study procedure if:

1. It follows a reasonable temporal sequence from administration of the study procedure;
2. It cannot be reasonably explained by the known characteristics of the participant's clinical state, or by environmental or toxic factors;
3. It follows a known pattern of response to the study procedure;

Possible: This category applies to those AEs in which the connection with the study procedure appears unlikely but cannot be ruled out with certainty. An AE may be considered as possibly related if it has at least two of the following:

1. It follows a reasonable temporal sequence from the study procedure
2. It may readily have been produced by the participant's clinical state, or by environmental or toxic factors;
3. It follows a known response pattern to the study procedure.

Unrelated: This category applies to those AEs which are judged to be clearly and incontrovertibly due to extraneous causes (disease, environment, etc.) and do not meet the criteria for study procedure relationship listed under possible or probable.

11.2 Serious Adverse Events

A Serious Adverse Event (SAE) is defined as any AE that results in any of the following outcomes:

- death
- a life-threatening adverse experience
- inpatient hospitalization or prolongation of existing hospitalization
- a persistent or significant disability/incapacity
- a congenital anomaly/birth defect

Other important medical events may also be considered an SAE when, based on appropriate medical judgment, they jeopardize the participant or require intervention to prevent one of the outcomes listed.

An AE is considered to be life-threatening if, in the view of the Principal Investigator, the participant was at immediate risk of death from the reaction as it occurred. It does not include a reaction that, had it occurred in a more serious form, might have caused death.

11.2.1 Serious Adverse Experience Reporting

SAEs (as defined in Section 11.2) must be reported to the Sponsor immediately and in no case later than within 24 hours of awareness of the event.

All SAEs that occur (whether or not related to study procedures) will be documented. The collection period for all SAEs will begin from the Sampling Visit and end after procedures for the final study visit have been completed.

In accordance with the standard operating procedures and policies of the REC, the Principal Investigator will report SAEs to the REC.

11.3 Post-study Follow-up of Adverse Events

Any AE, including clinically significant physical examination findings, must be followed until the event resolves, the condition stabilises, the event is otherwise explained, or the participant is lost to follow-up. If resolved, a resolution date should be documented on the eCRF and in the source documents. The Principal Investigator is responsible for ensuring that follow-up includes any supplemental investigations as may be indicated to elucidate the nature and/or causality of the AE. This may include additional laboratory tests or investigations, histopathological examinations, or consultation with other health care professionals as is medically indicated.

12. Statistical Methodology

12.1 Determination of Sample Size

Power calculations were based on a 12-subject CSF analysis of mutant huntingtin using a novel single molecule counting immunoassay1. Detecting cross-sectional differences between control and HD requires very small numbers (<5 per group for >90% power at 5% significance). 20 subjects per group gives >90% power to detect predicted longitudinal change in mutant huntingtin over two years.

For the biomarkers discovered and analysed, it may be important to understand the stability of the biomarker within participants over relatively short time periods. Thus, approximately 20 participants per cohort will be invited to return for a repeat sampling visit 4-8 weeks after their first visit.

13. Study Management

13.1 Ethics and Regulatory Considerations

The investigator will conduct the study in compliance with the protocol and in accordance with the ICH for GCP and the appropriate regulatory requirement(s). The study will also be conducted in accordance with the recommendations for physicians involved in research on human subjects adopted by the 18th World Medical Assembly, Helsinki 1964 and later revisions.

Participants must give informed consent prior to undertaking study procedures and these informed consents must be obtained by clinical site staff using approved processes. Signed consent forms will be maintained in a secure designated location.

13.1.1 Audits and Inspections

The study may be subject to inspection and audit by University College London under their remit as sponsor and other regulatory bodies to ensure adherence to GCP and the NHS Research Governance Framework for Health and Social Care (2nd edition). Audits and/or inspections may also be carried out by local authorities, or authorities to which information on this trial has been submitted. All documents pertinent to the trial will be made available for such inspection after an adequate announcement.

13.1.2 Ethics Committee Approval

The Investigator will obtain approval from the Local Research Ethics Committee (REC) The Investigator will require a copy of the R&D/NHS approval letter before accepting participants into the study. Substantial amendments to the protocol will require written approval / favourable opinion from the REC prior to implementation, except when the modification is needed to eliminate an immediate hazard(s) to subjects. Deviation from the protocol required to eliminate an immediate hazard(s) to subjects will be fully documented in the CRF and source documentation.

13.1.3 Confidentiality

In order to maintain subject privacy, all case report forms (CRFs), study reports and communications will identify the subject by initials and the assigned Subject number. The investigator will preserve the confidentiality of participants taking part in the study in accordance with the Data Protection Act.

13.1.4 Sponsor

University College London will act as the Sponsor for this study.

13.1.5 Indemnity

University College London holds negligent harm and non-negligent harm insurance policies which apply to this study.

13.2 Informed Consent Procedure

Consent to enter the study will be sought from each participant only after a full explanation of the study has been given, a patient information sheet offered and time allowed for consideration. Signed participant consent will be obtained. The method of obtaining and documenting the informed consent and the contents of the consent will comply with ICH-GCP and all applicable regulatory requirement(s).

The right of the participant to refuse to participate without giving reasons will be respected. After the participant has entered the study the investigator remains free to give alternative treatment to that specified in the protocol at any stage if he/she feels it is in the participant's best interest, but the reasons for doing so should be recorded. In these cases the participants remain within the study for the purposes of follow-up and data analysis. All participants are free to withdraw at any time from the protocol treatment without giving reasons and without prejudicing further treatment.

13.3 Biological samples (handling, processing and storage)

In the study, blood and CSF will be collected from participants in accordance with the patient consent form and patient information sheet and shall include all biological materials and any derivatives, portions, progeny or improvements as well as all patient information and documentation supplied in relation to them. These biological samples will be stored at UCL Institute of Neurology for the processing described in section 8 of this protocol. This will prepare samples for shipment to collaborators in accordance with the analytical plan agreed with the Principal Investigator. The PI and his delegated representatives will process, store and dispose of samples in accordance with all applicable legal and regulatory requirements, including the Human Tissue Act 2004 and any amendments thereto**.**

13.4 Data Collection, Retention and Monitoring

13.4.1 Data transfer (handling, processing and storage)

In the study, Name, date of birth, medical history, ethnicity and cognitive data will be collected from patients in accordance with the patient consent form, patient information sheet and sections 5 and 5.1 of this protocol.

The patient data will be stored securely at UCL Institute of Neurology and collaborators authorized by the principal investigator for statistical analysis, and UCL will act as the data controller of such data for the study.

The PI and his delegated representatives will process, store and dispose of patient data in accordance with all applicable legal and regulatory requirements, including the Data Protection Act 1998 and any amendments thereto. Data held on paper will be stored at the UCL Institute of Neurology Huntington's Disease Research Centre under secure access control, in a locked filing cabinet controlled by the Investigator.

All transfers of data and/or samples will be covered by materials transfer agreements.

13.4.2 Data Entry/Electronic Data Capture System

Data will be entered electronically via secure internet-based technology provided by the Enroll-HD platform. Access to the eCRF is limited by password and can only be authorized by the PI. Monitoring of clinical data will be carried out by the Enroll-HD data monitors. The data managers are responsible for study monitoring and ensuring compliance with the study protocol.

13.4.3 Data Quality Control and Reporting

After data have been entered into the study database, a system of computerized data validation checks will be implemented and applied to the database on a regular basis. Query reports pertaining to data omissions and discrepancies will be forwarded to the Principal Investigator and site investigators for resolution. The study database will be updated in accordance with the resolved queries. All changes to the study database will be documented.

13.4.4 Archival of Data

The database is safeguarded against unauthorized access by established security procedures; appropriate backup copies of the database and related software files will be

maintained. Databases are backed up by the database administrator in conjunction with any updates or changes to the database.

13.4.5 Source Documents

The Principal Investigator will maintain source documents for each participant enrolled in the study. Source documents such as local laboratory ranges and reports, participant charts and doctors' notes will be kept as part of the participants' medical records. For participants who do not have a medical record per se, another method of documentation and record keeping will be employed, along with the obligation to retain source documents, such as laboratory reports, for the period of time specified in the site agreement. Participant files including medical records and signed participant informed consent forms must be available for review in the event the site is selected for monitoring, audits, or inspections.

13.4.6 Monitoring

The Principal Investigator, on behalf of the Sponsor, is responsible for ensuring the proper conduct of the study with regard to ethics, protocol adherence, site procedures, integrity of the data, and applicable laws and/or regulations.

The Principal Investigator will make study data accessible to the clinical monitors, to other authorized representatives of the Sponsor, and to regulatory inspectors.

13.4.7 Intellectual Property Rights

All background intellectual property rights (including licences) and know-how used in connection with the study shall remain the property of the party introducing the same and the exercise of such rights for purposes of the study shall not infringe any third party's rights.

All intellectual property rights and know-how in the protocol and in the results arising directly from the study, but excluding all improvements thereto or clinical procedures developed or used by each participating site, shall belong to UCL. Each participating site agrees that by giving approval to conduct the study at its respective site, it is also agreeing to effectively assign all such intellectual property rights ("IPR") to UCL and to disclose all such know-how to UCL.

Each participating site agrees to, at the request and expense of UCL, execute all such documents and do all acts necessary to fully vest the IPR in UCL.

Nothing in this section shall be construed so as to prevent or hinder the participating site from using know-how gained during the performance of the study in the furtherance of its normal activities of providing or commissioning clinical services, teaching and research to the extent that such use does not result in the disclosure or misuse of confidential information or the infringement of an intellectual property right of UCL. This does not permit the disclosure of any of the results of the study, all of which remain confidential.

13.5 Amendments

Any amendments to the protocol will be written and approved by the Principal Investigator and submitted to the REC for approval prior to implementing the changes. In some instances, an amendment may require changes to the informed consent form, which also must be submitted for REC and JRO approval prior to administration to study participants.

13.6 Record Keeping

13.6.1 Statutory compliance

The Principal Investigator agrees to comply with all applicable laws and regulations relating to the privacy of patient health information.

13.6.2 Retention of Study Documents

Study-related records must be retained for the period of at least five years.

14. Appendix A –Principal Investigator Obligations

The study protocol and the final version of the participant informed consent form will be approved by a REC before enrollment of any participants. The opinion of the IRB/ERB will be dated and given in writing.

The Principal Investigator will ensure that the REC will be promptly informed of all changes in the research activity and of all unanticipated problems including risk to participants. The Principal Investigator will not proceed with changes to the protocol until REC approval has been obtained.

Written informed consent must be given freely and obtained from every participant prior to clinical study participation. The rights, safety, and well-being of the study participants are the most important considerations and should prevail over interests of science and society.

As described in GCP guidelines, study personnel involved in conducting this study will be qualified by education, training, and experience to perform their respective task(s). Study personnel will not include individuals against whom sanctions have been invoked after scientific misconduct or fraud (e.g., loss of medical licensure, debarment). Quality assurance systems and procedures will be implemented to assure the quality of every aspect of the study.

REC Review/Approval/Reports

The protocol and informed consent for this study, including advertisements used to recruit participants, must be reviewed and approved by an appropriate REC prior to enrolment of participants in the study. It is the responsibility of the Principal Investigator to ensure that all aspects of the ethical review are conducted in accordance with the current Declaration of Helsinki, ICH, GCP, and/or local laws, whichever provide the greatest level of protection. Amendments to the protocol will be subject to the same requirements as the original protocol.

A progress report with a request for re-evaluation and re-approval will be submitted by the Principal Investigator to the REC at intervals required by the REC.

After completion or termination of the study, the Principal Investigator will submit a final report to the REC. This report should include: deviations from the protocol, the number and types of participants evaluated, and significant AEs, including deaths.

Study Documentation

The Principal Investigator is required to maintain complete and accurate study documentation in compliance with current Good Clinical Practice standards and all applicable federal, state, and local laws, rules, and regulations related to the conduct of a clinical study. Study documentation includes REC correspondence, protocol and amendments, information regarding monitoring activities, participant exclusion records, eCRFs, and data queries.

Confidentiality

The anonymity of study participants must be maintained. Study participants will be identified by an assigned participant number on eCRFs and other documents submitted to the clinical monitor. Documents that will be submitted to the clinical monitor and that identify the participant (e.g., the signed informed consent document) must be maintained

in strict confidence by the Principal Investigator, except to the extent necessary to allow auditing by regulatory authorities or the clinical monitor.

Study Facilities

The Principal Investigator must ensure that there is a robust institutional policy on freezer failure that includes checks, alarms, emergency contact details, backup power supplies, CO_2 cylinders and an infrastructure to transfer samples to an off-site facility if necessary.

15. References

1. Wild, E. J. *et al.* Quantification of mutant huntingtin protein in cerebrospinal fluid from Huntington's disease patients. *The Journal of Clinical Investigation* **125**, 1979-1986 (2015).
2. Ross, C. A. *et al.* Huntington disease: natural history, biomarkers and prospects for therapeutics. *Nat Rev Neurol* **10**, 204-216 (2014).
3. Vecsei, L., Szalardy, L., Fulop, F. & Toldi, J. Kynurenines in the CNS: recent advances and new questions. *Nature reviews. Drug discovery* **12**, 64-82 (2013).
4. Wild, E. J. & Tabrizi, S. J. Targets for future clinical trials in Huntington's disease: what's in the pipeline? *Mov. Disord.* **29**, 1434-1445 (2014).
5. Wild, E. J. & Tabrizi, S. J. Biomarkers for Huntington's disease. *Expert Opinion on Medical Diagnostics* **2**, 47-62 (2008).
6. Tabrizi, S. J. *et al.* Biological and clinical manifestations of Huntington's disease in the longitudinal TRACK-HD study: cross-sectional analysis of baseline data. *The Lancet Neurology* **8**, 791-801 (2009).
7. Tabrizi, S. J. *et al.* Potential endpoints for clinical trials in premanifest and early Huntington's disease in the TRACK-HD study: analysis of 24 month observational data. *Lancet Neurol* **11**, 42-53 (2012).
8. Tabrizi, S. J. *et al.* Biological and clinical changes in premanifest and early stage Huntington's disease in the TRACK-HD study: the 12-month longitudinal analysis. *The Lancet Neurology* **10**, 31-42 (2011).
9. Tabrizi, S. J. *et al.* Predictors of phenotypic progression and disease onset in premanifest and early-stage Huntington's disease in the TRACK-HD study: analysis of 36-month observational data. *The Lancet Neurology* **12**, 637-649 (2013).